



**HAL**  
open science

# Searching sustainable solvents for high-performance organic solar cells by reverse engineering

Jing Wang

► **To cite this version:**

Jing Wang. Searching sustainable solvents for high-performance organic solar cells by reverse engineering. Material chemistry. Université de Strasbourg, 2020. English. NNT : 2020STRAD040 . tel-03636491

**HAL Id: tel-03636491**

**<https://theses.hal.science/tel-03636491v1>**

Submitted on 10 Apr 2022

**HAL** is a multi-disciplinary open access archive for the deposit and dissemination of scientific research documents, whether they are published or not. The documents may come from teaching and research institutions in France or abroad, or from public or private research centers.

L'archive ouverte pluridisciplinaire **HAL**, est destinée au dépôt et à la diffusion de documents scientifiques de niveau recherche, publiés ou non, émanant des établissements d'enseignement et de recherche français ou étrangers, des laboratoires publics ou privés.

**ÉCOLE DOCTORALE Mathématiques, Sciences de l'information et de l'Ingenieur**  
**[ Matériaux pour Composants Electroniques et Photovoltaïques ]**

**THÈSE** présentée par :

**Jing WANG**

soutenue le : 14 Octobre 2020

pour obtenir le grade de : **Docteur de l'université de Strasbourg**

Discipline/ Spécialité : Physique / Photovoltaïque

**Searching Sustainable Solvents For  
High-Performance Organic Solar Cells  
By Reverse Engineering**

**THÈSE dirigée par :**

**M. HEISER Thomas**

Professeur, Université de Strasbourg

**RAPPORTEURS :**

**M. WANTZ Guillaume**

Maître de Conférences HDR, Bordeaux INP, École Nationale Supérieure de Chimie, de Biologie et de Physique (ENSCBP)

**M. AUBRY Jean-Marie**

Professeur, École Nationale Supérieure de Chimie de Lille

---

**AUTRES MEMBRES DU JURY :**

**Mme. RODRIGUEZ-DONIS Ivonne**

Docteur, INP, Laboratoire de Chimie Agro-Industrielle, Université de Toulouse

**M. ULRICH Gilles**

Professeur, Université de Strasbourg

**INVITED MEMBRES DU JURY :**

**Mme. THIEBAUD-ROUX Sophie**

Professeur, INP, Laboratoire de Chimie Agro-Industrielle, Université de Toulouse

凡心所向，素履所往；  
生如逆旅，一苇以航。

## Acknowledgements

This thesis work was carried out under the supervision of **Dr. Thomas Heiser**, Professor at the University of Strasbourg. I would like to express sincere gratitude to him for his guidance, encouragement and support throughout these three years. I could not have imagined a better advisor and mentor for my PhD studies.

I would like to thank my reporters, **Dr. Guillaume Wantz**, Maître de Conférences HDR of Bordeaux INP, École Nationale Supérieure, de Chimie, de Biologie et de Physique (ENSCBP), and **Dr. Jean-Marie Aubry**, Professor of École Nationale Supérieure de Chimie de Lille, for their interest in my work. I would also like to thank the members of the Jury: **Dr. Ivonne Rodriguez-Donis**, **Dr. Gilles Ulrich** and **Ms. Sophie Thiebaud-Roux**, who gave me good advice in their respective fields.

I would like to thank the laboratory collaborators: **Dr. Nicolas Leclerc**, **Ms. Stéphanie Ferry**, **Dr. Stéphane Méry** and **Dr. Kamatham Narayanaswamy** for providing the polymers; **Dr. Ivonne Rodriguez-Donis** and **Dr. Sophie Thiebaud-Roux** guided me in use of the IBSS®CAMD tool; **Dr. Markus Kohlstädt** provided help with Hansen's parameter theory.

I would like to thank all the staff of the MaCEPV team, especially **Dr. Patrick Levêque**, **Dr. Sadiara Fall**, **Dr. Olzhas Ibraikulov** and **Mr. Nicolas Zimmermann** with whom I worked closely during the fabrication of the devices. Thanks to the good atmosphere of the team and the mutual help within the team, it is really fun to come to work every day.

In closing, I would like to thank my entire family for their emotional support and for their continued encouragement, which helped me persevere and complete my PhD.

## Table of Contents

Table of Contents .....	II
Figures .....	VII
Tables .....	X
List of variables and abbreviations .....	XII
1 General Introduction .....	17
2 Organic Photovoltaics.....	25
2.1 Organic Semiconducting Materials .....	25
2.2 Working Principle of OPV .....	26
2.2.1 Light absorption and exciton generation .....	27
2.2.2 Exciton diffusion and dissociation at the D/A Interface.....	28
2.2.3 Charge carrier transport.....	29
2.2.4 Charge-carrier extraction at electrodes.....	30
2.3 Functionality of the active Layer .....	31
2.4 Device Structures and working principle .....	32
2.4 Current – Voltage Characteristics.....	33
2.4.1 Short Circuit Current Density ( $J_{sc}$ ).....	34
2.4.2 Open Circuit Voltage ( $V_{oc}$ ) .....	35
2.4.3 Fill Factor (FF).....	35
2.5 Fabrication of OPVs .....	36
2.5.1 Materials and Substrates .....	36
2.5.2 Experimental details .....	37
2.6 Characterization of OPV devices .....	39
2.6.1 JV characteristics.....	39
2.6.2 Thickness measurement .....	39
2.6.3 Ultraviolet-visible spectroscopy .....	39
3 Strategies for Controlling the Active Layer Morphology and Methods for Solvents	

Selection .....	41
3.1 Active Layer Morphology .....	41
3.2 Role of Processing Solvents.....	41
3.2.1 Solubility .....	42
3.2.2 Boiling Point of Processing Solvents .....	45
3.2.3 Solvent mixtures .....	47
3.3 Methods for Solvent Selection.....	52
3.3.1 Trial and Error Approach .....	52
3.3.2 Hansen Solubility Parameters Theory (HSPs).....	54
3.3.3 IBSS® CAMD .....	57
4    IBSS®CAMD Tool.....	61
4.1 Fundamental Principles of IBSS®CAMD .....	61
4.1.1 Property calculation models .....	63
4.1.2 Performance criteria .....	66
4.1.3 Resolution method .....	68
4.1.4 Molecular representation model.....	70
4.2 Reverse Engineering Method for Alternative Solvents Design .....	73
4.2.1 Definition of the Initial Problem .....	74
4.2.2 Translation of functionalities into physicochemical properties and definition of target values.....	74
4.2.3 Molecular design parameters .....	75
4.2.4 Candidate ranking and final choice.....	80
4.3 Conclusion.....	80
5    Case Studies: Alternative Solvent Selection for P3HT Based OPV Devices By IBSS®CAMD .....	83
5.1 Defining the Conditions to Apply IBSS®CAMD to OPV .....	84
5.1.1 Initial problem definition: Functionalities of existing solvent.....	84
5.1.2 Translation of functionalities into physicochemical properties and definition of	

	target values.....	85
	5.1.3 Selection of the predictive models .....	91
	5.1.4 Definition of the global performance function .....	93
	5.1.5 Molecular design parameters .....	93
	5.1.6 Candidate ranking and final choice .....	94
	5.2 Photovoltaic Performance.....	100
	5.3 Conclusion.....	104
6	Case studies: Alternative Solvent Selection For New Donor Polymers by IBSS®CAMD ..	107
	6.1 Major Properties for Polymers.....	109
	6.1.1 UV-Vis characterization .....	109
	6.1.2 Solubility and HSPs.....	111
	6.2 Solvent selection by IBSS®CAMD .....	113
	6.3 Photovoltaic Performance.....	123
	6.4 Conclusion.....	126
7	Conclusion and Perspectives .....	128
8	Bibliography.....	132
9	Appendix .....	152

## Figures

Figure 1.1 Evolution of record photovoltaic conversion efficiencies for different families of semiconductors and technologies. <sup>19</sup> .....	19
Figure 1.2 Photographs of (a) a flexible OPV (Source: Fraunhofer ISE), and (b) a transparent OPV <sup>31</sup> .....	20
Figure 2.1 (a) Chemical structure of ethylene and polyacetylene, and (b) $p_z$ orbital overlap to form $\pi$ (bonding) and $\pi^*$ (anti-bonding) band in C-C system. ....	26
Figure 2.2 Band alignment of donor and acceptor materials for a heterojunction. ....	28
Figure 2.3 (a) The structure of OPV and (b) key steps involved in active layer (Red area: donor domains, Blue area: acceptor domains, Mixture: bulk heterojunction). ....	31
Figure 2.4 Schematic view of standard (a) and inverted (b) OPV devices.....	33
Figure 2.5 J-V characteristics of OPVs. The black and symbolic red lines represent dark and light curves, respectively. The navy point indicates the maximum power point (MPP) of a solar cell ( $V_{MPP}$ ). Green points show the open circuit voltage $V_{OC}$ and the short circuit current density $J_{SC}$ of the solar cell. The fill factor (FF) is determined by the area ratio of the yellow rectangle to the gray dashed rectangle. ....	34
Figure 2.6 Diagram of the interfacial layer on the ITO after cleaning from one side.....	38
Figure 2.7 (a) The OPV sample and (b) shadow mask used for JV characteristics. ....	38
Figure 3.1 AFM topography images ( $2\ \mu\text{m} \times 2\ \mu\text{m}$ ) of as-cast of MDMO-PPV:PC <sub>61</sub> BM spin-casted from (a) CB, (c) CS <sub>2</sub> , (e) CF, (g) pyridine, (i) trichloroethylene, (k) toluene, and (m) 1-methylpyrrole. [From REF. <sup>87</sup> ] (The solubilities of PC <sub>61</sub> BM in various solvents are shown at the top of the corresponding AFM images.) .....	43
Figure 3.2 Atomic force microscopy (AFM) micrographs ( $5 \times 5\ \mu\text{m}$ ) of thin films of 1:1 TQ1:PC <sub>71</sub> BM (a–c) and 1:3 PC <sub>71</sub> BM (d–f) spin-coated from CF (a,d), CB (b,e), o-DCB (c,f). Scale bar indicates $1\ \mu\text{m}$ . Surface roughness (RMS), as well as the	



corresponding height scale, is added to each image. <sup>92</sup> .....	44
Figure 3.3 The AFM images (size: 5 $\times$ 5 $\mu$ m) of (a) BDT-2T-DCV-Me: IDIC and (b) BDT-2T-CNAB: IDIC blend films processed from CF. <sup>87</sup> .....	45
Figure 3.4 AFM height images of spin-casted PFB/PCBM blends from xylene under (a) “no vapor” conditions, (b) “high vapor” conditions, (c) from toluene under “no vapor” conditions and (d) from mesitylene under “no vapor” conditions. <sup>60</sup> .....	47
Figure 3.5 Examples of processing additives for BHJ morphological control.....	48
Figure 3.6 (a)–(d) Represents surface topography images of PTB7: PC <sub>71</sub> BM photoactive layer with different concentration of DIO (0 ,1, 3 and 5 vol%) respectively. <sup>100</sup> .....	49
Figure 3.7 (a) HSPs diagrams with the good and bad solvents resulting from the solubility tests and the fitted solubility sphere. Radius R <sub>0</sub> of the solubility sphere as a function of temperature. The radius is fixed at a solubility limit of 10mg/mL. The dashed line is a guide to the eye. <sup>127</sup> .....	56
Figure 4.1 Division of N-phenyl-1,4-benzenediamine molecule by group contribution methods.....	64
Figure 4.2 (a) shows an example corresponding to a property whose x value is within a target range defined by two boundary values and thus two different $\sigma$ parameters. (b) examples corresponding to properties, whose x values need either to be higher or equal to a given target value, and (c) examples corresponding to a property whose x values need either to be lower or equal to a given target value.....	68
Figure 4.3 Steps of a genetic algorithm in IBSS <sup>®</sup> CAMD.....	69
Figure 4.4 Molecular graph representation of acetone.....	71
Figure 4.5 Simple and complex groups representation.....	73
Figure 4.6 Systematic methodology based on reverse engineering and CAPD to design alternative solvents.....	73
Figure 4.7 Examples of chemical groups and connection types for building alternative solvents using IBSS <sup>®</sup> CAMD tool. (R <sub>1</sub> and R <sub>2</sub> are randomly selected chemical groups from the IBSS <sup>®</sup> CAMD data base that are connected to other chemical groups by	

either simple or double bonds.....	76
Figure 4.8 Mutation operator example.....	77
Figure 4.9 Crossover operator example.....	78
Figure 4.10 Insertion operator example.....	78
Figure 4.11 Deletion operator example.....	79
Figure 4.12 Substitution operator example.....	80
Figure 5.1 Chemical structure of donors and acceptors.....	84
Figure 5.2 Differences between experimental data and IBSS®CAMD predicted values for various properties.....	86
Figure 5.3 (a) The positions of P3HT and PC <sub>71</sub> BM in Hansen solubility space, (b) the positions of P3HT and EH-IDTBR in Hansen solubility space.....	89
Figure 5.4 (a) The JV characteristics of P3HT:PC <sub>71</sub> BM based OPV devices processed from various solvents without DPE, and (b) with DPE.....	101
Figure 5.5 JV curves of P3HT:EH-IDTBR based OPVs processed from various solvents.....	103
Figure 6.1 The chemical structures of donor PF2 (side chain: R <sub>1</sub> ) and KNSF2 (side chain: R <sub>2</sub> ).....	109
Figure 6.2 UV-Vis absorption spectra of (a) PF2 and (b) KNSF2 in solution as a function of temperature and in thin film.....	111
Figure 6.3 The position of (a) PF2:PC <sub>71</sub> BM, (b) PF2:PEH-IDTBR and (c) KNSF2:PC <sub>71</sub> BM in Hansen space.....	112
Figure 6.4 a) The J-V curves of PF2 from o-DCB and PX/DPE solutions, and b) the JV curves of PF2 based devices processed from PX/DPE mixture solvents at different processing temperature.....	124
Figure 6.5 The JV characteristics of PF2:EH-IDTBR based OPVs processed from o-DCB and p- xylene.....	125

## Tables

Table 2.1 The list of processing solvents and additives used in this thesis. ....	37
Table 3.1 Solubility of PC <sub>61</sub> BM in various solvents. ....	42
Table 3.2 Solubilities of BDT-2T-DCV-Me and BDT-2TCNAB in CF, and PCEs of the OPVs devices based on BDT-2T-DCV-Me: IDIC films and BDT-2T-CNAB: IDIC films under the illumination of AM 1.5G, 100 mW cm <sup>-2</sup> . <sup>87</sup> .....	45
Table 3.3 Effects of processing additive on the PCE of several type of donor/acceptor OPVs.....	50
Table 3.4 Examples of alternative solvents for several type of donor/acceptor OPVs by trial and error approach. ....	53
Table 3.5 Examples of alternative solvents for several type of donor/acceptor OPVs by HSPs theory.....	57
Table 4.1 Estimation of normal boiling point of N-phenyl-1,4-benzenediamine. <sup>142</sup> .....	65
Table 4.2 Examples of available basic groups and their encoding in IBSS <sup>®</sup> CAMD.....	72
Table 5.1 The target properties, corresponding values for P3HT:PC <sub>71</sub> BM blends and P3HT:EH-IDTBR blends. ( <sup>a</sup> P3HT:PC <sub>71</sub> BM blends, and <sup>b</sup> P3HT:EH-IDTBR blends.).....	88
Table 5.2 The physicochemical properties and corresponding values of o-DCB and CB.....	91
Table 5.3 Group contribution method-based property models and Universal constants for the target properties.....	92
Table 5.4 The candidates provided for P3HT:PC <sub>71</sub> BM blends by IBSS <sup>®</sup> CAMD with a GloPerf > 0.6. (/: non-available data) .....	96
Table 5.5 The candidates provided for P3HT:EH-IDTBR blends by IBSS <sup>®</sup> CAMD with a GloPerf > 0.6. (/: non-available data) .....	97
Table 5.6 List of the best solvent candidates selected from the results of molecular design provided by IBSS <sup>®</sup> CAMD. (Y: yes, N: no, NA: non-available data) .....	99
Table 5.7 OPV device parameters of P3HT:PC <sub>71</sub> BM based devices fabricated from various solvents. ....	102

Table 5.8 The corresponding photovoltaic device parameters of P3HT:EH-IDTBR based devices fabricated from selected candidates.....	104
Table 5.9 $R_a$ and RED values between various solvents and two acceptor materials. ....	104
Table 6.1 HSPs for PF2, KNSF2, PC <sub>71</sub> BM and EH-IDTBR. ....	112
Table 6.2 The target properties, corresponding values for PF2:PC <sub>71</sub> BM, PF2:EH-IDTBR, and KNSF2:PC <sub>71</sub> BM. ( <sup>a</sup> PF2:PC <sub>71</sub> BM blends, <sup>b</sup> PF2:EH-IDTBR blends, and <sup>c</sup> KNSF2:PC <sub>71</sub> BM blends.).....	114
Table 6.3 The candidates provided for PF2:PC <sub>71</sub> BM by IBSS®CAMD with a GloPerf > 0.6. ....	117
Table 6.4 The candidates provided for PF2:EH-IDTBR by IBSS®CAMD with a GloPerf > 0.6. ....	118
Table 6.5 List of the best solvent candidates selected from the results of molecular design provided by IBSS®CAMD for PF2:PC <sub>71</sub> BM blends. (Y: yes, N: no, NA: non-available data).....	119
Table 6.6 List of the best solvent candidates selected from the results of molecular design provided by IBSS®CAMD for PF2:EH-IDTBR blends. (Y: yes, N: no, NA: non-available data).....	120
Table 6.7 The candidates provided for KNSF2:PC <sub>71</sub> BM by IBSS®CAMD with a GloPerf > 0.6.....	123
Table 6.8 Summary of PF2:PC <sub>71</sub> BM device performance for various solvents.....	125
Table 6.9 The corresponding photovoltaic device parameters of PF2:EH-IDTBR based devices fabricated from various solvents.....	126

## List of variables and abbreviations

AB	Allylbenzene
AN	Anisole
BA	Butyl acetate
BME	Benzyl methyl ether
CN	1,4-Cineol
CNAB	n-butyl cyanoester
CPME	Cyclopentyl methyl ether
DBE	Dibutyl ether
d-LM	d-Limonene
DMA	N,N-Dimethylaniline
IA	Isoamyl acetate
MB	Methyl Benzoate
MPE	Methyl phenethyl ether
PA	Phenylallene
PNA	Pinane
AA	p-Anisaldehyde
AFM	Atomic Force Microscopy
Ag	Silver
Al	Aluminum
AM1.5G	Global standard spectrum
AN	Anisole
ANR	Agence National de la Recherche
Au	Gold
BBzo	Benzyl benzoate
BDT	Benzo[1,2-b:4,5-b']dithiophene
BHJ	Bulk heterojunction
Ca	Calcium
CAMD	Computer assisted molecular design
CB	Chlorobenzene
CF	Chloroform
CN	1-chloronaphthalene
CS	charge separated
CS <sub>2</sub>	Carbon disulfide
CT	charge transfer
D/A	Donor/acceptor
DCVMe	Dicyanovinyl
DGEBA	Diglycidyl ether
DIO	1,8-diiodooctane

DPE	Diphenyl ether
EB	Ethyl benzenecarboxylate
$E_c$	Cohesive energy density
$E_D$	Dispersion interactions
EDOT	Ethylenedioxythiophene
$E_{Fn}$	Electron quasi-Fermi energy levels
$E_{Fp}$	Hole quasi-Fermi energy levels
$E_g$	Band gap energy
EH	Hydrogen binding interactions
EH-IDTBR	Ethylhexyl-rhodanine-benzothiadiazole-coupled indacenodithiophene
EP	Permanent dipole molecular interactions
EPBT	Energy payback time
ETL	Electron Transport Layer
FF	Fill factor
GTE	Glycerol -1,2,3-triethyl ether
HOMO	Highest Occupied Molecular Orbital
HSPs	Hansen solubility parameters theory
HTL	Hole Transport Layer
IC <sub>60</sub> BA	Indene-C60 bisadduct
ITO	Indium Tin Oxide
J	Current density
$J_{MPP}$	Current density of point of maximum power
$J_{SC}$	Short circuit current density
$L_{ex}$	Exciton diffusion length
LUMO	Lowest Unoccupied Molecular Orbital
MB	Methyl Benzoate
MEK	Methyl ethyl ketone
MeTHF	2-methyltetrahydrofuran
MoO <sub>3</sub>	Molybdenum trioxide
MPP	Maximum power point
MS	Molecular structures
NB	Nitrobenzene
NFPA	National Fire Protection Association
NMP	N-methyl-2-pyrrolidone
o-DCB	ortho-Dichlorobenzene
OFET	Organic field-effect transistors
OLED	Organic light emitting diode
OPV	Organic photovoltaics
OT	1,8-Octanedithiol
OX	o-Xylene
P3HT	Poly(3-hexylthiophene)

PC	p-Cymene
PC <sub>61</sub> BM	[6,6]-phenyl-C61-butyric acid methyl ester
PC <sub>71</sub> BM	[6,6]-phenyl-C71-butyric acid methyl ester
PCE/η	Power conversion efficiency
PEDOT:PSS	Poly(3,4-ethylenedioxythiophene) polystyrene sulfonate
PFB	poly[(9,9-dioctylfluorenyl-2,7-diyl)-alt-co-(N,N'-diphenyl-N,N'di(p-butylphenyl)-1,4-diaminobenzene)]
P <sub>in</sub>	Power of incident light
P <sub>M</sub>	Point of maximum power
PVE	Phenyl Vinyl Ether
PX	p-Xylene
QSAR/QSPR	Quantitative structure activity/propriety relationship
R <sub>0</sub>	Radius of solute in Hansen space
R <sub>a</sub>	Distance between two materials in Hansen space
RED	Relative energy difference
RFID	Radio-frequency identification
R <sub>s</sub>	Series resistance
R <sub>SH</sub>	Shunt resistance
Si	Silicon
SMILES	Simplified Molecular Input Line Specification
T	Temperature
T <sub>b</sub>	Boiling Point
T <sub>f</sub>	Flash Point
TGPA	Triglycidyl p-aminophenol ether
THF	Tetrahydrofuran
T <sub>m</sub>	Melting Point
TMB	1,2,4-trimethylbenzene
TPO	Terpinolene
TQ1	Quinoxaline-based co-polymer
UV	Ultra-Violet
V	Voltage
V <sub>m</sub>	Molecular volume
V <sub>MPP</sub>	Voltage of point of maximum power
V <sub>OC</sub>	Open-circuit voltage
WF	Work function
ZnO	Zinc oxide
α-PNE	α-Pinene
β-PNE	β-Pinene
δ <sub>D</sub>	Dispersion interactions
δ <sub>H</sub>	Hydrogen bonding type interactions
δ <sub>P</sub>	Permanent dipole molecular interactions
η	Viscosity

$\Delta H_{\text{vap}}$

1-4-MB

1-M-2-B

1-MN

1-P-2-B

1,2-DMN

1-MN

1-P-2-B

2-MA

2-MS

3-BTB

3-EC-1-C

4-ET

4-MPVE

4-MS

Vaporization enthalpy

1-(3-Buten-2-yl)-4-methylbenzene

1-Methyl-2-(2-propyn-1-yl) benzene

Methylnaphthalene

1-Phenyl-2-butene

1,2-dimethylnaphthalene

1-Methylnaphthalene

1-Phenyl-2-butene

2-methyl anisole

2-Methylstyrene

3-Butenylbenzene

3-Ethylcyclopentane-1-Carbaldehyde

4-Ethynyltoluene

4-Methylphenyl Vinyl Ether

4-Methylstyrene



# CHAPTER 1

---

---

## GENERAL INTRODUCTION

---

---

## 1 General Introduction

While for the past sixty years, inorganic semiconductors (such as silicon or gallium arsenide) and metals have formed the backbone of the semiconductor industry, today organic semiconductors are increasingly being used in various electronic devices, such as organic light emitting diodes (OLEDs), radio-frequency identification (RFID), organic field-effect transistors (OFET) and organic photovoltaics (OPVs). In 1977, Chiang et al. reported a chemically doped polyacetylene, the first highly conductive polymer that could be used as an electrically active material.<sup>1</sup> Since then, conjugated organic materials have been the focus of significant research efforts. While initially the development of organic semiconductor devices has been hampered by the poor performance and stability of early organic semiconductors, significant improvements in the synthesis and processing of new molecular materials, such as conjugated polythiophenes<sup>2</sup>, have increased the prospects for commercialization of organic semiconductor.<sup>3-6</sup> For example, OLEDs are now being used in many flat panel displays for smartphones.<sup>7</sup> Simplicity and lower costs of organic semiconductor device manufacturing have been the primary reasons driving these devices towards commercialization.

The development of functional organic materials that can be processed from solution has inspired many research groups to explore the potential of applying printing technologies to the large-scale manufacturing of organic electronic devices.<sup>8-10</sup> Solution-based printing technologies achieve the integration of advanced functions onto large-area substrates, such as flexible paper, plastic sheets, or large-area rigid glass, at a lower manufacturing cost than traditional manufacturing techniques.<sup>11-13</sup> For these technologies, the processing solvents play a critical role both in the performance of the organic devices and in their environmental impact. Therefore, the development and application of green solvents in the organic semiconductor field has attracted a lot of interest.<sup>14-17</sup>

The industrial revolution has caused a serious transformation of the human standard of living, leading to major advances that have contributed to improvements in life expectancy, quality of life and comfort. These developments have been accompanied by a dramatic increase in the world's population and, with it, a dramatic rise in energy demand. Today, the energy supply issue, more than ever, is a global problem, with a wide audience, from politicians to the scientific community. To date, energy demand has mostly been met by conventional hydrocarbons (oil, gas, coal). However, the greenhouse gases emitted into the Earth's atmosphere from the burning of fossil fuels are causing enormous environmental damage and have a significant impact on global climate change. Moreover, fossil fuels are a finite source of energy, leading to a shortage of these resources as societies develop, with political and social crises ensuing at the different places of today's world. In this case, solar energy offers many privileges as a clean and renewable energy source. The primary motivation for further development of solar energy research is the enormous amount of energy that the sun delivers to the Earth's surface every day. Considering simple assumptions and rough estimates, it has been reported that solar power plants could provide up to 67 TW of electricity by 2050, more than twice the world's energy demand, provided they cover 2% of the land area with an average power conversion efficiency (PCE) of about 12%.<sup>18</sup>

Solar cells, also known as photovoltaic cells, are devices that convert sunlight directly into electricity. They can be fabricated from a variety of materials (organic, inorganic, etc.) and their PCE over time is shown in the National Renewable Energy Laboratory chart<sup>19</sup> (Figure 1.1). By far, silicon solar cells (mono- and multicrystalline silicon) have controlled the commercial solar cells market, reaching a PCE of 22.9% for mono-crystalline and 18.5% for multicrystalline silicon in commercial modules in 2016.<sup>20</sup> However, silicon-based solar cells have obvious drawbacks that reduce their competitiveness with fossil fuels, including high production costs, heavy weight, high energy payback time (EPBT) (of the order of 3 years). In order to reduce the production

costs and the EPBT, different thin film technologies are being developed intensively. Organic Photovoltaics (OPV) is seen as a promising alternative to conventional photovoltaic systems, due to the possibility of producing light weight and flexible modules at low cost. Also, the recently reported significant increase in power conversion efficiency (PCE) of OPV devices strengthen the potential for this technology to contribute to large-scale renewable energy production.

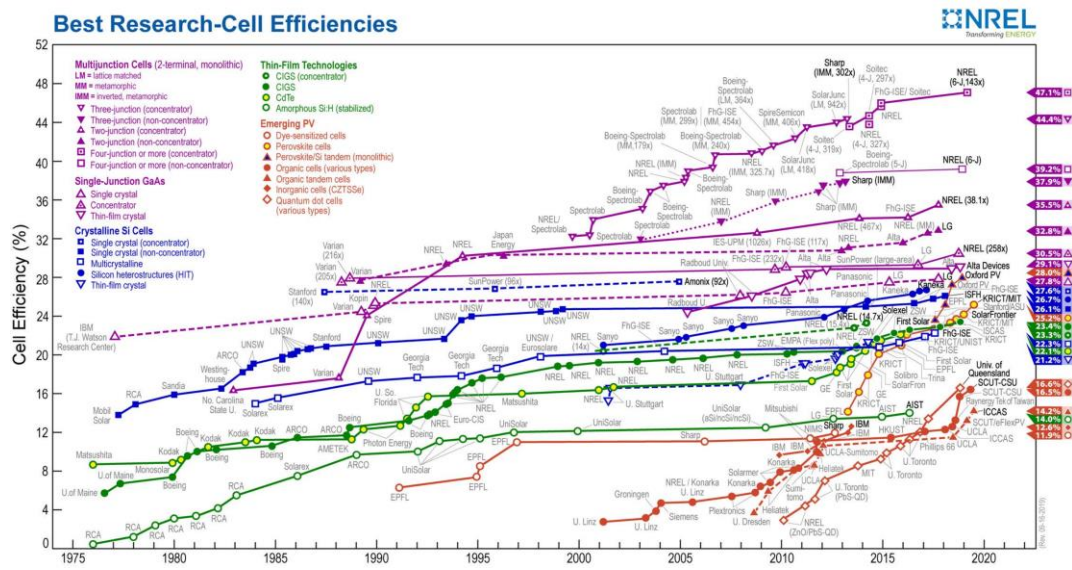


Figure 1.1 Evolution of record photovoltaic conversion efficiencies for different families of semiconductors and technologies.<sup>19</sup>

The history of organic electronics began with the discovery of conductive  $\pi$ -conjugated polymers by Shirakawa, MacDiarmid and Heeger in the late 1970s.<sup>21</sup> Traditionally, polymers are regarded as insulating materials; however, the presence of delocalized  $\pi$  electrons can attribute semi-conductive properties to polymers. In 1986, Tang et al. reported the first organic solar cell with a PCE of 0.95%.<sup>22</sup> In 1995, Yu et al. made an important breakthrough in PCE of OPVs by introducing the concept of donor-acceptor heterogeneous junction.<sup>23</sup> Until the early 2000s, the PCEs of solution-processed bulk heterogeneous junction solar cells remained around 3%.<sup>24,25</sup> However, despite low cost and simple manufacturing methods, these low efficiency values

remain a major impediment to the industrial development of organic technologies. As a result, many efforts have been made to improve their optoelectronic properties. To date, at the lab scale, a PCE of 18.22% has been reported for a single-junction OPV device based on a new electron donor copolymer “D18” and a new acceptor molecule “Y6”<sup>26</sup>. These achievements demonstrate the potential of OPVs in becoming a market reality. In addition, OPV devices can be processed from solutions, suggesting that it is easier to fabricate large-area, low-cost photovoltaic modules. Some innovative devices, such as flexible, transparent and lightweight solar cells (Figure 1.2) have already been reported<sup>27–30</sup>. At last, OPV modules have a much lower energy payback time (around 0.4 -1 year)<sup>31,32</sup> and an excellent power/weight ratio than silicon-based devices.

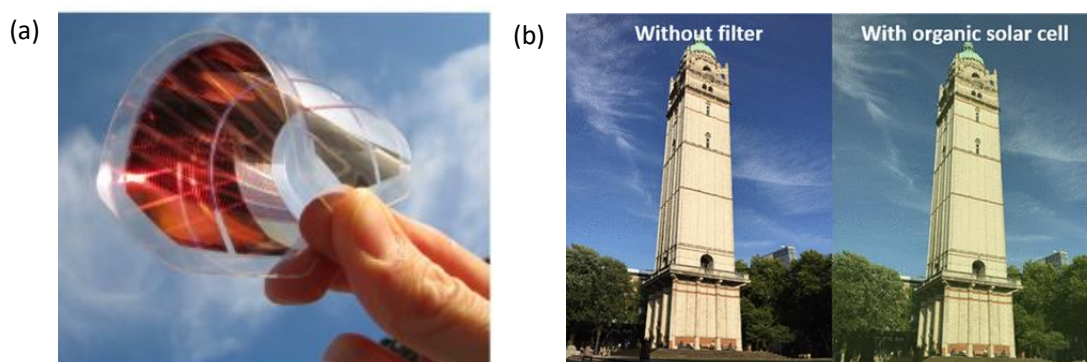


Figure 1.2 Photographs of (a) a flexible OPV (Source: Fraunhofer ISE), and (b) a transparent OPV<sup>31</sup>.

“Green” processing of OPV devices involves the use of non-toxic solvents, eco-friendly functional layers that are compatible with large-scale, low-cost fabrication methods. Essentially, green processing should suppress the emission of toxic substances into the environment while, simultaneously, leading to high-performance devices (in comparison with the performances of devices manufactured by conventional methods). Therefore, balancing low environmental impact with device performance is the key for successful green fabrication.

Over the past decades, great efforts were made to increase the PCE of organic solar cells up to 18% and to reach the threshold value required for industrialization

and commercialization.<sup>26-28</sup> However, when it comes to the industrial development of OPV modules, safe, eco-friendly and economical manufacturing is of paramount importance and will depend on the availability of non-toxic solvents for roll-to-roll production of organic modules. Historically, OPV devices were typically manufactured by standard solution printing techniques using laboratory equipment, and halogenated and/or aromatic solvents were chosen as processing solvents to meet thin film quality requirements.<sup>33,34</sup> However, since such solvents are harmful to human health of humans and to the environment, they impede sustainable development and are therefore not suitable for mass production and commercialization of OPV modules. It is thus urgent that environment-friendly or “green” solvents are found, which allow to reach power conversion efficiencies similar to those obtained from halogenated solutions.

Current research results on less/non-toxic processing solvents for OPV devices are rather limited. Up to now, the selection of alternative solvents was mostly the result of tedious experimental trial and error approaches, which may have left out suitable candidate solvents. Importantly, no solvent can be considered as a “universal” one for all organic semiconductors, because solubility depends both on the molecular structure of the solute and on the solvent. The search for new solvents is indeed a complex problem, requiring the simultaneous consideration of many properties, which may compete with each other in the sense that an increase in one property’s performance may reduce the performance in another. Hence finding a suitable solvent is often the compromise of a multi-objective problem. Properties such as solubility, viscosity, safety, durability, toxicity..., are altogether important for the final application and all have an impact on the performance of the device. In addition, as donor and acceptor materials are continually being modified to achieve OPV devices with still higher performance, the development of a more effective method for identifying non-toxic solvents that allow processing of these new materials is a critical issue. It should also be noted that the demand for non-toxic solvents is likewise important for other

organic devices processed from solution, such as OLEDs, OFETs, or photodiodes.<sup>35–37</sup> As sustainability is equally desirable, solvents based on agricultural resources, or so-called “biosolvents”, are initiating a growing interest as they usually exhibit low health and environmental impacts. However, regarding primary functions such as solubility, biosolvents are less versatile than most chlorinated or hydrocarbon solvents that need to be replaced. Therefore, new methodologies based on a reverse engineering approach have been developed to make the screening and selection of biosolvents less empirical.

In this thesis, we explore the effectiveness of reverse engineering based on a computer assisted molecular design (CAMD) tool to find alternative biosolvents for organic photovoltaic materials. The method is applied to blends of reference organic photovoltaic materials as well as to synthesized high-performance donor polymers. The reference materials were studied in order to understand the relationship between OPV performance and alternative solvent properties. The method is then applied to synthetic polymers to achieve high performance of “green-processed” OPVs in an efficient way.

**Chapter 2** details the basic principles of organic semiconductors and organic solar cells. Current understanding of the mechanisms of generation, transport and recombination of charge carriers is presented, as well as the state-of-the-art of the latest remarkable achievements in polymer photovoltaics. The main methods and detailed experimental steps used throughout the paper are described.

**Chapter 3** describes the relationship among processing solvents, morphology of the active layer and performance of OPV devices. The state-of-the-art methods of solvent selection applied in OPVs are shown.

**Chapter 4** reports the fundamentals of the IBSS<sup>®</sup>CAMD tool, including the basic principles and application steps.

**Chapter 5** focuses on the application of IBSS<sup>®</sup>CAMD to P3HT/PC<sub>71</sub>BM and

P3HT/EH-IDTBR based OPV devices. The alternative solvents identified and ranked by IBSS®CAMD are used to prepare the devices, and the photovoltaic performances are compared.

**Chapter 6** depicts the IBSS®CAMD application to two highly efficient donor polymers: PF2 and KNSF2. The UV-Vis absorption and solubility properties of both polymers are measured and analyzed. Then, related OPV devices prepared by alternative solvents are described.



# CHAPTER 2

---

---

## ORGANIC PHOTOVOLTAICS

---

---

## 2 Organic Photovoltaics

This chapter presents the current knowledge of the physical mechanisms of organic solar cell operation and the main parameters that determine the energy conversion efficiency. First, a brief introduction is provided to the physical properties of organic semiconductors. Then, the key physical steps that occur during the photon energy conversion are described in detail. After that, the main parameters of the solar cells are presented.

### 2.1 Organic Semiconducting Materials

Organic semiconductors are carbon-based materials, composed of organic molecules which include a  $\pi$ -conjugated system as molecular backbone. Within a  $\pi$ -conjugated carbon chain, the carbon atoms adopt a “ $sp^2$ ” configuration: three out of four valence electrons of each C atom occupy  $sp^2$  hybridized orbitals, with the fourth valence electron being in a  $p_z$  orbital. The  $sp^2$  electrons form strong  $\sigma$ -bonds with neighboring atoms and are responsible for most of the molecular binding energy, while the  $p_z$  electrons form weaker  $\pi$ -bond with neighboring C atoms. The bond-length between neighboring carbon atoms forming a conjugated  $\pi$ -electron system undergoes a slight periodic variation. The molecular backbone is therefore represented symbolically by an alternation of single and double bonds. Figure 2.1 illustrates a simple example of polyacetylene, which consists of repeating ethylene units. Within the conjugated  $\pi$ -electron system, the  $\pi$ -electrons are highly delocalized, allowing electrons to move freely along the conjugated carbon backbone. The spatial extension of electron delocalization is referred to as conjugation length.

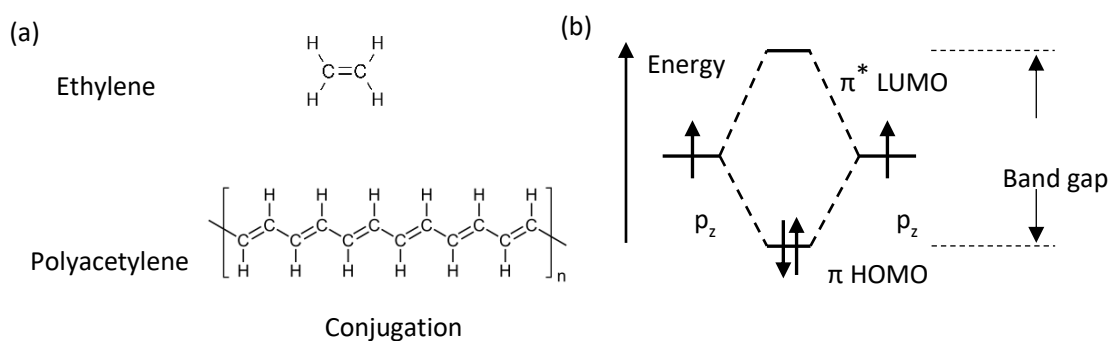


Figure 2.1 (a) Chemical structure of ethylene and polyacetylene, and (b)  $p_z$  orbital overlap to form  $\pi$  (bonding) and  $\pi^*$  (anti-bonding) band in C-C system.

The overlap of the  $p_z$  orbitals of neighboring C atoms results in the formation of bonding and antibonding orbitals. The bonding orbital is filled with electrons and is lower in energy. It contributes to the Highest Occupied Molecular Orbital (HOMO). The antibonding orbital is unoccupied and at higher energy and involved in the Lowest Unoccupied Molecular Orbital (LUMO). In organic semiconductors, the distribution of HOMO and LUMO levels are the analogs of respectively the valence and conduction bands of conventional inorganic semiconductors. The difference between the HOMO and LUMO levels is called energy bandgap. Organic materials are expected to behave as semiconductors when the energy bandgap is below  $\sim 3\text{eV}$ . In organic solar cells, the active layer is generally composed of two organic semiconductors. If the HOMO and LUMO levels of one semiconductor are higher than those of the second component (i.e., lower in absolute terms), this semiconductor behaves as an electron-donor. Accordingly, the semiconductor with the deeper lying HOMO and LUMO levels is referred to as an electron-acceptor material.

## 2.2 Working Principle of OPV

The overall working principle of OPV devices can be summarized in four steps as follows:

- (1) light absorption leading to exciton generation,
- (2) exciton diffusion and dissociation into free charge-carriers at the donor/acceptor heterojunction,
- (3) the free carriers are transported to their respective electrodes via the drift/diffusion mechanisms and,
- (4) collection of the free carriers at the electrodes.

### 2.2.1 Light absorption and exciton generation

In a conventional inorganic semiconductor, the Coulomb interaction of holes and electrons are efficiently reduced due to the large dielectric constant ( $\sim 10$ ). Correspondingly, the exciton binding energy is in the range of a few meV, and therefore excitons can be dissociated by thermal energy at room temperature. On the contrary, the dielectric constant of organic semiconductors is around 3, much smaller than that of inorganic semiconductors, and the electron and hole wavefunctions are generally delocalized over only a few molecular segments, causing a strong Coulomb interaction between electron-hole pairs. Hence, the consequently high exciton binding energy (100 ~ 1400 meV) prevents excitons from being dissociated into free charges directly by thermal energy at ambient temperature.<sup>38-41</sup> For example, P3HT (poly(3-hexylthiophene)), a common donor material for OPV devices, an exciton binding energy of 300~700 meV has been reported.<sup>42</sup> Since excitons have generally a lifetime of the order of nanoseconds<sup>43</sup>, most excitons recombine before being dissociated. A fast and effective method to avoid geminate recombination is therefore needed. An efficient way to solve this issue has been proposed in 1986 by Tang et al. They introduced the concept of donor-acceptor heterojunction, a bilayer composed of two different organic materials with properly aligned energy levels, which is used as light absorbing layer of a photovoltaic device.<sup>22</sup>

### 2.2.2 Exciton diffusion and dissociation at the D/A Interface

Excitons generated by photon absorption need to be dissociated to generate free charges. Because of the high exciton binding energy, an additional driving force is required to promote exciton dissociation. This driving force is provided by the energy offset between the frontier orbital energy levels of the donor and acceptor materials that compose the organic heterojunction. When the excitons are separated on a heterojunction, electrons will be transferred and dominate the acceptor material, which has deeper levels of HOMO and LUMO, while the holes remain on the donor material. In 2007, Derouiche and Djara have reported that energy differences in HOMO and LUMO levels of donor/acceptor organic materials could be proven to be responsible for the improvement of all photovoltaic properties of organic solar cells.<sup>44</sup> Figure 2.2 illustrates the exciton dissociation into free charges in the case the exciton is generated in the donor material.

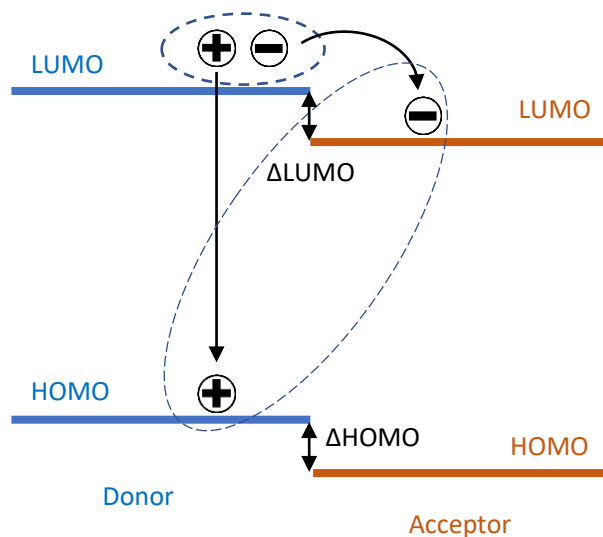


Figure 2.2 Band alignment of donor and acceptor materials for a heterojunction.

The energy difference in the LUMO levels of the donor/acceptor materials ( $\Delta\text{LUMO}$ ) will drive the exciton dissociation, which has to be greater than the binding energy of the excitons.<sup>45</sup> For many donor/acceptor systems using a fullerene

derivative as electron acceptor a  $\Delta\text{LUMO}$  greater than 0.3 eV has been found to be sufficient.<sup>46,47</sup> Koen Vandewal has reported that a  $\Delta\text{LUMO}$  as low as 0.1 eV is sufficient to achieve exciton dissociation in the active layer.<sup>48</sup> After exciton generation, the excitons need to reach the donor/acceptor interface by diffusion to be dissociated. If  $\Delta\text{LUMO}$  is large enough, a charge transfer from the donor to the acceptor occurs, giving rise to a charge transfer (CT) state. The CT process occurs at a very short timescale (around 45~100 fs),<sup>49,50</sup> which is roughly 10 000 times smaller than the exciton lifetime (around 1ns). After CT, the electron-hole pairs, although still influenced by coulomb interactions, are able to dissociate into a charge separated (CS) state corresponding to a free electron in the acceptor domain and a free hole in the donor domain. The CT is hence an intermediate state between the Coulomb bounded exciton and free charges. It is currently believed that the delocalized nature of holes and electrons on their respective materials could weaken the coulomb interactions enough to allow the formation of the CS state.<sup>51</sup> In some cases, the presence of an electric field may also contribute to the CS formation. The average distance covered by excitons before recombination (in the absence of a D/A interface) corresponds to the exciton diffusion length ( $L_{\text{ex}}$ ), which is generally of the order of a few nanometers. Excitons generated at a distance from the heterojunction longer than  $L_{\text{ex}}$  will recombine before reaching the heterojunction, reducing the energy conversion efficiency. Therefore, the concept of D/A bulk heterojunction, consisting of a mixture of donor and acceptor domains, has been introduced (Figure 2.3).

### 2.2.3 Charge carrier transport

Once excitons are dissociated into free charge-carriers, the latter have to travel towards their respective electrodes for collection within their lifetimes. The main driving forces for the transport of free charge-carriers are drift and diffusion currents. The charge-carriers may drift along the build-in electric field lines, with the electric field being generated by dissymmetric electrodes. In a planar heterojunction, the

recombination probability of free carrier is very low because they are spatially separated. On the other hand, in a bulk heterojunction, electrons and holes are more likely to meet at the D/A interface and recombine before charge extraction may occur.

The mobilities of free charges in the active layer is a major limitation for charge collection.<sup>49</sup> Balanced hole and electron mobilities are required to avoid accumulation of electrons or holes in the active layer and the formation of space charge that may impact the internal electric field. If for instance the electron mobility in organic semiconductors is higher than hole mobility, the electrons are transported more efficiently to the electrode. That is, the rate of electrons reaching the cathode is higher than that of holes to the anode, resulting in that the electrons tend to gather near the cathode interface, generating space charge in the active layer. This effect modifies the electric field distribution in the active layer and limit the current output of a solar cell. As a consequence, organic semiconductors with high and similar hole and electron mobilities are being developed to overcome this weakness.<sup>52-56</sup>

#### **2.2.4 Charge-carrier extraction at electrodes**

Free charge-carriers can be collected by electrodes when they reach the active layer/electrode interface. The potential barrier for the given charge carrier type (electrons at the anode or holes at the cathode) at the interface needs to be minimized to avoid charge accumulation and recombination, and achieve efficient charge-carrier extraction. Moreover, carrier accumulation causes the misalignment of active layer/electrode energy level, and strongly influences the  $V_{oc}$  (open-circuit voltage) and fill factor (FF) of the solar cells.<sup>57</sup> The ideal situation corresponds to the work function of the anode matching well the donor HOMO level, and the work function of the cathode matching the acceptor LUMO level. In this case, the contacts are ohmic and  $V_{oc}$  correlates with the difference between the donor HOMO and acceptor LUMO. In addition, charge collection at the wrong electrodes, i.e., electrons at the anode or holes at the cathode, can be another factor that reduces device performance.

Therefore, electrical and hole transport layer (ETL and HTL) are often implemented between the active layer and the electrode. For example, the low valence band and large band gap of ZnO ( $E_v \sim 4.4$  eV,  $E_g \sim 7.8$  eV) prevent holes from reaching the cathode while allowing efficient electron extraction.<sup>58,59</sup>

### 2.3 Functionality of the active Layer

As discussed in Section 2.2, excitons diffuse towards the D/A interface before their dissociation (Figure 2.3 b). Ideally, the phase separation between donor and acceptor materials in bulk heterojunctions should lead to domain sizes of the order of the exciton diffusion length, thereby minimizing exciton recombination and allowing excitons to be dissociated into a charge transfer state at the D/A interface (Figure 2.3 b). Phase separation between both materials is therefore critical to the electronic processes underlying the operation of the device. Importantly, the intermolecular interactions between both organic components and the means of manufacturing the OPV devices can influence the thin film morphology considerably.

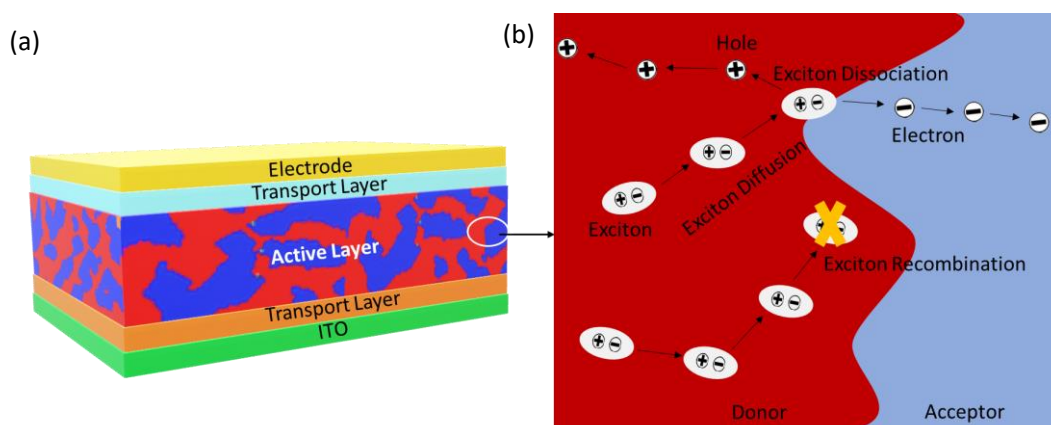


Figure 2.3 (a) The structure of OPV and (b) key steps involved in active layer (Red area: donor domains, Blue area: acceptor domains, Mixture: bulk heterojunction).



In general, phase separation of the active layer can be manipulated by designing the molecular structure and optimizing the device processing, e.g., by using different solvents, additives, co-solvents, thermal annealing or solvent vapor annealing. Selecting an appropriate solvent is a simple and common way to optimize the active layer morphology and to achieve high performance devices.<sup>34,51,60</sup> On the other hand, phase separation can be addressed, to some extent, by molecular engineering of the D and A molecules. For instance, fluorine substitution (see Chapter 6), which has been introduced to adjust frontier orbital energy levels and to improve charge carrier transport, also influences the phase separation and molecular assembly by enhancing intermolecular interactions. In general, controlling and optimizing the morphology of the active layer is necessary to achieve high photovoltaic performances.

## 2.4 Device Structures and working principle

Figure 2.4 illustrates two different OPV structures that are known as “standard” and “inverted”, respectively. For the “standard” structure, holes are extracted at the transparent bottom electrode and electrons at the top metal electrode. On the contrast, in the “inverted” structure, electrons are collected at the transparent bottom electrode and holes at the top metal electrode. In the “standard” structure, a low work function (WF) metal electrode like aluminum (Al), calcium/aluminum (Ca/Al) etc. is generally used. However, these low work function metals are easily oxidized in air causing poor device stability. Moreover, poly(3,4-ethylenedioxythiophene)-poly(styrenesulfonate) (PEDOT:PSS) is a widely used hole transporting layer (HTL) to modify the work function and improve the surface uniformity of indium-tin-oxide (ITO) transparent electrode. But on the long term, the acidity of PEDOT:PSS was shown to lead to a degradation of the electronic properties of ITO in “standard” solar cells. In the “inverted” structure”, a high work function metal (for hole extraction) that is more resistant to the oxidation in air, such as silver (Ag) or gold (Au) is utilized as a back contact. The bottom transparent electrode (ITO) is modified by electron transporting

layers (ETL) such as zinc oxides (ZnOx)<sup>61–64</sup> or titanium oxides (TiOx)<sup>65–68</sup>. Taking this into account, “inverted” device structures are accepted to be more stable than “standard” ones and they were shown to perform better.<sup>69–72</sup> More details on device architecture differences can be found in Ref 73. The inverted device structure was used throughout this work.

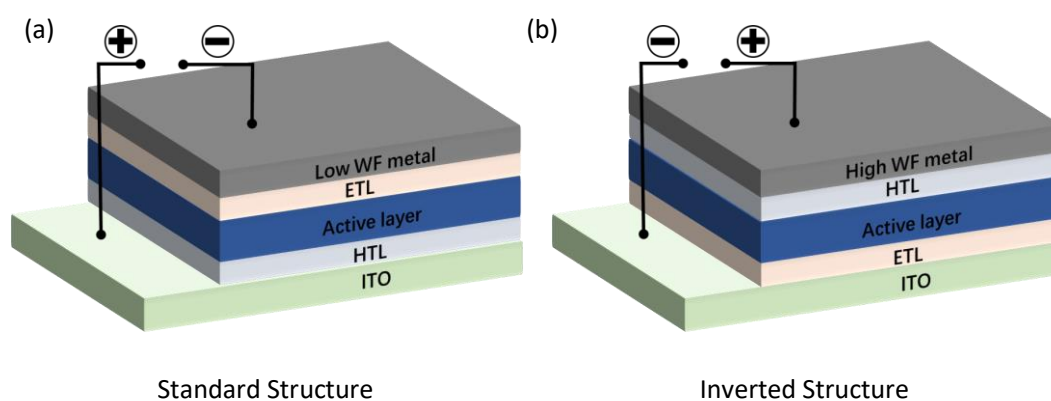


Figure 2.4 Schematic view of standard (a) and inverted (b) OPV devices.

## 2.4 Current – Voltage Characteristics

The main parameter that describes the performance of a solar cell is its power conversion efficiency ( $\eta$  or PCE), defined by:

$$\eta(\%) = \frac{P_{\max}}{P_{\text{in}}} \times 100\% \quad (1)$$

where  $P_{\max}$  is the highest electrical power per unit area delivered by the solar cell, and  $P_{\text{in}}$  the incident light intensity.

The values of  $\eta$  is generally measured by exposing the solar cell to a  $1000\text{W m}^{-2}$  light source characterized by a AM 1.5 solar spectrum. The current density  $J$  as a function of an applied DC voltage ( $V$ ) is recorded subsequently under darkness and under illumination. Figure 2.5 reports the illustrative dark and illuminated J-V curves. The maximum power point (MPP) represents the device operational point at which

the product of  $J \times V$  is maximum and corresponds to the highest power delivered by the solar cell under AM1.5 illumination conditions.

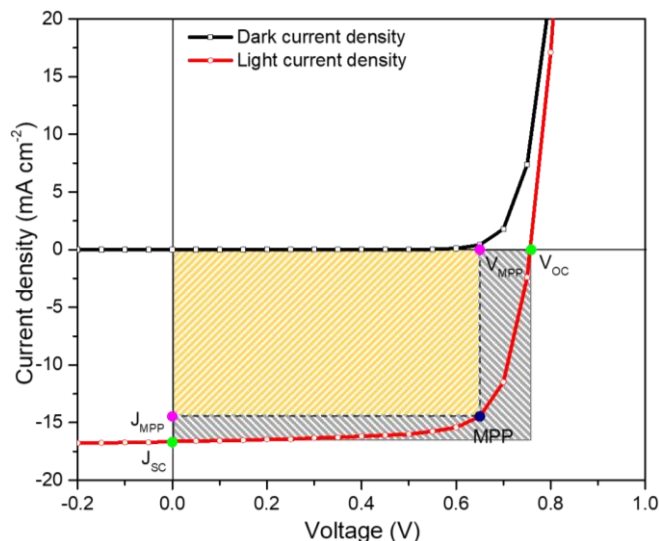


Figure 2.5 J-V characteristics of OPVs. The black and symbolic red lines represent dark and light curves, respectively. The navy point indicates the maximum power point (MPP) of a solar cell ( $V_{MPP}$ ). Green points show the open circuit voltage  $V_{OC}$  and the short circuit current density  $J_{SC}$  of the solar cell. The fill factor (FF) is determined by the area ratio of the yellow rectangle to the gray dashed rectangle.

### 2.4.1 Short Circuit Current Density ( $J_{SC}$ )

As shown in Figure 2.5, the short circuit current density ( $J_{SC}$ ) is obtained from the solar cell under short circuit conditions ( $V = 0$  V).  $J_{SC}$  represents the number of charge-carriers that are collected under illumination when the built-in electric field is at its maximum.  $J_{SC}$  is generally proportional to the number of absorbed photons in the active layer. It is often considered that enhanced optical/electrical parameters such as a high photon absorption coefficient and high carrier mobilities improve  $J_{SC}$ . Besides, phase separation plays a significant role in charge carrier generation. For domain sizes of the order of the exciton diffusion length (typically less than 10 nm), most photons are absorbed at a sufficiently short distance from the donor/acceptor interface to allow excitons to reach the donor/acceptor interface and to be dissociated into free

charge carriers before recombination.<sup>74–76</sup> During the free charge carrier extraction process, the free charges have to cross the active layer to reach the respective electrodes. Hence, interconnected donor and acceptor pathways must be present within the active layer.<sup>1,77</sup> Moreover, the domain purity should be as high as possible to avoid charge carrier trapping or recombination at bulk defect sites.<sup>78,79</sup>

### 2.4.2 Open Circuit Voltage ( $V_{oc}$ )

The open-circuit voltage ( $V_{oc}$ ) represents the maximum voltage that a solar cell can provide to an external circuit. Under open circuit conditions and steady state illumination, free charge carriers will accumulate at their respective electrodes, generating a potential difference which cancels out the built-in potential. Under this condition, charge carrier generation and recombination exactly compensate, therefore, no net current is flowing. If the contacts are ohmic,  $V_{oc}$  is dependent on the separation between the electron ( $E_{Fn}$ ) and hole ( $E_{Fp}$ ) quasi-Fermi energy levels:

$$V_{oc} = \frac{E_{Fn} - E_{Fp}}{q} \quad (2)$$

Due to the energetic disorder of organic semiconductors, the energy level distributions of the HOMO and LUMO bands of an organic semiconductor are approximately gaussian shaped, causing the quasi-Fermi levels to be pinned to the tail energy states. These tail states lead to a downshift of the electron and an upshift of the hole quasi-Fermi levels and thereby reduce the  $V_{oc}$ . In general, the factors that play a crucial importance in determining the  $V_{oc}$  are therefore energetic disorder, CT states distribution, carrier density and the quality of the semiconductor/electrode interfaces. A more detailed information about the origin of  $V_{oc}$  can be found in the Refs 80,81.

### 2.4.3 Fill Factor (FF)

The FF can be considered as a measure of how efficiently photo-generated charge

carriers can be extracted under the maximum power point operating conditions. It is defined as the ratio of the maximum power delivered by the device over the product of the open circuit voltage and short circuit current:

$$FF = \frac{J_{MPP} \times V_{MPP}}{J_{SC} \times V_{OC}} \quad (3)$$

where  $J_{MPP}$  and  $V_{MPP}$  correspond to the maximum power (MPP) point of the cell (Figure 2.5).

FF reflects the competition between recombination and extraction rates of free charges and is influenced, among others, by the series resistance ( $R_S$ ) and shunt resistance ( $R_{SH}$ ) of the OPV device.  $R_S$  depends on the conductivity of the electrodes (especially ITO), the active layer and the interfacial layers.  $R_{SH}$  may be caused by different types of leakage currents, e.g. imperfect active layer quality, aggregates etc.<sup>23</sup> Finally, the power conversion efficiency of the solar cell can be written as:

$$\eta(\%) = \frac{V_{OC} \times J_{SC} \times FF}{P_{in}} \times 100\% \quad (4)$$

## 2.5 Fabrication of OPVs

An inverted structure is used throughout this thesis due to its advantages mentioned above. Firstly, a brief description of the materials and substrates used is given. Next the elaboration procedures of “inverted” photovoltaic device structures and the device characterization methods are presented.

### 2.5.1 Materials and Substrates

P3HT, PC<sub>71</sub>BM and EH-IDTBR were purchased from Solaris Chem Inc., Solenne BV and 1-Material Inc, respectively. A ZnO nanoparticle dispersion (N-10) was purchased from Avantama. The properties of standard processing solvents and additives used for the active layer deposition and purchased at Sigma Aldrich are shown in Table 2.1. The

solvents were used as received. Pre-structured ITO-coated glass substrates, whose dimensions were 20 x 20 x 1 mm (L x W x H), were purchased from Luminescence Technology (LumTech) Corporation. The sheet resistance of substrates was around 10  $\Omega$ /sq.

Table 2.1 The list of processing solvents and additives used in this thesis.

Solvents	Purity
1,2-Dichlorobenzene	$\geq 99\%$
p-Xylene	$\geq 99\%$
Anisole	99.7%
Terpinolene	$\geq 85\%$ (GC)
2-Methylanisole	99%
p-Cymene	99%
Diphenyl Ether (additive)	99%

### 2.5.2 Experimental details

First, ITO-coated glass substrates were systematically cleaned in ultrasonic bath of deionized water, acetone and 2-propanol at 45°C for 15 minutes for each step. They were then dried under nitrogen flow and treated in a UV/Ozone oven to remove residual organic contaminants.

Before depositing the active layer, a 7-10 nm thin layer of ZnO nanoparticles was deposited by spin-coating, using the following steps:

- a) filtering the ZnO suspension by nylon filter with pore diameter of 0.45  $\mu\text{m}$ ;
- b) spin-coating at 5000 rpm, with acceleration of 1000 rpm/s, during 60 sec;
- c) cleaning the ZnO with ethanol from part of the substrate (Figure 2.6);

- d) annealing of ZnO layer at 110°C for 12 minutes in air to remove the residual solvent.

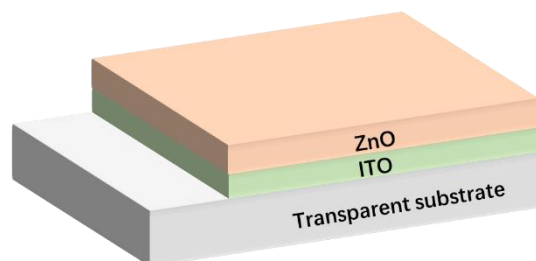


Figure 2.6 Diagram of the interfacial layer on the ITO after cleaning from one side.

Then, the active layer was spin-coated under nitrogen ambient (glove box). The organic semiconductors were weighted with the desired proportion in vials. Solvents were introduced to the vials to solubilize the organic semiconductors. These vials were put on a hotplate and stirred overnight at 60°C. For each polymer used in this thesis, the spin-coating conditions of the active layer were optimized to obtain homogeneous films. The corresponding thin film deposition parameters will be presented in the related chapters. For the inverted photovoltaic structure, thin layers of MoO<sub>3</sub> (~7 nm) and silver (120 nm) were thermally evaporated sequentially under vacuum (Pressure  $\approx 1 \times 10^{-6}$  mbar) and used as top electrodes. The OPV sample and shadow mask used for JV measurements are shown in Figure 2.7 a and b, respectively. There are four cells on a sample, each with an active layer area of 12 mm<sup>2</sup> (Figure 2.7 b), as defined by the shadow masks of all the solar cell devices discussed in this thesis.

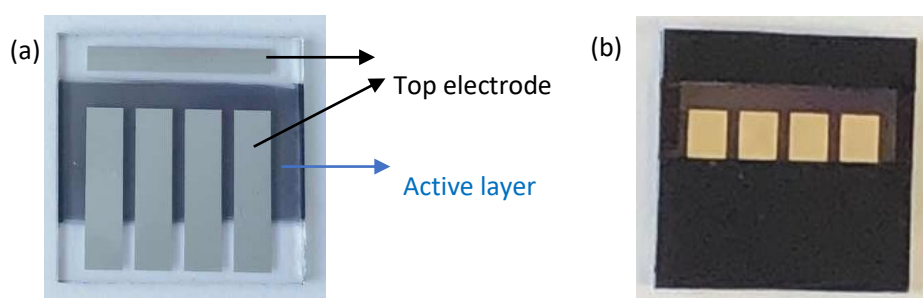


Figure 2.7 (a) The OPV sample and (b) shadow mask used for JV characteristics.

## 2.6 Characterization of OPV devices

### 2.6.1 JV characteristics

The JV curves of OPV devices were measured under a BET Technologies Sun 3000 AM 1.5G-100 mW/cm<sup>2</sup> solar simulator, using a LabView-controlled Keithley 2400 SMU device parameter analyzer. JV characterizations were carried out at room temperature in a glove box filled with N<sub>2</sub>. All the photovoltaic parameters ( $V_{OC}$ ,  $J_{SC}$ , FF and PCE) were extracted using a LabView program. The JV measurements shown in this thesis (chapter 5 and 6) are averaged over 24 cells (6 samples).

### 2.6.2 Thickness measurement

The thickness of the active layer was measured by a DektakXT stylus profiler. In our study, the average thickness was obtained from 6 measurement points on two samples.

### 2.6.3 Ultraviolet-visible spectroscopy

The absorption a material either in solution or in thin films can be measured by ultraviolet-visible (UV/Vis) spectroscopy by a UV/Vis spectrophotometer. In this thesis, all the absorption profiles of pure polymers in solid state were characterized using a Shimadzu 082395 spectrophotometer at ICPEES with the assistance of Dr. Nicolas Leclerc. In-situ temperature dependent UV/Vis measurements in solutions were carried out with the help of Dr. Laure Biniek at ICS on the Agilent Cary 60 UV-VIS spectrophotometer.



# CHAPTER 3

---

---

STRATEGIES FOR CONTROLLING THE  
ACTIVE LAYER MORPHOLOGY AND  
METHODS FOR SOLVENTS SELECTION

---

---

## **3 Strategies for Controlling the Active Layer Morphology and Methods for Solvents Selection**

### **3.1 Active Layer Morphology**

A key property that controls the solar cell performances is the morphology of the photoactive layer, which consists of intimately mixed electron donor and electron acceptor domains. Large donor and acceptor domains provide a percolating pathway for efficient charge transport and collection, but lead to a loss of interfacial area, low exciton dissociation rates and thus low free charge generation rates.<sup>82</sup> On the other hand, strong intermixing results in a large donor/acceptor interface, but hinder charge transport and increase the charge recombination rate. Consequently, the morphology of the active layer composed of a given donor/acceptor blend needs generally to be optimized in order to provide simultaneously a high exciton dissociation rate, minimum charge recombination and efficient charge transport and extraction. For solution-processed OPV devices, processing solvents and additives play a crucial role in this optimization process.

### **3.2 Role of Processing Solvents**

For solution-processed devices, the BHJ morphology is strongly dependent on the thermodynamic properties and drying kinetics of the solution used to elaborate the organic layers.<sup>83,84</sup> The thermodynamic properties of the system are related to various physicochemical properties of the donor and acceptor materials and the processing solvents, such as intermolecular interactions, miscibility, and solid state phases (crystallization).<sup>85</sup> The film-drying kinetics are related mostly to the properties of solvents such as boiling point and vapor pressure.<sup>86</sup> Currently, the choice of a processing solvent for OPV devices is mainly determined by its capacity to solubilize the organic semiconductors and its boiling point.

### 3.2.1 Solubility

The solubility properties of the donor and acceptor materials in a processing solvent affect the aggregation and the phase separation in the thin film. The work of Duc T. Duong et al. highlights the relationship between the quality of solvents and the morphology of a BHJ (MDMO-PPV: PC<sub>61</sub>BM system).<sup>87</sup> Figure 3.1 depicts the AFM topography images of MDMO-PPV: PC<sub>61</sub>BM system, showing that the size of phased-separated PC<sub>61</sub>BM domains is dependent on the maximum solubility of PC<sub>61</sub>BM in the solvent. Large sized aggregates of PC<sub>61</sub>BM can be found in the active layer when using a poor solubility solvent for PC<sub>61</sub>BM (such as toluene) to prepare the film. While the PC<sub>61</sub>BM is dispersed homogeneously and no over-sized aggregates are formed in the BHJ film when it is processed from a good solvent. The solubilities of PC<sub>61</sub>BM for some common solvents such as chloroform (CF), chlorobenzene (CB), ortho-dichlorobenzene (*o*-DCB) are summarized in Table 3.1.

Table 3.1 Solubility of PC<sub>61</sub>BM in various solvents.

Solvents	Solubility limited (mg/mL)	References
<i>o</i> -DCB	42~107	87–89
CF	24~27	60,87,90,91
CB	25~59.5	60,87,90,91
Toluene	9~15.6	60,87,90,91
Carbon disulfide (CS <sub>2</sub> )	~207	87
Trichloroethylene	~41.8	87
Mesitylene	29~48.1	60,88

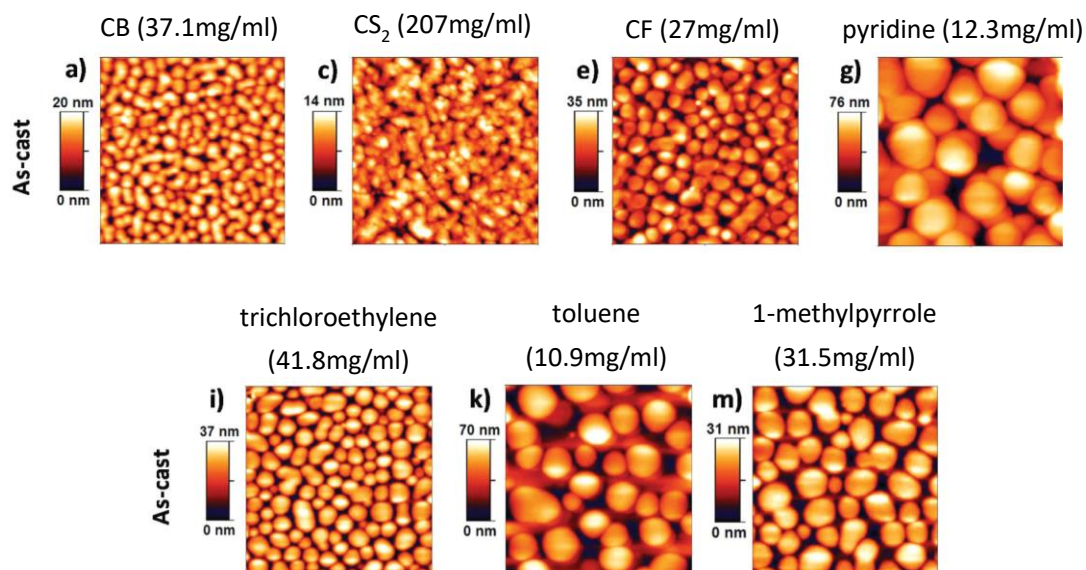


Figure 3.1 AFM topography images ( $2 \mu\text{m} \diamond 2 \mu\text{m}$ ) of as-cast of MDMO-PPV:PC<sub>61</sub>BM spin-casted from (a) CB, (c) CS<sub>2</sub>, (e) CF, (g) pyridine, (i) trichloroethylene, (k) toluene, and (m) 1-methylpyrrole. [From REF.<sup>87</sup>] (The solubilities of PC<sub>61</sub>BM in various solvents are shown at the top of the corresponding AFM images.)

Similarly, the study of Camilla Lindqvist et al. on a blend film with different ratios of quinoxaline-based co-polymer (TQ1) and a fullerene acceptor PC<sub>71</sub>BM illustrates the relationship between solubility limits of PC<sub>71</sub>BM and the morphology of a BHJ.<sup>92</sup> The AFM images (Figure 3.2) show that phase-separated, PC<sub>71</sub>BM-rich domains become larger when the films are processed from a solvent with a poorer solubility for PC<sub>71</sub>BM. In the series of decreasing PC<sub>71</sub>BM solubility, i.e., CF (34 mg/mL), CB (56 mg/mL), and *o*-DCB (66 mg/mL), this phenomenon is more pronounced for the 1:3 donor:acceptor blend ratio than for the 1:1 ratio. Thus, the PC<sub>71</sub>BM solubility significantly affects the aggregation of fullerene derivatives in polymer:fullerene blends.

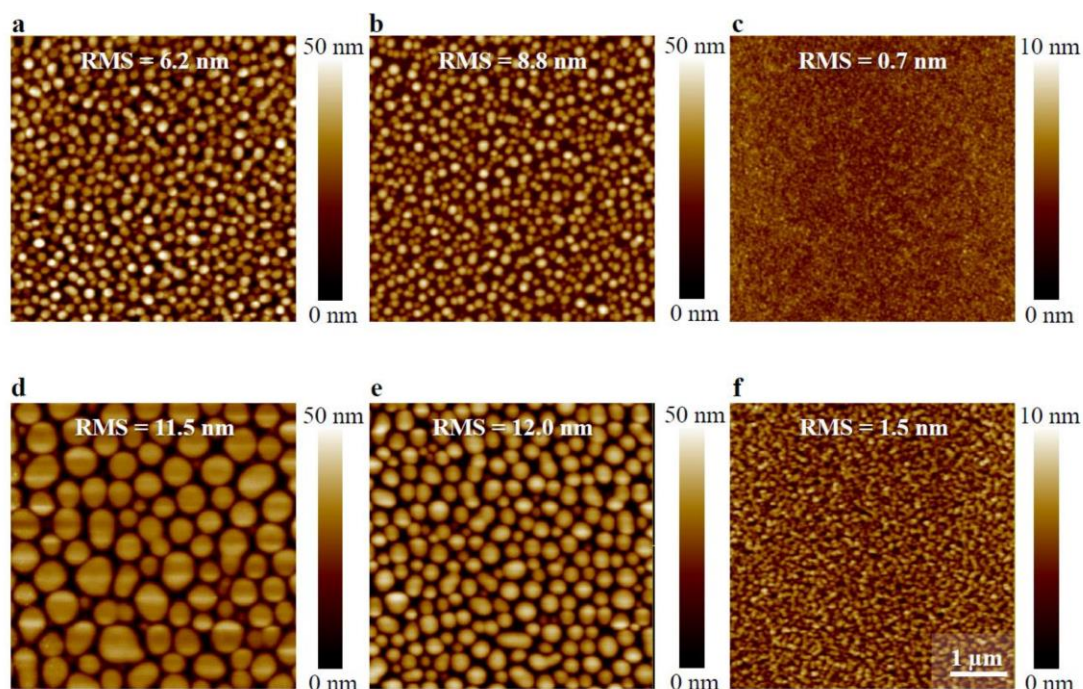


Figure 3.2 Atomic force microscopy (AFM) micrographs ( $5 \times 5 \mu\text{m}$ ) of thin films of 1:1 TQ1:PC<sub>71</sub>BM (a–c) and 1:3 PC<sub>71</sub>BM (d–f) spin-coated from CF (a,d), CB (b,e), o-DCB (c,f). Scale bar indicates  $1 \mu\text{m}$ .

Surface roughness (RMS), as well as the corresponding height scale, is added to each image.<sup>92</sup>

Likewise, the donor domains are influenced by the donor solubility limit in the processing solvent. A study by Jie Guo et al.<sup>93</sup> on two new small molecules: BDT-2T-DCV-Me and BDT-2T-CNAB illustrates the dependency between the solubility of donor molecules and the morphology of the active layer. These two small molecules were modified by end groups, dicyanovinyl (DCVMe) and n-butyl cyanoester (CNAB), to increase the charge transport rate. Table 3.2 displays the solubilities of both molecules in CF and the power conversion efficiency of related OPV devices. The AFM images (Figure 3.3) reveal a more homogeneous interpenetrating donor/acceptor network for BDT-2T-DCV-Me:IDIC blend films than for BDT-2T-CNAB:IDIC blend films. The BDT-2T-CNAB:IDIC films do have indeed a rougher surface than BDT-2T-DCV-Me:IDIC films, with RMS values of 0.843 nm and 2.927 nm respectively<sup>87</sup>. Note that the solubility of BDT-2T-CNAB (7.9 mg/mL) in CF is higher than that of BDT-2T-DCV-Me (1.7 mg/mL). The results reported by Jie Guo are thus in contrast with those reported on fullerene

acceptors by Ca. Lindqvist, where a higher solubility led to smaller domains. This discrepancy points out the complexity of the processes underlying the morphology of BHJ films, which is influenced by a range of properties other than solubility, and illustrates the difficulty to anticipate the optimum processing conditions.

Table 3.2 Solubilities of BDT-2T-DCV-Me and BDT-2TCNAB in CF, and PCEs of the OPVs devices based on BDT-2T-DCV-Me: IDIC films and BDT-2T-CNAB: IDIC films under the illumination of AM 1.5G, 100 mW  $cm^{-2}$ .<sup>87</sup>

Materials	solvents	Solubility (mg/mL)	PCE (%)
BDT-2T-DCV-Me	CF	1.7	1.56
BDT-2T-CNAB	CF	7.9	6.17

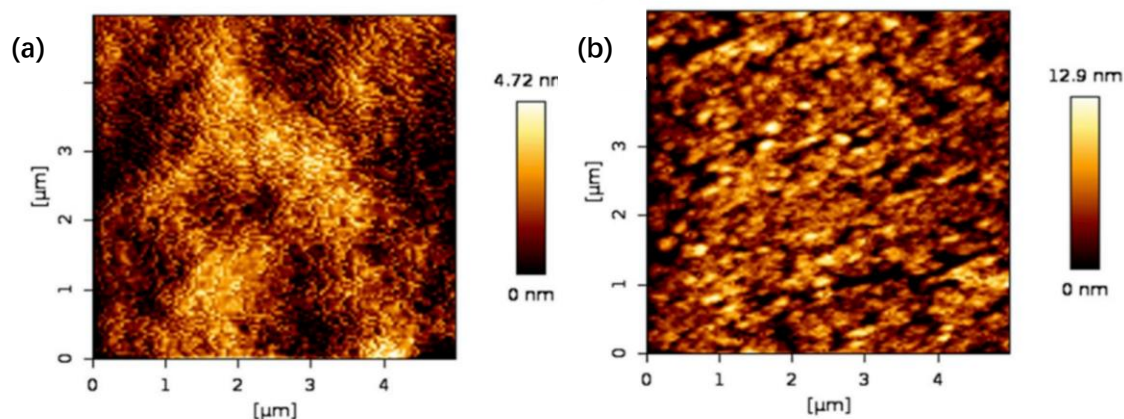


Figure 3.3 The AFM images (size:  $5 \times 5 \mu m$ ) of (a) BDT-2T-DCV-Me: IDIC and (b) BDT-2T-CNAB: IDIC blend films processed from CF.<sup>87</sup>

### 3.2.2 Boiling Point of Processing Solvents

The organization of donor and acceptor domains are in particular impacted by the drying kinetics. The solvent evaporation and crystallization of the organic materials

occur simultaneously. Evaporation rates will be higher than the crystallization rate if highly volatile solvents are used, restraining the crystallization of donor and acceptor materials into large domains. The relationship between drying kinetics and aggregation has been widely reported. Taking poly[(9,9-dioctylfluorenyl-2,7-diyl)-alt-co-(N,N'-diphenyl-N,N'-di(p-butylphenyl)-1,4-diaminobenzene)] (PFB):PCB<sub>61</sub>M system as an example, S. Nilsson et al. reported different morphologies of BHJ films which were obtained under different solvent evaporation rates.<sup>60</sup> Figure 3.4 displays the morphologies of PFB/PC<sub>61</sub>BM films when spin-coated from o-xylene (boiling point=138 °C) under “no vapor” conditions, i.e. without using extra solvent vapor, as well as “high vapor” conditions, i.e. using solvent vapor to reduce the evaporation rate. A more homogenous BHJ film was observed under high vapor conditions, when the rate of solvent evaporation is lower. Similar changes in the morphology of BHJ films occurred when using different processing solvents with different boiling points. Comparing Figure 3.4 a and d, the films spin-coated from mesitylene (boiling point=166 °C) are flatter and more homogenous than those spin-coated from either toluene or o-xylene with boiling points of 110°C and 138°C respectively.

A similar behavior was also observed in other blends such as P3HT:PC<sub>61</sub>BM. For example, Yu prepared P3HT:PC<sub>61</sub>BM OPV devices by using 4 processing solvents (CF, CB, o-DCB, and 1,2,4-trichlorobenzene).<sup>94</sup> It was observed that P3HT crystallinity is improved when the processing solvent boiling point is increased. This result was ascribed to the fact that a high boiling point solvent provides a low drying speed, offering more time for self-assembly of polymer chains during solvent evaporation. Thus, P3HT can adopt a low energy state (higher crystallinity) when the films are prepared from a high boiling point solvent. The OPVs achieved a PCE of 3.69% when using 1,2,4-trichlorobenzene compared to 0.94% for CF processed devices.

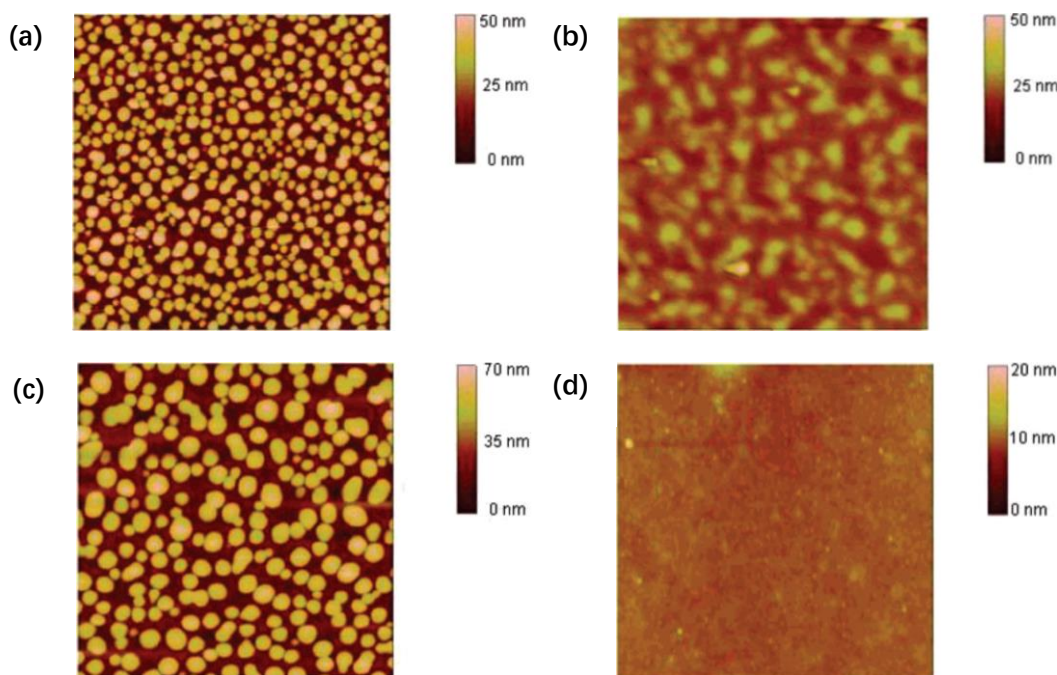


Figure 3.4 AFM height images of spin-casted PFB/PCBM blends from xylene under (a) “no vapor” conditions, (b) “high vapor” conditions, (c) from toluene under “no vapor” conditions and (d) from mesitylene under “no vapor” conditions.<sup>60</sup>

However, the solvents with high boiling points are difficult to remove and can lead to solvent residues after the devices processing. Zhang et al. has reported the study about the relationship between the solvent residues and the performance of devices, indicating that 1,8-diiodooctane (DIO), a solvent additive with a high boiling point (363.3 °C), is difficult to completely remove from the blend films, and results in an unstable state of the acceptor phase even though the films appear dry.<sup>95</sup> DIO residuals allow the acceptor domains to grow further in size, leading to excessively large domain sizes.

### 3.2.3 Solvent mixtures

Films cast from single solvents often have nonideal morphologies with either insufficient or excessive phase separation between the donor and acceptor materials, and/or disordered domains, resulting in poor device performances. The utilization of



cosolvents or additives provide a simple and fast way to optimize the morphology of the active layer.

*-Use of additives.* This method requires that a processing solvent is introduced in very small proportions (commonly a few volume ~%) into the host solvent. Generally, the additives should have a high boiling point and provide a good solubility for both the donor and the acceptor. Under these conditions, additives can optimize the active layer morphology of various of donor and acceptor BHJs. They may for instance, promote the polymer crystallization after evaporation of the main solvent (the polymer chains have more time to self-organize themselves), and increase the purity of the domains, thereby improving the performance of OPV devices. Common additives include 1,8-diiodooctane (DIO)<sup>76,96–101</sup>, 1,8-octanedithiol (OT)<sup>102–105</sup>, 1-chloronaphthalene (CN)<sup>106,107</sup>, nitrobenzene (NB)<sup>108</sup>, N-methyl-2-pyrrolidone (NMP)<sup>109</sup>, 1-Methylnaphthalene (1-MN)<sup>110</sup>, and diphenyl ether (DPE)<sup>37,96,98,111,112</sup>. Figure 3.5 depicts the chemical structures of some of the processing additives found in the literature.

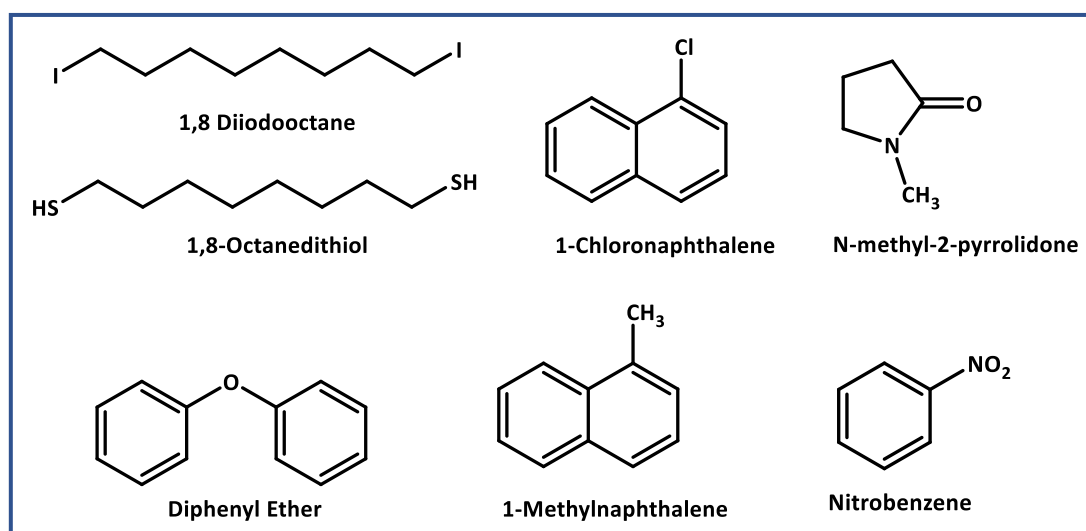


Figure 3.5 Examples of processing additives for BHJ morphological control.

A large number of studies indicate that these additives can dramatically enhance

the device performance by improving the charge generation and transport, as well as decreasing the charge recombination. The DIO is a favorable additive for fullerene derivatives. Large PC<sub>71</sub>BM domains were generated when PTB7:PC<sub>71</sub>BM BHJ films were processed from pure *o*-DCB, leading to less donor/acceptor interfacial area and weak exciton dissociation rates.<sup>100</sup> The large PC<sub>71</sub>BM domains were found to decrease in number and even disappear with the introduction of DIO (Figure 3.6). The power conversion efficiency was increased from 3.82% to 8.20% by adding 3% DIO. Note that the very high boiling point (363.3°C) of DIO, when used in a larger proportion, slows down the drying kinetics too much and yields large PC<sub>71</sub>BM domains that are detrimental to the device.

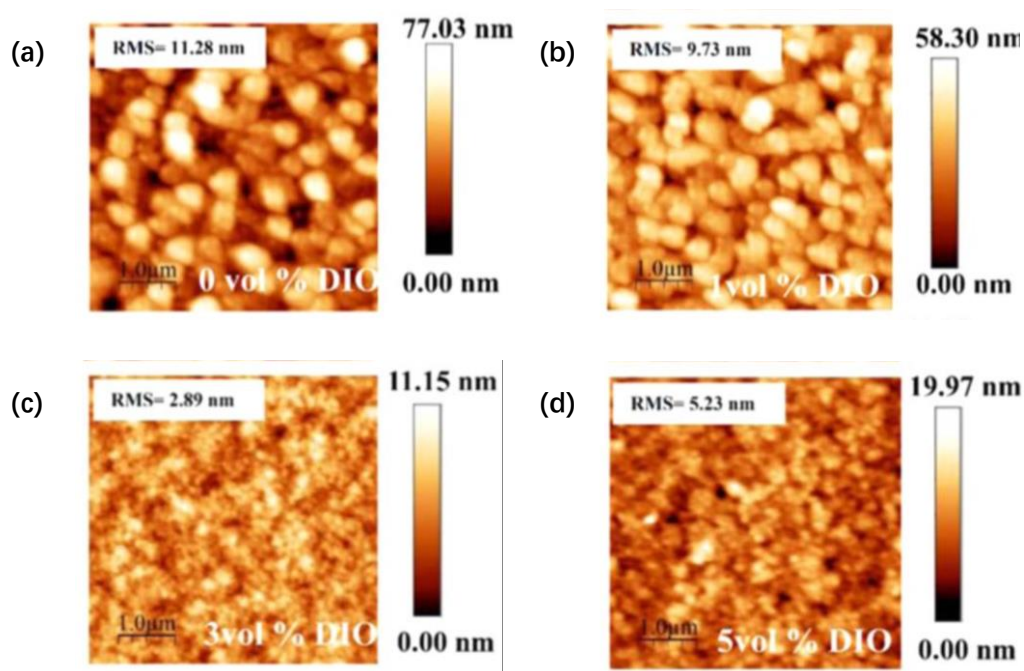


Figure 3.6 (a)–(d) Represents surface topography images of PTB7: PC<sub>71</sub>BM photoactive layer with different concentration of DIO (0, 1, 3 and 5 vol%) respectively.<sup>100</sup>

Table 3.3 Effects of processing additive on the PCE of several type of donor/acceptor OPVs.

Donor/acceptors	Host solvent	Processing additive	PCE (%)	
			Without additives	With additives
P3HT/PC <sub>61</sub> BM	CB	OT	0.29	2.9 <sup>89</sup>
			0.56	3.02 <sup>103</sup>
	<i>o</i> -DCB	1.6-hexanedithiol	1.0	2.8 <sup>102</sup>
	CB	NB	0.61	3.04 <sup>108</sup>
P3HT/PC <sub>71</sub> BM	Toluene	Ethyl benzenecarboxylate	0.80	4.11 <sup>113</sup>
PTB7/PC <sub>71</sub> BM	CB	DIO	2.9	6.9 <sup>114</sup>
				8.22 <sup>115</sup>
	<i>o</i> -Xylene	<i>p</i> -Anisaldehyde (AA)	0.9	7.4 <sup>114</sup>
	Toluene	NMP		11.28 <sup>116</sup>
PBQ-4/PC <sub>71</sub> BM	Anisole	DPE	3.60	8.37 <sup>99</sup>
PDTSTPD/PC <sub>71</sub> BM	CB	DIO	1.37	7.32 <sup>117</sup>
PBDT-TS1/PC <sub>71</sub> BM	<i>o</i> -DCB	DIO	6.94	9.15 <sup>97</sup>
	<i>o</i> -Xylene	NMP	2.78	9.11 <sup>97</sup>

Yao et al. introduced OT into the host solvent CB to study how the additive impacts the morphology of a P3HT:PC<sub>61</sub>BM system.<sup>89</sup> The different boiling points between the processing additive OT (270 °C) and the host solvent *o*-DCB (178 °C), lead to different evaporation rates. A fast evaporation rate for the host solvent causes an increase in the additive concentration in the solvent mixture during film formation. The redistribution of PC<sub>61</sub>BM and P3HT in blend films is due to the residual OT. Due to the presence of OT, PC<sub>61</sub>BM is finely dispersed between P3HT chains on a molecular basis, leading to the redistribution of PC<sub>61</sub>BM and P3HT in the blend films, and optimizing the morphology of active layer. Experimental results demonstrate that the

PCE of OT-processed OPVs is 5-6 times higher than that of OPVs without additive. Based on these examples, it is obvious that the use of processing additives represents a widely applicable and effective way to optimize the morphology of a wide range of donor/acceptor systems and, consequently, to improve the performance of organic solar cells. Table 3.3 displays examples of some donor/acceptor systems along with the PCEs with and without processing additives.

*-Use of cosolvents.* Cosolvents generally constitute a larger proportion of the solvent mixtures, and cosolvents and host solvents have close evaporation rates, e.g. vapor pressure, melting point, etc. The "new solvent" made from the mixture of cosolvent and host solvent needs to provide high solubility for both donor and acceptor. Since the chlorinated solvents cannot be used for large-area OPV products because of their high toxicity and large environmental impact, nontoxic or less toxic alternative solvents are required for OPV up-scaling. If no single less toxic solvents that lead to an ideal morphology can be identified, the utilization of cosolvents can be an interesting alternative, as it broadens the choice of solvents.

As an example, carbon disulphide (CS<sub>2</sub>) and acetone were chosen to replace CB for processing PCDTBT: PC<sub>71</sub>BM blends. A higher solubility of PCDTBT: PC<sub>71</sub>BM blends was achieved in the solvent mixture by optimizing the CS<sub>2</sub> /acetone ratio.<sup>118</sup> CS<sub>2</sub> and acetone are mutually miscible and have similar boiling points (46°C and 56 °C respectively). This close boiling point of both solvents ensures that the solvents in the blend evaporate at a similar rate during the drying process. Besides, the CS<sub>2</sub> /acetone mixtures provide a higher solubility for PCDTBT (20 mg/ml) than CB (10 mg/ml). The OPV devices that were processed by CS<sub>2</sub>/acetone (80:20 by volume) mixtures obtained a comparable PCE of 6.62% to the PCE of devices processed by pure CB (5.52%). The results from Jung et al. suggest that the use of cosolvents represents an efficient approach to optimize the morphology of BHJ films and the OPV fabrication from less toxic processing solvents.<sup>118</sup>

### 3.3 Methods for Solvent Selection

There are two main reasons for selecting alternative solvents: to improve the performance of organic materials for OPV (for instance due to a better morphology), and to replace toxic solvents to make OPV module fabrication more environmentally friendly. Currently, most active layers of state-of-the-art OPV systems are still processed with toxic solvents such as CF, CB, and o-DCB at the laboratory scale. It should be noted that the quantity of solvents used during processing increases dramatically with large-scale production, making environmental damage and impact on human health critical issues. Also, toxic solvents are expensive and energy-intensive to remove as waste. Therefore, the usage of toxic solvents to process both well-known and new organic materials is a major bottleneck for the development of the OPV industry. It is thus urgent to develop “greener” alternative solvents to process efficient OPV devices. Many efforts have already been made for a safe, eco-friendly and economical OPV fabrication and were based on two methodologies: a trial and error approach and the Hansen solubility parameters theory (HSPs).

#### 3.3.1 Trial and Error Approach

The trial and error approach is a basic experimental problem-solving method built on practical experiments. For a conventional (generally toxic) solvent to be replaced, one or several alternative solvents are empirically selected and tested. If these candidates do not match the requirements, they are removed from the candidate list and others are proposed and tested, until achieving the target properties. The efficacy of the alternative solvent generally takes into account application-relevant properties, such as solubility power, toxicity and energy consumption. For determining the final choice, a compromise between different selection criteria is often ineluctable.

Table 3.4 Examples of alternative solvents for several type of donor/acceptor OPVs by trial and error approach.

Donor/acceptor system	Alternative solvents/additives	PCE (%)	Ref.
PTB-EDOTS/ITIC	MeTHF	10.18	106
PTB7/PC <sub>71</sub> BM	2-MA	9.6	95
	o-xylene/DIO	7.1	119
	Thiophene/DPE	8.92	98
PBDTTT-C/oo-2PDlate	Anisole	2.24	120
BDTSTNTTR/PC <sub>71</sub> BM	CS <sub>2</sub>	11.53	121
BTR/PC <sub>71</sub> BM	Toluene/DPE	6.56	122
FTAZ/IT-M	TMB	9.1	123
	o-xylene	9.6	123
	Toluene	11.0	123
T1/BTP-4F-12	o-xylene	15.3	124
	TMB	14.9	124
	Tetrahydrofuran	16.1	124
PBBDTBT/PC <sub>71</sub> BM	o-xylene/NMP	4.57	109

This method is widely used in the OPV field for the selection of alternative solvents and processing additives. For instance, Liao et al. added ethylenedioxythiophene (EDOT) side chains to the benzo[1,2-b:4,5-b']dithiophene (BDT) donor units to improve the solubility of the PTB7 donor material in non-halogenated solvents.<sup>106</sup> Yet, the final halogen-free solvent 2-methyltetrahydrofuran (MeTHF) that was used to prepare the OPV devices and led to a maximum PCE of 10.18%, was selected by a trial and error method. Another recent example is 2-methyl

anisole (2-MA) which has been considered as alternative solvent in many studies, because of its low toxicity and widespread use as food additive.<sup>95</sup> 2-MA was selected by a trial and error method to replace the toxic halogenated solvent CB and processing additive DIO during the device manufacturing. Highly efficient PTB7: PC<sub>71</sub>BM-based OPV devices with a highest PCE of 9.6%. were prepared with 2-MA. Table 3.4 represents some examples of alternative solvents for different donor/acceptor systems.

### 3.3.2 Hansen Solubility Parameters Theory (HSPs)

As noted in section 3.2, processing solvents and additives can improve the morphology of BHJ by modifying the miscibility between solvents and photovoltaic materials. The solubility of photovoltaic materials in various solvents can be predicted by the Hansen solubility parameters methodology (HSPs). Hildebrand and Scott were first to propose the term solubility parameter. The Hildebrand solubility parameter is defined as the square root of the cohesive energy density ( $E_C$ ) (or energy of evaporation per unit volume) over the molar volume of the pure solution:

$$\delta = \sqrt{\left(\frac{E_C}{V}\right)} \quad (5)$$

Hansen extended this preliminary work by proposing the so-called Hansen solubility theory that decomposes the cohesive energy into three major types of intermolecular interactions<sup>125</sup>, namely: (1) dispersion interactions  $E_D$ , (2) permanent dipole molecular interactions  $E_P$ , and (3) hydrogen binding interactions  $E_H$ . The total cohesive energy and solubility parameter are then given by:

$$E_C = E_D + E_P + E_H \quad (6)$$

$$\delta = \sqrt{(\delta_D)^2 + (\delta_P)^2 + (\delta_H)^2} \quad (7)$$

where  $\delta_D = \sqrt{\left(\frac{E_D}{V}\right)}$ ,  $\delta_P = \sqrt{\left(\frac{E_P}{V}\right)}$ , and  $\delta_H = \sqrt{\left(\frac{E_H}{V}\right)}$  are Hansen solubility

parameters. Each molecule can be represented by its position in a three-dimension space (Hansen solubility space), and the corresponding coordinates are defined by the three solubility parameters. The basic concept for describing the miscibility between two molecules is “like dissolves like.” Therefore, the solute can be soluble in a solvent when they have similar molecular interactions, i.e. the similar HSPs. Such a similarity is quantified by the distance  $R_a$  between the HSPs of a solvent ( $\delta_{D1}$ ,  $\delta_{P1}$ , and  $\delta_{H1}$ ) and that of a solute ( $\delta_{D2}$ ,  $\delta_{P2}$ , and  $\delta_{H2}$ ) in the Hansen space. The distance  $R_a$  is defined by the following equation:

$$R_a = \sqrt{4(\delta_{D1} - \delta_{D2})^2 + (\delta_{P1} - \delta_{P2})^2 + (\delta_{H1} - \delta_{H2})^2} \quad (8)$$

Furthermore, a solubility “boundary” for a solute is required to define and differentiate “good solvents” from “bad solvents”. This has led to the concept of the Hansen solubility sphere, which is defined by a center position whose coordinates are the HSPs of the solute and by a radius ( $R_0$ ).  $R_0$  corresponds to the largest distance (equation (9)) between a solute and miscible solvents and can be determined by solubility experiments.<sup>126</sup> In other words, a solute is insoluble in a given solvent if  $R_a$  between the solute and solvent is larger than the  $R_0$  of the solute. The affinity between both molecules increases with decreasing  $R_a$  and is described by the relative energy difference ( $RED$ ), with:

$$RED = \frac{R_a}{R_0} \quad (9)$$

A  $RED$  less than 1 implies that the solvent HSPs are inside the Hansen solubility sphere of the solute and can be considered as a good solvent. Note that the Hansen solubility sphere radius is somewhat misleading since it can depend to some extent on the experimental conditions such as temperature, annealing and stirring time of the solution. Generally,  $R_0$  increases with temperature and stirring time, as illustrated by the work of Strohm et al. on the temperature dependency of the P3HT-Solubility sphere (Figure 3.7).<sup>127</sup> As a consequence, solvents that are located near the boundary



of the solute solubility sphere may provide only a limited solubility for the solute.

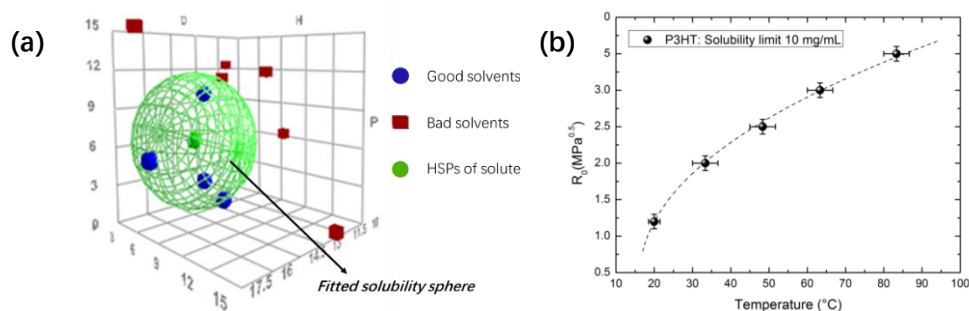


Figure 3.7 (a) HSPs diagrams with the good and bad solvents resulting from the solubility tests and the fitted solubility sphere. Radius  $R_0$  of the solubility sphere as a function of temperature. The radius is fixed at a solubility limit of 10mg/mL. The dashed line is a guide to the eye.<sup>127</sup>

In the OPV field, the HSP theory is generally used to predict the interactions between the processing solvents and additive, or correlate the solubility properties with the active layer and with the performances of OPV devices. This theory provides a more efficient way to select alternative solvents in comparison to the trial and error method. Kumari et al. selected the halogen-free solvents toluene and o-xylene by HSPs theory to prepare ternary PTB7/DR3TSBDT/PC<sub>71</sub>BM (75:25:150 wt%) based OPV devices and could achieve PCEs of 11.2 % and 11.75 % respectively.<sup>116</sup> In this study, the toluene and o-xylene are located inside the solubility spheres of PTB7, DR3TSBDT and PC<sub>71</sub>BM at the same time, indicating that these two halogen-free solvents provide a good solubility for the three organic semiconductors. The HSPs theory can also be used for the selection of processing additives. The non-halogenated solvent o-xylene and additive 1,2-DMN were selected by HSPs theory to replace CB/CN mixture solvents for the PIDT-FQT/PC<sub>71</sub>BM based OPV devices.<sup>128</sup> The HSPs of o-xylene/1,2-DMN mixture solvents exhibit similar HSPs than the CB/CN mixtures, inducing similar morphologies and mobilities of devices that were manufactured by both solvent mixtures. Recent examples of selected processing solvents for OPV devices are summarized in Table 3.5.

Table 3.5 Examples of alternative solvents for several type of donor/acceptor OPVs by HSPs theory.

Donor/acceptor system	Alternative solvents/additives	PCE (%)	Ref.
PTB7/DR3TSBDT/PC <sub>71</sub> BM	Toluene/NMP	11.28	116
	o-Xylene/NMP	11.75	116
DPP(TBFu) <sub>2</sub> /PC <sub>71</sub> BM	Thiophene	3.9	129
	CS <sub>2</sub>	4.2	129
	Trichloroethylene	4.2	129
P3HT/IDTBR	o-Xylene/1-MN	4.99	127
	p-Cymene/p-Bromoanisole	5.30	127
	2-MA	5.41	127
PIDT-FQ-T:PC <sub>71</sub> BM	o-Xylene/ 1,2-Dimethylnaphthalene	7.18	128
P3HT:IC <sub>60</sub> BA	Toluene/1-Methylnaphthalene	6.27	128
P3HT:PC <sub>60</sub> BM	1,2-Dichlorobenzene/Dimethyl phthalate	3.20	104

### 3.3.3 IBSS<sup>®</sup> CAMD

The trial and error method and HSPs theory are common methodologies for solvent selection in the OPV field. However, they are both time-consuming and may miss good solvent candidates. Searching for new solvents is indeed a complex problem, which requires considering multiple properties, such as solubility, viscosity, safety, sustainability, toxicity, where most of these may impact the device properties in a rather unpredictable way. Multiple properties of the candidate solvents need therefore to be taken into account simultaneously during the selection process. There is thus a considerable interest to develop more systematic methodologies to achieve the alternative solvent selection in a more efficient and accurate way. A possible route to achieve this goal is based on the concept of reverse engineering.

Reverse engineering follows the Computer Aided Molecular Design (CAMD) precepts by first defining a set of target values for a group of selected physicochemical properties and by leading the construction in silico of the molecular structures that best satisfy them. The IBSS<sup>®</sup> CAMD tool is an innovative CAMD tool dedicated to the design of biosolvents.<sup>130</sup> The main advantage of IBSS<sup>®</sup> CAMD lies on the construction of molecular structures by imposing bio-based building blocks as the starting fragment to ensure the development of biosolvents. Several applications of IBSS<sup>®</sup> CAMD appeared in the open literature to find new biosolvents as pure compound: substitution of acetone and methyl ethyl ketone (MEK) by furfural derivatives to dissolve two epoxy resin prepolymers, bisphenol A diglycidyl ether (DGEBA) and triglycidyl p-aminophenol ether (TGPA)<sup>131</sup> and glycerol derivatives to solubilize nitrocellulose<sup>132</sup>. IBSS<sup>®</sup> CAMD was also applied to generate ricinoleic acid derivatives aiming to find new biolubricants from a biomass feedstock.<sup>133</sup> Moreover, since the efficiency of a pure solvent can be improved thanks to the thermodynamic synergism of forming binary or multicomponent mixtures, special attention has been devoted to the use of azeotropic mixtures that behave as a pure compound at a given composition. For instance, new coolant azeotropic mixtures for heat-exchange devices in aerospace applications have been recently identified by using IBSS<sup>®</sup>CAMD tool<sup>134</sup>. It is worth to notice however that best proposed structures might be virtually excellent but infeasible at an industrial scale. Therefore, even if new molecular structures are identified by IBSS<sup>®</sup>CAMD as promising candidate, commercially available compounds are generally preferred to replace hazard solvents in the industry.

Up to now, the IBSS<sup>®</sup>CAMD method has not yet been used to search for alternative solvents for the processing of organic semiconductors. Yet, the successful implementations of IBSS<sup>®</sup>CAMD mentioned above suggest that it has a promising perspective for solving the toxic solvent issue for solution-processed organic devices such as OPVs, but also organic light-emitting diodes (OLEDs), organic solid-state field-effect transistors (OFETs), or organic photodiodes.<sup>35-37</sup> In this thesis, this tool is

introduced for the first time to select alternative solvents for polymer/fullerene and polymer/non-fullerene based OPV devices. A more detailed description of IBSS®CAMD is given in the following chapter.

# CHAPTER 4

---

---

IBSS<sup>®</sup>CAMD TOOL

---

---

## 4 IBSS®CAMD Tool

Reverse engineering is nowadays an established approach for designing solvents with multiple properties. It follows the Computer Aided Molecular Design (CAMD) precepts by first defining a set of target values for a group of selected physicochemical properties and by leading the construction in silico of molecular structures that best satisfy them. Recently, an innovative CAMD tool, called IBSS®CAMD,<sup>135</sup> has been developed by Juliette Heintz et al. to design alternative solvents and eventually biosolvents.<sup>136,137</sup> IBSS®CAMD designs molecular structures by imposing building blocks, including bio-based ones, as starting fragments to ensure the development of solvents that can be synthesized from agricultural resources. Some recent examples of the utilization of IBSS®CAMD to find new biosolvents include the substitution of acetone and methyl ethyl ketone (MEK) by furfural derivatives to dissolve two epoxy resin prepolymers, as well as bisphenol A diglycidyl ether (DGEBA), triglycidyl p-aminophenol ether (TGPA)<sup>132</sup> and glycerol derivatives to solubilize nitrocellulose<sup>133</sup>. IBSS®CAMD has also been applied to generate ricinoleic acid derivatives aiming to find new biolubricants from a biomass feedstock.<sup>133</sup> Since the efficiency of a pure solvent can be improved thanks to the thermodynamic synergism of forming binary or multicomponent mixtures, special attention has also been devoted to the use of azeotropic mixtures that behave as a pure compound at a given composition and pressure. For instance, new coolant azeotropic mixtures for heat-exchange devices in aerospace applications have been recently identified by using IBSS®CAMD tool<sup>134</sup>. Therefore, IBSS®CAMD is considered to be an effective tool for alternative solvent selection in different fields. This tool is described in detail in this chapter.

### 4.1 Fundamental Principles of IBSS®CAMD

Up to now, the selection of new molecules as alternative solvents for OPV has mostly been the result of a time-consuming trial-and-error approach. Searching for

---

new solvents is indeed a complex problem that requires taking into account multiple properties, such as Hansen solubility parameters, boiling temperature, toxicity ..., while most of these may impact the device performance in a rather unpredictable way. In order to cope with the challenging complexity of the problem, it is therefore highly desirable to replace the conventional "trial and error" approach by more efficient methods, capable to take into account multiple functional, economic, health, safety and lifecycle constraints simultaneously.

IBSS®CAMD can generate molecular structures "from scratch" by starting from a fixed number of chemical groups, including for instance biobased building blocks. The final solution is constrained by the nature of the selected chemical groups and their maximal number in the molecules to be constructed. A molecular structure is appropriate to replace a hazardous solvent if the corresponding physicochemical properties are within specifications. This "appropriateness" is quantified by defining and calculating a global performance index *GloPerf* for each designed molecule (see below). The initial chemical structures are continuously modified according to a genetic algorithm optimization strategy (see below) in order to maximize the *GloPerf* index. The final list of the solvent candidates comes from the solution of the optimization problem of *GloPerf* on the optimization variables.

Two different methods to predict the properties of alternative solvents can be applied: the database approach and the group contribution-based approach. The database approach is achieved by using existing databases of physicochemical properties of given molecules. The group contribution-based approach decomposes molecules into chemical fragments for which property databases are available and estimates the molecular properties by a linear combination of the fragment properties (see below). The molecules are evaluated by the group contribution methods (see below) and then identified so that only the best molecules are retained. In addition, IBSS®CAMD is based on four major concepts: (1) property calculation models, (2) performance criteria, (3) molecular representation model and (4) resolution method.

#### 4.1.1 Property calculation models

A list of property calculation models can be used in IBSS<sup>®</sup>CAMD to calculate the property values of alternative solvents. The accuracy of the selected calculation techniques must be sufficient to get a meaningful final list of candidates. The property calculation models must be distinguished between a pure compound model and a mixture model.

##### 4.1.1.1 Pure compound property estimation model

For a pure component, the user retrieves the required property models from the property package library available in CAMD tools. They should be able to compute properties for a wide diversity of chemical structures by applying group contribution models or quantitative structure activity/property relationship (QSAR/QSPR).<sup>138,139</sup> Group contribution models are widely used for alternative solvents design due to their simplicity and availability in CAMD tools.<sup>140,141</sup>

In principle, the properties of a compound are calculated from the contributions of three types of chemical groups: first order groups, second order groups and third order groups. The first order groups are the basic ones such as -CH<sub>3</sub>, -OH, =O, -NH<sub>2</sub>, etc., and intended to describe a wide variety of organic compounds. The second and third order groups use the connectivity between basic groups in order to distinguish between isomers and to describe the proximity effects in a molecule arising from polyfunctionality. However, the second order groups are inadequate to provide an exact representation of compounds when the latter include more than one ring, or in some cases, open-chain polyfunctional compounds with more than four carbon atoms in the main chain. Thus, a further level (third order groups) is required to describe the more complex chemical structures, such as systems of fused aromatic rings, systems of fused aromatic and nonaromatic rings, etc. For the group contribution approach, a large database is required, which reports the physicochemical properties of functional



groups. Any physicochemical property,  $P$ , such as phase transition temperature, viscosity, heat capacity, etc. of full molecules can then be estimated by the following general form:

$$P = \sum_{k \in G1} n_{1k} A_k + w \sum_{k \in G2} n_{2k} B_k + z \sum_{k \in G3} n_{3k} C_k \quad (10)$$

where  $G1$ ,  $G2$  and  $G3$  are the sets of first, second and third order groups respectively,  $A_k$  is the contribution of the first order group  $k$  to the property  $P$  that occurs  $n_{1k}$  times in the molecule,  $B_k$  is the contribution of the second order group  $k$  that occurs  $n_{2k}$  times and  $C_k$  is the contribution of the third order group  $k$  that occurs  $n_{3k}$  times. For some properties, an additional adjustable model parameter (or universal constant) is used (see chapter 5).

For most properties, the  $A_k$ ,  $B_k$  and  $C_k$  coefficients have been regressed from experimental data obtained over a large range of chemical families.<sup>142</sup> The series of  $A_k$ ,  $B_k$  and  $C_k$  coefficients for numerous physicochemical properties estimated by Marrero and Gani<sup>142</sup> are used as a database by IBSS®CAMD. The corresponding additional adjustable model parameter can be found in Ref 142.

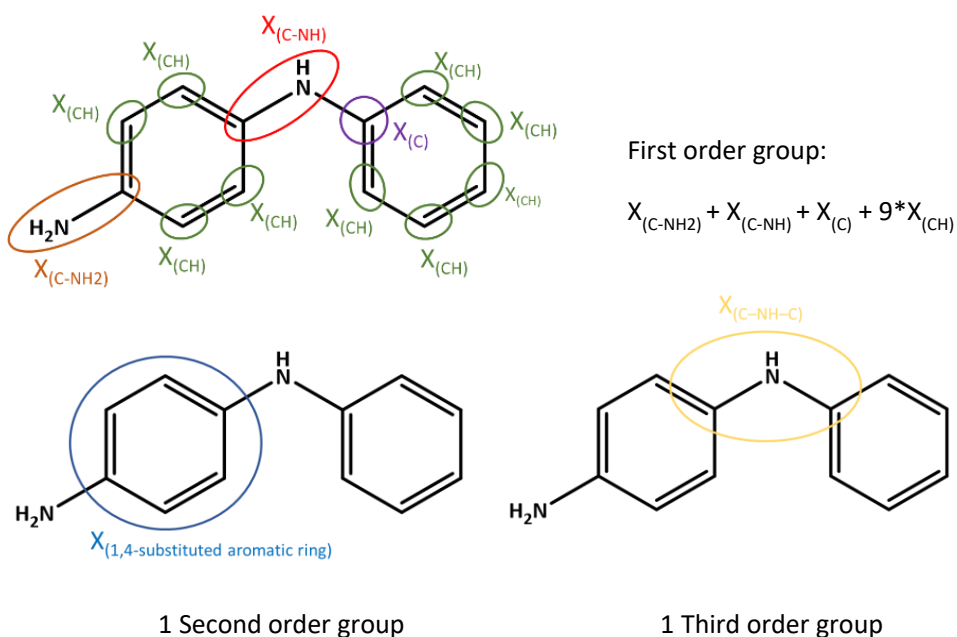
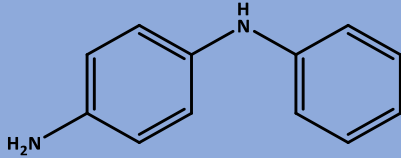


Figure 4.1 Division of *N*-phenyl-1,4-benzenediamine molecule by group contribution methods.

For simple molecules, the property  $P$  can be estimated by using only the first term with  $A_k$  values, which are known for all first order groups that are relevant to organic molecules. For more complex structures,  $B_k$  and  $C_k$  coefficients can improve the accuracy of the estimates, provided that they are available in the CAMD database. The  $w$  and  $z$  coefficients in equation (10) will be set to 1 or 0 depending on the availability of  $B_k$  and  $C_k$  in the CAMD database.

Table 4.1 Estimation of normal boiling point of *N*-phenyl-1,4-benzenediamine.<sup>142</sup>

N-phenyl-1,4-benzenediamine (experimental value: $T_b = 627$ K)		Molecular structure	
			
<i>First order groups</i>	$n_{1k}$	$A_k$	$\sum n_{1k}A_k$
$X_{(C-NH_2)}$	1	3.8298	15.8281
$X_{(C-NH)}$	1	2.9230	
$X_{(C)}$	1	1.5468	
$X_{(CH)}$	9	0.8365	
<i>Second order groups</i>	$n_{2k}$	$B_k$	$\sum n_{2k}B_k$
$X_{(1,4\text{-substituted aromatic ring})}$	1	0.1007	0.1007
<i>Third order groups</i>	$n_{3k}$	$C_k$	$\sum n_{3k}C_k$
$X_{(C-NH-C)}$	1	0.5768	0.5768
$P = \sum_{k \in G1} n_{1k}A_k + \sum_{k \in G2} n_{2k}B_k + \sum_{k \in G3} n_{3k}C_k = 15.8281 + 0.1007 + 0.5768 = 16.5056$			
$T_b^{est} = c \times \ln(P) = 624K$ , calculated with the universal constant for the boiling point $c = 222.543$ . (error = $627 - 624 = 3K$ )			

---

As an example, the N-phenyl-1,4-benzenediamine molecule was decomposed by the group contribution method, as shown in Figure 4.1. The boiling point of N-phenyl-1,4-benzenediamine can be estimated according to the data given in Table 4.1, leading to an estimated boiling point,  $T_b^{est}$ , that matches well the experimental value. The related parameters including  $n_{1k}$ ,  $A_k$ ,  $n_{2k}$ ,  $B_k$ ,  $n_{3k}$ ,  $C_k$ , and adjustable parameters for the target properties are taken from Ref 142.

#### 4.1.1.2 Mixture property estimation model

The estimation of the properties of organic mixtures is based on the calculation of the pure compound property. Within IBSS<sup>®</sup>CAMD, a linear dependency model is used. Taking the molecular mass as an example:

$$P_{mixture} = \sum_{i=1}^{nc} z_i P_i \quad (11)$$

where  $z$  is a molar fraction.

The accuracy of the linear dependency model is limited and may result in a poor quality estimations as a consequence of nonlinear property dependencies. However, in the case of mixtures that include a minor component (or additive), the linear approximation is expected to yield meaningful results. Appendix 9.1 presents a list of properties that are included in IBSS<sup>®</sup>CAMD and their associated default calculation models.

#### 4.1.2 Performance criteria

The tailor-made molecular design problem is inherently multi-objective since several physicochemical properties (section 4.2.3) must be satisfied at the same time for each molecular structure. Different molecular structures ( $MS$ ) are ranked according to a *GloPerf* parameter that represents a weighted average performance.<sup>143</sup> *GloPerf* is

itself formulated as the average of  $m$  individual performance factors  $ProPerf_p(MS, cond_j)$  each related to a single property prediction model, as shown in equation (12):

$$GloPerf(MS, cond_j) = \frac{\sum_{p=1}^m w_p * ProPerf_p(x(MS, cond_j))}{\sum_{p=1}^m w_p} \quad (12)$$

where  $w_p$  are weighting factors that are selected by the user based on its knowledge of the property significance for the targeted application.  $GloPerf$  equals unity in the ideal case, where all target properties are matched and all  $ProPerf_p$  factors are equal to one.

The  $ProPerf_p$  factor corresponding to a given property  $P$  compares the property value  $x$ , predicted by the selected methods (section 4.2.2), with the targeted value  $V$ . The  $ProPerf_p$  factors depend obviously on the molecular structures  $MS$  and can also be a function of  $j$  specific “conditions” ( $cond_j$ ) set by the user, such as for instance the temperature and/or pressure under which the experimental process is to be performed.

The  $ProPerf_p$  factors are calculated by using a Gaussian-type distance function defined by equation 13:

$$ProPerf_p(x(MS, cond_j)) = \exp \left[ - \left( \frac{V - x(MS, cond_j)}{\sigma} \right)^2 \right] \quad (13)$$

where parameter  $\sigma$  is used to define a “tolerance” margin around a given target value  $V$ .  $ProPerf_p$  takes the value 1 if the estimated value  $x$  meets the target value  $V$  for  $P$ . The  $\sigma$  parameter determines the rate at which  $ProPerf_p$  decreases when  $x$  deviates from  $V$ .

Three types of Gaussian function were defined based on the property constraints, as shown in Figure 4.3. For instance, if the target is to achieve a flashpoint level above a specified value to enhance safety, the distance function is characterized by a lower target value and a single tolerance margin (figure 4.3b). On the other hand, if the target

is a viscosity at 298 K within a given range, two target values and tolerance margins are needed (figure 4.3a).

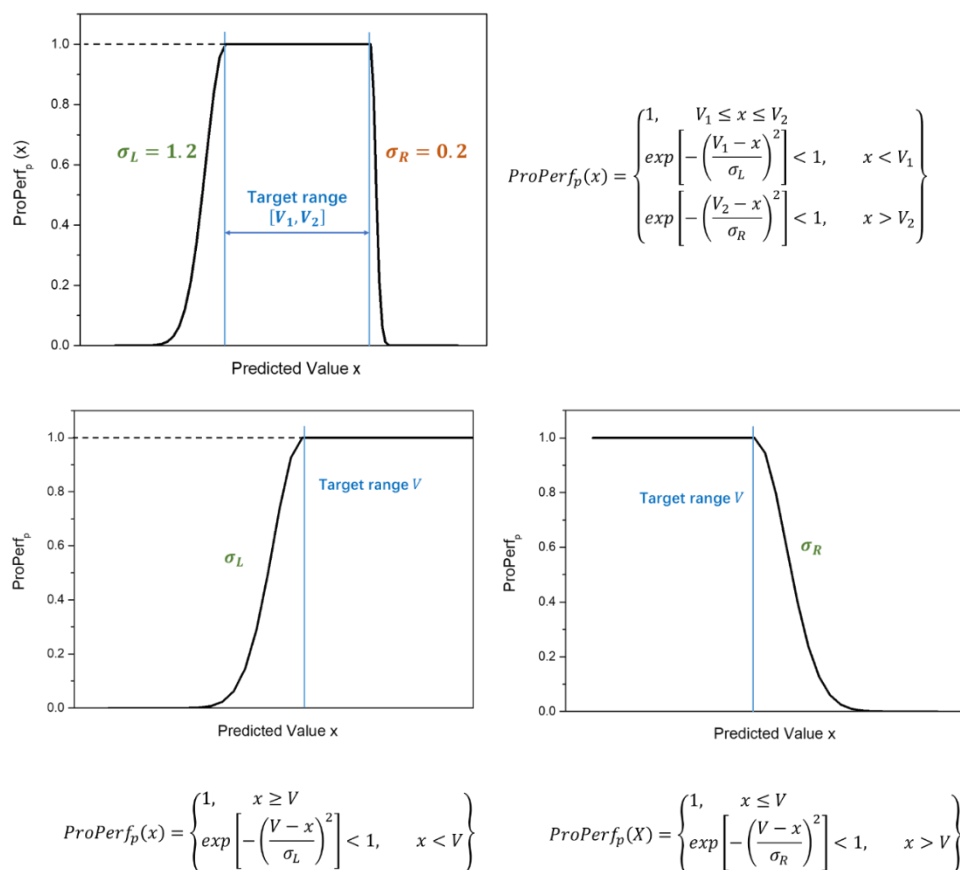


Figure 4.2 (a) shows an example corresponding to a property whose  $x$  value is within a target range defined by two boundary values and thus two different  $\sigma$  parameters. (b) examples corresponding to properties, whose  $x$  values need either to be higher or equal to a given target value, and (c) examples corresponding to a property whose  $x$  values need either to be lower or equal to a given target value.

### 4.1.3 Resolution method

To solve the combinatorial problem of the design of molecules with target properties, meta-heuristic research methods are used by IBSS<sup>®</sup>CAMD. They consist of iterative improvement of candidate molecules or “solutions”. In IBSS<sup>®</sup>CAMD, they are based on the probabilistic evolution of the solution and can therefore be called random or stochastic search methods.

The most frequently used algorithm in IBSS®CAMD is the genetic algorithm. At first, the genetic algorithm explores the solution space using the principle of natural selection and the laws elaborated by Darwin. Holland (1975) has introduced the fundamentals of this algorithm.<sup>144</sup> The population  $n$  is evaluated using a performance-biased method and the best solution in the population is modified randomly by genetic operators such as "crossover" and "mutation" to create population  $n+1$ . Population  $n+1$  (children), which differs from population  $n$  (parent generation), is again evaluated using the same performance-biased method and the best solutions are modified to yield generation  $n+2$  (grand-children), etc. The generation steps of the genetic algorithm are shown in Figure 4.3.

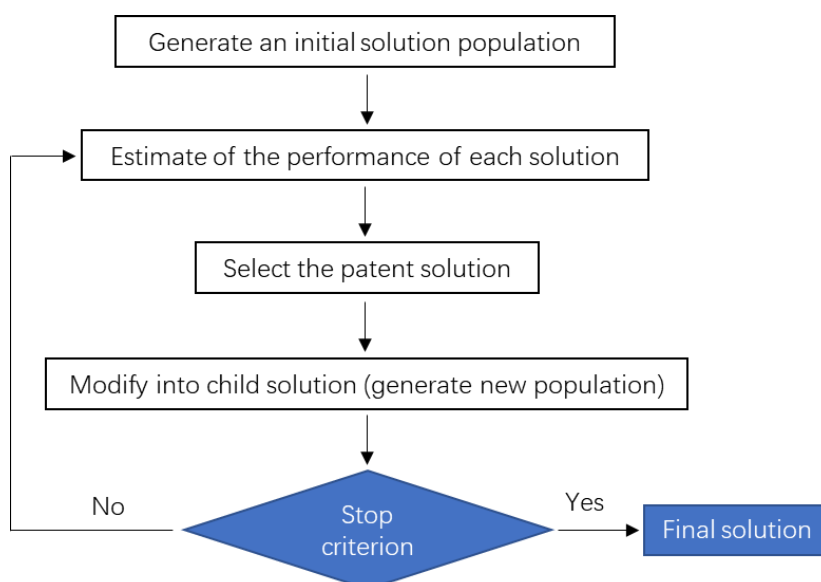


Figure 4.3 Steps of a genetic algorithm in IBSS®CAMD.

First, the initial population of  $N$  molecular structures (individuals) is generated randomly within predefined constraints (for instance the fixed number of basic groups, type of chemical bonds, ...) on the optimization variables (i.e. on the basic groups used to build the chemical structure). Second, target properties are evaluated by the selected group contribution model available in the property calculation library in order to calculate the performance of individual property and the corresponding global

---

performance of each solution is estimated. The molecules are then ranked according to their match with the target properties. Next, some structures are changed by using various molecule modification operators (deleting, adding or changing the chemical groups, see section 4.3 for details.). The population of molecular structures is modified and evaluated again until the stop criterion is satisfied putting an end to the search step and providing the final list of the best candidates.

#### 4.1.4 Molecular representation model

Molecular representation plays an important role for IBSS<sup>®</sup>CAMD because the property calculation methods and the resulting expression of candidate molecular structures depend on the molecular representation. Thus, it is a challenge to precisely represent the molecular structure. Various molecular representation methods have been reported in the literature, including string representation<sup>141</sup>, binary representation<sup>145</sup>, structure-composition matrix<sup>146</sup>, SMILES “Simplified Molecular Input Line Specification”<sup>147</sup>, as well as molecular graphs proposed by Korichi et al.<sup>148</sup> The latter is used in IBSS<sup>®</sup>CAMD. Once decomposed into suitable groups, molecular graphs provide inputs to a large variety of property estimation models. And this representation of molecules is also quite easy for users to understand. Molecular graphs are included in a matrix where each diagonal element contains a functional group coded as an integer identifier *EG*. The *EG* expresses the valence, integrated or not in a cyclic structure, and the number of hydrogens in a molecule or fragment. The molecular graph of a given molecule is the aggregation of its fragment graphs completed with the fragment interconnections. Figure 4.4 shows an example of the acetone molecular representation model.

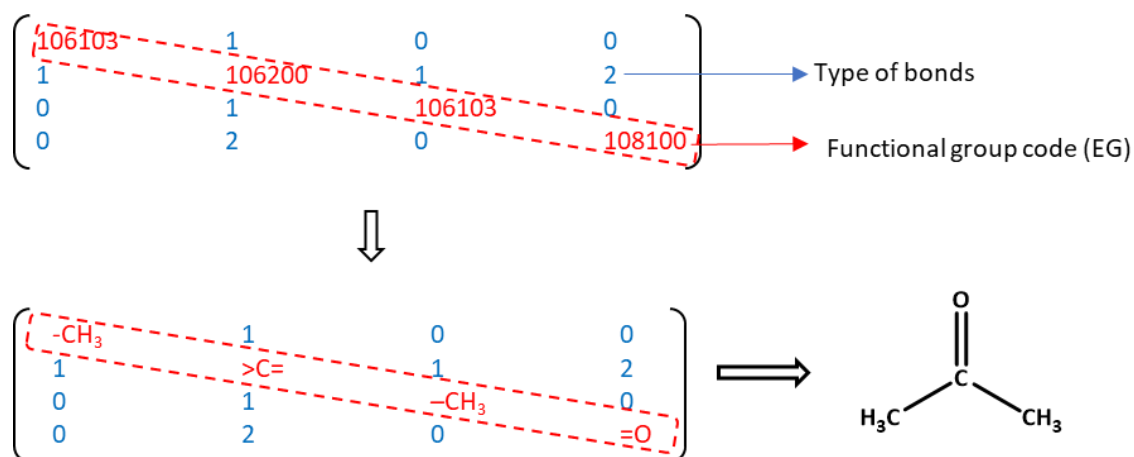


Figure 4.4 Molecular graph representation of acetone.

The basic functional group coding proposed by Korichi et al. (2008)<sup>148</sup>, is defined as diagonal atomic codes:

$$EG = P1P2P3P4. \quad (14)$$

where  $P1$  presents the atomic number, preceded with a 1 (106 for C, 107 for N, 108 for O, 117 for Cl...).

$P2$  expressed the highest bond order on the atom (ex. 1 for « -C- », 2 for « -N= », 3 for « -C≡ » and a special case 4 for =C=).

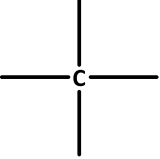
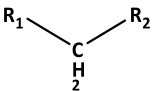
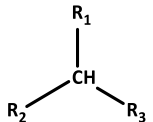
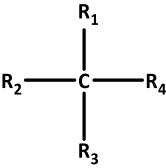

$P3$  represents the bond type (0 for bond with C or with the same atom. e.g. C-C-C; N-N; 1 for bond with at least one non-similar atom (C-O, C=O, C≡N, N-O); 2 for atom in a non-aromatic cycle e.g. pyridine, 3 in an aromatic ring e.g. benzene; 4 for an atom shared by two aromatic rings e.g. naphthalene; 5 for an atom shared by two cycles, one of them aromatic e.g. indane, 6 for other aromatic cases e.g. biphenyl; 7 for an atom shared by two non-aromatic rings.

$P4$  is the number of implicit hydrogens.

Examples of the available basic groups and their encoding is shown in Table 4.2. More available basic groups and their encoding can be found in Appendix 9.2.



Table 4.2 Examples of available basic groups and their encoding in IBSS®CAMD.

Atom	Type of bond	Basic groups	EG
C	 Four single bonds	$\text{H}_3\text{C}-\text{R}_1$	106103
			106102
			106101
			106100
O	 One double bond	Connection to C only	108200
		One non-C connection	108210
		Ring (non-aromatic)	108220

Molecular fragments are represented in the same way. But they need additional information related to their external connections. An example is shown in Figure 4.5. The molecular structure of acetaldehyde can be decomposed by showing how both fragments are connected. The fragments are detailed by their graph and a vector to show their position and the connection way in a whole molecule. Each EG code identifies a unique complex group available in a database. IBSS® CAMD uses a database of more than 200 fragments for molecular design.

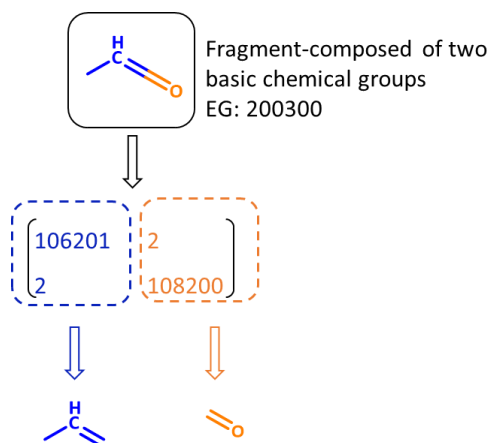


Figure 4.5 Simple and complex groups representation.

## 4.2 Reverse Engineering Method for Alternative Solvents Design

The methodology to design alternative solvents involves five essential steps as displayed in Figure 4.6 and described in the following.

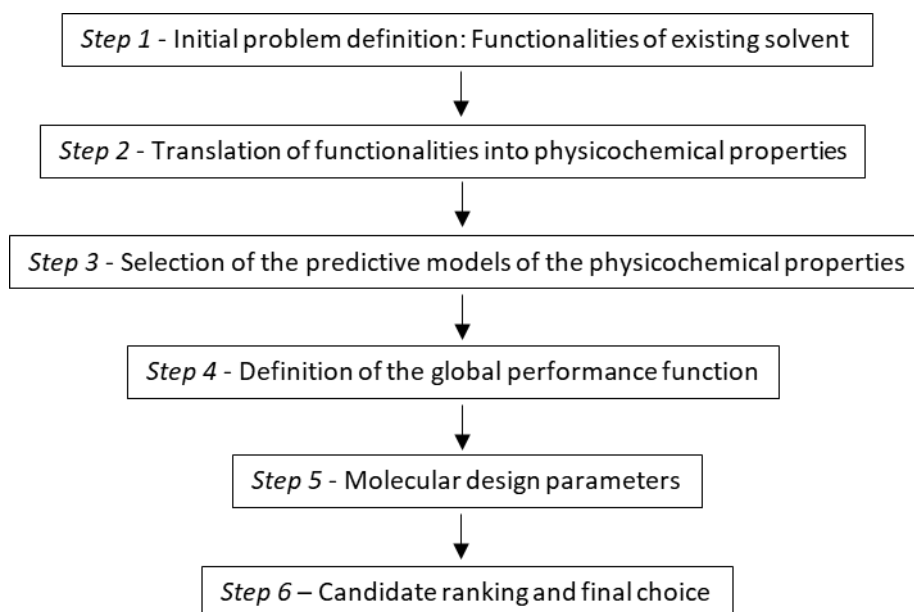


Figure 4.6 Systematic methodology based on reverse engineering and CAPD to design alternative solvents.

---

#### 4.2.1 Definition of the Initial Problem

A list of functionalities has to be set taking into account the properties of the solvents to be substituted. Typical examples are: high solubility power, Newtonian fluid, low energy consumption, good capillarity, safety, non-toxicity. In our case, the goal is to replace toxic solvents during processing with safer alternative solvents, in keeping with legislation (for instance, with the Registration Evaluation, Authorization of Chemical Substances regulations (REACH) (EC/1907/2006) implemented by the EU on June 1st 2007), environmental protection and customer needs. The translation of such solvent functionalities into physicochemical properties that can be reevaluated by IBSS® CAMD tool is further required.

#### 4.2.2 Translation of functionalities into physicochemical properties and definition of target values

This step is commonly done by using knowledge-based analysis. For instance, Hansen parameters are a good indicator for the capability of a solvent to dissolve a given molecule. A Newtonian fluid is related to its viscosity. A liquid solvent requires a low melting temperature, while low energy consumption can be associated with a low boiling temperature and vaporization enthalpy.

Target values for physicochemical properties can be defined in two different ways. In the case a property needs to reach a well-defined value that is already achieved with the initial solvent to be replaced, for instance a given surface tension, the target value is set to the corresponding experimental value of the initial solvent. Otherwise, the target values may differ from those of the initial solvent, if the related properties can be improved by the alternative solvent. For instance, a safer solvent implies to seek a higher flash point.

Step 2 is commonly done by using knowledge-based analysis. For instance, Hansen parameters are a good indicator for the capability of a solvent to dissolve a

given molecule. A Newtonian fluid is related to its viscosity. A liquid solvent requires a low melting temperature, while low energy consumption can be associated with a low boiling temperature and vaporization enthalpy.

### 4.2.3 Molecular design parameters

The steps 3 (Selection of the predictive models of the physicochemical properties) and 4 (Definition of the global performance function) have been described above (section 4.1.1 and 4.1.2, respectively).

IBSS<sup>®</sup>CAMD can be used in two different ways: (1) to evaluate only the performance of a given pre-selected list of existing solvents, or (2) to design new molecules and evaluate their performances, so as to rank them. Both modes have been used in this thesis. Step 5 (molecular design) is for mode (2) only.

When using the first mode, a list of SMILES (simplified molecular input line entry specification) codes of existing solvents must be entered and is used by IBSS<sup>®</sup>CAMD to evaluate the solvents performances.

In the molecular design mode, thousands of molecular structures are methodically generated by IBSS<sup>®</sup>CAMD and the *GloPerf* value is calculated for each of them. The tailor-made molecular design problem is a multi-objective optimization problem because several properties must be satisfied simultaneously. A genetic algorithm optimization method is implemented in IBSS<sup>®</sup>CAMD that allows the molecular structures to be modified in order to improve the *GloPerf* closer to one. In other words, the maximum *GloPerf* value is obtained by numerically resolving the objective function (*OF*) defined by:

$$OF = \text{MIN}\{GloPerf(MS, cond_j) - 1\} \quad (15)$$

As discussed before (section 4.1.2), the property values of a molecule are predicted by a group contribution method. The chemical nature of each group and the

connections between chemical moieties determine the *GloPerf* values. An important input issue for IBSS®CAMD is the definition of the chemical groups or fragments to create a platform molecule. Common chemical fragments *MS* (simple ones like -CH<sub>3</sub>, -OH or more complex ones such as -COOH) are usually listed in the library of CAMD tools as elementary blocks. A large number of molecular structures can be generated from these building-blocks. IBSS®CAMD generates molecules with a maximum predefined size (or number of blocks) using only the elementary blocks or attaching them to a fixed building-core. Namely, a molecule is built from the fixed fragments (contained in every potential molecule) and the free groups (connected to the fixed part). Figure 4.7 represents some examples of elementary/fixed blocks and different types of bonds among these building blocks. The chemical groups for molecular design are shown in Appendix 9.3.

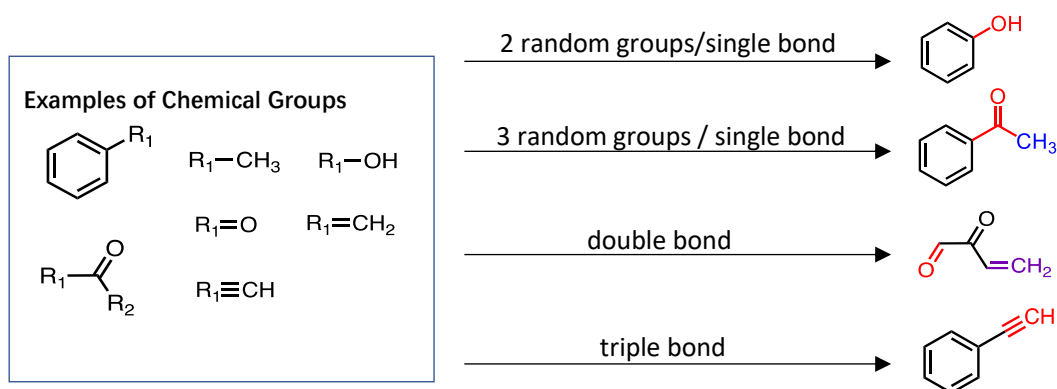


Figure 4.7 Examples of chemical groups and connection types for building alternative solvents using IBSS®CAMD tool. ( $R_1$  and  $R_2$  are randomly selected chemical groups from the IBSS®CAMD data base that are connected to other chemical groups by either simple or double bonds.

The optimal search of molecular structures better satisfying the target values of the selected physicochemical properties is based on the genetic algorithm method. As discussed in section 4.2.2, the initial population of molecular structures (individuals) is randomly generated under predefined constraints of optimization variables related to the chemical structure  $MG_i$ . Then the offspring generation of molecular structures

can be modified by using different molecule modification operators (deleting, adding or changing the chemical groups  $MG_i$ ). Several molecule modification operators are given in below.

*i. Mutation operator*

The mutation operator is a classic genetic operator and is not limited to CAMD. In CAMD, the mutation is used when the replacement of a single group by a group with the same connections occurs in a molecule, e.g.  $>CH_2$  by  $>O$  (see Figure 4.8). The group is changed randomly.

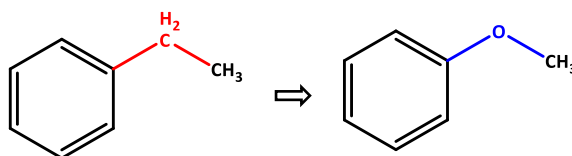


Figure 4.8 Mutation operator example.

*ii. Crossover operator*

The crossover involves two molecules. A non-cyclic fragment with the same bond type (single, double or triple bond) is randomly chosen in two molecular graph matrices thereby creating four semi-graphs. An example is shown in Figure 4.9. The red dashed lines show the positions of the cut in both molecules. The fragments are switched and recombined to form two new molecules. The recombined bonds are symbolized by solid red lines.

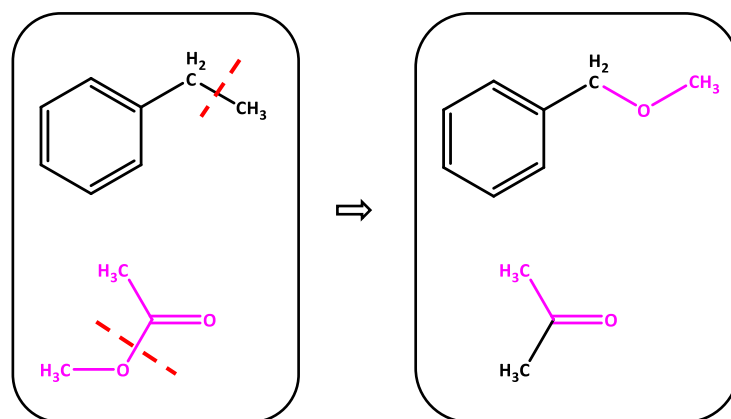


Figure 4.9 Crossover operator example.

### iii. Insertion operator

This operator involves the addition of a group into a molecular structure. In general, the inserted group has more than two connections, which makes it possible to complete the molecular structure with some branches. An example is reported in Figure 4.10. A bond is chosen randomly, here symbolized by a red dashed line. Then a group having at least two connections of the same type of the bond is randomly selected ( $-\text{CH}<$ ) (in magenta in Figure 4.8). The fragment with its branches is then inserted into the selected bond. The available connections to other groups are marked by  $R_i$ . If the inserted group has more branches ( $=\text{O}$  in Figure 4.8), these branches are added into the original group.

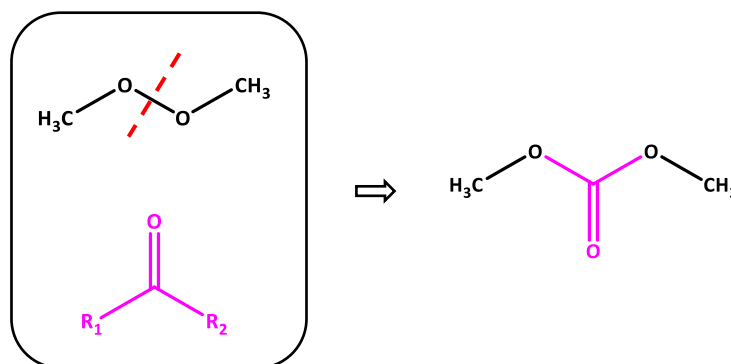


Figure 4.10 Insertion operator example.

*iv. Deletion operator*

The deletion operator is used to remove a group from a given molecular structure (Figure 4.9). It can lead to the deletion of whole branches of the molecule. A group of the graph is randomly chosen ( $-C<$ ). The group can be deleted if it has two bonds of the same type. As a result, the extra branches are deleted and two remaining bonds (same type) are directly recombined. In Figure 4.11, the  $>CH-CH=CH-CH_3$  (blue coloured) is deleted, and the group  $-CH_3$  is connected directly to the remaining fragment (black coloured), resulting in a new molecule.

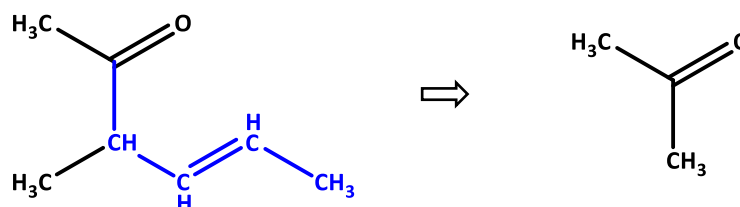


Figure 4.11 Deletion operator example.

*v. Substitution operator*

This operator is typically adopted to modify aromatic rings, which cannot be done by the previous operators. It combines the principles of mutation and insertion, which includes the replacement of a group with a group that has more connections. In Figure 4.12, the  $-CH=$  group is replaced by a more complex fragment (orange in colour). Both groups are selected at random and the same method as insertion is used to complete the new connections.



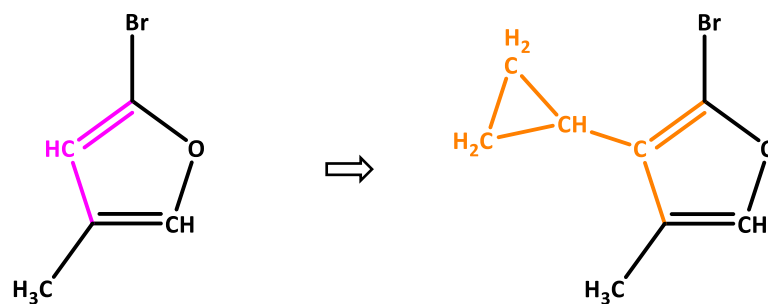


Figure 4.12 Substitution operator example.

#### 4.2.4 Candidate ranking and final choice

While the IBSS<sup>®</sup>CAMD results allow the ranking of the solvent candidates according to their *GloPerf* values, a final selection by the user is often still required to take into account properties that are out-of-reach to IBSS<sup>®</sup>CAMD. For instance, the final toxicity levels for the selected solvents are not provided by IBSS<sup>®</sup>CAMD. Neither do the results allow to evaluate the complexity and related costs for the synthesis of the new solvents. Also, experimental values are needed to confirm the actual performance of each candidate.

### 4.3 Conclusion

The IBSS<sup>®</sup>CAMD tool presented in this chapter has several features that makes it particularly well suited for many applications.

- 1) the target properties can be freely chosen in view of the target application.
- 2) the relative importance of each target property can be adjusted by weight factors to take into account their possible impact on the solvent desired functionality
- 3) the Gaussian performance functions can be selected in accordance with the actual application.
- 4) the tolerance margins counterweigh to some extent the uncertainty of the

property estimation methods.

Due to these advantages, the IBSS<sup>®</sup>CAMD can be seen as an efficient tool for the solvent selection and new solvent design in the organic photovoltaic field. In the following chapter, we will describe the case study of selecting alternative solvents for the elaboration of OPV devices.

# CHAPTER 5

---

CASE STUDY: ALTERNATIVE SOLVENT  
SELECTION FOR P3HT BASED OPV DEVICES  
BY IBSS<sup>®</sup>CAMD

---

## 5 Case Studies: Alternative Solvent Selection for P3HT Based OPV Devices By IBSS®CAMD

In this thesis, we apply the IBSS®CAMD reverse engineering tool to find alternative biosolvents for processing organic photovoltaic materials. The method is applied to blends of poly (3-hexylthiophene) (P3HT) and [6,6]-phenyl-C71-butyric acid methyl ester (PC<sub>71</sub>BM) as well as to P3HT blended with Ethylhexyl-rhodanine-benzothiadiazole-coupled indacenodithiophene (EH-IDTBR). The chemical structure of P3HT, PC<sub>71</sub>BM and EH-IDTBR are shown in Figure 5.1. P3HT is a well-known electron-donor polymer that has been extensively studied for OPV applications and is therefore a good reference for testing our methodology.<sup>149</sup> In addition, despite the extensive literature data on P3HT based solar cells, only few examples have dealt with the green solvent issue. Toluene and ethyl benzenecarboxylate (EB), an additive, have been used by Shen et al. and resulted in a maximum PCE of almost 5%.<sup>113</sup> Chueh et al. used o-xylene and processing additive 1,2-dimethylnaphthalene (1,2-DMN) to replace o-DCB on P3HT: indene-C60 bisadduct (IC<sub>60</sub>BA) based devices leading to a PCE of 5.7%.<sup>150</sup> EH-IDTBR is a promising non-fullerene acceptor that has recently generated a lot of interest in replacing fullerene derivatives and improving the PCE of P3HT-based devices.<sup>127,151,152</sup> We have therefore chosen P3HT:EH-IDTBR as a second example to illustrate how IBSS®CAMD applies to different materials and paves the way towards a more versatile and efficient approach for identifying alternative solvents.

As we discussed in Chapter 3, the morphology of the organic layer is usually the result of a phase separation between both organic constituents that occurs during processing of the film from solution.<sup>114,153</sup> Pure domains are essential for exciton generation and charge carrier transport, while exciton dissociation into free charge carriers occurs at the interface between donor and acceptor domains.<sup>153–155</sup> The morphology of the active layer at the nanoscale is therefore a key factor underlying the performance of BHJ OPV devices. Although many studies have highlighted the existing correlations between various solvent properties and blend morphology, it is not yet possible to fully anticipate the solvent properties that are best suited to

process a given blend to its optimum.<sup>24,35,87,156</sup> Extensive optimization of the blend composition and processing conditions is therefore still required to achieve the highest power conversion efficiency with a given donor/acceptor system. It should be noted that in many cases solvent additives have been necessary to reach maximum efficiency.

In the following, we will first present the multiple steps that need to be considered when applying IBSS®CAMD to the identification of alternative solvents for OPV. Next, the method is applied to P3HT:PC<sub>71</sub>BM and P3HT:EH-IDTBR blends to identify new biosolvents for the fabrication of OPV devices. Finally, the photovoltaic performances of devices processed from these solvents are compared to those obtained from halogenated solutions.

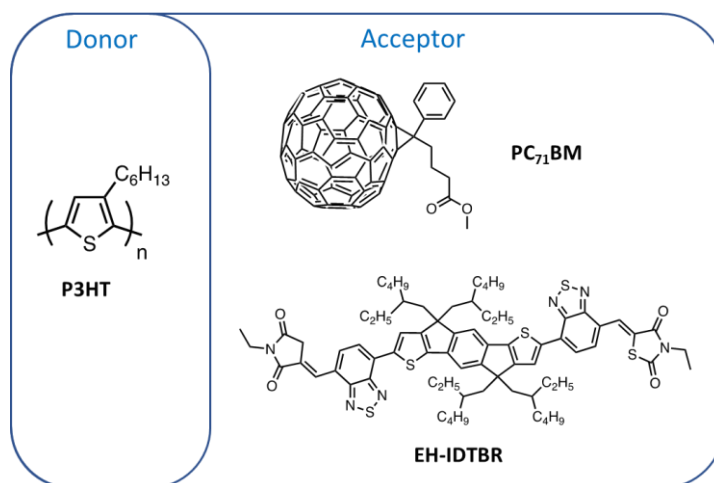


Figure 5.1 Chemical structure of donors and acceptors.

## 5.1 Defining the Conditions to Apply IBSS®CAMD to OPV

In the following, we apply the IBSS®CAMD tool described in Chapter 4 to both blends. Six steps are required for IBSS®CAMD to search alternative solvents (see section 4.2).

### 5.1.1 Initial problem definition: Functionalities of existing solvent

For the solution-processed BHJ OPV devices, the active layer is processed from a solution containing both donor and acceptor materials. It is thus essential that the

alternative solvents provide good solubility with respect to both organic materials. The morphology of the active layer is strongly dependent on the kinetics of the film-forming and drying processes and needs to match closely the configuration that leads to a maximum PCE. In addition, the alternative solvents should be Newtonian fluids, so that the active layer can be formed by a standard printing process. Keeping solvents in the liquid state at room temperature is also a prerequisite to elaborate thin films and reduce the difficulty and energy consumption during the process. Furthermore, the safety of solvents is obviously an important “functionality”.

### **5.1.2 Translation of functionalities into physicochemical properties and definition of target values**

The physicochemical properties and the corresponding target values are defined so as to achieve the functionalities set above. In some cases, several properties are associated with one functionality, for instance, surface tension and boiling point both have an effect on film drying. It is noted that the IBSS®CAMD tool is a computer-based prediction method, therefore the reliability and limitations of these property prediction models can directly affect the final results. For example, the boiling point is easily predicted and the predictions match the experimental results. However, surface tension predictions were poorly matched to experimental results. The match between the predicted and experimental values of several properties has been illustrated in Figure 5.2. For required properties that have less accurate predictive models, such as melting point, a low  $w_p$  value reduces the impact on the final results.

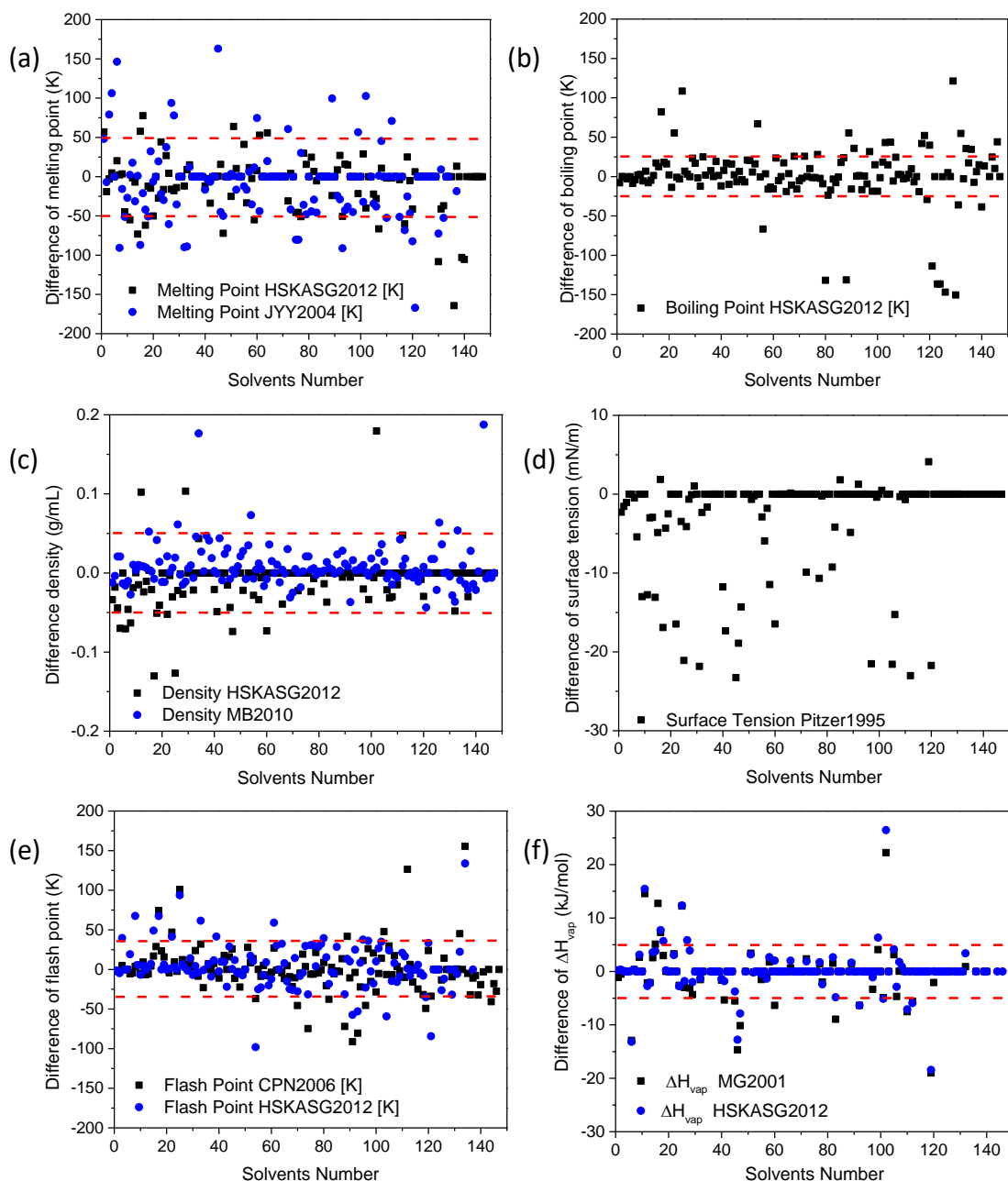


Figure 5.2 Differences between experimental data and IBSS®CAMD predicted values for various properties.

The miscibility between alternative solvents and organic materials can be predicted by the Hansen solubility parameter theory (HSPs). Within this theoretical framework, the cohesive energy is divided into three intermolecular interactions which are: the dispersion interactions ( $\delta_D$ ), the permanent dipole molecular interactions ( $\delta_P$ ), and the hydrogen bonding type interactions ( $\delta_H$ ).<sup>125</sup> The miscibility between a solvent and a solute can be estimated by the relative energy difference (*RED*) in the Hansen space (see Chapter 3). Following the classical rule “like dissolves

like”, the affinity between a solvent and a solute increase with decreasing *RED*. A *RED* value below 1 indicates that the material is miscible to some extent. The lower the *RED* value the higher the solubility limit. In addition,  $R_a$  is the “effective distance” between solvent and solute coordinates in Hansen space. A smaller  $R_a$  means a higher affinity between the solvent and the solute.

The kinetics of film-drying primarily depend on the boiling point and vaporization enthalpy of the solvents during film printing. The boiling point is known to impact the polymer crystallinity (in case of a semi-crystalline polymer such as P3HT) and the donor/acceptor average domain sizes.<sup>60,157</sup> These parameters are therefore critical for the final device performance.

The Newtonian fluid behavior is related to moderate viscosity and density of solvents, two parameters that have to be taken into account for achieving high quality films (optimized thickness, homogeneity). A solvent that remains in the liquid state at room temperature needs to have a low melting point. Finally, the flash point, which determines the flammability of solvents and therefore the risks for explosion during the devices processing, should also be considered.

Based on the above, we have selected 11 target properties to be used by IBSS®CADM to evaluate the performance of alternative solvents, as summarized in Table 5.1.

For each property the target values can in principle be defined following two approaches based either on preliminary experimental measurements or on reference solvents. We followed the first approach to specify the target solubility properties. The alternative solvents need to solubilize both the donor and acceptor molecules, i.e. in our case P3HT and PC<sub>71</sub>BM or EH-IDTBR. Therefore, the HSPs of P3HT, PC<sub>71</sub>BM and EH-IDTBR have been determined experimentally.

Firstly, the solubility of a solute is tested in a list of solvents. The solvents are ranked into 1 (“good” solvents), 0 (“bad” solvents) and 2 (between “good” and “bad” solvents), depending on their capacity to solubilize the solute. The software HSPiP uses the scores to build a solubility sphere which separates good and bad solvents. The center of the HSP solubility sphere yields the HSP parameters of the solute. The radius



of the sphere,  $R_0$ , defines the region in HSP space corresponding to the solvents that are able to solubilize the solute. The larger  $R_0$  the more easily soluble is the solute.

Table 5.1 The target properties, corresponding values for P3HT:PC<sub>71</sub>BM blends and P3HT:EH-IDTBR blends. (<sup>a</sup> P3HT:PC<sub>71</sub>BM blends, and <sup>b</sup> P3HT:EH-IDTBR blends.)

Functionalities	Target properties	Target values	Parameters		
			$w_p$	$\sigma_L$	$\sigma_R$
Solubility	$\delta_D$ (MPa) <sup>1/2</sup>	18 < $\delta_D$ < 20 <sup>a</sup>	1	0.48	0.21
	$\delta_P$ (MPa) <sup>1/2</sup>	4 < $\delta_P$ < 6 <sup>a</sup>	1	0.56	0.48
	$\delta_H$ (MPa) <sup>1/2</sup>	3.5 < $\delta_H$ < 6	1	0.24	0.48
	$R_a$ (MPa) <sup>1/2</sup>	$R_a$ < 3	3		0.84
	$RED$	< 1	2		0.28
Film drying	Boiling point ( $T_b$ /K)	373 < BP < 473	2	8.4	10.6
	Vaporization enthalpy ( $\Delta H_{vap}$ kJ/mol)	40 < $\Delta H_{vap}$ < 55	1	1.7	1.7
Film processing/ Newtonian fluid	Density (kg/m <sup>3</sup> )	800 < $\rho$ < 1500	1	19.8	19.8
	Viscosity (mPa/s)	0.5 < $\mu$ < 1.5	1	0.13	0.13
Safety	Flash Point ( $T_{ff}$ /K)	> 296	1	2.8	
Liquid state	Melting point ( $T_m$ /K)	< 283	0.5		4.2

In this work, a series of solutions were prepared with a solute concentration of 2 mg/ml. Mostly common solvents, already available in the lab, were used for the HSP measurements. The prepared solutions were annealed at 40°C overnight. The Hansen parameters of EH-IDTBR were found to be  $\delta_D=18.8 \pm 0.3$ ,  $\delta_P=4.4 \pm 0.75$ ,  $\delta_H=4.3 \pm 0.80$ , and  $R_0$  was found to be 6.1. The error margins correspond to the standard deviation of the mean values.

The solubility experiments of P3HT were done by Dr. Markus Kohlstädt at the Albert Ludwigs Universität Freiburg. The HSPs of P3HT were estimated to  $\delta_D=18.5$ ,

$\delta_P=4.7$ ,  $\delta_H=5.0$ , and  $R_0=4.7$ . The HSPs of PC<sub>71</sub>BM have been reported in literature and are given by  $\delta_D=20.2$ ,  $\delta_P=5.4$ ,  $\delta_H=4.5$ ,  $R_0=8.4$ .<sup>113</sup> The positions of P3HT/PC<sub>71</sub>BM and P3HT/EH-IDTBR in Hansen space are shown in Figure 5.3a and 5.3b, respectively.

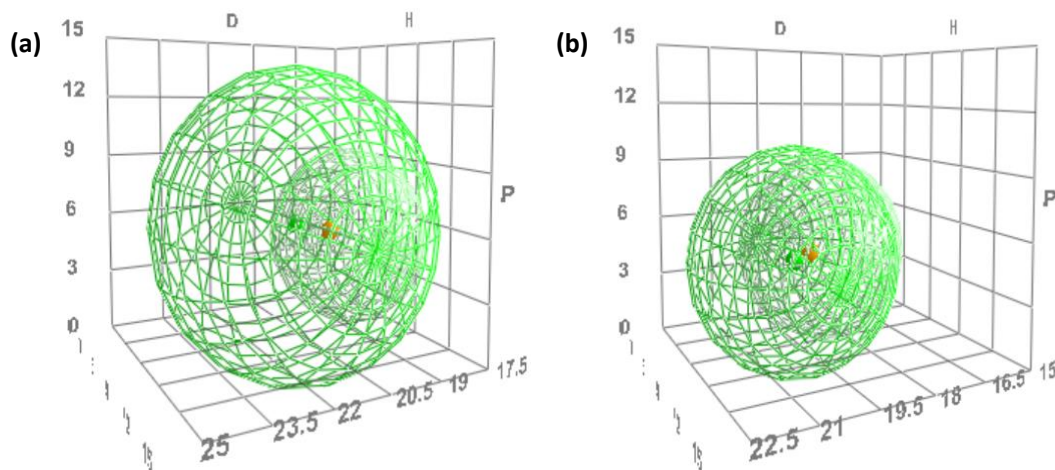


Figure 5.3 (a) The positions of P3HT and PC<sub>71</sub>BM in Hansen solubility space, (b) the positions of P3HT and EH-IDTBR in Hansen solubility space.

For P3HT:PC<sub>71</sub>BM blends, the overlap between Hansen spheres (or Hansen junction) of both molecules defines the HSP space for solvents that solubilize both molecules. The Hansen junction “barycenter”, which defines the coordinates of the solvent that should interact most efficiently with both materials, can be estimated by the HSPiP software<sup>158</sup>. For P3HT:PC<sub>71</sub>BM, the junction barycenter values are 19.1, 5.0, 4.8 for  $\delta_D$ ,  $\delta_P$  and  $\delta_H$ , respectively. Therefore, the HSP target ranges for P3HT:PC<sub>71</sub>BM blends are chosen as  $18 < \delta_D < 20$ ,  $4 < \delta_P < 6$ , and  $3.5 < \delta_H < 6$ , respectively. Note that the inequalities for the HSP target values given above are not enough to warrant a good solubility for both materials in the selected solvent. It is indeed necessary that the solvent HSPs also lead to  $RED < 1$  for each compound. In our case, the rather high solubility radius  $R_0$  of PC<sub>71</sub>BM leads the Hansen solubility spheres of P3HT to be located fully inside of the solubility sphere of PC<sub>71</sub>BM (Figure 5.2a). Therefore, an alternative solvent for which  $RED < 1$  for P3HT will necessarily be miscible with PC<sub>71</sub>BM as well.

The junction values of P3HT:EH-IDTBR are 18.6, 4.5, 4.8 for  $\delta_D$ ,  $\delta_P$  and  $\delta_H$ , therefore the target ranges of HSPs are set to  $17.5 < \delta_D < 19.5$ ,  $3.5 < \delta_P < 5.5$ , and  $3.5 < \delta_H < 6$ , respectively. The position of P3HT and EH-IDTBR in the HSP solubility space can be found in Figure 5.2b. Again, the solubility spheres of P3HT and EH-IDTBR fully overlap, so that the solubility requirement can be satisfied with  $RED < 1$  for P3HT only. For the solvent not to be classified as dangerous according to flammable and combustible liquid hazard classifications (National Fire Protection Association, NFPA)<sup>159</sup>, its flash point needs to be larger than 296.15K. Similarly, a melting point lower than 283.15K is requested to keep the solvents in its liquid state at the processing temperature.

For the properties  $R_a$ , boiling point,  $\Delta H_{vap}$ , density, and viscosity, the target values have been defined by using the second approach mentioned above, i.e. using the key properties of a “reference” solvent that is known to yield high-performance OPV devices. For the investigated materials, *o*-DCB is a good choice as it dissolves efficiently P3HT and has led to the highest power conversion efficiencies with the P3HT:PC<sub>70</sub>BM blends. For the P3HT:EH-IDTBR system, CB is considered to be the best “reference” solvent for the OPV field. The experimental database of the target properties for *o*-DCB and CB are summarized in Table 5.2. As the  $R_a$  values between *o*-DCB/CB and P3HT are 2.83 and 3.19 respectively, the target value for  $R_a$  is set to be lower than 3. Note that by taking into account simultaneously  $R_a$ , HSPs and RED, a significant weight is put onto the solubility of the polymer (which is a critical functionality), while keeping the impact of the error margin of RED on the global performance factor reasonably low, unlike what would occur if the weight  $w_p$  for the RED property would have been increased instead.

Table 5.2 The physicochemical properties and corresponding values of *o*-DCB and CB.

Physicochemical properties	Property values	
	<i>o</i> -DCB	CB
Non-polar interactions ( $\delta_D$ , MPa <sup>1/2</sup> )	19.2	19.0
Polar interactions ( $\delta_P$ , MPa <sup>1/2</sup> )	6.3	4.3
Hydrogen bonds ( $\delta_H$ , MPa <sup>1/2</sup> )	3.3	2.0
Distance ( $R_a$ , MPa <sup>1/2</sup> ) with P3HT	2.83	3.19
Relative energy difference (RED) with P3HT (defined by $R_a/R_o$ )	0.64	0.68
Boiling Point ( $T_b$ , K)	453	405
Evaporation enthalpy ( $\Delta H_{vap}$ , kJ/mol)	49.08	40.76
Density ( $\rho$ , g/cm <sup>3</sup> )	1.31	1.11
Viscosity ( $\eta$ , mPa s)	1.30	0.76
Flash Point ( $T_f$ , K)	339	301
Melting Point ( $T_m$ , K)	256	228

As shown in table 5.2, the experimental values for the boiling point, vaporization enthalpy, density, and viscosity are relatively close for both reference solvents. Therefore, same target ranges for a given target property were chosen identical for both systems. More precisely, for the boiling point the target range for the alternative solvent is set to [373 K, 473 K]<sup>151,160</sup>, while for the vaporization enthalpy, density, and viscosity, the target ranges are [35 kJ/mol, 55 kJ/mol], [0.8 g/cm<sup>3</sup>, 1.5 g/cm<sup>3</sup>], and [0.5 mPa/s, 1.5 mPa/s] respectively. All the target values are summarized in Table 5.1.

### 5.1.3 Selection of the predictive models

As mentioned above, the group contribution method is used in IBSS®CADM to predict the solvent properties. The value of a given property,  $P$ , can be calculated using a property-estimation model and additional adjustable model parameters which

depend on the property involved. The property-estimation model is based on the group contribution method and has the form of equation (10). The universal constants for each individual property were determined by a regression scheme that can be found in Table 5.3.

The density,  $\rho$ , of a given molecule is calculated using equation (16).

$$\rho = \frac{M_W}{V_m} = \frac{M_W}{V_m(P)} \quad (16)$$

where  $M_W$  is the molecular weight and  $V_m$  the molecular volume. The molecular volume is calculated based on the group contribution method from equation (17) The universal constant for the molecular volume,  $V_{m0}$ , is summarized in Table 5-3.

$$V_m - V_{m0} = \sum_{k \in G1} n_{1k} A_k + w_2 \sum_{k \in G2} n_{2k} B_k + w_3 \sum_{k \in G3} n_{3k} C_k \quad (17)$$

Table 5.3 Group contribution method-based property models and Universal constants for the target properties.

Property (X)	$P =$	Universal constants	Refs
$\delta_D$ (MPa <sup>1/2</sup> )	$\delta_D$		161
$\delta_P$ (MPa <sup>1/2</sup> )	$\delta_P$		161
$\delta_H$ (MPa <sup>1/2</sup> )	$\delta_H$		161
Boiling Point ( $T_b$ , K)	$EXP(T_b/T_{b0})$	222.543	142
Evaporization enthalpy ( $\Delta H_{vap}$ , kJ/mol)	$H_{vap} - H_{vap0}$	11.733	142
Molecular volume ( $V_m$ , cm <sup>3</sup> /kmol)	$V_m - V_{m0}$	0.0160	162
Viscosity ( $\eta$ , mPa s)	$\ln \eta$		163
Flash Point ( $T_f$ , K)	$T_f - T_{f0}$	170.7058	162
Melting Point ( $T_m$ , K)	$EXP(T_m/T_{m0})$	147.450	142

#### 5.1.4 Definition of the global performance function

Table 5.1 displays the functionalities and the associated target properties for alternative solvents together with the chosen  $\sigma$  and  $w_p$  parameters. The  $\sigma$  values are set by considering the uncertainty on the selected target values and the estimated tolerance margin on the corresponding property. The  $w_p$  values are chosen by pondering the possible influence of the property on the performances of the devices, as indicated in table 1. For instance, the solvent evaporation rate, which depends on both the boiling point and  $\Delta H_{vap}$ , influences the amount of residual solvents in deposited films as well as the degree of phase separation between donor and acceptor molecules during the film processing. We therefore set  $w_p$  to 2 and 1 for the boiling point and  $\Delta H_{vap}$  respectively, i.e., a cumulative weight of 3 on the solvent evaporation kinetics.

#### 5.1.5 Molecular design parameters

As mentioned above, IBSS®CAMD tool can be used in two different modes: to evaluate the performances of existing solvents with respect to target properties or to design new molecules and optimize their structure to fit the target properties. We have used the first mode for both P3HT:PC<sub>71</sub>BM and P3HT:EH-IDTBR blends, and the second mode for P3HT:PC<sub>71</sub>BM only.

*Existing solvents performance evaluation:* 139 biosolvents<sup>164</sup> were selected as target solvents (see appendix 9.4), represented by their SMILES (simplified molecular input line entry specification) code and evaluated by IBSS®CAMD through its first operating mode.

*Molecular design:* New molecules have been built from a list of chemical groups connected randomly by specifying possible positions and bond types (single or double) for each group. The complete chemical groups are used in IBSS®CAMD for P3HT:PC<sub>71</sub>BM blend are shown in appendix 9.3. Halogen elements like -Cl, -Br -I are discarded from the chemical group list to avoid a-priori toxic solvents.

During the molecular design mode, thousands of molecular structures are generated and their performance evaluated using IBSS®CAMD, ending up with a list of 10102 candidate solvents.

### 5.1.6 Candidate ranking and final choice

*Selection from the list of existing solvents.* For P3HT:PC<sub>71</sub>BM and P3HT:EH-IDTBR blends, nine evaluated candidate solvents achieved a *GloPerf* > 0.6 and are reported in Table 5.4 and 5.5, respectively. The corresponding full sets of *ProPerf<sub>p</sub>* values are given in Appendix 9.5 and 9.6. Among these best ranked solvents, eight solvents, namely anisole (AN), p-xylene (PX), butyl acetate (BA), tetrahydrofuran (THF), terpinolene (TPO) and p-cymene (PC), isoamyl acetate (IA), d-limonene (LM) are selected for both P3HT:PC<sub>71</sub>BM and P3HT:EH-IDTBR blends, while Benzyl benzoate (BBzo) occurs only for P3HT:PC<sub>71</sub>BM, and cyclopentyl methyl ether (CPME) for P3HT:EH-IDTBR. The performance evaluation for the remaining solvents is given in Appendix 9.5 and 9.6.

Further analysis of the individual *ProPerf<sub>p</sub>* values leads us to dismiss some of these solvents:

- BBzo is removed because its boiling point,  $\Delta H_{vap}$  and viscosity lead to a *ProPerf<sub>p</sub>*  $\approx 0$ , their estimated values being far above the target, and may hinder film formation and drying.<sup>95</sup>

- CPME should be removed due to its low flash point (280 K) in order to avoid safety problems during usage and storage. Also, the low  $\Delta H_{vap}$  of CPME (37 kJ/mol) should give rise to rapid evaporation and result in insufficient phase separation between donor and acceptor materials and low P3HT crystallinity.<sup>60</sup> Importantly, today the commercial CPME is currently produced from fossil resources although it could be bio-based.<sup>165</sup>

- Similarly, THF is not retained because of its low boiling point (338 K). The RED of

P3HT in *THF* is 0.728 under a concentration of 2 mg/ml, while a concentration of 10 mg/ml for P3HT is needed for OPV devices processing. A high processing temperature can improve the solubility of P3HT in a solvent, but the low boiling point of *THF* limits this. In addition, commercial *THF* is also currently Petro-sourced.

- *IA* and *BA* are omitted because their *REDs* are larger than 1 for P3HT ( $ProPerf_p(RED) \approx 0$ ).

For the remaining candidate solvents *AN* shows the best performance with the *GloPerf* values of 0.997 and 0.946 for P3HT:PC<sub>71</sub>BM and P3HT:EH-IDTBR respectively. Only the  $ProPerf_p$  value for  $\delta_H$  is slightly off the target value ( $ProPerf_p = 0.957$ ).

*PX* shows high *GloPerf* values of 0.853 for P3HT:PC<sub>71</sub>BM and 0.861 for P3HT:EH-IDTBR, however, the low  $ProPerf_p$  values of  $\delta_H$  ( $\approx 0$ ) and  $R_a$  (0.66) for both blends, indicating that *PX* is a poorer solvent for P3HT than *o*-DCB. Yet, the *RED* of *PX* is 0,75 (<1), showing that *PX* can still dissolve P3HT, PC<sub>71</sub>BM and EH-IDTBR.

Compared to *An* and *PX*, *PC*, *TPO* and *LM* have lower *GloPerf*, meaning that more properties show a poor match with the corresponding target properties (Appendix 9.5, 9.6). For example, the  $ProPerf_p$  of  $\Delta H_{vap}$  of 0.34 for *TPO* may impact the film drying kinetics of the active layer. In addition, these three solvents have a low  $ProPerf_p$  value for  $R_a$  due to the poor match of their HSPs' properties with the corresponding target properties (Appendix 9.5, 9.6). But their *RED* values are still lower than 1, indicating that P3HT can be dissolved in these three solvents despite the poorer solubility than that in *AN*.

We finally retained *AN*, *PX*, *TPO*, *PC* and *LM* for both blends and investigated the device performances that could be achieved using these solvents as alternative to *o*-DCB.



Table 5.4 The candidates provided for P3HT:P<sub>71</sub>BM blends by IBSS®CAMD with a GloPerf > 0.6. (/: non-available data)

Candidates	CAS	GloPerf	T <sub>b</sub>	ProPerf <sub>P-T<sub>b</sub></sub>	$\Delta H_{vap}$	ProPerf <sub>P-<math>\Delta H_{vap}</math></sub>	RED	ProPerf <sub>P-RED</sub>	Viscosity	ProPerf <sub>P-Viscosity</sub>
o-DCB	95-50-1	1	449	1	50.1	1	0.59	1	1.089	1
Anisole (AN)	100-66-3	0.997	428	1	46.5	1	0.3	1	0.569	1
p-Xylene (PX)	106-42-3	0.853	419	1	43.4	1	0.75	1	0.568	1
Isoamyl acetate (IA)	123-92-2	0.674	420	1	48.9	1	1.19	0.64	0.903	1
Benzyl Benzoate (BBzo)	120-51-4	0.667	573	≈ 0	85.8	≈ 0	0.65	1	5.224	0
p-Cymene (PC)	99-87-6	0.628	450	1	50.1	1	0.89	1	0.897	1
Terpinolene (TPO)	586-62-9	0.626	448	1	38.3	0.34	0.93	1	0.748	1
Butyl acetate (BA)	123-86-4	0.621	407	1	46	1	1.21	0.58	0.724	1
Tetrahydrofuran (THF)	109-99-9	0.609	323	≈ 0	32	≈ 0	0.73	1	0.557	1
d-Limonene (LM)	138-86-3	0.598	452	1	44.4	1	0.94	1	/	0

Table 5.5 The candidates provided for P3HT:EH-IDTBR blends by IBSS®CAMD with a  $GI_{\text{Perf}} > 0.6$ . (/: non-available data)

Candidates	CAS	$GI_{\text{Perf}}$	$T_f$	$ProPerf_p$ - $T_f$	$\Delta H_{\text{vap}}$	$ProPerf_p$ - $\Delta H_{\text{vap}}$	$R_o$	$ProPerf_p$ - $R_o$	RED	$ProPerf_p$ -RED	Viscosity	$ProPerf_p$ - Viscosity
CB	108-90-7	1	300	1		1	1.58	1		1		1
Anisole (AN)	100-66-3	0.997	314	1	46.5	1	1.39	1	0.3	1	0.569	1
p-Xylene (PX)	106-42-3	0.861	301	1	43.4	1	3.54	0.66	0.75	1	0.568	1
p-Cymene (PC)	99-87-6	0.680	323	1	50.1	1	4.20	0.13	0.89	1	0.897	1
Isoamyl acetate (IA)	123-92-2	0.674	312	1	48.9	1	5.59	$\approx 0$	1.19	0.64	0.903	1
Terpinolene (TPO)	586-62-9	0.640	308	1	38.3	0.34	4.35	0.08	0.93	1	0.748	1
Tetrahydrofuran (THF)	109-99-9	0.624	243	$\approx 0$	32	$\approx 0$	3.42	0.78	0.73	1	0.557	1
Butyl acetate (BA)	123-86-4	0.621	305	1	46	1	5.67	$\approx 0$	1.21	0.58	0.724	1
Cyclopentyl methyl ether (CPME)	5614-37-9	0.612	281	$\approx 0$	37.3	0.07	4.20	0.13	0.89	1	0.494	0.87
d-Limonene (LM)	138-86-3	0.603	311	1	44.4	1	4.42	0.06	0.94	1	/	0

*Molecular design.* A total of 10102 designed solvents were evaluated by IBSS®CAMD, leading to a significantly larger number of solvents with a high global performance factor. The purpose of using the IBSS®CAMD tool in OPVs is to find alternative solvents to replace toxic halogenated solvents. Therefore, 14 designed solvents with high *GloPerf* values over 0.9 for further investigation, which were listed in Table 5.6. The complete predicted values of solvents whose *GloPerf* values are larger than 0.9 are given in Appendix 9.7 together with the performance factors. 4-Ethynyltoluene (4-ET) and 3-Ethylcyclopentane-1-Carbaldehyde (3-EC-1-C) are two perfect solvents with a *GloPerf* value of 1, indicating that the estimated values of both have a perfect match with the target values. The next best ranked solvent is 4-Methylphenyl Vinyl Ether (4-MPVE) with a *GloPerf* of 0.998, because the boiling point (474 K) and  $\Delta H_{vap}$  (55.26 kJ/mol) of 4-MPVE are slightly larger than the corresponding target values resulting in a non-perfect match. Interestingly, AN, which were included in the list of pre-selected solvents (see above) also occurs in the list of designed solvents among the best ranked solvent, pointing out the consistency between both methods. All designed solvents (listed in Table 5.6) show a *ProPerf<sub>p</sub>* of 1 for RED, meaning these candidates can dissolve P3HT:PC<sub>71</sub>BM blends.

Obviously, molecular design provides a large choice for alternative solvents with a high global performance factor that is not limited by the list of existing solvents defined by the user. However, further evaluation of the best ranked candidates is required to verify predicted performance by using experimental values and to take into account non-evaluated properties such as cost, commercial availability, established synthesis method, chemical structure stability in air, toxicity.... Table 5.6 summarizes three non-evaluated properties which have been considered in the further selection of the best alternative solvent for P3HT:PC<sub>71</sub>BM blends. 10 out of 14 candidates are commercially available. But considering their cost, only 3 candidates, which are AN, 2-Methyl Anisole (2-MA) and Methyl Benzoate (MB), have been retained. In addition, the chemical stability in air of alternative solvents is another important non-evaluated

property that is associated with the active layer treatment method and device stability and needs to be taken into account.

Table 5.6 List of the best solvent candidates selected from the results of molecular design provided by IBSS®CADM. (Y: yes, N: no, NA: non-available data)

Candidates	CAS	<i>GloPerf</i>	Commerciality	Cost (€/g)	Stable (at room temperature)
4-Ethynyltoluene	766-97-2	1	Y	9.3	N
3-Ethylcyclopentane-1-carbaldehyde	NA	1	N	NA	N
4-Methylphenyl vinyl ether	1005-62-5	0.998	N	NA	NA
Anisole	100-66-3	0.997	Y	0.4	Y
Allyl phenyl ether	1746-13-0	0.989	Y	1.9	Y
Phenyl vinyl ether	766-94-9	0.978	Y	4230	N
4-Acetylcyclohexene	7353-76-6	0.977	Y	1961.6	NA
2-Methyl anisole	578-58-5	0.946	Y	0.7	Y
2-Vinyl anisole	612-15-7	0.931	Y	39.8	N
Methyl benzoate	93-58-3	0.923	Y	0.9	Y
4-Methoxystyrene	637-69-4	0.923	Y	20.0	Y
(1R,2R)-2-Vinylcyclohexanecarbaldehyde	NA	0.920	N	NA	N
3-Cyclohexen-1-yl methyl ether	15766-93-5	0.916	Y	3712	NA
Cyclopentyl formate	62781-99-1	0.901	N	NA	N

4-Ethynyltoluene (4-ET) is an “ideal” solvent with a *GloPerf* value of 1, indicating that the estimated values have a perfect match with the target values. Phenyl Vinyl

Ether (*PVE*) is susceptible to moisture deterioration, therefore it needs to be stored and handled under nitrogen. Thus, *PVE* has also been avoided. At last, among the three remaining designed solvents, *AN*, *2-MA* and *MB*, *MB* has a higher boiling point (470 K) and a larger  $\Delta H_{vap}$  (55.6 KJ/mol). Therefore, taking into account the energy consumption for film drying, we considered *4-ET*, *AN* and *2-MA* as the better options for processing OPV devices. Since *AN* has already been selected from the list of existing candidates (Table 5.4), we have limited our device investigations to blends that were processed from the commercially available *4-ET* and *2-MA*.

## 5.2 Photovoltaic Performance

To evaluate the quality of the alternative solvents identified by IBSS®CADM, we have elaborated OPV devices using each of the previously selected biosolvents. Reference devices processed from *o*-DCB and CB solutions were also investigated. An inverted OPV structure is adopted in this thesis. It includes ITO as transparent electrode, ZnO as electron transporting layer, MoO<sub>3</sub> as hole transporting layer and Ag as top electrode. The active layer was composed of either P3HT:PC<sub>71</sub>BM or P3HT:EH-IDTBR blends with a 1:0.7 weight ratio. The solutions were annealed and stirred overnight at various processing temperatures in nitrogen ambient (see Table 5.7). A slightly higher processing temperature was adopted for the poorer solvents *PC*, *TPO* and *LM*. The thin films were elaborated by spin-coating onto substrates previously heated at the same temperature. After deposition, the films were further annealed at 135°C for 10 min, under an inert atmosphere to improve the polymer crystallinity.

The electrical properties of the devices under darkness and under illumination are recorded in Figure 5.3 and Table 5.7. In the case of *P3HT:PC<sub>71</sub>BM* blends, the performances of devices processed from *pure 4-ET*, *AN*, *PX*, *PC*, *TPO* and *LM* solutions were much lower than those of the reference device (see Figure 5.3). This brought us to add 3% of the non-halogenated diphenyl ether (DPE) as processing additive to these

solvents. It is indeed widely known that DPE can dramatically improve the OPV performances by optimizing the morphology of the active layer.<sup>97,99</sup> It is generally believed that adding DPE enhances the solubility of PC<sub>71</sub>BM and retards the formation of PC<sub>71</sub>BM aggregates. Finally, the devices processed from each of the 6 selected alternative biosolvents could achieve comparable performances to those processed from *o*-DCB.

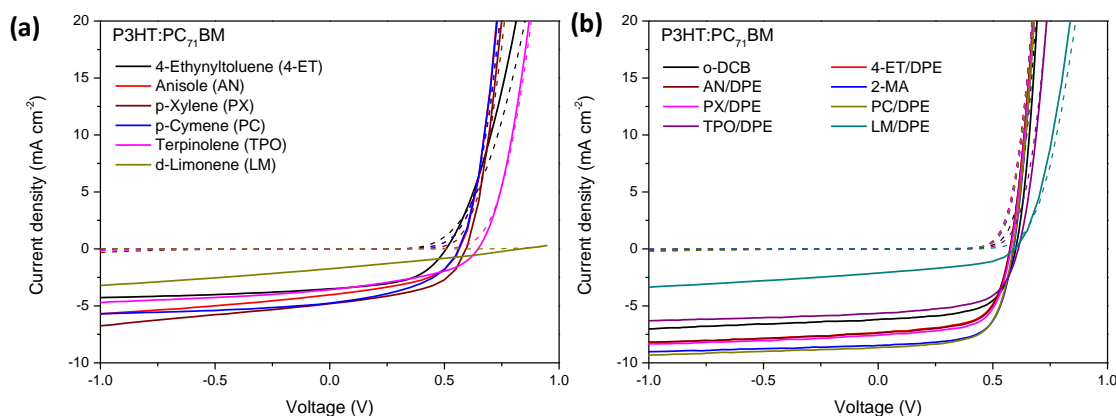


Figure 5.4 (a) The JV characteristics of P3HT:PC<sub>71</sub>BM based OPV devices processed from various solvents without DPE, and (b) with DPE.

Note that the processing conditions were kept identical to the reference solvent, except for the eventual introduction of DPE as solvent additive and the slight change in processing temperature for *PC*, *TPO* and *LM*. Interestingly, no additive was needed for devices processed from pure *2-MA*. This behavior correlates with the higher solubility of PC<sub>71</sub>BM in *2-MA* in comparison to the other alternative solvents. Also, its relatively high boiling point (443 K) should enhance the phase separation between donor and acceptor materials, presumably leading to domains of higher purity. In fact, the slight differences in performances between biosolvents may be attributed to the absence of full optimization of the deposition parameters. The latter would require additional experimental variables such as spin-coating parameters, solution concentration, processing temperature... to be optimized.

Using *TPO* and *LM* as alternative solvent led to significantly lower performance, even after the introduction of *DPE*. This is in good agreement with the lower *GloPerf* factors of *TPO* and *LM* and suggests that solvents with still lower *GloPerf* values are no more appropriate to process P3HT:PC<sub>71</sub>BM into efficient devices.

Table 5.7 OPV device parameters of P3HT:PC<sub>71</sub>BM based devices fabricated from various solvents.

Processing solvents	Processing temperature	V <sub>oc</sub> (mV)	J <sub>sc</sub> (mA/cm <sup>2</sup> )	FF (%)	PCE (%)	Thickness (nm)
<i>o</i> -DCB	80	594±5	6.3±0.1	59.0±3	2.3±0.2	~100
<i>4-ET/DPE</i>	100	575±3	7.2±0.2	61.5±2	2.6±0.1	~110
<i>4-ET</i>	100	540±6	3.3±0.5	49.2±5	0.9±0.2	~110
<i>AN/DPE</i>	100	575±3	7.4±0.1	62.9±1	2.7±0.1	~140
<i>AN</i>	100	571±5	4.2±0.2	45.7±3	1.1±0.2	~140
<i>2-MA</i>	100	587±2	8.3±0.1	64.5±1	3.1±0.2	~90
<i>PX/DPE</i>	90	577±2	7.5±0.1	63.6±1	2.7±0.2	~130
<i>PX</i>	90	585±5	4.5±0.3	50.7±2	1.1±0.3	~130
<i>PC/DPE</i>	110	585±6	8.5±0.2	65.3±1	3.3±0.1	~120
<i>PC</i>	110	555±7	5.0±0.3	42.8±4	1.2±0.2	~120
<i>TPO/DPE</i>	110	606±6	5.5±0.2	57.3±2	1.9±0.2	~90
<i>TPO</i>	110	645±8	3.5±0.2	41.8±2	1.0±0.1	~90
<i>LM/DPE</i>	110	669±7	3.3±0.2	42.8±3	1.0±0.1	~100

The JV curves of *P3HT:EH-IDTBR* devices and the extracted physical parameters are depicted in Figure 5.4 and Table 5.8. Similar photovoltaic performances could again be achieved with all the selected solvents. Also in this case, the solvent-to-solvent variations may be attributed to the incomplete optimization of the processing conditions. The highest PCE value, observed for *AN*-based devices, results mostly from

the higher fill factor and photocurrent, which in turn may be the outcome of purer domains, and therefore less recombination. However, clarifying the origin of the performance fluctuations would need more in-depth investigations that lie beyond the scope of this thesis. It is nevertheless noteworthy that no processing additive was needed to achieve efficient P3HT:EH-IDTBR based devices for none of the solvents, in contrast with the behavior of P3HT:PC<sub>71</sub>BM devices. We attribute this difference to the smaller  $R_a$  and  $RED$  values estimated for EH-IDTBR for each solvent (Table 5.9), indicating that the solubility of EH-IDTBR is higher than that of PC<sub>71</sub>BM in the corresponding solvents. In other words, a higher solubility of the small molecule acceptors is likely to retard acceptor aggregation, to reduce the domain size and increase donor/acceptor interfacial area.

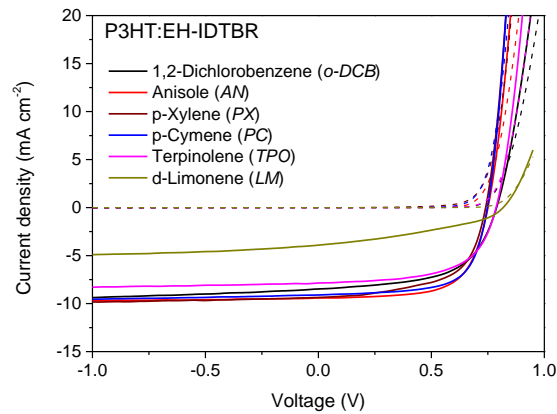


Figure 5.5 JV curves of P3HT:EH-IDTBR based OPVs processed from various solvents.



Table 5.8 The corresponding photovoltaic device parameters of P3HT:EH-IDTBR based devices fabricated from selected candidates.

Processing solvents	Processing temperature (°C)	V <sub>oc</sub> (mV)	J <sub>sc</sub> (mA/cm <sup>2</sup> )	FF (%)	PCE (%)	Thickness (nm)
CB	80	780±5	8.1±0.3	53.4±4	3.4±0.4	~120
AN	80	752±3	9.2±0.2	65.6±2	4.55±0.1	~140
PX	80	742 ±3	8.9±0.4	57.0±2	3.79±0.3	~150
PC	90	749±6	8.9±0.3	65.3±1	4.42±0.1	~120
TPO	90	787±5	7.8 ±0.1	58.8±1	3.59±0.1	~100
LM	100	816±7	3.6±0.3	35.7±2	1.04 ±0.2	~100

Table 5.9 R<sub>a</sub> and RED values between various solvents and two acceptor materials.

Processing solvents	PC <sub>71</sub> BM		EH-IDTBR	
	R <sub>a</sub>	RED	R <sub>a</sub>	RED
<i>o</i> -DCB	2.50	0.30	2.11	0.35
AN	4.52	0.54	2.24	0.37
PX	4.61	0.55	2.85	0.47
PC	6.74	0.80	3.93	0.64
TPO	7.52	0.90	4.51	0.74

### 5.3 Conclusion

A systematic reverse engineering methodology applied via IBSS®CAMD tool has been successfully used to design and select alternative solvents for OPV devices, in replacement of current toxic solvents. The method required the identification of the solvent specifications, their translation to target physicochemical properties, and for

the setting of target property values. By solving a multi-objective optimization problem with a computer assisted molecular design tool (IBSS®CADM), the alternative solvents were ranked according to a global performance value, which evaluates the matching of the behavior of alternative solvents with a set of multiple target physicochemical properties. In our cases, 11 target properties were defined to evaluate the performance of alternative solvents to achieve high-performance OPV devices. By exploring the diversity of molecular structure, the reverse engineering approach greatly expands the list of candidate solvents compared to the trial-and-error list established beforehand and can give rise to solvents that exhibit better performances. The method was applied successfully to two series of bulk heterojunctions solar cells using P3HT as electron donor and either PC<sub>71</sub>BM or EH-IDTBR as electron acceptor. For P3HT:PC<sub>71</sub>BM, five alternative solvents were found suitable to be used for OPV device processing, with an average PCE of 3.26% obtained by using p-cymene as processing solvent. For the second blend P3HT:EH-IDTBR, four alternative solvents could be identified, with anisole giving rise to the highest average PCE of 4.55%. Importantly, the selected solvents are all bio-sourced and are therefore of particular interest for future industrial up-scaling.

# CHAPTER 6

---

CASE STUDY: ALTERNATIVE SOLVENT  
SELECTION FOR NEW DONOR POLYMERS  
BY IBSS<sup>®</sup>CAMD

---

## 6 Case studies: Alternative Solvent Selection For New Donor Polymers by IBSS®CADM

Since the IBSS®CADM tool has been proven efficient on two “reference” D/A systems in the previous chapter, it is now of interest to apply it to more recent “high performance” D/A systems. In this chapter, two efficient di-fluorinated copolymers are investigated. Fluorination of conjugated polymers was first used to fine-tune the frontier molecular orbital energy levels of electron-donor polymers.<sup>166,167</sup> Surprisingly, many authors found other positive effects of fluorinated polymers. For example, mixed “face-on” and “edge-on” backbone orientations of fluorinated polymers with respect to the device substrate were frequently observed and provide high out-of-plane hole mobilities.<sup>168–172</sup> Moreover, it has been found that the purity of the domains in polymer:fullerene blends is improved when fluorine atoms are introduced into the polymer backbone.<sup>173</sup> As a consequence, fluorinated polymers led to a significant increase in the PCE of BHJ solar cells. In 2014, T. L. Nguyen et al. synthesized for instance an efficient fluorinated copolymer, poly[(2,5-bis(2-hexyldecyloxy)phenylene)-*alt*-(5,6-difluoro-4,7-di(thiophen-2-yl)benzo[*c*]-[1,2,5]thiadiazole)] (PPDT<sub>2</sub>FBT), reaching power conversion efficiencies of 9.39% for PPDT<sub>2</sub>FBT:PC<sub>71</sub>BM OPVs.<sup>171</sup> In 2018, O. A. Ibraikulov et al. has reported a study of a series of fluorinated co-polymers with different numbers of fluorine atoms. Efficiencies over 10% could be reached on 12 mm<sup>2</sup>-sized devices, elaborated from hot 1,2-dichlorobenzene (*o*-DCB) solutions, when using a bi-fluorinated copolymer, named PF2, as electron donor and PC<sub>71</sub>BM as electron acceptor.<sup>174</sup> PF2 exhibits outstanding characteristics, such as well-adjusted frontier orbital energy levels, excellent light-harvesting capabilities, high out-of-plane charge transport properties together with a high morphology robustness upon blending, that translate into high PCE.<sup>174</sup>

Up to recently, PF2-based OPV devices have been prepared using toxic *o*-DCB,

which limited the large-scale application of PF2 devices. In 2019 however, we succeeded to use non-halogenated *o*-xylene (OX) and 1,2,4-trimethylbenzene (TMB) solvents to prepare large-scale (an active area larger than 60 cm<sup>2</sup>) PF2-based ITO-free modules, obtaining a high-power conversion efficiency (PCE) of above 6%.<sup>175</sup> These two alternative solvents are less toxic than standard halogenated solvents and have been selected by a trial and error approach. However, OX and TMB cannot be bio-sourced and TMB is still classified as hazardous. Accordingly, this chapter focuses on the selection of alternative solvents from biosolvents by using IBSS®CADM for PF2-based devices.

In addition, the impact of "side chains" on organic photovoltaic polymers has attracted considerable interest. Side chains are not only necessary for conjugated polymers to allow solution processing, they also impact molecular ordering, packing, and thin-film morphology and hence organic electronics performance.<sup>176–182</sup>

In this work, we applied our solvent selection methodology based on IBSS®CADM to study the consequences of side-chain engineering on the selection of efficient green solvents. In particular, the replacement of branched alkyl-chains by linear siloxane chains on the same conjugated backbone has been considered.

Mei et al. have reported in 2011 the introduction of siloxane functional groups as side chains in isoindigo conjugated polymers to provide sufficient polymer solubility.<sup>176</sup> They found that siloxane side chain could induce an unusual face-on orientation in isoindigo conjugated polymers, giving the polymer a dual face-on and edge-on orientation and improving the charge carrier mobility in transistor devices. Tang et al. introduced siloxane functional groups as side chains for the modification of the benzodithiophene–benzotriazole alternated wide band gap copolymer, named PBDFBTA-2Si.<sup>182</sup> They found that the introduction of siloxane functional groups has only a minor effect on the absorption and frontier orbital energy levels of the polymers but a significant impact on the miscibility with nonfullerene acceptors. The blends of

PBDTFBTA-2Si and acceptor Y6 exhibited more balanced miscibility, carrier mobility, and phase separation, achieving a high PCE of 14.18% for OPVs.

Recently, the group of S. Mery synthesized PF2 derivatives with linear siloxane functional groups (instead of C<sub>20</sub>H<sub>41</sub> branched alkyl chains), named KNSF2, in order to improve the photovoltaic performance.

Here, we apply the reverse engineering method to both PF2 and KNSF2 polymers blended with either PCBM or EH-IDTBR.

## 6.1 Major Properties for Polymers

### 6.1.1 UV-Vis characterization

The chemical structures of PF2 and KNSF2 are shown in Figure 6.1. The acceptors used in this chapter are PC<sub>71</sub>BM and EH-IDTBR, the molecular structure of which can be found in Figure 5.1. The PF2 and KNSF2 polymers were synthesized by the groups of Dr. Nicolas Leclerc and Dr. Stéphane Mery.

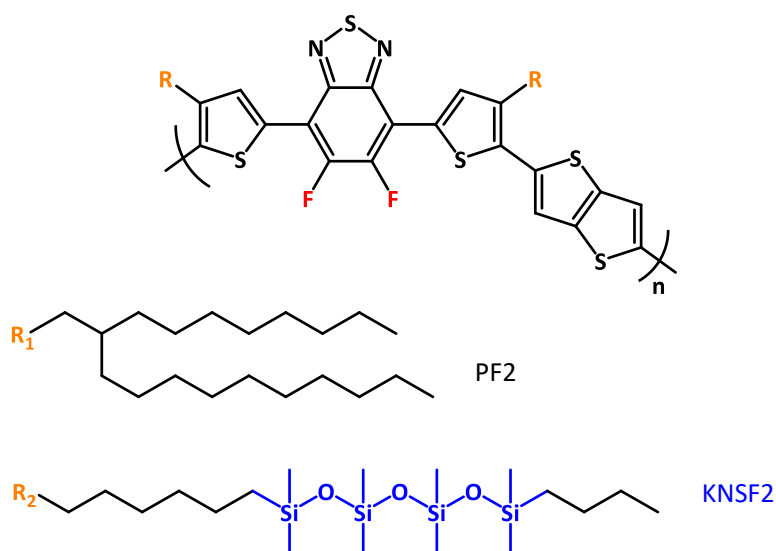


Figure 6.1 The chemical structures of donor PF2 (side chain: R<sub>1</sub>) and KNSF2 (side chain: R<sub>2</sub>).

Figure 6.2 shows the normalized UV-vis absorption spectra of pure PF2 and KNSF2 in diluted *o*-DCB solution at different temperatures and in thin films. At room temperature, the peak positions of the absorption bands in the PF2 solution were 440, 636 and 695 nm, respectively, which match closely the absorption peaks in the solid state (dashed line in Figure 6.2a). This behavior was attributed to temperature-dependent aggregation in solution, which is now considered to be responsible for the coexistence of face-on and edge-on polymer orientations in thin films.<sup>183–187</sup> There are two main processes involved in the absorption of PF2 solution: (1) at high temperatures (above 75°C), the absorption is dominated by the dissolved polymer; and (2), when the temperature is below 75°C, the absorption is dominated by the aggregated polymer. At room temperature, the absorption peaks of KNSF2 in solution appears at 698, 644, and 427 nm, respectively, which are similar to the peak positions of the PF2 solution. In addition, the absorption peaks of KNSF2 solution at room temperature coincided with the absorption peaks in film (dash line in Figure 6.2b), demonstrating that the KNSF2 forms aggregates when the active layer is processed from a solution. The absorption of KNSF2 solution exhibits a weak temperature-dependent behavior, which means that KNSF2 forms aggregates even at high temperature (95°C).

PF2 has an optical bandgap of about 1.60 eV, which is almost optimal for photovoltaic energy conversion<sup>188</sup>. The HOMO level was estimated electrochemically to -5.42 eV<sup>189</sup> while the LUMO level was calculated to be -3.83 eV, taking into account the optical band gap. KNSF2 has an optical bandgap of about 1.63 eV that is similar to PF2, which has a HOMO level of -5.25 eV.

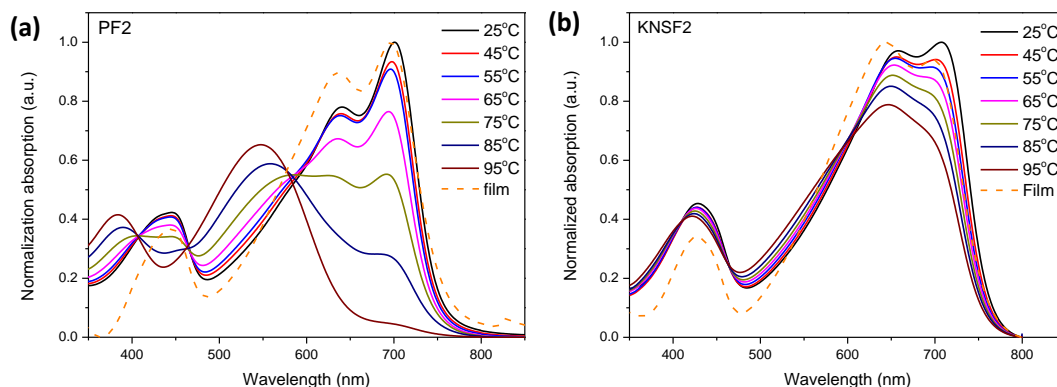


Figure 6.2 UV-Vis absorption spectra of (a) PF2 and (b) KNSF2 in solution as a function of temperature and in thin film.

### 6.1.2 Solubility and HSPs

HSPs for both polymers were measured using common solvents, covering a large portion of the Hansen space. A list of solutions were prepared with a solute concentration of 2 mg/ml. The prepared solutions were annealed at 40 °C overnight. The solvent list and related PF2/KNSF2 solubility scores are shown in Appendix 9.8. The HSPs of PF2 were found to be  $\delta_D=19.15$ ,  $\delta_P=3.87$ ,  $\delta_H=2.83$ , and  $R_0$  was estimated to 4.0, while the HSPs of KNSF2 were  $\delta_D = 17.47$ ,  $\delta_P = 4.28$ ,  $\delta_H = 1.53$ ,  $R_0 = 4.9$ , respectively. Comparing the  $R_0$  of PF2 to KNSF2 and P3HT, PF2 is less soluble than P3HT ( $R_0 = 4.7$ ) and KNSF2.

The HSPs of PC<sub>71</sub>BM have been reported in literature and are given by  $\delta_D=20.2$ ,  $\delta_P=5.4$ ,  $\delta_H=4.5$ ,  $R_0=8.4$ .<sup>113</sup> The HSPs measurements of EH-IDTBR have been described in Chapter 5, and the HSPs values of EH-IDTBE were  $\delta_D=18.8$ ,  $\delta_P=4.4$ ,  $\delta_H=4.3$ , as well as  $R_0$  is equal to 6.1. The positions of PF2/PC<sub>71</sub>BM and PF2/EH-IDTBR in Hansen space are shown in Figure 6.3 a and b, indicating that the solubility sphere of PF2 is completely within the solubility sphere of PC<sub>71</sub>BM and EH-IDTBR. Figure 6.3 c shows the position of KNSF2 and PC<sub>71</sub>BM in Hansen solubility space, exhibiting only a partial overlap of both solubility spheres. For KNSF2 and PC<sub>71</sub>BM, the good solvent should have HSPs located in the overlapping part in HSP solubility space. The work on KNSF2:non-



fullerene acceptors blends is still on-going. The HSPs for these four materials are summarized in Table 6.1.

Table 6.1 HSPs for PF2, KNSF2, PC<sub>71</sub>BM and EH-IDTBR.

Materials	$\delta_D$	$\delta_P$	$\delta_H$	$R_0$
PF2	19.2	3.9	2.8	4.0
KNSF2	17.5	4.3	1.5	4.9
PC <sub>71</sub> BM	20.2	5.4	4.5	8.4
EH-IDTBR	18.8	4.4	4.3	6.1

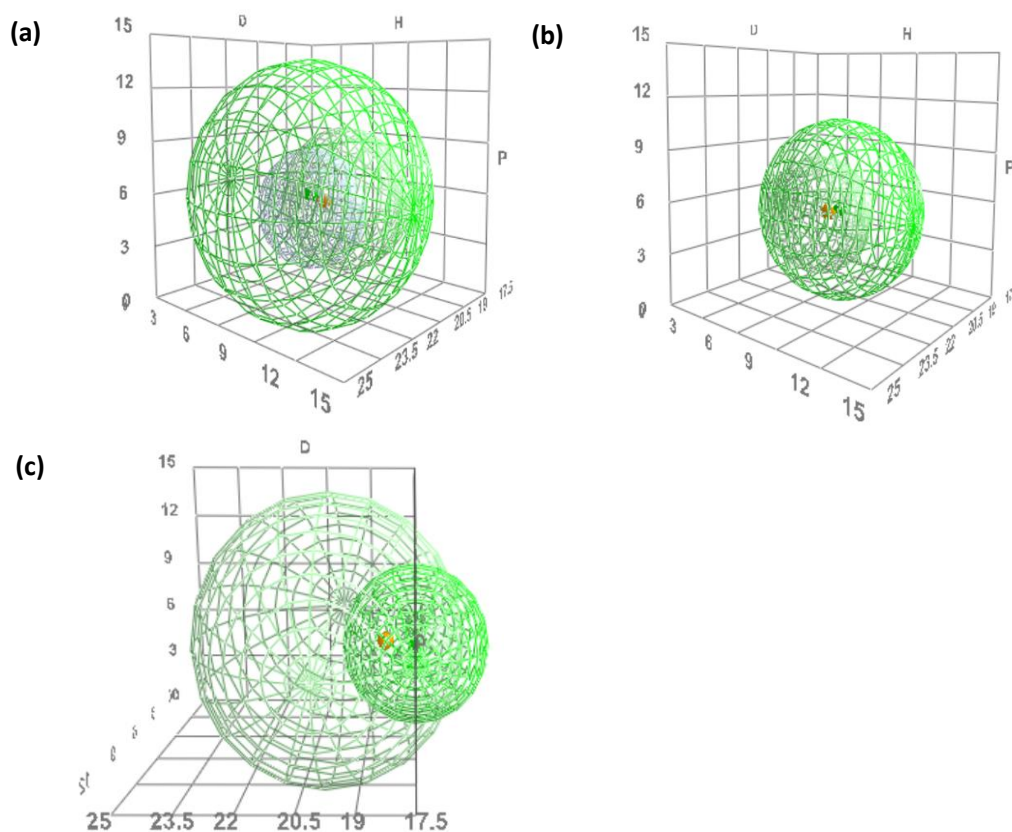


Figure 6.3 The position of (a) PF2:PC<sub>71</sub>BM, (b) PF2:PEH-IDTBR and (c) KNSF2:PC<sub>71</sub>BM in Hansen space.

## 6.2 Solvent selection by IBSS<sup>®</sup>CAMD

As mentioned in Chapter 4, six steps are required when using IBSS<sup>®</sup>CAMD to search for alternative solvents.

The same target properties (11 properties) have been chosen for PF2 and KNSF2-based OPV devices, than for P3HT-based devices. However, the target values of the target properties may differ for the different donor:acceptor blends.

In this study, the target values for each target property are still adopted using two approaches mentioned in Chapter 5, which are based on preliminary experimental measurements and on reference solvents. All the target values are summarized in Table 6.2. The target values of solubility properties are specified according to the first approach. Suitable alternative solvents are required to solubilize both the donor and acceptor materials, i.e. in our case PF2:PC<sub>71</sub>BM, PF2:EH-IDTBR, or KNSF2:PC<sub>71</sub>BM.

The junction barycenter values of PF2:PC<sub>71</sub>BM blends are  $\delta_D=19.5$ ,  $\delta_P=4.4$ ,  $\delta_H=3.4$ . Therefore, the HSP target ranges for PF2:PC<sub>71</sub>BM blends are defined as  $18.5 < \delta_D < 20.5$ ,  $3.4 < \delta_P < 5.4$ , and  $2.4 < \delta_H < 4.4$ , respectively. The junction values of PF2:EH-IDTBR are 19.0, 4.1, 3.4 for  $\delta_D$ ,  $\delta_P$  and  $\delta_H$ , therefore the target ranges of HSPs are set to  $18 < \delta_D < 20$ ,  $3.1 < \delta_P < 5.1$ , and  $2.4 < \delta_H < 4.4$ , respectively. The position of PF2 and EH-IDTBR in the HSP solubility space can be found in Figure 6.3b. Again, as the solubility spheres of PF2 and EH-IDTBR fully overlap, the solubility requirement can be satisfied with *RED* <1 for PF2 only.

For the KNSF2:PC<sub>71</sub>BM blends, the junction barycenter values are  $\delta_D=18.5$ ,  $\delta_P=4.7$ ,  $\delta_H=2.6$ , hence the corresponding HSP target ranges were defined as  $17.5 < \delta_D < 19.5$ ,  $3.5 < \delta_P < 6$ , and  $1.5 < \delta_H < 3.5$ . Considering that the solubility spheres of KNSF2 and PC<sub>71</sub>BM only partially overlap, *RED* will be defined twice, once for KNSF2 and the other for PC<sub>71</sub>BM. The target range of both *RED* is <1.

Table 6.2 The target properties, corresponding values for PF2:PC<sub>71</sub>BM, PF2:EH-IDTBR, and KNSF2:PC<sub>71</sub>BM. (<sup>a</sup> PF2:PC<sub>71</sub>BM blends, <sup>b</sup> PF2:EH-IDTBR blends, and <sup>c</sup> KNSF2:PC<sub>71</sub>BM blends.)

Specifications	Target properties	Target values	Parameter values		
			$w_p$	$\sigma_L$	$\sigma_R$
Solubility	$\delta_D$ (MPa) <sup>1/2</sup>	18.5 < $\delta_D$ < 20.5 <sup>a</sup>	1	0.48	0.21
		18 < $\delta_D$ < 20 <sup>b</sup>			
		17.5 < $\delta_D$ < 19.5 <sup>c</sup>			
	$\delta_P$ (MPa) <sup>1/2</sup>	3.4 < $\delta_P$ < 5.4 <sup>a</sup>	1	0.56	0.48
		3.1 < $\delta_P$ < 5.1 <sup>b</sup>			
		3.5 < $\delta_P$ < 6 <sup>b</sup>			
	$\delta_H$ (MPa) <sup>1/2</sup>	2.4 < $\delta_H$ < 4.4 <sup>a,b</sup>	1	0.24	0.48
		1.5 < $\delta_H$ < 3.5 <sup>c</sup>			
	$R_a$ (MPa) <sup>1/2</sup> -PF2	$R_a$ < 3	3	0.84	
	$R_a$ (MPa) <sup>1/2</sup> -KNSF2	$R_a$ < 4	2		
	$R_a$ (MPa) <sup>1/2</sup> -PC <sub>71</sub> BM	$R_a$ < 3	2		
	RED-PF2	< 1	2	0.28	
RED-KNSF2	1				
RED-PC <sub>71</sub> BM	1				
Film drying	Boiling point ( $T_b$ /K)	373 < $T_b$ < 473	2	8.4	10.6
	Vaporization enthalpy ( $\Delta H_{vap}$ kJ/mol)	40 < $\Delta H_{vap}$ < 55	1	1.7	1.7
Film processing	Density (g/cm <sup>3</sup> )	0.8 < $\rho$ < 1.5	1	19.8	19.8
	Viscosity (mPa/s)	0.5 < $\eta$ < 1.5	1	0.13	0.13
Safety	Flash Point ( $T_f$ /K)	$T_f$ > 296	1	2.8	
Liquid state	Melting point ( $T_m$ /K)	$T_m$ < 283	0.5		4.2

The solvent should be safe to use, thus requiring a flash point greater than 296.15 K.<sup>159</sup> Similarly, in order for the solvent to remain liquid at the processing temperature, a melting point of less than 283.15 K is required.

For the properties  $R_o$ , boiling point,  $\Delta H_{vap}$ , density, and viscosity, the target values have been defined by using the key properties of a “reference” solvent that is known to yield high-performance OPV devices. For the investigated materials, *o*-DCB is a good choice as it dissolves efficiently PF2 and has led to the highest power conversion efficiencies with the PF2:PC<sub>71</sub>BM blends (~10%) and P3HT:EH-IDTBR blends (~7.3%). As well, the KNSF2:PC<sub>71</sub>BM devices achieve a PCE of about 8% when using *o*-DCB as a process solvent. The experimental database of the target properties for *o*-DCB are summarized in Table 5.2. As the  $R_o$  values between *o*-DCB and PF2 is 2.48, the target value for  $R_o$  is set to be lower than 3. Since the solubility spheres of KNSF2 and PC<sub>71</sub>BM partially overlap, different  $R_o$  target values will be set for each of the two materials. The  $R_o$  between *o*-DCB and KNSF2 is 4.4, which is close to the  $R_o$  of KNSF2 ( $R_o = 4.9$ ). The solvent provides poor solubility for the solute when it is at the boundary of the sphere of solubility of the solute. Therefore, the target value of  $R_o$  for KNSF2 is defined as less than 4. The target value of  $R_o$  for PC<sub>71</sub>BM is less than 3, because the  $R_o$  of PC<sub>71</sub>BM and *o*-DCB is 2.50.

As shown in table 5.2, the experimental values for the boiling point, vaporization enthalpy, density, and viscosity are relatively close for *o*-DCB. For the boiling point the target range for the alternative solvent is set to [373 K, 473 K]<sup>151,160</sup>, while for the vaporization enthalpy, density, and viscosity, the target ranges are [35 kJ/mol, 55 kJ/mol], [0.8 g/cm<sup>3</sup>, 1.5 g/cm<sup>3</sup>], and [0.5 mPa/s, 1.5 mPa/s] respectively.

The third step is the selection of predictive models, which are the same as those used for the P3HT-based blends, and the list of predictive models can be found in Appendix 9.1. The fourth step is definition of the global performance function. The parameter used by IBSS<sup>®</sup>CAMD include  $w_p$ ,  $\sigma_L$ , and  $\sigma_R$ , which are defined in the same

way as the rules discussed in Chapters 4 and 5. Note that the weight of each *RED* is reduced to 1 and the weight of each  $R_a$  is reduced to 2 as they are defined for KNSF2 and PC<sub>71</sub>BM, respectively.

For the existing solvent performance evaluation, 139 biosolvents (see Appendix 9.4) were also selected as target solvents for PF2 and KNSF2-based OPVs. For molecular design, the chemical groups that are shown in Appendix 9.3, are selected to design new molecules only for PF2:PC<sub>71</sub>BM blends and PF2:EH-IDTBR blends.

*-PF2: PC<sub>71</sub>BM blends and PF2:EH-IDTBR blends:*

3 best ranked alternative solvents candidates for PF2:PC<sub>71</sub>BM blends and 3 best ranked alternative solvents candidates for PF2:EH-IDTBR blends with a *GloPerf* >0.6 are displayed in table 6.3 and 6.4. The full target property values and *ProPerf<sub>p</sub>* values for candidate solvents with a *GloPerf* >0.5 for PF2:PC<sub>71</sub>BM blends are presented in Appendix 9.9, and those for candidate solvents with a *GloPerf* >0.5 for PF2:EH-IDTBRE blends are presented in Appendix 9.10.

According to IBSS<sup>®</sup>CAMD, the best candidate solvent turns out to be p-xylene (*PX*), with a *GloPerf* of 0.931 for both blends. All individual performance functions of *PX* do indeed equal unity except  $\delta_H$  (*ProPerf<sub>p</sub>*  $\approx$  0). The estimated viscosity and density of *PX* are similar with the values of *o*-DCB, allowing similar conditions to be applied when processing PF2 solutions. Also, the  $R_a$  and *RED* values of *PX* are smaller than those of the other alternative solvents, providing a good solubility for PF2.

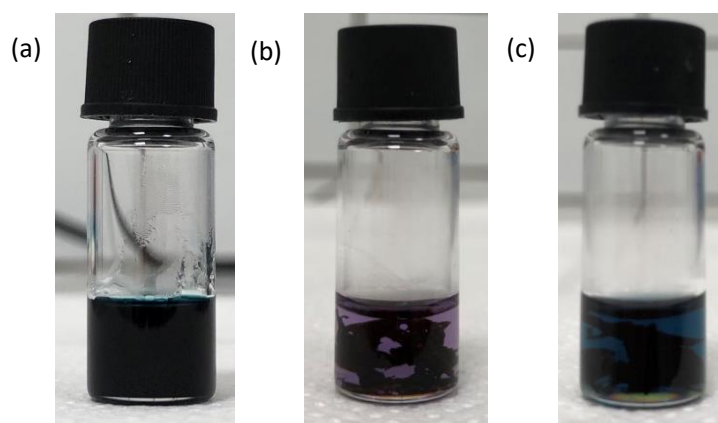
Table 6.3 The candidates provided for PF2:PC<sub>71</sub>BM by IBSS®CADM with a *GloPerf* > 0.6.

Properties	o-DCB	p-Xylene	Anisole	p-Cymene
CAS	95-50-1	106-42-3	100-66-3	99-87-6
<i>GloPerf</i>	1	0.931	0.724	0.693
$\delta_D$	19.5	18.6	18.1	17.4
<i>ProPerf<sub>p</sub></i> - $\delta_D$	1	1	0.50	0.01
$\delta_P$	5.1	3.8	4.9	2.3
<i>ProPerf<sub>p</sub></i> - $\delta_P$	1	1	1	0.02
$\delta_H$	3.1	1.6	6.1	2.4
<i>ProPerf<sub>p</sub></i> - $\delta_H$	1	≈ 0	≈ 0	1.00
$R_a$	1.37	1.70	4.12	4.10
<i>ProPerf<sub>p</sub></i> - $R_a$	1	1	0.17	0.18
RED	0.34	0.42	1.03	1.03
<i>ProPerf<sub>p</sub></i> -RED	1	1	0.99	0.99

For anisole (AN), the low *GloPerf* is caused by the *ProPerf<sub>p</sub>* values of  $R_a$  (*ProPerf<sub>p</sub>*- $R_a = 0.17$ ) and a low match to the target values of HSPs, for instance the *ProPerf<sub>p</sub>* of  $\delta_H$  is 0. The RED of PF2 in AN is 1.03, meaning that AN is located in the boundary of the solubility sphere of PF2. p-Cymene (PC) is similar with AN, which is located in the boundary of the solubility sphere of PF2 (RED=1.03,  $R_a=4.10$ ) leading to a low *ProPerf<sub>p</sub>* value of  $R_a$  (*ProPerf<sub>p</sub>*- $R_a = 0.18$ ). The *ProPerf<sub>p</sub>* values of  $\delta_D$  and  $\delta_P$  are 0.01 and 0.02, respectively, a poor match with the target HSPs. AN and PC should therefore provide a poor solubility to PF2, as confirmed by solubility experiments with a PF2 concentration of 4mg/ml. Figure 6.4 shows pure PF2 solutions in PC and AN stirred overnight at 80°C. As a consequence, PX is the only remaining candidate solvent for PF2:PC<sub>71</sub>BM blends and PF2:EH-IDTBR blends.

Table 6.4 The candidates provided for PF2:EH-IDTBR by IBSS®CAMD with a  $GloPerf > 0.6$ .

Properties	o-DCB	p-Xylene	Anisole	p-Cymene
CAS	95-50-1	106-42-3	100-66-3	99-87-6
$GloPerf$	1	0.931	0.758	0.714
$\delta_D$	19.5	18.60	18.1	17.40
$ProPerf_p-\delta_D$	1	1	1	0.21
$\delta_P$	5.1	3.80	4.9	2.30
$ProPerf_p-\delta_P$	1	1.00	1	0.13
$\delta_H$	3.1	1.60	6.1	2.40
$ProPerf_p-\delta_H$	1	$\approx 0$	$\approx 0$	1
$R_a$	1.37	1.70	4.12	4.10
$ProPerf_p-R_a$	1	1	0.17	0.18
RED	0.34	0.42	1.03	1.03
$ProPerf_p-RED$	1	1	0.99	0.99

Figure 6.4 Pictures of pure PF2 solutions (a) in  $PX$ , (b) in  $AN$  and (c)  $PC$  stirred overnight at  $80^\circ C$ .

For molecular design, numerical molecular structures are designed and properties of these molecules are evaluated by IBSS®CAMD. Table 6.5 lists 8 designed solvents with a  $GloPerf$  values over 0.9 for further investigation for PF2:PC<sub>71</sub>BM blends,

and 13 designed solvents with a *GloPerf* values over 0.9 for PF2:EH-IDTBR blends are shown in table 6.6. The full property values together with the *ProPerf* values of solvents whose *GloPerf* values are greater than 0.9 are presented in Appendix 9.11 (for PF2:PC<sub>71</sub>BM blends) and Appendix 9.12 (for PF2:EH-IDTBR blends). Interestingly, *PX*, which were included in the list of pre-selected solvents (see above) also occurs in the list of designed solvents, pointing out the consistency between both methods. 8 identical designed solvents are found for both donor:acceptor blends: benzyl methyl ether (*BME*), methyl phenethyl ether (*MPE*), *PX*, N,N-Dimethylaniline (*DMA*), 1-(3-Buten-2-yl)-4-methylbenzene (*1-4-MB*), 4-methylstyrene (*4-MS*), 1-phenyl-2-butene (*1-P-2-B*), and 1-Methyl-2-(2-propyn-1-yl)benzene (*1-M-2-B*). Allylbenzene (*AB*), 3-butenylbenzene (*3-BTB*), 4-ethynyltoluene (*4-ET*), 2-methylstyrene (*2-MS*), and phenylallene (*PA*) are only for PF2:EH-IDTBR blends. These candidate solvents need to be further screened taking into account non-evaluated properties.

Table 6.5 List of the best solvent candidates selected from the results of molecular design provided by IBSS®CADM for PF2:PC<sub>71</sub>BM blends. (Y: yes, N: no, NA: non-available data)

Candidates	CAS	<i>GloPerf</i>	Commerciality	Cost (€/g)	Stability
Benzyl methyl ether ( <i>BME</i> )	538-86-3	0.975	Y	2.66	Y
Methyl phenethyl ether ( <i>MPE</i> )	3558-60-9	0.966	Y	1.32	Y
<i>PX</i>	106-42-3	0.931	Y	0.18	Y
N,N-Dimethylaniline ( <i>DMA</i> )	121-69-7	0.931	Y	0.21	Y
1-(3-Buten-2-yl)-4-methylbenzene ( <i>1-4-MB</i> )	97664-18-1	0.931	N	NA	N
4-Methylstyrene ( <i>4-MS</i> )	622-97-9	0.912	Y	0.52	N
1-Phenyl-2-butene ( <i>1-P-2-B</i> )	935-00-2	0.909	N	NA	N
1-Methyl-2-(2-propyn-1-yl)benzene ( <i>1-M-2-B</i> )	NA	0.901	N	NA	N



Table 6.6 List of the best solvent candidates selected from the results of molecular design provided by IBSS®CADM for PF2:EH-IDTBR blends. (Y: yes, N: no, NA: non-available data)

Candidates	CAS	<i>GloPerf</i>	Commerciality	Cost (€/g)	Stability
Methyl phenethyl ether ( <i>MPE</i> )	3558-60-9	1	Y	1.32	Y
Benzyl methyl ether ( <i>BME</i> )	538-86-3	0.997	Y	2.66	Y
1-(3-Buten-2-yl)-4-methylbenzene ( <i>1-4-MB</i> )	97664-18-1	0.989	N	NA	N
Allylbenzene ( <i>AB</i> )	300-57-2	0.932	Y	2.84	N
1-Phenyl-2-butene ( <i>1-P-2-B</i> )	935-00-2	0.932	N	NA	N
<i>PX</i>	106-42-3	0.931	Y	0.18	Y
4-Methylstyrene ( <i>4-MS</i> )	622-97-9	0.931	Y	0.52	N
N,N-Dimethylaniline ( <i>DMA</i> )	121-69-7	0.931	Y	0.21	Y
3-Butenylbenzene ( <i>3-BTB</i> )	768-56-9	0.930	Y	9.73	N
1-Methyl-2-(2-propyn-1-yl)benzene ( <i>1-M-2-B</i> )	NA	0.929	N	NA	N
4-Ethynyltoluene ( <i>4-ET</i> )	622-96-8	0.923	Y	7.04	N
2-Methylstyrene ( <i>2-MS</i> )	611-15-4	0.914	Y	19.01	N
Phenylallene ( <i>PA</i> )	2327-99-3	0.903	N	NA	N

For the 8 identical solvents, 5 candidates are commercially available. However, taking the cost into account, only 3 candidates, which are *PX*, *DMA* and *4-MS*, have been retained. Considering the toxicity of above three solvents, *PX* and *4-MS* are less toxic than *DMA*, which is in fact a highly toxic solvent. In addition, *4-MS* must be removed from the list of alternative solvents due to its low chemical stability in air. The reason is that *4-MS* has a double-bond in its chemical structure, which is unstable and prone to break, which may lead to OPV device instability.

For the other 5 designed solvents, *PA* is not commercially available. *AB*, *3-BTB*, *4-*

*ET*, and *2-MS* are costly compared to other commonly used solvents such as *PX* and anisole. In addition, *AB*, *3-BTB*, *4-ET* and *2-MS* are unstable when exposed in air, due to the fact that either double-bond or triple-bond in their chemical structure tend to break in air. Therefore, only *PX* has been retained as candidate solvent for *PF2:PC<sub>71</sub>BM* blends and *PF2:EH-IDTBR* blends.

--> *KNSF2: PC<sub>71</sub>BM* blends:

Table 6.7 lists 13 candidate alternative solvents with *GloPerf* > 0.6 for the *KNSF2:PC<sub>71</sub>BM* blends. They are *p*-xylene (*PX*), *p*-cymene (*PC*), 1,4-cineol (*CN*), anisole (*AN*), cyclopentyl methyl ether (*CPME*),  $\alpha$ -pinene ( $\alpha$ -*PNE*), glycerol -1,2,3-triethyl ether (*GTE*), pinane (*PNA*), dibutyl ether (*DBE*),  $\beta$ -pinene ( $\beta$ -*PNE*), terpinolene (*TPO*), d-limonene (*d-LM*), isoamyl acetate (*IA*). The full target property values and *ProPerf<sub>p</sub>* values for candidate solvents with a *GloPerf* > 0.6 for *KNSF2:PC<sub>71</sub>BM* blends are presented in Appendix 9.13.

The *GloPerf* value for *o*-DCB is 0.977 rather than 1 because the  $R_a$  value between *o*-DCB and *KNSF2* is greater than 4, which results in a *ProPerf<sub>p-R<sub>a</sub></sub>* value of 0.824 for *KNSF2*. This result was expected because of the previous setting of the *KNSF2* target value for  $R_a$ . The boiling point,  $\Delta H_{vap}$ , density, and viscosity of the candidates are almost identical to the target values, which means that they are good alternative solvents for film formation and drying. In addition, they are liquid at room temperature, meeting the requirement for reduced energy consumption in device manufacturing. For the flash point, *CPME* has a low *ProPerf<sub>p</sub>* of 0, therefore a safety issue for usage and storage. Moreover, commercial *CPME* is currently produced from fossil resources although it could be bio-based. Therefore, *CPME* should be removed from the list of alternative solvents for *KNSF2:PC<sub>71</sub>BM* blends.

For solubility, different  $R_a$  and *RED* were set for *KNSF2* and *PC<sub>71</sub>BM*. Thus, the two materials need to be discussed separately to screen for the suitable alternative solvents.

- *PX* is the first candidate in the list with a *GloPerf* of 0.874. The imperfectly matched property is *Ra-PC<sub>71</sub>BM* with a *ProPerf<sub>p</sub>* of 0.026, indicating that *PC<sub>71</sub>BM* has poor solubility in *PX*. However, *PX* provides good solubility for *KNSF2* (*ProPerf<sub>p</sub>-R<sub>o</sub>*=1). As in the case of the *P3HT:PC<sub>71</sub>BM* copolymer, the solubility of *PC<sub>71</sub>BM* was improved by adding *DPE*.
- *PC* and *CN* were similar to *PX* for *KNSF2:PC<sub>71</sub>BM* blends. They provide good solubility of *KNSF2*, but have poor miscibility with *PC<sub>71</sub>BM*. In this case, high processing temperatures and additives should be used to optimize the solubility of *PC<sub>71</sub>BM* in the blend solution to achieve high performance devices with improved morphology.
- *AN*, *GTE*, *DBE*, *TPO* and *d-LM* are located in the boundary of the solubility sphere of *KNSF2*, providing a bad miscibility with *KNSF2*. Importantly, *GTE* and *DBE* are located outside the solubility sphere of *PC<sub>71</sub>BM*, indicating that *PC<sub>71</sub>BM* is not miscible with them. *AN*, *d-LM* and *TPO* have a large *R<sub>o</sub>* with *PC<sub>71</sub>BM*, indicating low miscibility with *PC<sub>71</sub>BM*.
- *α-PNE*, *β-PNE* and *PNA* are located in the boundary of *PC<sub>71</sub>BM*, although they can provide a good solubility of *KNSF2*. Considering that temperature is a key factor in material solubility, a solubility measurement should be taken for *α-PNE*, *β-PNE* and *PNA*.
- *IA* will be removed from the list, as neither material is soluble in it.

Consequently, *PX*, *PC* and *CN* are selected as alternative solvents for *KNSF2:PC<sub>71</sub>BM* blends, while *AN*, *d-LM*, *TPO*, *α-PNE*, *β-PNE* and *PNA* requires additional solubility measurements to evaluate their potential for processing *KNSF2:PC<sub>71</sub>BM*. The investigation of OPV devices processed from these alternative solvents is still on-going. We may nevertheless already conclude that the introduction of siloxane functional groups as solubilizing side chains onto the fluorinated conjugated backbone of *PF2*, has broadened the choice for candidate solvents.

Table 6.7 The candidates provided for KNSF2:PC<sub>71</sub>BM by IBSS®CADM with a GloPerf > 0.6.

Candidates	CAS	GloPerf	R <sub>σ</sub> -KNSF2	ProPerf <sub>p</sub> -R <sub>σ</sub> -KNSF2	R <sub>σ</sub> -PC <sub>71</sub> BM	ProPerf <sub>p</sub> -R <sub>σ</sub> -PC <sub>71</sub> BM
<i>o</i> -DCB	95-50-1	0.977	4.37	0.824	0.88	1
<i>p</i> -Xylene (PX)	106-42-3	0.874	2.31	1	4.61	0.026
<i>p</i> -Cymene (PC)	99-87-6	0.812	2.66	1	5.11	0.002
1,4-Cineol (CN)	470-67-7	0.751	2.47	1	6.75	≈ 0
Anisole (AN)	100-66-3	0.742	4.74	0.465	4.52	0.038
Cyclopentyl methyl ether (CPME)	5614-37-9	0.725	2.80	1	7.44	≈ 0
α-Pinene (α-PNE)	80-56-8	0.699	3.13	1	8.00	≈ 0
Glycerol -1,2,3-triethyl ether (GTE)	162614-45-1	0.694	4.46	0.741	9.46	≈ 0
Pinane (PNA)	473-55-2	0.689	2.83	1	8.06	≈ 0
Dibutyl ether (DBE)	142-96-1	0.640	4.50	0.703	10.08	≈ 0
β-Pinene (β-PNE)	127-91-3	0.626	2.90	1	8.08	≈ 0
Terpinolene (TPO)	586-62-9	0.619	4.21	0.940	7.52	≈ 0
<i>d</i> -Limonene ( <i>d</i> -LM)	138-86-3	0.610	4.20	0.945	7.71	≈ 0
Isoamyl acetate (IA)	123-92-2	0.600	5.55	0.034	9.04	≈ 0

### 6.3 Photovoltaic Performance

Since KNSF2:PC<sub>71</sub>BM OPV devices will be prepared after completion of selection of alternative solvents, this paragraph focuses on PF2-based devices. One reason is the solubility of PC<sub>71</sub>BM in the solvent candidates limited green-processing of KNSF2-based OPVs. More efficient acceptors need to be used in the KNSF2:acceptor-based OPVs. An inverted OPV structure is used in this study. Reference devices processed from *o*-DCB solutions were also studied. For PF2:PC<sub>71</sub>BM based devices, the active layer was prepared from a mixture solution of PF2 and PC<sub>71</sub>BM with an overall

concentration of 10 mg/ml. The ratio of donor and acceptor is 1:1.5. The blend films were processed from hot *o*-DCB and *PX*/DPE solutions ( $\approx 100^\circ\text{C}$ ) and spin-coated onto substrates previously heated at the same temperature. For the PF2:EH-IDTBR based devices, the active layer was composed of PF2:EH-IDTBR blends with a 1:1 weight ratio from hot *o*-DCB and *PX* solutions that were annealed and stirred overnight at  $100^\circ\text{C}$  in nitrogen ambient. The overall concentration of PF2:EH-IDTBR blends is 8mg/ml.

The photovoltaic properties of the devices are recorded in Figure 6.4 and Table 6.8. PF2 devices worked efficiently in inverted devices without any post-treatment. The devices processed from *PX*/DPE mixture solvents showed an impressive maximum PCE of 9.47%. In this study, 3% of DPE was added as processing additive to improve the morphology of the active layer. The slightly lower efficiency compared to devices processed from *o*-DCB is caused by the lower  $J_{sc}$  ( $16.5\text{ mA cm}^{-2}$ ) for *PX* processed devices. The latter may be the consequence of a less optimal blend morphology (larger domain sizes). The high FF of 76.5% clearly points out excellent charge carrier extraction. Interestingly, the devices processed by *PX* could be manufactured at a lower temperature ( $70^\circ\text{C}$ ) than from *o*-DCB solutions. We attribute this behavior to the lower viscosity of *PX*: the active layer can be spin-coated at a lower processing temperature for achieving a similar thickness than with *o*-DCB.

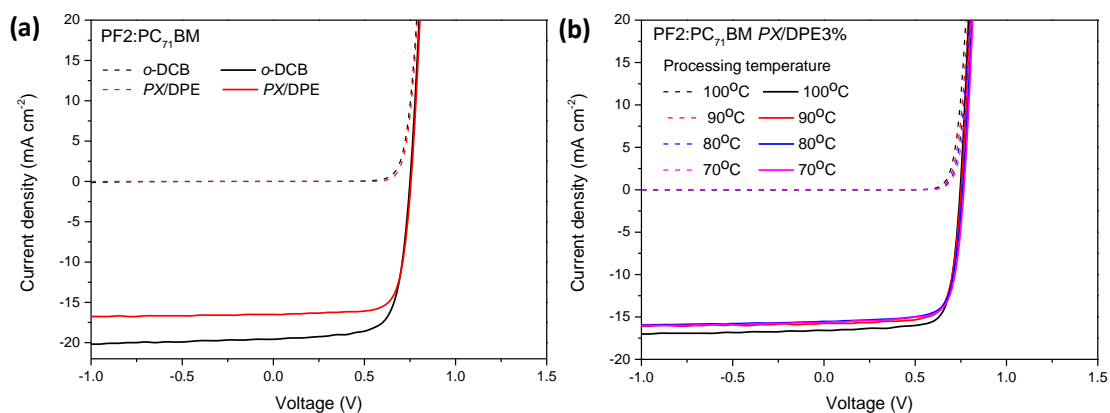


Figure 6.4 a) The J-V curves of PF2 from *o*-DCB and *PX*/DPE solutions, and b) the JV curves of PF2 based devices processed from *PX*/DPE mixture solvents at different processing temperature.

Table 6.8 Summary of PF2:PC<sub>71</sub>BM device performance for various solvents.

Processing solvents	Processing temperature	V <sub>oc</sub> (mV)	J <sub>sc</sub> (mA cm <sup>-2</sup> )	FF (%)	PCE (%)	Thickness (nm)
<i>o</i> -DCB	100°C	754±5	17.9±1.3	73.5±0.5	9.8±0.7	~115
PX/DPE3%	100°C	753±3	15.9±0.6	75.5±1	9.1±0.4	~130
PX/DPE3%	90°C	753±5	15.3±0.5	75.5±1	8.8±0.2	~120
PX/DPE3%	80°C	758±3	15.4±0.2	74.5±1	8.8±0.1	~125
PX/DPE3%	70°C	761±6	15.3±0.4	74.8±1	8.8±0.2	~135

The JV curves and corresponding parameters of PF2:EH-IDTBR cell devices are shown in Figure 6.5 and table 6.9. The average PCE equals 8.0 when processed from PX solutions, exceeding the PCE of devices processed from *o*-DCB (7.29%). Interestingly, the EH-IDTBR based devices could be fabricated by a single biosolvent (without additive). The  $R_a$  and RED values of EH-IDTBR are smaller than those of PC<sub>71</sub>BM (table 6.9), indicating that the solubility of EH-IDTBR is higher than that of PC<sub>71</sub>BM in PX. A higher solubility of the small molecule acceptors is likely to retard acceptor aggregation, to reduce the domain size and to increase donor/acceptor interfacial area.

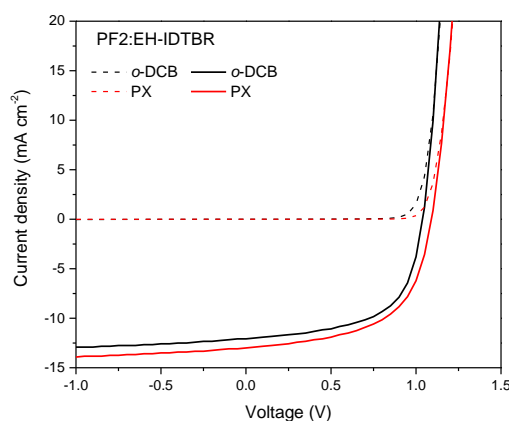
Figure 6.5 The JV characteristics of PF2:EH-IDTBR based OPVs processed from *o*-DCB and *p*-xylene.

Table 6.9 The corresponding photovoltaic device parameters of PF2:EH-IDTBR based devices fabricated from various solvents.

Materials	Processing solvents	V <sub>oc</sub> (mV)	J <sub>sc</sub> (mA/cm <sup>2</sup> )	FF (%)	PCE (%)
PF2:EH-IDTBR	<i>o</i> -DCB	1040±5	12.87±0.2	57.9±1	7.3±0.2
	<i>PX</i>	1070±3	13.21±0.1	55.8±1	8.0±0.1

## 6.4 Conclusion

In summary, the IBSS<sup>®</sup>CAMD tool has been successfully used to design and select alternative solvents for PF2-based OPV devices. *PX* was defined as the best candidate for both blends and allowed to achieve an average PCE of 9.10% with PF2:PC<sub>71</sub>BM based devices when using DPE as the processing additive. For the second blend PF2:EH-IDTBR, *PX* gave rise to the average PCE of 8.03%. It is important to note, that the small number of alternative solvents with a high GloPerf is due to the small solubility sphere radius ( $R_0$ ) and underlines the low miscibility of PF2 in most solvents, which is itself a consequence of the high planarity and strong intermolecular stacking of the fluorinated polymer backbone.

The IBSS<sup>®</sup>CAMD results further reveal a larger  $R_0$  for KNSF2, in comparison to PF2, and consequently a broader choice of alternative solvents, suggesting that the insertion of siloxane functional groups on the side chains is an effective way to improve the solubility properties of fluorinated polymers. Nevertheless, the small overlap of the solubility spheres of KNSF2 and PC<sub>71</sub>BM is a limiting factor and suggests that other acceptors should be considered for KNSF2-based OPV devices.

Finally, the study on the fluorinated polymers corroborates the universal applicability of the reverse engineering methodology based on IBSS<sup>®</sup>CAMD for various donor and acceptor blends used for bulk heterojunctions solar cells.

# CHAPTER 7

---

---

## CONCLUSION AND PERSPECTIVES

---

---



## 7 Conclusion and Perspectives

My PhD project was devoted to improving the performance of organic photovoltaic devices and reducing the environmental impact of the device manufacturing. OPV is seen as an important green technology to replace conventional energy sources in the future. In recent years, the focus on research and development of organic solar cells has contributed to improving the performance of organic cells and making them economically viable. However, there is undoubtedly a need for devices to be prepared in a "greener" manner when marketing OPV modules, for example by using biodegradable organic materials or non-toxic processing solvents. In this thesis, the selection of non-toxic alternative solvents has been the focus of the work.

Taking into account that the organic electron-donor and electron-acceptor materials are continually evolving to further improve the power conversion efficiency of OPV devices and that the traditional "trial-and-error" approach for the selection of non-toxic solvents is hindered by the multiple parameters that may impact the device performances, we have introduced a reverse engineering approach, based on the IBSS®CAMD numerical tool, to select alternative solvents and applied the methodology to different organic photovoltaic materials.

IBSS®CAMD can be used in two different modes for solvents selection: (a) to evaluate the performance of a list of pre-selected existing solvents, or (b) to design new molecules and evaluate their performances. Both ways are used in this thesis, with a particular focus on bio-sourced solvents, as these are expected to exhibit low health and environmental impacts.

The utilization of IBSS®CAMD for organic photovoltaic applications required a preliminary work to identify the physico-chemical parameters of the solvent that have a strong impact on the photovoltaic performances. For each of these properties, target

values, which the alternative solvent must satisfy, had to be defined. IBSS<sup>®</sup>CAMD was then used to estimate the physico-chemical properties of a large number of solvents and to evaluate the “performance” of the solvents for each property and rank them according to an overall performance criterion. Thus, eleven target properties were defined and applied to four different donor/acceptor blends:

1) P3HT:PC<sub>71</sub>BM system

This blend has been used as a reference system, even though its photovoltaic performance is nowadays largely outdated. Indeed, this material has been the subject of numerous studies throughout the world and today represents the donor/acceptor system whose properties are best understood.

5 alternative solvents could be identified through the two modes of IBSS<sup>®</sup>CAMD (anisole, 2-methyl anisole, p-xylene, p-cymene and terpinolene) and allowed to reach similar device performances as with the original toxic solvent (*o*-DCB).

2) P3HT:EH-IDTBR system

EH-IDTBR is an electron-acceptor molecule recently developed to replace fullerene derivatives (such as PC<sub>71</sub>BM) and improve the performance of OPV devices. Four alternative non-toxic solvents were selected through the first mode of IBSS<sup>®</sup>CAMD tool: anisole, p-xylene, p-cymene and terpinolene. A high average PCE of 4.55% could be obtained using anisole as processing solvent.

3) PF2:PC<sub>71</sub>BM system

The same approach was used to identify a bio-based solvent, p-xylene, for the implementation of the PF2:PC<sub>71</sub>BM mixture with only minor loss of performance, and allowed us to achieve a conversion efficiency of 9% with an experimental protocol requiring a lower annealing temperature than that based on chlorinated solvents.

4) PF2:EH-IDTBR system

Due to the limited solubility of PF2, p-xylene was the only alternative solvent selected according to the candidate list of IBSS<sup>®</sup>CADM results. P-xylene allowed the OPV device to achieve a PCE of 8.03%, showing better performance than o-DCB processed devices.

5) KNSF2:PC<sub>71</sub>BM system

KNSF2 is an efficient polymer that was synthesized by the groups of Dr. Nicolas Leclerc and Dr. Stéphane Mery, and for which siloxane functional groups were introduced to replace the alkyl side-chains of the PF2 polymer. HSP measurements demonstrated that KNSF2 is more soluble than PF2. The IBSS<sup>®</sup>CAMD results also validate this conclusion by providing more solvent candidates. However, the solubility of PC<sub>71</sub>BM in the solvent candidates limited green-processing of KNSF2-based OPVs. The next step will therefore be to use other acceptors instead of PC<sub>71</sub>BM to prepare green processable KNSF2-based OPVs. The molecular design model will also be used to search for alternative solvents for KNSF2-based OPVs.

In summary, the five cases studied in this PhD clearly demonstrate that the reverse engineering approach is an efficient way to select alternative solvents for organic semiconductors and to avoid the time-consuming trial and error approach. It should further be noted that while the method has only been applied to materials designed for OPV applications, it should also be of interest for the selection of solvents for other solution-processed organic semiconductor devices.

# CHAPTER 8

---

---

## BIBLIOGRAPHY

---

---

## 8 Bibliography

- (1) Audenaert, M.; Gusman, G.; Deltour, R. Electrical Conductivity of I<sub>2</sub>-Doped Polyacetylene. *Phys. Rev. B* **1981**, *24* (12), 7380–7382.
- (2) Shaw, J. M. Seidler, P. F. Organic Electronics; Introduction. *IBM J. Res. Dev.* **2001**, *45* (1), 3–9.
- (3) Jo, G.; Jung, J.; Chang, M. Controlled Self-Assembly of Conjugated Polymers via a Solvent Vapor Pre-Treatment for Use in Organic Field-Effect Transistors. *Polymers (Basel)*. **2019**, *11* (2).
- (4) Lee, C.; Lee, H. R.; Choi, J.; Kim, Y.; Nguyen, T. L.; Lee, W.; Gautam, B.; Liu, X.; Zhang, K.; Huang, F.; Oh, J. H.; Woo, H. Y.; Kim, B. J. Efficient and Air-Stable Aqueous-Processed Organic Solar Cells and Transistors: Impact of Water Addition on Processability and Thin-Film Morphologies of Electroactive Materials. *Adv. Energy Mater.* **2018**, *8* (34), 1–12.
- (5) Li, P.; Mainville, M.; Zhang, Y.; Leclerc, M.; Sun, B.; Izquierdo, R.; Ma, D. Air-Processed, Stable Organic Solar Cells with High Power Conversion Efficiency of 7.41%. *Small* **2019**, *15* (7), 1–11.
- (6) Li, M.; Qiu, Z.; Zhang, G.; Liu, Y.; Xiong, L.; Bai, D.; Zhu, M.; Peng, Q.; Zhu, W. Efficient Chemical Structure and Device Engineering for Achieving Difluorinated 2,2'-Bithiophene-Based Small Molecular Organic Solar Cells with 9.0% Efficiency. *J. Mater. Chem. A* **2018**, *6* (26), 12493–12505.
- (7) OLED Smartphones: introduction and market status <https://www.oled-info.com/oled-mobile-phones>.
- (8) Berny, S.; Blouin, N.; Distler, A.; Egelhaaf, H. J.; Krompiec, M.; Lohr, A.; Lozman, O. R.; Morse, G. E.; Nanson, L.; Pron, A.; Sauermann, T.; Seidler, N.; Tierney, S.; Tiwana, P.; Wagner, M.; Wilson, H. Solar Trees: First Large-Scale Demonstration of Fully Solution Coated, Semitransparent, Flexible Organic Photovoltaic Modules. *Adv. Sci.* **2015**, *3* (5), 1–7.
- (9) Zhang, T.; Miao, J.; Ali, M. U.; Shi, M.; He, Y.; Fu, T.; Meng, H. Phosphorescent OLEDs with Extremely Low Efficiency Roll-off Enabled via Rationally Designed Benzimidazole-Based Bipolar Hosts. *Dye. Pigment.* **2020**, *180* (April), 108477.
- (10) Yang, L.; Tong, S.; Gong, C.; Xia, H.; Wang, C.; Liu, B.; Liu, B.; Xie, H.; Xiao, S.; He, J.; Zhang, D.; Dai, G.; Yang, J. Large-Scale Roll-to-Roll Micro-Gravure Printed Flexible PBDB-T/IT-M Bulk Heterojunction Photodetectors. *Appl. Phys. A Mater. Sci. Process.* **2020**, *126* (6).
- (11) Lee, B. R.; Kim, J. T.; Lee, J.; Jang, S.; Yu, Z.; Park, J. H.; Jung, E. D.; Lee, S.; Song,

- M. H.; Whang, D. R.; Wu, S.; Park, S. H.; Chang, D. W. Solution Processable Small Molecules as Efficient Electron Transport Layers in Organic Optoelectronic Devices. *J. Mater. Chem. A* **2020**, 13501–13508.
- (12) Planes, E.; Juillard, S.; Matheron, M.; Charvin, N.; Cros, S.; Qian, D.; Zhang, F.; Berson, S.; Flandin, L. Encapsulation Effect on Performance and Stability of Organic Solar Cells. *Adv. Mater. Interfaces* **2020**, 2000293, 1–13.
- (13) Song, S.; Lee, K. T.; Koh, C. W.; Shin, H.; Gao, M.; Woo, H. Y.; Vak, D.; Kim, J. Y. Hot Slot Die Coating for Additive-Free Fabrication of High Performance Roll-to-Roll Processed Polymer Solar Cells. *Energy Environ. Sci.* **2018**, 11 (11), 3248–3255.
- (14) Gao, S.; Hu, Y.; Duan, Z.; Gao, X. N-Channel Organic Transistors Processed from Halogen-Free Solvents: Solvent Effect on Thin-Film Morphology and Charge Transport. *Chinese J. Chem.* **2016**, 34 (7), 689–695.
- (15) Wang, H.; Wu, J.; Zhang, Y.; Song, J.; Chen, L.; Xiao, Y.; Qu, J.; Wong, W. Y. Achieving Efficient Green-Solvent-Processed Organic Solar Cells by Employing Ortho-Ortho Perylene Diimide Dimer. *Org. Electron.* **2020**, 83 (September 2019), 105732.
- (16) Li, W.; Liu, Q.; Zhang, Y.; Li, C.; He, Z.; Choy, W. C. H.; Low, P. J.; Sonar, P.; Kyaw, A. K. K. Biodegradable Materials and Green Processing for Green Electronics. *Adv. Mater.* **2020**, 2001591, 1–40.
- (17) Ribeiro, A. H.; Fakhri, A.; Van Der Zee, B.; Veith, L.; Glaser, G.; Kunz, A.; Landfester, K.; Blom, P. W. M.; Michels, J. J. Green and Stable Processing of Organic Light-Emitting Diodes from Aqueous Nanodispersions. *J. Mater. Chem. C* **2020**, 8 (19), 6528–6535.
- (18) Darling, S. B.; You, F. The Case for Organic Photovoltaics. *RSC Adv.* **2013**, 3 (39), 17633–17648.
- (19) NREL. Best Research-Cell Efficiency Chart <https://www.nrel.gov/pv/cell-efficiency.html>.
- (20) Lewis S. Nathan. Research Opportunities to Advance Solar Energy Utilization. *Science (80-. )*. **2016**, 351 (6271), aad1920-1–9.
- (21) Shirakawa, H.; Louis, E. J.; MacDiarmid, A. G.; Chiang, C. K.; Heeger, A. J. Synthesis of Electrically Conducting Organic Polymers: Halogen Derivatives of Polyacetylene, (CH)<sub>x</sub>. *J. Chem. Soc. Chem. Commun.* **1977**, No. 16, 578–580.
- (22) Tang, C. W. Two-Layer Organic Photovoltaic Cell. *Appl. Phys. Lett.* **1986**, 48 (2), 183–185.
- (23) G. Yu, J. Gao, J. C. Hummelen, F. Wudl, A. J. H. Polymer Photovoltaic Cells:

- Enhanced Efficiencies via a Network of Internal Donor-Acceptor Heterojunctions. *Science* (80-. ). **1995**, *270*, 1–3.
- (24) Shaheen, S. E.; Brabec, C. J.; Sariciftci, N. S.; Padinger, F.; Fromherz, T.; Hummelen, J. C. 2.5% Efficient Organic Plastic Solar Cells. *Appl. Phys. Lett.* **2001**, *78* (6), 841–843.
- (25) Padinger, F.; Rittberger, R. S.; Sariciftci, N. S. Effects of Postproduction Treatment on Plastic Solar Cells. *Adv. Funct. Mater.* **2003**, *13* (1), 85–88.
- (26) Liu, Q.; Jiang, Y.; Jin, K.; Qin, J.; Xu, J.; Li, W.; Xiong, J.; Liu, J.; Xiao, Z.; Sun, K.; Yang, S.; Zhang, X.; Ding, L. 18% Efficiency Organic Solar Cells. *Sci. Bull.* **2020**, *65* (4), 272–275.
- (27) Koo, D.; Jung, S.; Seo, J.; Jeong, G.; Choi, Y.; Lee, J.; Lee, S. M.; Cho, Y.; Jeong, M.; Lee, J.; Oh, J.; Yang, C.; Park, H. Flexible Organic Solar Cells Over 15% Efficiency with Polyimide-Integrated Graphene Electrodes. *Joule* **2020**, *4* (5), 1021–1034.
- (28) Qu, T. Y.; Zuo, L. J.; Chen, J. De; Shi, X.; Zhang, T.; Li, L.; Shen, K. C.; Ren, H.; Wang, S.; Xie, F. M.; Li, Y. Q.; Jen, A. K. Y.; Tang, J. X. Biomimetic Electrodes for Flexible Organic Solar Cells with Efficiencies over 16%. *Adv. Opt. Mater.* **2020**, 2000669, 1–9.
- (29) Anctil, A.; Lee, E.; Lunt, R. R. Net Energy and Cost Benefit of Transparent Organic Solar Cells in Building-Integrated Applications. *Appl. Energy* **2020**, *261* (December 2019), 114429.
- (30) Lee, J.; Cha, H.; Yao, H.; Hou, J.; Suh, Y. H.; Jeong, S.; Lee, K.; Durrant, J. R. Toward Visibly Transparent Organic Photovoltaic Cells Based on a Near-Infrared Harvesting Bulk Heterojunction Blend. *ACS Appl. Mater. Interfaces* **2020**, *12* (29), 32764–32770.
- (31) Anctil, A.; Lee, E.; Lunt, R. R. Net Energy and Cost Benefit of Transparent Organic Solar Cells in Building-Integrated Applications. *Appl. Energy* **2020**, *261* (August 2019), 114429.
- (32) Zhou, Z.; Carbajales-Dale, M. Assessing the Photovoltaic Technology Landscape: Efficiency and Energy Return on Investment (EROI). *Energy Environ. Sci.* **2018**, *11* (3), 603–608.
- (33) Huang, T. Y.; Patra, D.; Hsiao, Y. S.; Chang, S. H.; Wu, C. G.; Ho, K. C.; Chu, C. W. Efficient Ternary Bulk Heterojunction Solar Cells Based on Small Molecules Only. *J. Mater. Chem. A* **2015**, *3* (19), 10512–10518.
- (34) Diao, Y.; Shaw, L.; Bao, Z.; Mannsfeld, S. C. B. Morphology Control Strategies for Solution-Processed Organic Semiconductor Thin Films. *Energy Environ. Sci.* **2014**, *7* (7), 2145–2159.

- (35) Zheng, L.; Xu, J.; Feng, Y.; Shan, H.; Fang, G.; Xu, Z. X. Green Solvent Processed Tetramethyl-Substituted Aluminum Phthalocyanine Thin Films as Anode Buffer Layers in Organic Light-Emitting Diodes. *J. Mater. Chem. C* **2018**, *6* (42), 11471–11478.
- (36) Wang, Y.; Yan, C.; Cheng, S. Y.; Xu, Z. Q.; Sun, X.; Xu, Y. H.; Chen, J. J.; Jiang, Z.; Liang, K.; Feng, Z. S. Flexible RFID Tag Metal Antenna on Paper-Based Substrate by Inkjet Printing Technology. *Adv. Funct. Mater.* **2019**, *29* (29), 1–11.
- (37) Hong, J.; Wang, C.; Cha, H.; Kim, H. N.; Kim, Y.; Park, C. E.; An, T. K.; Kwon, S. K.; Kim, Y. H. Morphology Driven by Molecular Structure of Thiazole-Based Polymers for Use in Field-Effect Transistors and Solar Cells. *Chem. - A Eur. J.* **2019**, *25* (2), 649–656.
- (38) Knupfer, M. Exciton Binding Energies in Organic Semiconductors. *Appl. Phys. A Mater. Sci. Process.* **2003**, *77* (5), 623–626.
- (39) Hummer, K.; Ambrosch-Draxl, C. Oligoacene Exciton Binding Energies: Their Dependence on Molecular Size. *Phys. Rev. B - Condens. Matter Mater. Phys.* **2005**, *71* (8), 1–4.
- (40) Van Der Horst, J. W.; Bobbert, P. A.; Michels, M. A. J.; Bäessler, H. Calculation of Excitonic Properties of Conjugated Polymers Using the Bethe-Salpeter Equation. *J. Chem. Phys.* **2001**, *114* (15), 6950–6957.
- (41) Clarke, T. M.; Durrant, J. R. Charge Photogeneration in Organic Solar Cells. *Chem. Rev.* **2010**, *110* (11), 6736–6767.
- (42) Deibel, C.; MacK, D.; Gorenflot, J.; Schöll, A.; Krause, S.; Reinert, F.; Rauh, D.; Dyakonov, V. Energetics of Excited States in the Conjugated Polymer Poly(3-Hexylthiophene). *Phys. Rev. B - Condens. Matter Mater. Phys.* **2010**, *81* (8), 1–5.
- (43) De, S.; Kesti, T.; Maiti, M.; Zhang, F.; Inganäs, O.; Yartsev, A.; Pascher, T.; Sundström, V. Exciton Dynamics in Alternating Polyfluorene/Fullerene Blends. *Chem. Phys.* **2008**, *350* (1–3), 14–22.
- (44) Derouiche, H.; Djara, V. Impact of the Energy Difference in LUMO and HOMO of the Bulk Heterojunctions Components on the Efficiency of Organic Solar Cells. *Sol. Energy Mater. Sol. Cells* **2007**, *91* (13), 1163–1167.
- (45) Athanasopoulos, S.; Schauer, F.; Nádaždy, V.; Weiß, M.; Kahle, F. J.; Scherf, U.; Bäessler, H.; Köhler, A. What Is the Binding Energy of a Charge Transfer State in an Organic Solar Cell? *Adv. Energy Mater.* **2019**, *9* (24), 1–11.
- (46) Scharber, M. C.; Mühlbacher, D.; Koppe, M.; Denk, P.; Waldauf, C.; Heeger, A. J.; Brabec, C. J. Design Rules for Donors in Bulk-Heterojunction Solar Cells -



- Towards 10 % Energy-Conversion Efficiency. *Adv. Mater.* **2006**, *18* (6), 789–794.
- (47) Jean-Luc Bre´das, David Beljonne, Veaceslav Coropceanu, and J. C. Charge-Transfer and Energy-Transfer Processes in  $\pi$ -Conjugated Oligomers and Polymers: A Molecular Picture. *Chem. Rev.* **2004**, *104* (11), 4971–5003.
- (48) Vandewal, K. Interfacial Charge Transfer States in Condensed Phase Systems. *Annu. Rev. Phys. Chem.* **2016**, *67*, 113–133.
- (49) N . S . Sariciftci , L . Smilowitz , A . J . Heeger , F . . W. Photoinduced Electron Transfer from a Conducting Polymer to Buckminsterfullerene Author ( s ): N . S . Sariciftci , L . Smilowitz , A . J . Heeger , F . Wudl Published by : American Association for the Advancement of Science Stable URL : [Http://www.jstor.org](http://www.jstor.org). *Adv. Sci.* **2009**, *258* (5087), 1474–1476.
- (50) Brabec, C. J.; Zerza, G.; Cerullo, G.; De Silvestri, S.; Luzzati, S.; Hummelen, J. C.; Sariciftci, S. Tracing Photoinduced Electron Transfer Process in Conjugated Polymer/Fullerene Bulk Heterojunctions in Real Time. *Chem. Phys. Lett.* **2001**, *340* (3–4), 232–236.
- (51) Han, G.; Yi, Y.; Shuai, Z. From Molecular Packing Structures to Electronic Processes: Theoretical Simulations for Organic Solar Cells. *Adv. Energy Mater.* **2018**, *8* (28).
- (52) Li, J.; Zhang, Y.; Yuan, J.; Zhu, C.; Peng, H.; Zou, Y. Fine-Tuning of Non-Fullerene Acceptor Gives over 14% Efficiency for Organic Solar Cells. *Dye. Pigment.* **2020**, *181* (April), 108559.
- (53) Zhang, W.; Huang, J.; Xu, J.; Han, M.; Su, D.; Wu, N.; Zhang, C.; Xu, A.; Zhan, C. Phthalimide Polymer Donor Guests Enable over 17% Efficient Organic Solar Cells via Parallel-Like Ternary and Quaternary Strategies. *Adv. Energy Mater.* **2020**.
- (54) Sun, H.; Sun, P.; Zhang, C.; Yang, Y.; Gao, X.; Chen, F.; Xu, Z.; Chen, Z. K.; Huang, W. High-Performance Organic Solar Cells Based on a Non-Fullerene Acceptor with a Spiro Core. *Chem. - An Asian J.* **2017**, *12* (7), 721–725.
- (55) Bilal Ahmed Siddique, M.; Hussain, R.; Ali Siddique, S.; Yasir Mehboob, M.; Irshad, Z.; Iqbal, J.; Adnan, M. Designing Triphenylamine-Configured Donor Materials with Promising Photovoltaic Properties for Highly Efficient Organic Solar Cells. *ChemistrySelect* **2020**, *5* (25), 7358–7369.
- (56) Hou, J.; Inganäs, O.; Friend, R. H.; Gao, F. Organic Solar Cells Based on Non-Fullerene Acceptors. *Nat. Mater.* **2018**, *17* (2), 119–128.
- (57) Wagenpfahl, A.; Rauh, D.; Binder, M.; Deibel, C.; Dyakonov, V. S-Shaped Current-Voltage Characteristics of Organic Solar Devices. *Phys. Rev. B* -

- Condens. Matter Mater. Phys.* **2010**, *82* (11), 1–8.
- (58) Wang, F.; Tan, Z.; Li, Y. Solution-Processable Metal Oxides/Chelates as Electrode Buffer Layers for Efficient and Stable Polymer Solar Cells. *Energy Environ. Sci.* **2015**, *8* (4), 1059–1091.
- (59) Liang, Z.; Zhang, Q.; Jiang, L.; Cao, G. ZnO Cathode Buffer Layers for Inverted Polymer Solar Cells. *Energy Environ. Sci.* **2015**, *8* (12), 3442–3476.
- (60) Nilsson, S.; Bernasik, A.; Budkowski, A.; Moons, E. Morphology and Phase Segregation of Spin-Casted Films of Polyfluorene/PCBM Blends. *Macromolecules* **2007**, *40* (23), 8291–8301.
- (61) McDowell, C.; Bazan, G. C. Organic Solar Cells Processed from Green Solvents. *Curr. Opin. Green Sustain. Chem.* **2017**, *5*, 49–54.
- (62) Kong, J.; Hwang, I. W.; Lee, K. Top-down Approach for Nanophase Reconstruction in Bulk Heterojunction Solar Cells. *Adv. Mater.* **2014**, *26* (36), 6275–6283.
- (63) Jagadamma, L. K.; Al-Senani, M.; El-Labban, A.; Gereige, I.; Ngongang Ndjawa, G. O.; Faria, J. C. D.; Kim, T.; Zhao, K.; Cruciani, F.; Anjum, D. H.; McLachlan, M. A.; Beaujuge, P. M.; Amassian, A. Polymer Solar Cells with Efficiency >10% Enabled via a Facile Solution-Processed Al-Doped ZnO Electron Transporting Layer. *Adv. Energy Mater.* **2015**, *5* (12).
- (64) Liao, S. H.; Jhuo, H. J.; Yeh, P. N.; Cheng, Y. S.; Li, Y. L.; Lee, Y. H.; Sharma, S.; Chen, S. A. Single Junction Inverted Polymer Solar Cell Reaching Power Conversion Efficiency 10.31% by Employing Dual-Doped Zinc Oxide Nano-Film as Cathode Interlayer. *Sci. Rep.* **2014**, *4*, 4–10.
- (65) Steim, R.; Choulis, S. A.; Schilinsky, P.; Brabec, C. J. Interface Modification for Highly Efficient Organic Photovoltaics. *Appl. Phys. Lett.* **2008**, *92* (9), 93–96.
- (66) Hadipour, A.; Müller, R.; Heremans, P. Room Temperature Solution-Processed Electron Transport Layer for Organic Solar Cells. *Org. Electron.* **2013**, *14* (10), 2379–2386.
- (67) Litzov, I.; Brabec, C. J. Development of Efficient and Stable Inverted Bulk Heterojunction (BHJ) Solar Cells Using Different Metal Oxide Interfaces. *Materials (Basel)*. **2013**, *6* (12), 5796–5820.
- (68) Kuwabara, T.; Sugiyama, H.; Yamaguchi, T.; Takahashi, K. Inverted Type Bulk-Heterojunction Organic Solar Cell Using Electrodeposited Titanium Oxide Thin Films as Electron Collector Electrode. *Thin Solid Films* **2009**, *517* (13), 3766–3769.
- (69) Yuan, J.; Huang, X.; Dong, H.; Lu, J.; Yang, T.; Li, Y.; Gallagher, A.; Ma, W.

- Structure, Band Gap and Energy Level Modulations for Obtaining Efficient Materials in Inverted Polymer Solar Cells. *Org. Electron.* **2013**, *14* (2), 635–643.
- (70) Zhang, Z.; Zhang, Z.; Yu, Y.; Zhao, B.; Li, S.; Zhang, J.; Tan, S. Non-Conjugated Polymers as Thickness-Insensitive Electron Transport Materials in High-Performance Inverted Organic Solar Cells. *J. Energy Chem.* **2020**, *47*, 196–202.
- (71) Thambidurai, M.; Shini, F.; Kim, J. Y.; Lee, C.; Dang, C. Solution-Processed Ga-TiO<sub>2</sub> Electron Transport Layer for Efficient Inverted Organic Solar Cells. *Mater. Lett.* **2020**, *274*, 128003.
- (72) Abdallaoui, M.; Sengouga, N.; Chala, A.; Meftah, A. F.; Meftah, A. M. Comparative Study of Conventional and Inverted P3HT: PCBM Organic Solar Cell. *Opt. Mater. (Amst)*. **2020**, *105* (April), 109916.
- (73) Etxebarria, I.; Guerrero, A.; Albero, J.; Garcia-Belmonte, G.; Palomares, E.; Pacios, R. Inverted vs Standard PTB7:PC70BM Organic Photovoltaic Devices. the Benefit of Highly Selective and Extracting Contacts in Device Performance. *Org. Electron.* **2014**, *15* (11), 2756–2762.
- (74) Ma, Z.; Sun, W.; Himmelberger, S.; Vandewal, K.; Tang, Z.; Bergqvist, J.; Salleo, A.; Andreasen, J. W.; Inganäs, O.; Andersson, M. R.; Müller, C.; Zhang, F.; Wang, E. Structure-Property Relationships of Oligothiophene-Isoindigo Polymers for Efficient Bulk-Heterojunction Solar Cells. *Energy Environ. Sci.* **2014**, *7* (1), 361–369.
- (75) Bloking, J. T.; Giovenzana, T.; Higgs, A. T.; Ponec, A. J.; Hoke, E. T.; Vandewal, K.; Ko, S.; Bao, Z.; Sellinger, A.; McGehee, M. D. Comparing the Device Physics and Morphology of Polymer Solar Cells Employing Fullerenes and Non-Fullerene Acceptors. *Adv. Energy Mater.* **2014**, *4* (12).
- (76) Sharenko, A.; Gehrig, D.; Laquai, F.; Nguyen, T. Q. The Effect of Solvent Additive on the Charge Generation and Photovoltaic Performance of a Solution-Processed Small Molecule: Perylene Diimide Bulk Heterojunction Solar Cell. *Chem. Mater.* **2014**, *26* (14), 4109–4118.
- (77) Proctor, C. M.; Kher, A. S.; Love, J. A.; Huang, Y.; Sharenko, A.; Bazan, G. C.; Nguyen, T. Q. Understanding Charge Transport in Molecular Blend Films in Terms of Structural Order and Connectivity of Conductive Pathways. *Adv. Energy Mater.* **2016**, *6* (9).
- (78) Zhang, J.; Zhang, Y.; Fang, J.; Lu, K.; Wang, Z.; Ma, W.; Wei, Z. Conjugated Polymer-Small Molecule Alloy Leads to High Efficient Ternary Organic Solar Cells. *J. Am. Chem. Soc.* **2015**, *137* (25), 8176–8183.
- (79) Collins, B. A.; Li, Z.; Tumbleston, J. R.; Gann, E.; McNeill, C. R.; Ade, H. Absolute Measurement of Domain Composition and Nanoscale Size Distribution

- Explains Performance in PTB7:PC71bm Solar Cells. *Adv. Energy Mater.* **2013**, *3* (1), 65–74.
- (80) Shintaku, N.; Hiramoto, M.; Izawa, S. Doping for Controlling Open-Circuit Voltage in Organic Solar Cells. *J. Phys. Chem. C* **2018**, *122* (10), 5248–5253.
- (81) Elumalai, N. K.; Uddin, A. Open Circuit Voltage of Organic Solar Cells: An in-Depth Review. *Energy Environ. Sci.* **2016**, *9* (2), 391–410.
- (82) Oosterhout, S. D.; Savikhin, V.; Burgers, M. A.; Zhang, J.; Zhang, Y.; Marder, S. R.; Bazan, G. C.; Toney, M. F. Absence of Mixed Phase in Organic Photovoltaic Active Layers Facilitates Use of Green Solvent Processing. *J. Phys. Chem. C* **2018**, *122* (20), 11136–11144.
- (83) Cho, S.; Rolczynski, B. S.; Xu, T.; Yu, L.; Chen, L. X. Solution Phase Exciton Diffusion Dynamics of a Charge-Transfer Copolymer PTB7 and a Homopolymer P3HT. *J. Phys. Chem. B* **2015**, *119* (24), 7447–7456.
- (84) Yang, X.; van Duren, J. K. J.; Rispens, M. T.; Hummelen, J. C.; Janssen, R. A. J.; Michels, M. A. J.; Loos, J. Crystalline Organization of a Methanofullerene as Used for Plastic Solar-Cell Applications. *Adv. Mater.* **2004**, *16* (910), 802–806.
- (85) Hleli, E.; Alam, S.; Saaidia, A.; Kästner, C.; Hoepfener, S.; Ulbricht, C.; Romdhane, S.; Fredj, A. Ben; Egbe, D. A. M.; Schubert, U. S.; Bouchriha, H.; Hoppe, H. Improvement of Polymer:Fullerene Bulk Heterojunction Morphology via Temperature and Anti-Solvent Effect. *Synth. Met.* **2018**, *243* (March), 8–16.
- (86) S. Gurney, R.; Li, W.; Yan, Y.; Liu, D.; J. Pearson, A.; Wang, T. Morphology and Efficiency Enhancements of PTB7-Th:ITIC Nonfullerene Organic Solar Cells Processed via Solvent Vapor Annealing. *J. Energy Chem.* **2019**, *37*, 148–156.
- (87) Duong, D. T.; Walker, B.; Lin, J.; Kim, C.; Love, J.; Purushothaman, B.; Anthony, J. E.; Nguyen, T. Q. Molecular Solubility and Hansen Solubility Parameters for the Analysis of Phase Separation in Bulk Heterojunctions. *J. Polym. Sci. Part B Polym. Phys.* **2012**, *50* (20), 1405–1413.
- (88) Vongsaysy, U. Studies on Processing Additives Introduced for Increasing the Efficiency of Organic Solar Cells: Their Selections and Their Mechanistic Effects, University of Waterloo, 2014.
- (89) Yao, Y.; Hou, J.; Xu, Z.; Li, G.; Yang, Y. Effects of Solvent Mixtures on the Nanoscale Phase Separation in Polymer Solar Cells. *Adv. Funct. Mater.* **2008**, *18* (12), 1783–1789.
- (90) Ruderer, M. A.; Guo, S.; Meier, R.; Chiang, H. Y.; Körstgens, V.; Wiedersich, J.; Perlich, J.; Roth, S. V.; Müller-Buschbaum, P. Solvent-Induced Morphology in Polymer-Based Systems for Organic Photovoltaics. *Adv. Funct. Mater.* **2011**, *21*

- (17), 3382–3391.
- (91) Bernardo, G.; Melle-Franco, M.; Washington, A. L.; Dalglish, R. M.; Li, F.; Mendes, A.; Parnell, S. R. Different Agglomeration Properties of PC61BM and PC71BM in Photovoltaic Inks—a Spin-Echo SANS Study. *RSC Adv.* **2020**, *10* (8), 4512–4520.
- (92) Lindqvist, C.; Moons, E.; van Stam, J. Fullerene Aggregation in Thin Films of Polymer Blends for Solar Cell Applications. *Materials (Basel)*. **2018**, *11* (11), 16–19.
- (93) Guo, J.; Balakirev, D. O.; Gu, C.; Peregudova, S. M.; Ponomarenko, S. A.; Liu, Z.; Luponosov, Y. N.; Min, J.; Lei, A. End Group Tuning in Small Molecule Donors for Non-Fullerene Organic Solar Cells. *Dye. Pigment.* **2020**, *175* (November 2019), 108078.
- (94) Huangzhong, Y. Different Solvents Effect on the Performance of the Solar Cells Based on Poly(3-Hexylthiophene):Methanofullerenes. *Synth. Met.* **2010**, *160* (23–24), 2505–2509.
- (95) Zhang, K.; Chen, Z.; Armin, A.; Dong, S.; Xia, R.; Yip, H.-L.; Shoaee, S.; Huang, F.; Cao, Y. Efficient Large Area Organic Solar Cells Processed by Blade-Coating With Single-Component Green Solvent. *Sol. RRL* **2018**, *2* (1), 1700169.
- (96) Zheng, Y.; Wang, G.; Huang, D.; Kong, J.; Goh, T. H.; Huang, W.; Yu, J.; Taylor, A. D. Binary Solvent Additives Treatment Boosts the Efficiency of PTB7:PCBM Polymer Solar Cells to Over 9.5%. *Sol. RRL* **2018**, *2* (4), 1–8.
- (97) Zhao, W.; Ye, L.; Zhang, S.; Sun, M.; Hou, J. A Universal Halogen-Free Solvent System for Highly Efficient Polymer Solar Cells. *J. Mater. Chem. A* **2015**, *3* (24), 12723–12729.
- (98) Xu, Y.; Sun, L.; Wu, J.; Ye, W.; Chen, Y.; Zhang, S.; Miao, C.; Huang, H. Thiophene: An Eco-Friendly Solvent for Organic Solar Cells. *Dye. Pigment.* **2019**, *168* (January), 36–41.
- (99) Liu, D.; Wang, Z.; Zhang, S.; Zheng, Z.; Yang, B.; Ma, W.; Hou, J. Rational Selection of Solvents and Fine Tuning of Morphologies toward Highly Efficient Polymer Solar Cells Fabricated Using Green Solvents. *RSC Adv.* **2015**, *5* (85), 69567–69572.
- (100) Khan, J. A.; Sharma, R.; Sarkar, S. K.; Panwar, A. S.; Gupta, D. Combined Effect of ZnO Nanoripples and Solvent Additive on the Nanomorphology and Performance of PTB7-Th: PC71BM Organic Solar Cells. *Nanotechnology* **2019**, *30* (38).
- (101) Lou, S. J.; Szarko, J. M.; Xu, T.; Yu, L.; Marks, T. J.; Chen, L. X. Effects of Additives on the Morphology of Solution Phase Aggregates Formed by Active

- Layer Components of High-Efficiency Organic Solar Cells. *J. Am. Chem. Soc.* **2011**, *133* (51), 20661–20663.
- (102) Solanki, A.; Wu, B.; Salim, T.; Lam, Y. M.; Sum, T. C. Correlation between Blend Morphology and Recombination Dynamics in Additive-Added P3HT:PCBM Solar Cells. *Phys. Chem. Chem. Phys.* **2015**, *17* (39), 26111–26120.
- (103) Shin, N.; Richter, L. J.; Herzing, A. A.; Kline, R. J.; DeLongchamp, D. M. Effect of Processing Additives on the Solidification of Blade-Coated Polymer/Fullerene Blend Films via in-Situ Structure Measurements. *Adv. Energy Mater.* **2013**, *3* (7), 938–948.
- (104) Vongsaysy, U.; Pavageau, B.; Wantz, G.; Bassani, D. M.; Servant, L.; Aziz, H. Guiding the Selection of Processing Additives for Increasing the Efficiency of Bulk Heterojunction Polymeric Solar Cells. *Adv. Energy Mater.* **2014**, *4* (3), 1–9.
- (105) Vongsaysy, U.; Bassani, D. M.; Servant, L.; Pavageau, B.; Wantz, G.; Aziz, H. Formulation Strategies for Optimizing the Morphology of Polymeric Bulk Heterojunction Organic Solar Cells: A Brief Review. *J. Photonics Energy* **2014**, *4* (1), 040998.
- (106) Liao, C.; Zhang, M.; Xu, X.; Liu, F.; Li, Y.; Peng, Q. Green Solvent-Processed Efficient Non-Fullerene Organic Solar Cells Enabled by Low-Bandgap Copolymer Donors with EDOT Side Chains. *J. Mater. Chem. A* **2019**, *7* (2), 716–726.
- (107) Manley, E. F.; Strzalka, J.; Fauvell, T. J.; Marks, T. J.; Chen, L. X. In Situ Analysis of Solvent and Additive Effects on Film Morphology Evolution in Spin-Cast Small-Molecule and Polymer Photovoltaic Materials. *Adv. Energy Mater.* **2018**, *8* (23), 1–20.
- (108) Thomas, A.; Elsa Tom, A.; Rao, A. D.; Varman, K. A.; Ranjith, K.; Vinayakan, R.; Ramamurthy, P. C.; Ison, V. V. Solvent Polarity and Nanoscale Morphology in Bulk Heterojunction Organic Solar Cells: A Case Study. *J. Appl. Phys.* **2014**, *115* (10), 3–8.
- (109) Zhang, Z.; Zhang, X.; Zhang, J.; Gong, X.; Liu, Y.; Lu, H.; Li, C.; Bo, Z. Efficient Polymer Solar Cells Processed by Environmentally Friendly Halogen-Free Solvents. *RSC Adv.* **2016**, *6* (45), 39074–39079.
- (110) Chen, K. S.; Yip, H. L.; Schlenker, C. W.; Ginger, D. S.; Jen, A. K. Y. Halogen-Free Solvent Processing for Sustainable Development of High Efficiency Organic Solar Cells. *Org. Electron.* **2012**, *13* (12), 2870–2878.
- (111) Abdulahi, B. A.; Li, X.; Mone, M.; Kiros, B.; Genene, Z.; Qiao, S.; Yang, R.; Wang, E.; Mammo, W. Structural Engineering of Pyrrolo[3,4- F] Benzotriazole-5,7(2 H,6 H)-Dione-Based Polymers for Non-Fullerene Organic Solar Cells with an

- Efficiency over 12%. *J. Mater. Chem. A* **2019**, *7* (33), 19522–19530.
- (112) Lee, T. H.; Park, S. Y.; Walker, B.; Ko, S. J.; Heo, J.; Woo, H. Y.; Choi, H.; Kim, J. Y. A Universal Processing Additive for High-Performance Polymer Solar Cells. *RSC Adv.* **2017**, *7* (13), 7476–7482.
- (113) Shen, W.; Xiao, M.; Tang, J.; Wang, X.; Chen, W.; Yang, R.; Bao, X.; Wang, Y.; Jiao, J.; Huang, L.; Liu, J.; Wang, W.; Belfiore, L. A. Effective Regulation of the Micro-Structure of Thick P3HT:PC71BM Film by the Incorporation of Ethyl Benzenecarboxylate in Toluene Solution. *RSC Adv.* **2015**, *5* (59), 47451–47457.
- (114) Sprau, C.; Buss, F.; Wagner, M.; Landerer, D.; Koppitz, M.; Schulz, A.; Bahro, D.; Schabel, W.; Scharfer, P.; Colsmann, A. Highly Efficient Polymer Solar Cells Cast from Non-Halogenated Xylene/Anisaldehyde Solution. *Energy Environ. Sci.* **2015**, *8* (9), 2744–2752.
- (115) He, Z.; Zhong, C.; Huang, X.; Wong, W. Y.; Wu, H.; Chen, L.; Su, S.; Cao, Y. Simultaneous Enhancement of Open-Circuit Voltage, Short-Circuit Current Density, and Fill Factor in Polymer Solar Cells. *Adv. Mater.* **2011**, *23* (40), 4636–4643.
- (116) Kumari, T.; Lee, S. M.; Yang, C. Cubic-Like Bimolecular Crystal Evolution and over 12% Efficiency in Halogen-Free Ternary Solar Cells. *Adv. Funct. Mater.* **2018**, *28* (19), 1–10.
- (117) Cai, W.; Liu, P.; Jin, Y.; Xue, Q.; Liu, F.; Russell, T. P.; Huang, F.; Yip, H. L.; Cao, Y. Morphology Evolution in High-Performance Polymer Solar Cells Processed from Nonhalogenated Solvent. *Adv. Sci.* **2015**, *2* (8), 1–7.
- (118) Griffin, J.; Pearson, A. J.; Scarratt, N. W.; Wang, T.; Dunbar, A. D. F.; Yi, H.; Iraqi, A.; Buckley, A. R.; Lidzey, D. G. Organic Photovoltaic Devices with Enhanced Efficiency Processed from Non-Halogenated Binary Solvent Blends. *Org. Electron.* **2015**, *21*, 216–222.
- (119) Takahira, K.; Toda, A.; Suzuki, K.; Fukuda, T. Highly Efficient Organic Photovoltaic Cells Fabricated by Electrospray Deposition Using a Non-Halogenated Solution. *Phys. Status Solidi Appl. Mater. Sci.* **2017**, *214* (3), 6–10.
- (120) Wang, H.; Fan, Q.; Chen, L.; Xiao, Y. Amino-Acid Ester Derived Perylene Diimides Electron Acceptor Materials: An Efficient Strategy for Green-Solvent-Processed Organic Solar Cells. *Dye. Pigment.* **2019**, *164* (December 2018), 384–389.
- (121) Wan, J.; Xu, X.; Zhang, G.; Li, Y.; Feng, K.; Peng, Q. Highly Efficient Halogen-Free Solvent Processed Small-Molecule Organic Solar Cells Enabled by Material Design and Device Engineering. *Energy Environ. Sci.* **2017**, *10* (8), 1739–1745.

- (122) Heo, Y. J.; Jung, Y. S.; Hwang, K.; Kim, J. E.; Yeo, J. S.; Lee, S.; Jeon, Y. J.; Lee, D.; Kim, D. Y. Small-Molecule Organic Photovoltaic Modules Fabricated via Halogen-Free Solvent System with Roll-to-Roll Compatible Scalable Printing Method. *ACS Appl. Mater. Interfaces* **2017**, *9* (45), 39519–39525.
- (123) Ye, L.; Xiong, Y.; Zhang, Q.; Li, S.; Wang, C.; Jiang, Z.; Hou, J.; You, W.; Ade, H. Surpassing 10% Efficiency Benchmark for Nonfullerene Organic Solar Cells by Scalable Coating in Air from Single Nonhalogenated Solvent. *Adv. Mater.* **2018**, *30* (8), 1–9.
- (124) Hong, L.; Yao, H.; Wu, Z.; Cui, Y.; Zhang, T.; Xu, Y.; Yu, R.; Liao, Q.; Gao, B.; Xian, K.; Woo, H. Y.; Ge, Z.; Hou, J. Eco-Compatible Solvent-Processed Organic Photovoltaic Cells with Over 16% Efficiency. *Adv. Mater.* **2019**, *31* (39), 1–7.
- (125) Hansen, C. M. *HANSEN SOLUBILITY PARAMETERS A User's Handbook*; 2007.
- (126) Jalan, I.; Lundin, L.; van Stam, J. Using Solubility Parameters to Model More Environmentally Friendly Solvent Blends for Organic Solar Cell Active Layers. *Materials (Basel)*. **2019**, *12* (23).
- (127) Strohm, S.; Machui, F.; Langner, S.; Kubis, P.; Gasparini, N.; Salvador, M.; McCulloch, I.; Egelhaaf, H. J.; Brabec, C. J. P3HT: Non-Fullerene Acceptor Based Large Area, Semi-Transparent PV Modules with Power Conversion Efficiencies of 5%, Processed by Industrially Scalable Methods. *Energy Environ. Sci.* **2018**, *11* (8), 2225–2234.
- (128) Yao, K.; Xu, Y. X.; Wang, X.; Li, F.; Yuan, J. The Critical Role of Additives in Binary Halogen-Free Solvent Systems for the General Processing of Highly Efficient Organic Solar Cells. *RSC Adv.* **2015**, *5* (114), 93689–93696.
- (129) Walker, B.; Tamayo, A.; Duong, D. T.; Dang, X. D.; Kim, C.; Granstrom, J.; Nguyen, T. Q. A Systematic Approach to Solvent Selection Based on Cohesive Energy Densities in a Molecular Bulk Heterojunction System. *Adv. Energy Mater.* **2011**, *1* (2), 221–229.
- (130) Gerbaud, V. The InBioSynSolv Project: Virtual laboratory for synthons and biosolvent design based on reverse molecular engineering <http://www.axelera.org/>.
- (131) Axelsson, L.; Franzén, M.; Ostwald, M.; Berndes, G.; Lakshmi, G.; Ravindranath, N. H. Perspective: Jatropha Cultivation in Southern India: Assessing Farmers' Experiences. *Biofuels, Bioprod. Biorefining* **2012**, *6* (3), 246–256.
- (132) Moity, L.; Molinier, V.; Benazzouz, A.; Joossen, B.; Gerbaud, V.; Aubry, J. M. A “Top-down” in Silico Approach for Designing Ad Hoc Bio-Based Solvents: Application to Glycerol-Derived Solvents of Nitrocellulose. *Green Chem.* **2016**,



- 18 (11), 3239–3249.
- (133) Dos Santos, M. T.; Morgavi, P.; Le Roux, G. A. C. Exploring Amazonian Fats and Oils Blends by Computational Predictions of Solid Fat Content. *OCL - Oilseeds fats, Crop. Lipids* **2018**, 25 (1), 1–8.
- (134) US Patent App. 16/310,253, 2019.
- (135) Heintz, J.; Belaud, J. P.; Gerbaud, V. Chemical Enterprise Model and Decision-Making Framework for Sustainable Chemical Product Design. *Comput. Ind.* **2014**, 65 (3), 505–520.
- (136) Heintz, J. Systemic Approach and Decision Process for Sustainability in Chemical Engineering: Application to Computer Aided Product Design. PhD Thesis. **2012**, 256.
- (137) Manon Bergez-Lacoste, Sophie Thiebaud-Roux, Pascale De Caro, Jean-François Fabre, Vincent Gerbaud, Z. M. From Chemical Platform Molecules to New Biosolvents: Design Engineering as a Substitution Methodology. *Biofuels, Bioprod. Biorefining* **2012**, 6 (3), 246–256.
- (138) Samir Chtita, M. B. and T. L. Basic Approaches and Applications of QSAR / QSPR Methods. *Rev. Interdiscip.* **2016**, 1 (January).
- (139) Roy, K.; Kar, S.; Ambure, P. On a Simple Approach for Determining Applicability Domain of QSAR Models. *Chemom. Intell. Lab. Syst.* **2015**, 145, 22–29.
- (140) Bruce E. Poling, John M. Prausnitz, J. P. O. *THE PROPERTIES OF GASES AND LIQUIDS*; McGraw-Hill Professional, 2000.
- (141) Venkatasubramanian, P. R. P. & V. Genetic Algorithms Based CAMD. In *COMPUTER AIDED MOLECULAR DESIGN: THEORY AND PRACTICE*; Gani, R., Ed.; 2003; pp 95–128.
- (142) Marrero, J.; Gani, R. Group-Contribution Based Estimation of Pure Component Properties. *Fluid Phase Equilib.* **2001**, 183–184, 183–208.
- (143) Rodriguez-Donis, I.; Thiebaud-Roux, S.; Lavoine, S.; Gerbaud, V. Computer-Aided Product Design of Alternative Solvents Based on Phase Equilibrium Synergism in Mixtures. *Comptes Rendus Chim.* **2018**, 21 (6), 606–621.
- (144) Holland, J. H. *Adaptation in Natural and Artificial Systems: An Introductory Analysis with Applications to Biology, Control, and Artificial Intelligence*; University of Michigan Press, 1975.
- (145) Churi, N.; Achenie, L. E. K. Novel Mathematical Programming Model for Computer Aided Molecular Design. *Ind. Eng. Chem. Res.* **1996**, 35 (10), 3788–3794.

- (146) Ourique, J. E.; Silva Telles, A. Computer-Aided Molecular Design with Simulated Annealing and Molecular Graphs. *Comput. Chem. Eng.* **1998**, *22* (SUPPL.1), 0–3.
- (147) Weininger, D. SMILES, a Chemical Language and Information System: 1: Introduction to Methodology and Encoding Rules. *J. Chem. Inf. Comput. Sci.* **1988**, *28* (1), 31–36.
- (148) Korichi, M.; Gerbaud, V.; Floquet, P.; Meniai, A. H.; Nacef, S.; Joulia, X. Computer Aided Aroma Design I-Molecular Knowledge Framework. *Chem. Eng. Process. Process Intensif.* **2008**, *47* (11), 1902–1911.
- (149) Dang, M. T.; Hirsch, L.; Wantz, G. P3HT:PCBM, Best Seller in Polymer Photovoltaic Research. *Adv. Mater.* **2011**, *23* (31), 3597–3602.
- (150) Chueh, C. C.; Yao, K.; Yip, H. L.; Chang, C. Y.; Xu, Y. X.; Chen, K. S.; Li, C. Z.; Liu, P.; Huang, F.; Chen, Y.; Chen, W. C.; Jen, A. K. Y. Non-Halogenated Solvents for Environmentally Friendly Processing of High-Performance Bulk-Heterojunction Polymer Solar Cells. *Energy Environ. Sci.* **2013**, *6* (11), 3241–3248.
- (151) Wadsworth, A.; Hamid, Z.; Bidwell, M.; Ashraf, R. S.; Khan, J. I.; Anjum, D. H.; Cendra, C.; Yan, J.; Rezasoltani, E.; Guilbert, A. A. Y.; Azzouzi, M.; Gasparini, N.; Bannock, J. H.; Baran, D.; Wu, H.; de Mello, J. C.; Brabec, C. J.; Salleo, A.; Nelson, J.; Laquai, F.; McCulloch, I. Progress in Poly (3-Hexylthiophene) Organic Solar Cells and the Influence of Its Molecular Weight on Device Performance. *Adv. Energy Mater.* **2018**, *8* (28).
- (152) Zhang, K. N.; Bi, P. Q.; Wen, Z. C.; Niu, M. S.; Chen, Z. H.; Wang, T.; Feng, L.; Yang, J. L.; Hao, X. T. Unveiling the Important Role of Non-Fullerene Acceptors Crystallinity on Optimizing Nanomorphology and Charge Transfer in Ternary Organic Solar Cells. *Org. Electron.* **2018**, *62* (July), 643–652.
- (153) Hamid, Z.; Wadsworth, A.; Rezasoltani, E.; Holliday, S.; Azzouzi, M.; Neophytou, M.; Guilbert, A. A. Y.; Dong, Y.; Little, M. S.; Mukherjee, S.; Herzing, A. A.; Bristow, H.; Kline, R. J.; DeLongchamp, D. M.; Bakulin, A. A.; Durrant, J. R.; Nelson, J.; McCulloch, I. Influence of Polymer Aggregation and Liquid Immiscibility on Morphology Tuning by Varying Composition in PffBT4T-2DT/Nonfullerene Organic Solar Cells. *Adv. Energy Mater.* **2020**, *10* (8), 1–13.
- (154) Munshi, J.; Balasubramanian, G. Investigating Blend Morphology of P3HT:PCBM Bulk Heterojunction Solar Cells by Classical Atomistic Simulations—Progress and Prospects. *Soft Mater.* **2020**, *00* (00), 1–14.
- (155) Zhang, H.; Yao, H.; Zhao, W.; Ye, L.; Hou, J. High-Efficiency Polymer Solar Cells Enabled by Environment-Friendly Single-Solvent Processing. *Adv. Energy Mater.* **2016**, *6* (6), 1–6.

- (156) Zhu, L.; Zhang, M.; Zhou, G.; Hao, T.; Xu, J.; Wang, J.; Qiu, C.; Prine, N.; Ali, J.; Feng, W.; Gu, X.; Ma, Z.; Tang, Z.; Zhu, H.; Ying, L.; Zhang, Y.; Liu, F. Efficient Organic Solar Cell with 16.88% Efficiency Enabled by Refined Acceptor Crystallization and Morphology with Improved Charge Transfer and Transport Properties. *Adv. Energy Mater.* **2020**, *10* (18), 1–9.
- (157) Verploegen, E.; Miller, C. E.; Schmidt, K.; Bao, Z.; Toney, M. F. Manipulating the Morphology of P3HT-PCBM Bulk Heterojunction Blends with Solvent Vapor Annealing. *Chem. Mater.* **2012**, *24* (20), 3923–3931.
- (158) S. Abbott, C. M. Hansen, H. Y. HSPiP 4th Edition Version 4.1.07. CRC Press, Boca Raton FL 2013.
- (159) Howell, S. and S. E. Flammable and Combustible Liquid Hazard Classifications <https://ehs.princeton.edu/laboratory-research/chemical-safety/flammable-materials/flammable-and-combustible-liquid-hazard>.
- (160) Shalu, C.; Shukla, M.; Tiwari, A.; Agrawal, J.; Bilgaiyan, A.; Singh, V. Role of Solvent Used to Cast P3HT Thin Films on the Performance of ZnO/P3HT Hybrid Photo Detector. *Phys. E Low-Dimensional Syst. Nanostructures* **2020**, *115* (April 2019), 113694.
- (161) Yamamoto, H. Hansen Solubility Parameters(HSP) Application Notes <http://www.pirika.com/NewHP/Y-MB/Y-MB.html>.
- (162) Hukkerikar, A. S.; Sarup, B.; Ten Kate, A.; Abildskov, J.; Sin, G.; Gani, R. Group-Contribution + (GC +) Based Estimation of Properties of Pure Components: Improved Property Estimation and Uncertainty Analysis. *Fluid Phase Equilib.* **2012**, *321*, 25–43.
- (163) Conte, E.; Martinho, A.; Matos, H. A.; Gani, R. Combined Group-Contribution and Atom Connectivity Index-Based Methods for Estimation of Surface Tension and Viscosity. *Ind. Eng. Chem. Res.* **2008**, *47* (20), 7940–7954.
- (164) Clark, J. H.; Hunt, A. J.; Topi, C.; Paggiola, G.; Sherwood, J. *Sustainable Solvents (Perspectives from Research, Business and International Policy)*; 2017; Vol. 2017-Janua.
- (165) de Gonzalo, G.; Alcántara, A. R.; Domínguez de María, P. Cyclopentyl Methyl Ether (CPME): A Versatile Eco-Friendly Solvent for Applications in Biotechnology and Biorefineries. *ChemSusChem* **2019**, *12* (10), 2083–2097.
- (166) Chen, H. Y.; Hou, J.; Zhang, S.; Liang, Y.; Yang, G.; Yang, Y.; Yu, L.; Wu, Y.; Li, G. Polymer Solar Cells with Enhanced Open-Circuit Voltage and Efficiency. *Nat. Photonics* **2009**, *3* (11), 649–653.
- (167) Liang, Y.; Feng, D.; Wu, Y.; Tsai, S. T.; Li, G.; Ray, C.; Yu, L. Highly Efficient Solar Cell Polymers Developed via Fine-Tuning of Structural and Electronic

- Properties. *J. Am. Chem. Soc.* **2009**, *131* (22), 7792–7799.
- (168) Li, W.; Albrecht, S.; Yang, L.; Roland, S.; Tumbleston, J. R.; McAfee, T.; Yan, L.; Kelly, M. A.; Ade, H.; Neher, D.; You, W. Mobility-Controlled Performance of Thick Solar Cells Based on Fluorinated Copolymers. *J. Am. Chem. Soc.* **2014**, *136* (44), 15566–15576.
- (169) Leclerc, N.; Chávez, P.; Ibraikulov, O. A.; Heiser, T.; Lévêque, P. Impact of Backbone Fluorination on  $\pi$ -Conjugated Polymers in Organic Photovoltaic Devices: A Review. *Polymers (Basel)*. **2016**, *8* (1).
- (170) Jo, J. W.; Jung, J. W.; Ahn, H.; Ko, M. J.; Jen, A. K. Y.; Son, H. J. Effect of Molecular Orientation of Donor Polymers on Charge Generation and Photovoltaic Properties in Bulk Heterojunction All-Polymer Solar Cells. *Adv. Energy Mater.* **2017**, *7* (1).
- (171) Nguyen, T. L.; Choi, H.; Ko, S. J.; Uddin, M. A.; Walker, B.; Yum, S.; Jeong, J. E.; Yun, M. H.; Shin, T. J.; Hwang, S.; Kim, J. Y.; Woo, H. Y. Semi-Crystalline Photovoltaic Polymers with Efficiency Exceeding 9% in a  $\sim$ 300 Nm Thick Conventional Single-Cell Device. *Energy Environ. Sci.* **2014**, *7* (9), 3040–3051.
- (172) Jung, J. W.; Liu, F.; Russell, T. P.; Jo, W. H. Medium Bandgap Conjugated Polymer for High Performance Polymer Solar Cells Exceeding 9% Power Conversion Efficiency. *Adv. Mater.* **2015**, *27* (45), 7462–7468.
- (173) Stuart, A. C.; Tumbleston, J. R.; Zhou, H.; Li, W.; Liu, S.; Ade, H.; You, W. Fluorine Substituents Reduce Charge Recombination and Drive Structure and Morphology Development in Polymer Solar Cells. *J. Am. Chem. Soc.* **2013**, *135* (5), 1806–1815.
- (174) Ibraikulov, O. A.; Ngov, C.; Chávez, P.; Bulut, I.; Heinrich, B.; Boyron, O.; Gerasimov, K. L.; Ivanov, D. A.; Swaraj, S.; Méry, S.; Leclerc, N.; Lévêque, P.; Heiser, T. Face-on Orientation of Fluorinated Polymers Conveyed by Long Alkyl Chains: A Prerequisite for High Photovoltaic Performances. *J. Mater. Chem. A* **2018**, *6* (25), 12038–12045.
- (175) Ibraikulov, O. A.; Wang, J.; Kamatham, N.; Heinrich, B.; Méry, S.; Kohlstädt, M.; Würfel, U.; Ferry, S.; Leclerc, N.; Heiser, T.; Lévêque, P. ITO-Free Organic Photovoltaic Modules Based on Fluorinated Polymers Deposited from Non-Halogenated Solution: A Major Step Toward Large-Scale Module Production. *Sol. RRL* **2019**, *3* (12), 1–7.
- (176) Mei, J.; Kim, D. H.; Ayzner, A. L.; Toney, M. F.; Bao, Z. Siloxane-Terminated Solubilizing Side Chains: Bringing Conjugated Polymer Backbones Closer and Boosting Hole Mobilities in Thin-Film Transistors. *J. Am. Chem. Soc.* **2011**, *133* (50), 20130–20133.

- (177) Han, A. R.; Lee, J.; Lee, H. R.; Lee, J.; Kang, S. H.; Ahn, H.; Shin, T. J.; Oh, J. H.; Yang, C. Siloxane Side Chains: A Universal Tool for Practical Applications of Organic Field-Effect Transistors. *Macromolecules* **2016**, *49* (10), 3739–3748.
- (178) Yang, S. F.; Liu, Z. T.; Cai, Z. X.; Luo, H. W.; Qi, P. L.; Zhang, G. X.; Zhang, D. Q. Conjugated Donor-Acceptor Polymers Entailing Pechmann Dye-Derived Acceptor with Siloxane-Terminated Side Chains Exhibiting Balanced Ambipolar Semiconducting Behavior. *Macromolecules* **2016**, *49* (16), 5857–5865.
- (179) Liu, X.; Nian, L.; Gao, K.; Zhang, L.; Qing, L.; Wang, Z.; Ying, L.; Xie, Z.; Ma, Y.; Cao, Y.; Liu, F.; Chen, J. Low Band Gap Conjugated Polymers Combining Siloxane-Terminated Side Chains and Alkyl Side Chains: Side-Chain Engineering Achieving a Large Active Layer Processing Window for PCE > 10% in Polymer Solar Cells. *J. Mater. Chem. A* **2017**, *5* (33), 17619–17631.
- (180) Kamino, B. A.; Bender, T. P. The Use of Siloxanes, Silsesquioxanes, and Silicones in Organic Semiconducting Materials. *Chem. Soc. Rev.* **2013**, *42* (12), 5119–5130.
- (181) Kim, D. H.; Ayzner, A. L.; Appleton, A. L.; Schmidt, K.; Mei, J.; Toney, M. F.; Bao, Z. Comparison of the Photovoltaic Characteristics and Nanostructure of Fullerenes Blended with Conjugated Polymers with Siloxane-Terminated and Branched Aliphatic Side Chains. *Chem. Mater.* **2013**, *25* (3), 431–440.
- (182) Tang, Z.; Xu, X.; Li, R.; Yu, L.; Meng, L.; Wang, Y.; Li, Y.; Peng, Q. Asymmetric Siloxane Functional Side Chains Enable High-Performance Donor Copolymers for Photovoltaic Applications. *ACS Appl. Mater. Interfaces* **2020**, *12* (15), 17760–17768.
- (183) Liu, Y.; Zhao, J.; Li, Z.; Mu, C.; Ma, W.; Hu, H.; Jiang, K.; Lin, H.; Ade, H.; Yan, H. Aggregation and Morphology Control Enables Multiple Cases of High-Efficiency Polymer Solar Cells. *Nat. Commun.* **2014**, *5* (9).
- (184) Li, Z.; Jiang, K.; Yang, G.; Lai, J. Y. L.; Ma, T.; Zhao, J.; Ma, W.; Yan, H. Donor Polymer Design Enables Efficient Non-Fullerene Organic Solar Cells. *Nat. Commun.* **2016**, *7* (9), 1–9.
- (185) Chen, Z.; Cai, P.; Chen, J.; Liu, X.; Zhang, L.; Lan, L.; Peng, J.; Ma, Y.; Cao, Y. Low Band-Gap Conjugated Polymers with Strong Interchain Aggregation and Very High Hole Mobility towards Highly Efficient Thick-Film Polymer Solar Cells. *Adv. Mater.* **2014**, *26* (16), 2586–2591.
- (186) Kim, I. B.; Jang, S. Y.; Kim, Y. A.; Kang, R.; Kim, I. S.; Ko, D. K.; Kim, D. Y. The Effect of Fluorine Substitution on the Molecular Interactions and Performance in Polymer Solar Cells. *ACS Appl. Mater. Interfaces* **2017**, *9* (28), 24011–24019.
- (187) Li, M.; An, C.; Marszalek, T.; Baumgarten, M.; Yan, H.; Müllen, K.; Pisula, W.

- Controlling the Surface Organization of Conjugated Donor–Acceptor Polymers by Their Aggregation in Solution. *Adv. Mater.* **2016**, *28* (42), 9430–9438.
- (188) Fei, Z.; Boufflet, P.; Wood, S.; Wade, J.; Moriarty, J.; Gann, E.; Ratcliff, E. L.; Mcneill, C. R.; Siringhaus, H.; Kim, J. S.; Heeney, M. Influence of Backbone Fluorination in Regioregular Poly(3-Alkyl-4-Fluoro)Thiophenes. *J. Am. Chem. Soc.* **2015**, *137* (21), 6866–6879.
- (189) Ibraikulov, O. A. Bulk Heterojunction Solar Cells Based on Low Band-Gap Copolymers and Soluble Fullerene Derivatives, Université de Strasbourg, 2016.
- (190) Bouzid, H.; Prosa, M.; Bolognesi, M.; Chehata, N.; Gedefaw, D.; Albonetti, C.; Andersson, M. R.; Muccini, M.; Bouazizi, A.; Seri, M. Impact of Environmentally Friendly Processing Solvents on the Properties of Blade-Coated Polymer Solar Cells. *J. Polym. Sci. Part A Polym. Chem.* **2019**, *57* (4), 487–494.
- (191) Morvillo, P.; Grimaldi, I. A.; Diana, R.; Loffredo, F.; Villani, F. Study of the Microstructure of Inkjet-Printed P3HT:PCBM Blend for Photovoltaic Applications. *J. Mater. Sci.* **2013**, *48* (7), 2920–2927.
- (192) Meng, B.; Fu, Y.; Xie, Z.; Liu, J.; Wang, L. Phosphonated Conjugated Polymers for Polymer Solar Cells with a Non-Halogenated Solvent Process. *Polym. Chem.* **2015**, *6* (5), 805–812.
- (193) Constantinou, L.; Gani, R.; O’Connell, J. P. Estimation of the Acentric Factor and the Liquid Molar Volume at 298 K Using a New Group Contribution Method. *Fluid Phase Equilib.* **1995**, *103* (1), 11–22.
- (194) Chen, D. H.; Dinivahi, M. V.; Jeng, C. Y. New Acentric Factor Correlation Based on the Antoine Equation. *Ind. Eng. Chem. Res.* **1993**, *32* (1), 241–244.
- (195) Constantinou, L.; Gani, R. New Group Contribution Method for Estimating Properties of Pure Compounds. *AIChE J.* **1994**, *40* (10), 1697–1710.
- (196) Joback, K. G.; Reid, R. C. Estimation of Pure-Component Properties from Group-Contributions. *Chem. Eng. Commun.* **1987**, *57* (1–6), 233–243.
- (197) Riedel, L. Eine Neue Universelle Dampfdruckformel Untersuchungen Über Eine Erweiterung Des Theorems Der Übereinstimmenden Zustände. Teil I. *Chemie Ing. Tech.* **1954**, *26* (2), 83–89.
- (198) Curl Jr, R. F.; Pitzer, K. S. Volumetric and Thermodynamic Properties of Fluids - Enthalpy, Free Energy, and Entropy. *Ind. Eng. Chem.* **1958**, *50* (2), 265–274.
- (199) Brock, J. R.; Bird, R. B. Surface Tension and the Principle of Corresponding States. *AIChE J.* **1955**, *1* (2), 174–177.
- (200) Zuo, Y. X.; Stenby, E. H. Corresponding-States and Parachor Models for the Calculation of Interfacial Tensions. *Can. J. Chem. Eng.* **1997**, *75* (6), 1130–1137.

- (201) Laurent Catoire, Ste'phanie Paulmier, and V. N. Experimental Determination and Estimation of Closed Cup Flash Points of Mixtures of Flammable Solvents. *Process Saf. Prog.* **2006**, 25 (4), 326–330.
- (202) Jain, A.; Yang, G.; Yalkowsky, S. H. Estimation of Melting Points of Organic Compounds. *Ind. Eng. Chem. Res.* **2004**, 43 (23), 7618–7621.

# CHAPTER 9

---

---

APPENDIXS

---

---



## 9 Appendix

### Appendix 9.1: List of Calculation Models used in IBSS®CAMD

Properties	Models	Refs
Acentric Factor	HSKASG2012	Hukkerikar A.S. et al. 2012 <sup>162</sup>
	CGOC1995	Constantinou L. et. al. 1995 <sup>193</sup>
	LK1975	Lee B.I. et al. 1975 <sup>194</sup>
	CDJ1993	Chen D.H. et al. 1993 <sup>194</sup>
Enthalpy of vaporization at 298K	HSKASG2012	Hukkerikar A.S. et al. 2012 <sup>162</sup>
	MG2001	Marrero J. et al. 2001 <sup>142</sup>
	CG1994	Constantinou L. et al. 1994 <sup>195</sup>
Enthalpy of vaporization at the normal boiling point	HSKASG2012	Hukkerikar A.S. et al. 2012 <sup>162</sup>
	JR1987	Joback R. et al. 1987 <sup>196</sup>
$\delta_D$	HSKASG2012	Hukkerikar A.S. et al. 2012 <sup>162</sup>
	MB2010	<a href="http://www.pirika.com/NewHP/Y-MB/Y-MB.html">http://www.pirika.com/NewHP/Y-MB/Y-MB.html</a> <sup>161</sup>
$\delta_P$	HSKASG2012	Hukkerikar A.S. et al. 2012 <sup>162</sup>
	MB2010	<a href="http://www.pirika.com/NewHP/Y-MB/Y-MB.html">http://www.pirika.com/NewHP/Y-MB/Y-MB.html</a> <sup>161</sup>
$\delta_H$	HSKASG2012	Hukkerikar A.S. et al. 2012 <sup>162</sup>
	MB2010	<a href="http://www.pirika.com/NewHP/Y-MB/Y-MB.html">http://www.pirika.com/NewHP/Y-MB/Y-MB.html</a> <sup>161</sup>

R <sub>a</sub>	MB2010	Hansen C.M. <sup>125</sup>
Hildebrand Solubility parameter ( $\delta$ )	HSKASG2012	Hukkerikar A.S. et al. 2012 <sup>162</sup>
RED	MB2010	Hansen C.M. <sup>125</sup>
Critical Pressure	HSKASG2012	Hukkerikar A.S. et al. 2012 <sup>162</sup>
	MG2001	Marrero J. et al. 2001 <sup>142</sup>
	CG1994	Constantinou L. et al. 1994 <sup>195</sup>
	JR1987	Joback R. et al. 1987 <sup>196</sup>
Vapor Pressure	Riedel1954	Riedel L., 1954. <sup>197</sup>
Surface Tension at 298 K	CMMG2008	Conte E. et al. 2008 <sup>163</sup>
Surface Tension (as a function of temperature)	Ptizer1995	Curl R. F. Jr., and Pitzer K. S. 1958 <sup>198</sup>
	BrockBird55	Brock, J. R., and R. B. Bird, 1955 <sup>199</sup>
	ZuoStenby1997	Zuo Y-X, Stenby EH. 1997 <sup>200</sup>
Flash Point	HSKASG2012	Hukkerikar A.S. et al. 2012 <sup>162</sup>
	CPN2006	Catoire L. 2006 <sup>201</sup>
Boiling Point	HSKASG2012	Hukkerikar A.S. et al. 2012 <sup>162</sup>
	MG2001	Marrero J. et al. 2001 <sup>142</sup>
	CG1994	Constantinou L. et al. 1994 <sup>195</sup>
	JR1987	Joback R. et al. 1987 <sup>196</sup>
Melting Point	HSKASG2012	Hukkerikar A.S. et al. 2012 <sup>162</sup>
	MG2001	Marrero J. et al. 2001 <sup>142</sup>

	CG1994	Constantinou L. et al. 1994 <sup>195</sup>
	JR1987	Joback R. et al. 1987 <sup>196</sup>
	JYY2004	Jain A. et al. 2004 <sup>202</sup>
Viscosity at 300 K	CMMG2008	Conte E. et al. 2008 <sup>163</sup>
Viscosity as a function of temperature	JR1987	Joback R. et al. 1987 <sup>196</sup>
Liquid molar volume at 298 K	HSKASG2012	Hukkerikar A.S. et al. 2012 <sup>162</sup>
	CGOC1995	Constantinou L. et. al. 1995 <sup>193</sup>
Critical Volume	HSKASG2012	Hukkerikar A.S. et al. 2012 <sup>162</sup>
	MG2001	Marrero J. et al. 2001 <sup>142</sup>
	CG1994	Constantinou L. et al. 1994 <sup>195</sup>
	JR1987	Joback R. et al. 1987 <sup>196</sup>

## Appendix 9.2 Basic Function Group Coding

- Carbon (C)

Bond types	Comments		EG
Four single bonds	Bond with C	-CH <sub>3</sub>	106103
		-CH <sub>2</sub>	106102
		-CH	106101
		-C	106100
	One non-C connection	X-CH <sub>3</sub>	106113
		X-CH <sub>2</sub>	106112
		X-CH	106111
		X-C	106110
	Ring (non-aromatic)-CH <sub>2</sub>		106122
	Ring (non-aromatic)-CH		106121
	Ring (non-aromatic)-C		106120
	Ring-sp-CH		106161
	Ring-sp-C		106160
Two single bonds One double bond	Bond with C	=CH <sub>2</sub>	106202
		=CH	106201
		=C	106200
	One non-C connection	X=CH <sub>2</sub>	106212
		X=CH	106211
		X=C	106210
	Ring (non-aromatic)-CH		106221
	Ring (non-aromatic)-C		106220
	Aromatic cycle-CH		106231

	Aromatic cycle-C		106230
	Common atom between two aromatic cycles		106240
	Common atom between two – 1 aromatic and 1 non aromatic		106250
One single bond One triple bond	Bond with C	$\equiv \text{CH}$	106301
		$\equiv \text{C}$	106300
	One non-C connection	$\text{X} \equiv \text{CH}$	106311
		$\text{X} \equiv \text{C}$	106310
	Ring (non-aromatic) $\equiv \text{C}$		106320
Two double bonds	Bond with C		106400
	One non-C connection		106410
	Non-aromatic cycle		106420

## - Nitrogen (N)

Bond types	Comments		EG
Three single bonds	Bond with C or N	$-\text{NH}_2$	107102
		$-\text{NH}$	107101
		$-\text{N}$	107100
	One non-C or N connection	$\text{X}-\text{NH}_2$	107112
		$\text{X}-\text{NH}$	107111
		$\text{X}-\text{N}$	107110
	Ring (non-aromatic)-NH		107121
	Ring (non-aromatic)-N		107120
One single bond One double bond	Bond with C or N	$=\text{NH}$	107201
		$=\text{N}$	107200

	One non-C or N connection	X=NH	107211
		X=N	107210
	Bond with ring (non-aromatic)-N		107220
	Bond with aromatic cycle-N		107230
One triple bond	Bond with C only		107300
	One non-C connection		107310

- *Oxygen (O)*

Bond types	Comments		EG
Two single bonds	Bond with C	-OH	108101
		-O	108100
	One non-C connection	X-OH	108111
		X-O	108110
	Bond with ring (non-aromatic)		108120
	Bond with aromatic cycle		108130
One double bond	Bond with C only		108200
	One non-C connection		108210
	Bond with ring (non-aromatic)		108220

- *Halogens*

Atom	Comments	EG
-Cl	Bond with C only	117100
	One non-C connection	117110
-F	Bond with C only	109100

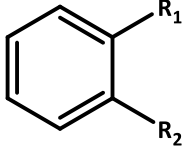
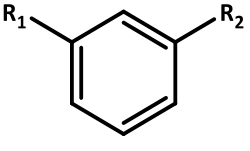
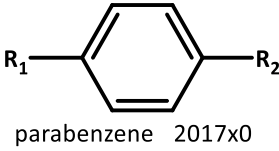
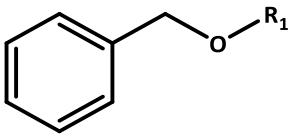
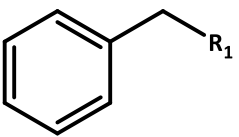
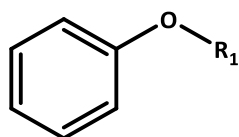
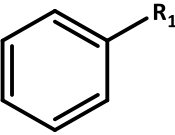
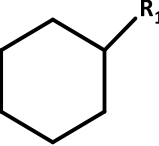
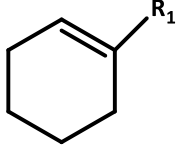
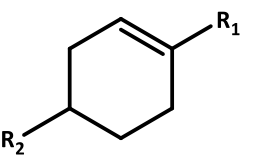
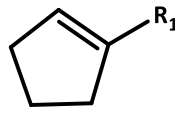
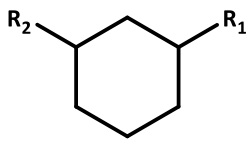
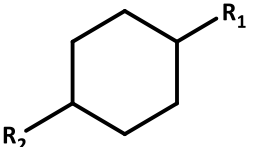
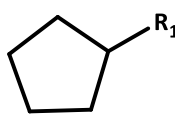
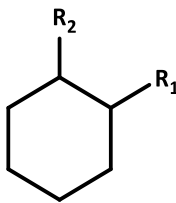
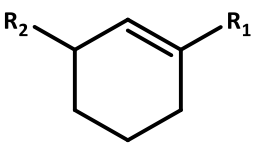
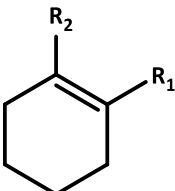
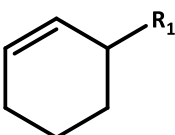
## 9. APPENDIX

---

	One non-C connection	109110
-Br	Bond with C only	135100
	One non-C connection	135110
-I	Bond with C only	153100
	One non-C connection	153110

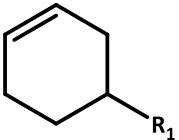
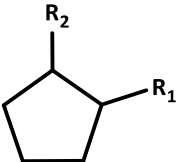

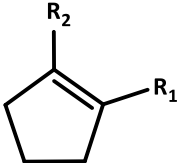

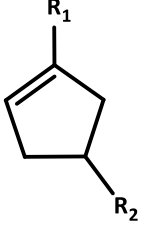
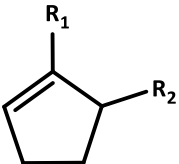
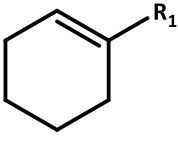
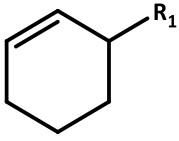
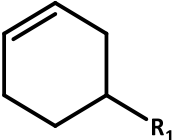
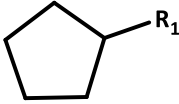
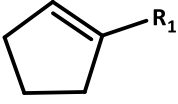
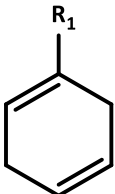
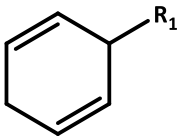
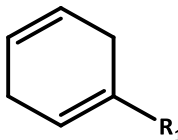
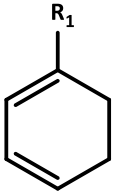
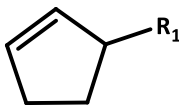
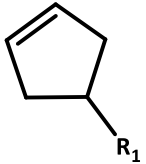
## Appendix 9.3: A list of chemical groups for new molecular design in

## IBSS®CAMD.

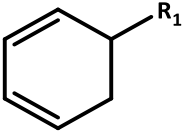
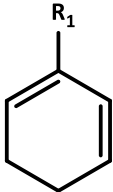
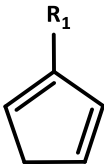
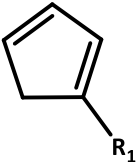
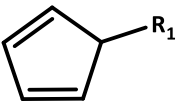
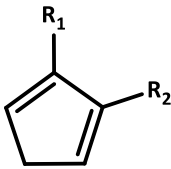
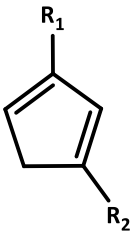
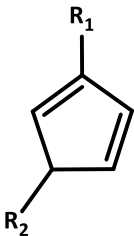
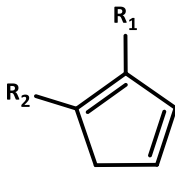
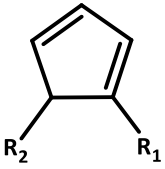
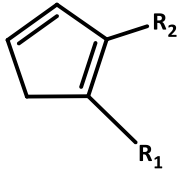
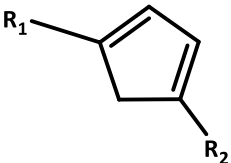
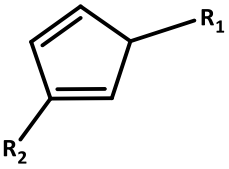
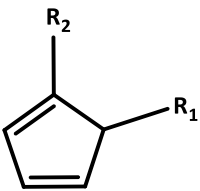
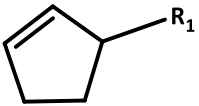
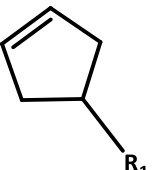
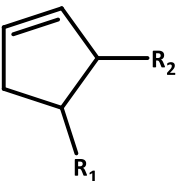
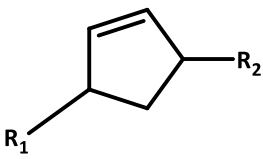
 <p>orthobenzene 2015x0</p>	 <p>methabenzene 2016x0</p>	 <p>parabenzene 2017x0</p>
 <p>phenilate_2?? 2021x0</p>	 <p>benzyle 2019x0</p>	 <p>phenolate 2020x0</p>
 <p>phenyle 2018x0</p>	 <p>cyclohexyle 2023x0</p>	 <p>cyclohexenyle 2024x0</p>
 <p>cyclohexenyle_1_4 2024x3</p>	 <p>cyclopentenyle 2026x0</p>	 <p>cyclohexyle_1_3 2023x2</p>
 <p>cyclohexyle 2023x3</p>	 <p>cyclopentyle 2025x0</p>	 <p>cyclohexyle_1_2 2023x1</p>
 <p>cyclohexenyle_1_3 2024x2</p>	 <p>cyclohexenyle_1_2 2024x1</p>	 <p>cyclohexenyle_2 2024x5</p>



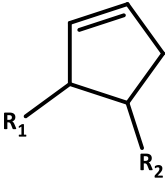
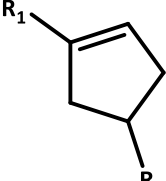
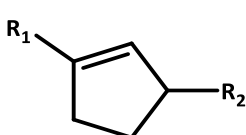
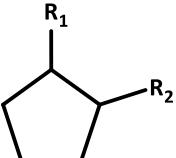

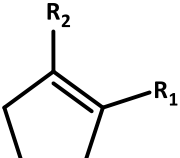

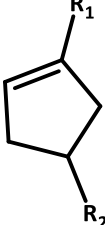
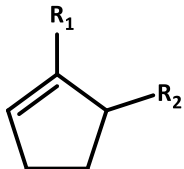
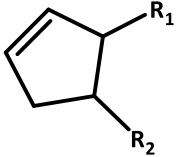
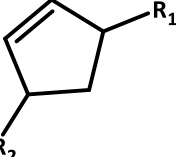
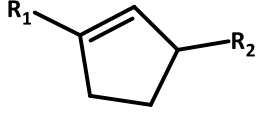
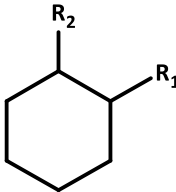
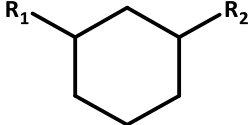
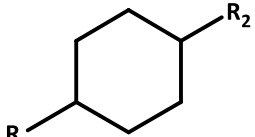
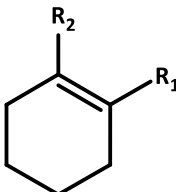
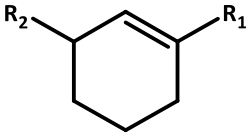
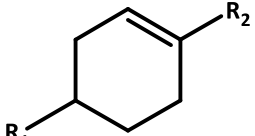
## 9. APPENDIX

 cyclohexenyle_3 2024x6	 Cyclopentyle_1_2 2025x1	 Cyclopentyle_1_3 2025x2
 Cyclopentenyle_1_2 2026x3	 Cyclopentenyle_1_3 2026x4	 Cyclopentenyle_1_4 2026x5
 Cyclopentenyle_1_5 2026x6	 cyclohexenyle 2024x0	 cyclohexenyle_2 2024x5
 cyclohexenyle_3 2024x6	 cyclopentyle 2025x0	 cyclopentyle_1 2026x0
 cyclohexene_diyle_1 2027x0	 cyclohexene_diyle_2 2027x1	 cyclohexene_diyle_3 2027x2
 cyclohexene_diyle_4 2027x3	 cyclopentenyle_2 2026x1	 cyclopentenyle_3 2026x2

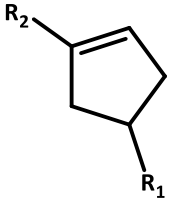
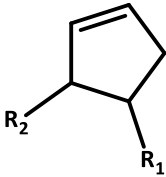
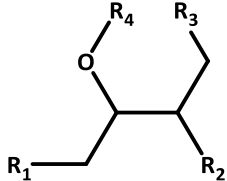
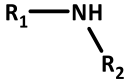


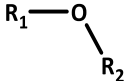
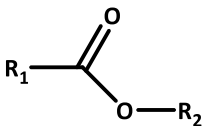
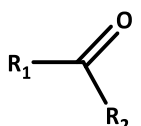
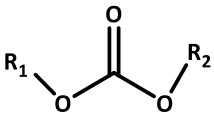
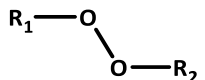
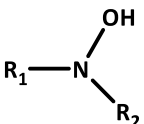
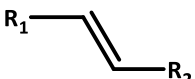
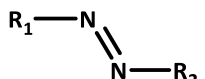
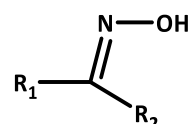
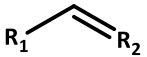
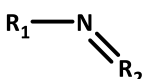

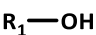
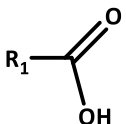
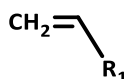
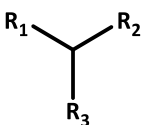
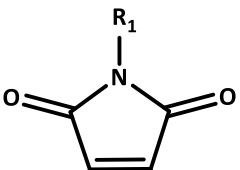
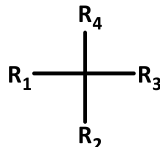
## 9. APPENDIX

 <p>cyclohexene_dyele_5 2027x4</p>	 <p>cyclohexene_dyele_6 2027x5</p>	 <p>cyclopentene_diyle_1 2028x0</p>
 <p>cyclopentene_diyle_2 2028x1</p>	 <p>cyclopentene_diyle_3 2028x2</p>	 <p>Cyclopentene_diyele_1_5 2028x3</p>
 <p>Cyclopentene_diyele_1_4 2028x4</p>	 <p>Cyclopentene_diyele_1_3 2028x5</p>	 <p>Cyclopentene_diyele_1_2 2028x6</p>
 <p>Cyclopentene_diyele_3_4 2028x7</p>	 <p>Cyclopentene_diyele_5_4 202809</p>	 <p>Cyclopentene_diyele_2_4 202808</p>
 <p>Cyclopentene_diyele_3_5 202810</p>	 <p>Cyclopentene_diyele_2_3 202811</p>	 <p>cyclopentyle_2 2026x1</p>
 <p>cyclopentyle_3 2026x2</p>	 <p>cyclopentenyle_5_4 2026x7</p>	 <p>cyclopentenyle_5_3 2026x8</p>

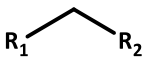
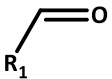
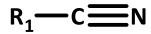
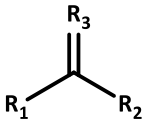
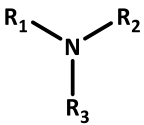
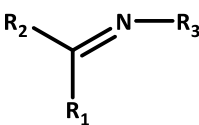
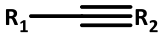


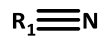
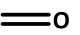

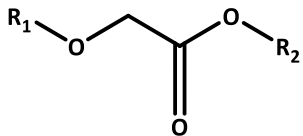
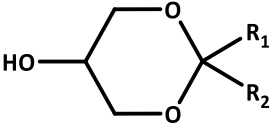

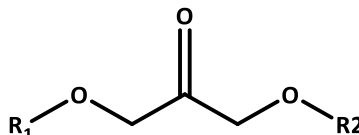
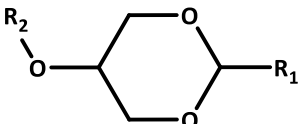
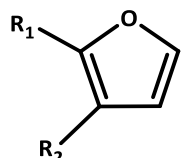
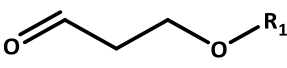
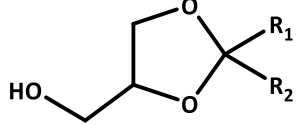
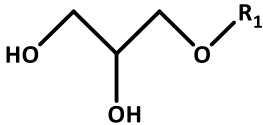
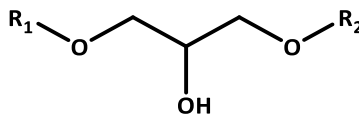
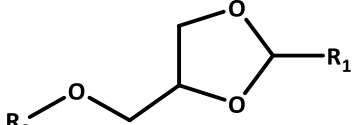
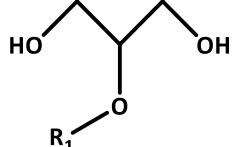
## 9. APPENDIX

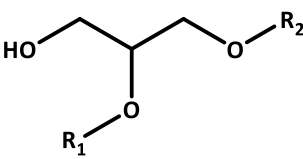
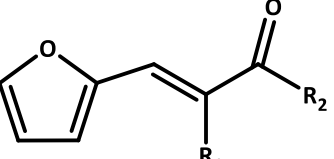
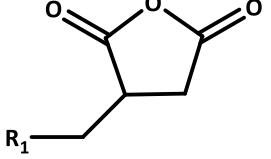
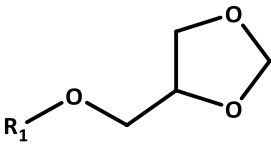
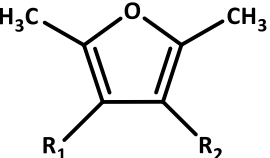
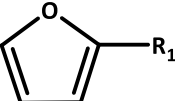
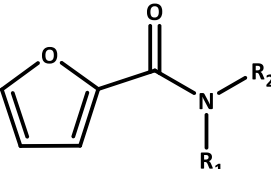
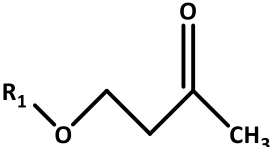
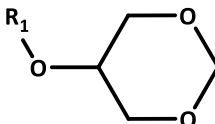
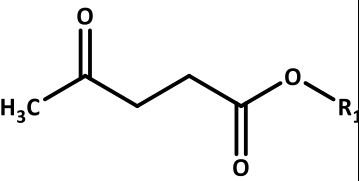
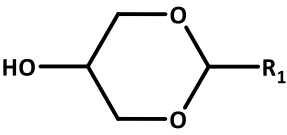
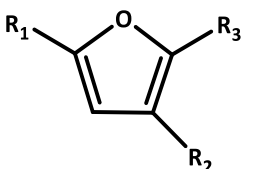
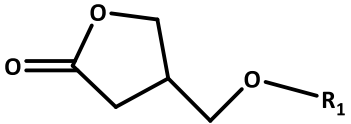
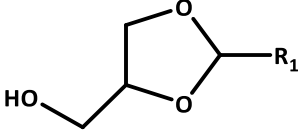
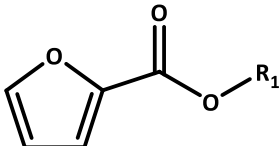
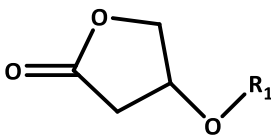
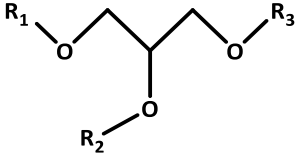
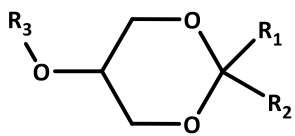
 <p>cyclopentenyle_4_2 202611</p>	 <p>cyclopentenyle_4_2 202610</p>	 <p>cyclopentenyle_5_2 2026x9</p>
 <p>cyclopentyle_1_2 2025x1</p>	 <p>cyclopentyle_1_3 2025x2</p>	 <p>cyclopentenyle_1_2 2026x3</p>
 <p>cyclopentenyle_1_3 2026x4</p>	 <p>cyclopentenyle_1_4 2026x5</p>	 <p>cyclopentenyle_1_5 2026x6</p>
 <p>cyclopentenyle_5_4 2026x7</p>	 <p>cyclopentenyle_5_3 2026x8</p>	 <p>cyclopentenyle_5_2 2026x9</p>
 <p>cyclohexyle_1_2 2023x1</p>	 <p>cyclohexyle_1_3 2023x2</p>	 <p>cyclohexyle_1_4 2023x3</p>
 <p>cyclohexenyle_1_2 2024x1</p>	 <p>cyclohexenyle_1_3 2024x2</p>	 <p>cyclohexenyle_1_4 2024x3</p>

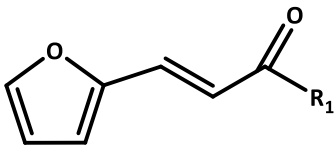
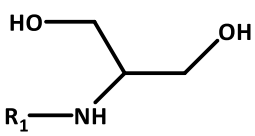
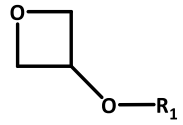
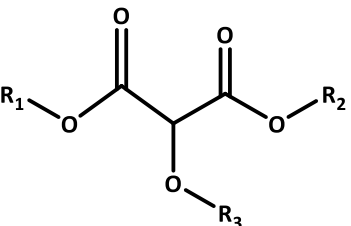
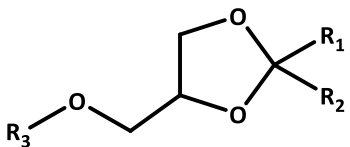
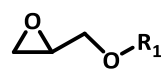
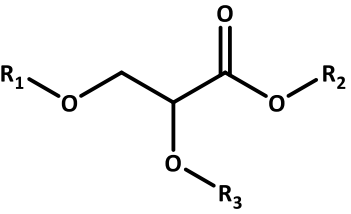
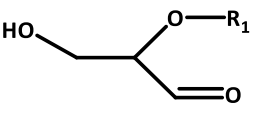
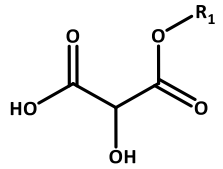
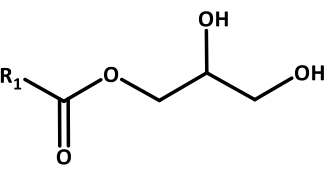
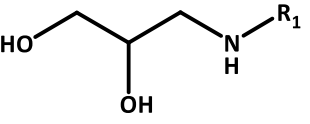
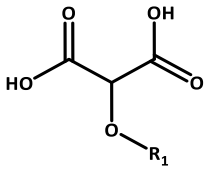
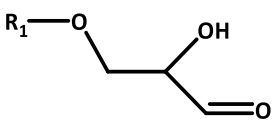
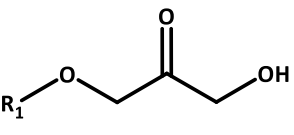
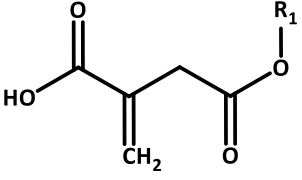
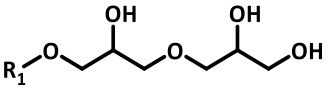
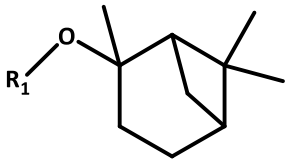
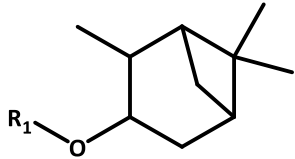
## 9. APPENDIX

 <p>cyclopentylene_4_2 202610</p>	 <p>cyclopentylene_4_3 202611</p>	 <p>4R butyl ether 2014x0</p>
 <p>1071x0</p>	 <p>1061x3</p>	 <p>1062x2</p>
 <p>1081x0</p>	 <p>ester 2001x0</p>	 <p>ketone 2002x0</p>
 <p>carbonate 2005x0</p>	 <p>peroxy 2006x0</p>	 <p>hydroxylamine 2008x0</p>
 <p>alkenyl 2009x0</p>	 <p>azo 2011x0</p>	 <p>ketoxime 2013x0</p>
 <p>1062x1</p>	 <p>1072x0</p>	 <p>1071x2</p>
 <p>1081x1</p>	 <p>carboxylic acid 2000x0</p>	 <p>vinyl 2010x0</p>
 <p>1061x1</p>	 <p>cyclic secondary amide 2004x0</p>	 <p>1061x0</p>

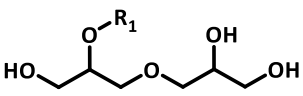
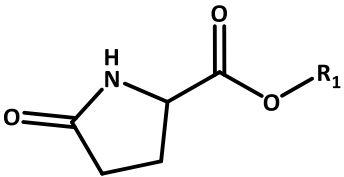
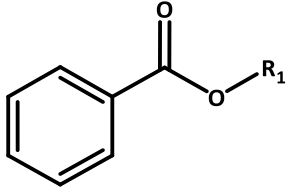
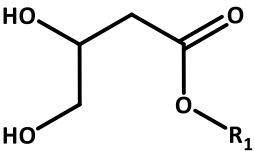
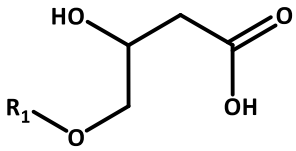
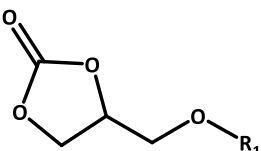
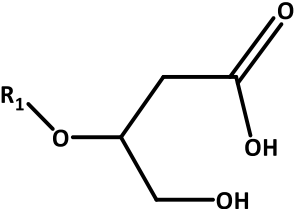
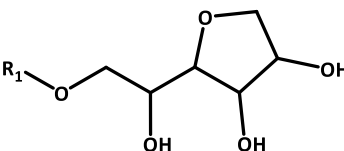
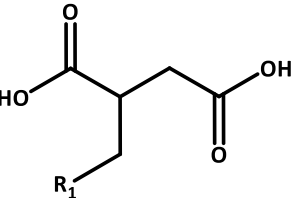
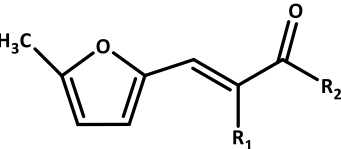
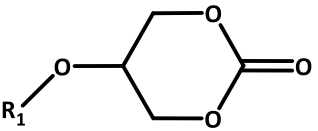
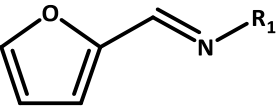
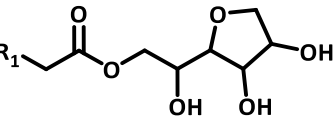
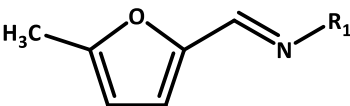
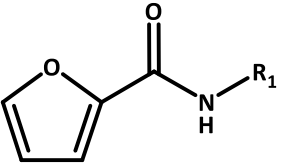
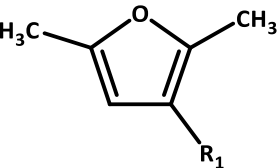
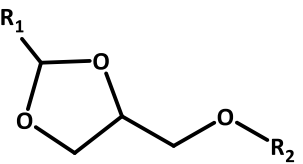
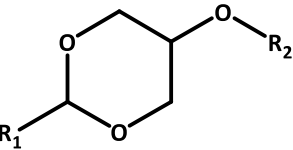
## 9. APPENDIX

 <p>1061x2</p>	 <p>aldehyde 2003x0</p>	 <p>nitrile 2012x0</p>
 <p>1062x0</p>	 <p>1071x0</p>	 <p>imide 2007x0</p>
 <p>1063x0</p>	 <p>1072x1</p>	 <p>1063x1</p>
 <p>1073x0</p>	 <p>1082x0</p>	 <p>1064x0</p>
 <p>glycerol 7 2207x0</p>	 <p>dioxane 5,5 2401x0</p>	 <p>furane 1,4 2612x0</p>
 <p>glycerol 10 2210x0</p>	 <p>dioxane 5,7 2403x0</p>	 <p>furane 1,2 2613x0</p>
 <p>glycerol 5 2205x0</p>	 <p>dioxolane 4,4 2406x0</p>	 <p>glycerol 6 (0) 2200x0</p>
 <p>glycerol 1,6 (4) 2204x0</p>	 <p>dioxolane 4,7 2408x0</p>	 <p>glycerol 4 (1) 2201x0</p>

 <p>glycerol 4,6 (2) 2202x0</p>	 <p>adol/croto furfural 6,7 2602x0</p>	 <p>acide itaconique cyclique 4 2254x0</p>
 <p>dioxolane 7 240700</p>	 <p>alkyls DMFurane 2,3 2609x0</p>	 <p>furane 1 2611x0</p>
 <p>nakamura 2610x0</p>	 <p>glycerol 6 1 2206x0</p>	 <p>dioxane 7 2402x0</p>
 <p>Llevulinc acid 2306x0</p>	 <p>dioxane5 2400x0</p>	 <p>furane 1,2,4 2614x0</p>
 <p>glycerol 15 2215x0</p>	 <p>dioxolane 4 2405x0</p>	 <p>furoate 2600x0</p>
 <p>3-Hydroxybutyrolactone 2207x0</p>	 <p>glycerol 1,4,6 2203x0</p>	 <p>dioxane 5,5,7 2404x0</p>

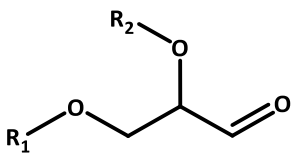
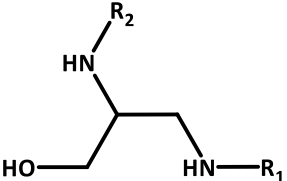
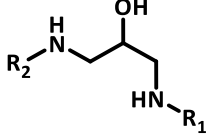
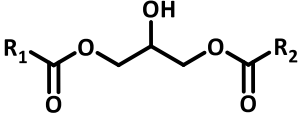
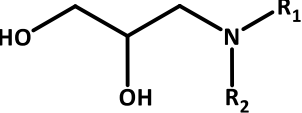
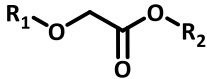
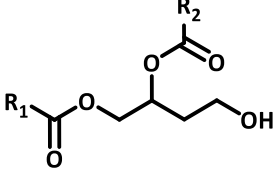
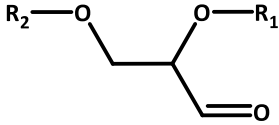
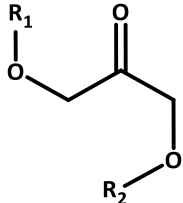
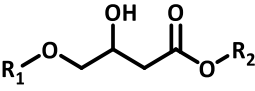
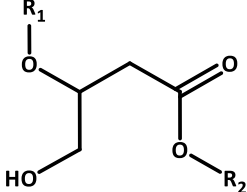
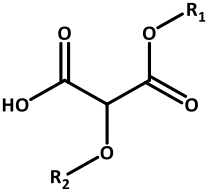
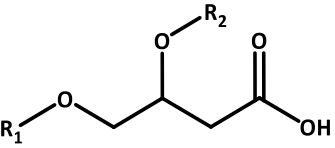
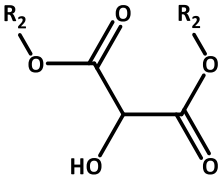
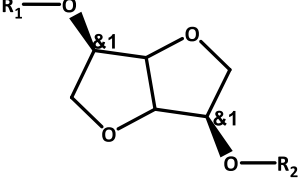
 <p>adol/ceoto furfural 7 2601x0</p>	 <p>glycerol 29 moiety2014 2229x0</p>	 <p>glycerol 34 moiety2014 2234x0</p>
 <p>glycerol 16 2214x0</p>	 <p>dioxolane 4,4,7 2409x0</p>	 <p>glycerol 35 moiety2014 2235x0</p>
 <p>malic acid (glycerol 14) 2214x0</p>	 <p>glycerol 3601 moiety 2014 2236x1</p>	 <p>glycerol 3904 moiety 2014 2239x4</p>
 <p>glycerol 23 moiety2014 2223x0</p>	 <p>glycerol 28 moiety2014 2228x0</p>	 <p>glycerol 3903 moiety 2014 2239x3</p>
 <p>glycerol 3602 moiety 2014 2236x2</p>	 <p>glycerol 3701 moiety 2014 2237x1</p>	 <p>acide itaconique 0 2250x0</p>
 <p>glycerol 4008 moiety 2014 2240x8</p>	 <p>alpha-pinene 0 2290x0</p>	 <p>alpha-pinene 1 2291x0</p>

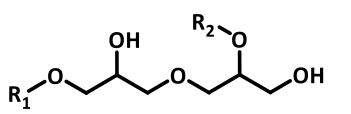
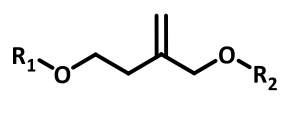
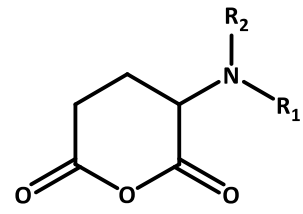
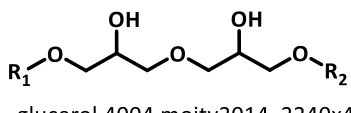
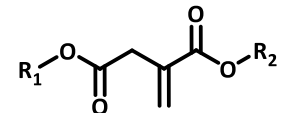
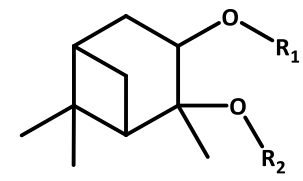
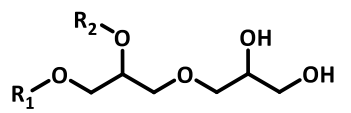
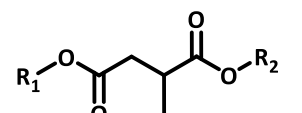
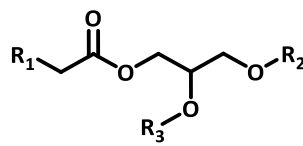
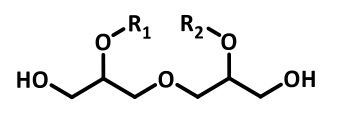
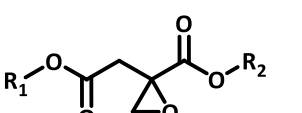
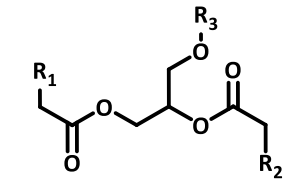
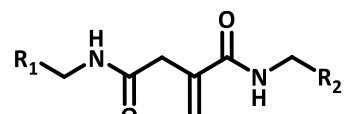
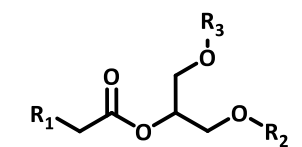
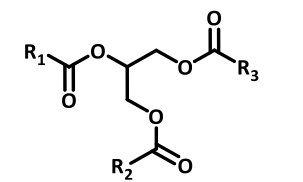
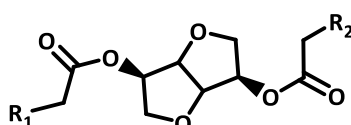
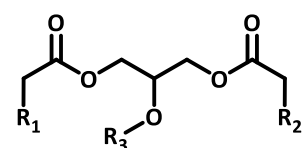
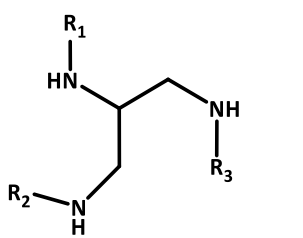
## 9. APPENDIX

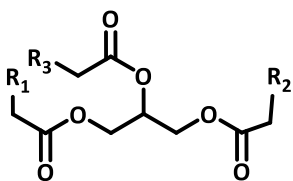
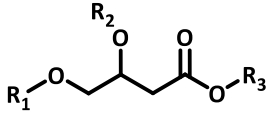
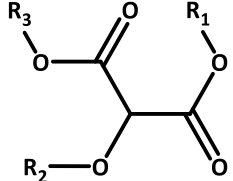
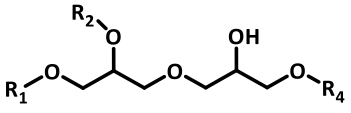
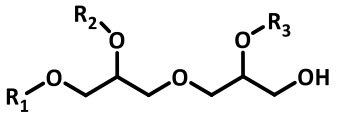
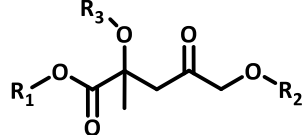
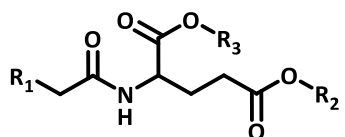
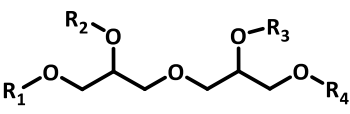
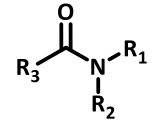
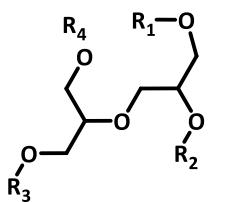
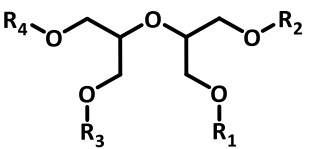
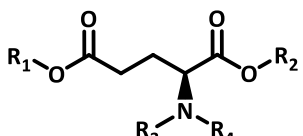
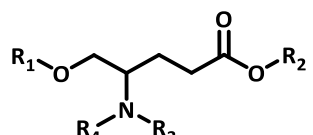
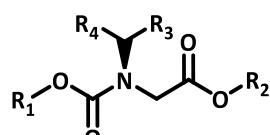
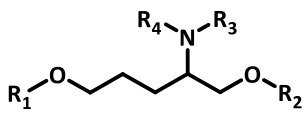
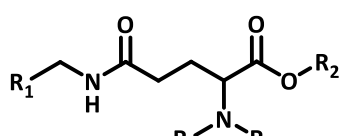
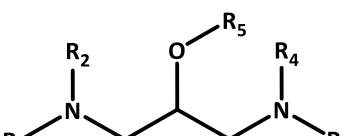
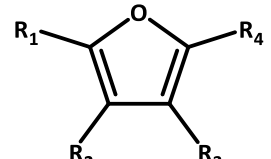
 <p>glycerol 4007 moiety 2014 2240x7</p>	 <p>glutamic acid 3 2283x0</p>	 <p>benzoate 2310x0</p>
 <p>glycerol 3804 moiety 2014 2238x4</p>	 <p>glycerol 3805 moiety 2014 2238x5</p>	 <p>dioxolane-one moiety 2411x0</p>
 <p>glycerol 3806 moiety 2014 2238x6</p>	 <p>sorbitol 4 2274x0</p>	 <p>acide itaconique 3 2253x0</p>
 <p>adol/croto methyl furfural 6,7 2604x0</p>	 <p>dioxane-one moiety 2410x0</p>	 <p>imine F 2605x0</p>
 <p>sorbitol 3 2273x0</p>	 <p>imine MF 2606x0</p>	 <p>amide 2607x0</p>
 <p>alkyls DMFurane 2 2608x0</p>	 <p>glycerol 12 221200</p>	 <p>glycerol 13 221300</p>



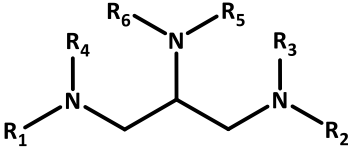
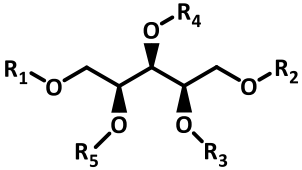
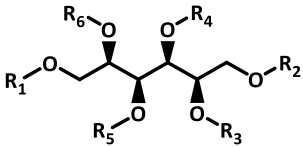
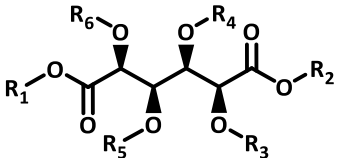
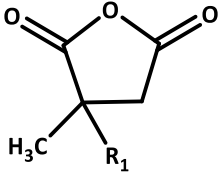
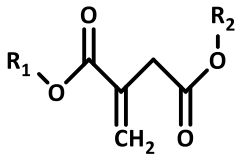
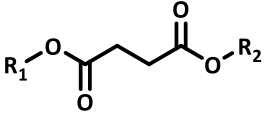
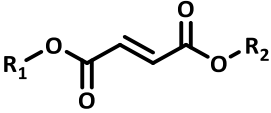
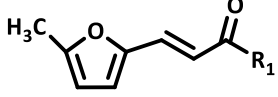
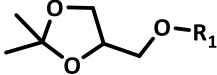
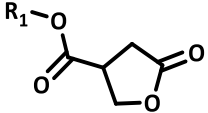
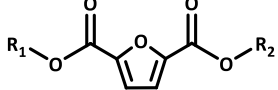
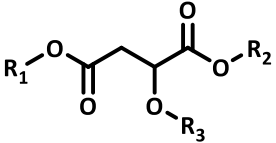
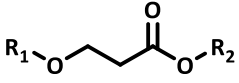
## 9. APPENDIX

 <p>glycerol 11 221100</p>	 <p>glycerol 31 moity2014 2231x0</p>	 <p>glycerol 32 moity2014 2232x0</p>
 <p>glycerol 25 moity2014 2225x0</p>	 <p>glycerol 28 moity2014 2228x1</p>	 <p>glycerol 33 moity2014 2233x0</p>
 <p>glycerol 26 moity2014 2226x0</p>	 <p>glycerol 36 moity2014 223600</p>	 <p>glycerol 37 moity2014 223700</p>
 <p>glycerol 3802 moity2014 223802</p>	 <p>glycerol 3803 moity2014 223803</p>	 <p>glycerol 3902 moity2014 223902</p>
 <p>glycerol 3801 moity2014 223801</p>	 <p>glycerol 3901 moity2014 223901</p>	 <p>sorbitol 1 227100</p>

 <p>glycerol 4003 moiety2014 2240x3</p>	 <p>acide itaconique 7 225700</p>	 <p>glutamic acid 228500</p>
 <p>glycerol 4004 moiety2014 2240x4</p>	 <p>acide itaconique 9 225900</p>	 <p>alpha-pinene 2 229200</p>
 <p>glycerol 4005 moiety2014 2240x5</p>	 <p>acide itaconique 11 226100</p>	 <p>glycerol 18 221800</p>
 <p>glycerol 4006 moiety2014 2240x6</p>	 <p>acide itaconique 12 226200</p>	 <p>glycerol 22 222200</p>
 <p>acide itaconique 10 226000</p>	 <p>glycerol 19 221900</p>	 <p>glycerol 27 moiety2014 222700</p>
 <p>sorbitol 2 227200</p>	 <p>glycerol 20 222000</p>	 <p>glycerol 30 moiety2014 223000</p>

 <p>glycerol 21 222100</p>	 <p>glycerol 38 moiety2014 223800</p>	 <p>glycerol 39 moiety2014 223900</p>
 <p>glycerol 4001 moiety2014 224001</p>	 <p>glycerol 4002 moiety2014 224002</p>	 <p>acid itaconique 8 225800</p>
 <p>glutamic acid 7 228700</p>	 <p>glycerol 40 moiety2014 224000</p>	 <p>3R amide 260701</p>
 <p>glycerol 41 moiety2014 224100</p>	 <p>glycerol 42 moiety2014 224200</p>	 <p>glutamic acid 0 228000</p>
 <p>glutamic acid 2 2282x0</p>	 <p>aspartic acid 2305x0</p>	 <p>glutamic acid 1 228100</p>
 <p>glutamic acid 6 2286x0</p>	 <p>glycerol 9 2209x0</p>	 <p>furane 1,2,3,4 2615x0</p>

## 9. APPENDIX

 <p>glycerol 8 2208x0</p>	 <p>xylitol 2309x0</p>	 <p>sorbitol 0 2270x0</p>
 <p>glucallic acid 2308x0</p>	 <p>acide itaconique cyclique 5 2255x0</p>	 <p>acide itaconique2 2252x0</p>
 <p>succinic acid 2301x0</p>	 <p>fumaric acid 2301x0</p>	 <p>adol/croto methyl furfural 7 2603x0</p>
 <p>Glycerol 17 2217x0</p>	 <p>acide itaconique cyclique 6 2256x0</p>	 <p>2,5-furandicarboxylic acid 2303x0</p>
 <p>malic acid 2302x0</p>	 <p>3-hydroxypropionic acid 2304x0</p>	

### Appendix 9.4: The list of selected existing solvents.

N.	Name	N.	Name
1	1,2-dichlorobenzene (reference solvent)	2	Chlorobenzene (reference solvent)
3	Anisole	4	Methyl 9,12- octadecadienoate
5	2-Methylanisole	6	Geranyl acetate
7	p-Xylene	8	Dimethyl Adipate
9	Isoamyl acetate	10	Nopol
11	Benzyl Benzoate	12	Methyl myristate
13	p-Cymene	14	2-Octanol
15	Terpinolene	16	2-Furylmethanol
17	Butyl acetate	18	1,3-Dioxolan-4-ylmethanol
19	Tetrahydrofuran	20	Ethyl myristate
21	d-Limonene	22	Ethyl palmitate
23	Cyclopentyl methyl ether	24	Bis(2-ethylhexyl) succinate
25	Isobutyl acetate	26	Methyl palmitate
27	2-Methyltetrahydrofuran	28	Dimethyl sulfoxide
29	Propylene carbonate	30	Dimethyl isosorbide
31	Ethylene carbonate	32	Butyl laurate
33	Glycerol -1,2,3-triethyl ether	34	9,12-Octadecadienoic acid (9Z,12Z)-, ethyl ester
35	Dimethyl Succinate	36	Propionic acid
37	1,2,3-Trimethoxypropane	38	Methyl 9-octadecenoate
39	Diethyl carbonate	40	Diethyl-succinate
41	Furfural	42	N,N-Dimethyldec-9-enamide
43	5-Methyldihydro-2(3H)- furanone	44	Methyl stearate

45	1,2-Ethanediy diacetate	46	P-ANISALDEHYDE
47	alpha-Pinene	48	Glycerol 1,3-diethyl ether
49	2-(4-Methylcyclohexyl)-2-propanyl acetate	50	Isopropyl myristate
51	Dimethyl Glutarate	52	Oleic Acid
53	1 – Butanol	54	1,3-Dioxan-5-ol
55	Pinane	56	Ethyl 9-octadecenoate
57	Isobutanol	58	2,6-Dimethyl-7-octen-2-ol
59	$\beta$ -Myrcene	60	Tetrahydro-2-furanylmethanol
61	Isosorbide dioctanoate	62	Menthanol
63	Methyl linolenate	64	N,N-Dimethyloctanamide
65	Isoamyl alcohol	66	Butyl palmitate
67	Isopropyl palmitate	68	Methyl 12-hydroxy-9-octadecenoate
69	2-Furanamine	70	Butyl myristate
71	Dimethyl 2-methylglutarate	72	Ethylene glycol
73	Bis(3-methylbutyl) succinate	74	Ethyl 2-hydroxypropanoate
75	Diisopropyl Adipate	76	3-Methoxy-1,2-propanediol
77	Ethyl linolenate	78	1,3-Dimethoxy-2-propanol
79	1,3-Dioxolane	80	Propylene glycol
81	$\beta$ –Pinene	82	Glycerol-1,2,3-tributyl ether
83	Methyl laurate	84	Glycerol -1,3-dibutyl ether (Dibuprol)
85	Ethyl Laurate	86	1-Octanol
87	N,N-Dimethyldecanamide	88	beta-Terpineol
89	Dibutyl ether	90	1,3-Propanediol
91	Terpineol acetate	92	Methanol
93	6,8-Dioxabicyclo[3.2.1]octan-4-one	94	1,1,1,3,3-Pentafluorobutane

95	Isopropyl Acetate	96	2,3-Dibutoxy-1-propanol
97	Diethoxymethane	98	5-(Hydroxymethyl)-2-furaldehyde
99	Acetic acid	100	4-(Hydroxymethyl)-1,3-dioxolan-2-one
101	Tributyl citrate acetate	102	Triethyl citrate
103	1,4-Butanediol	104	Hexamethyldisiloxane
105	2,3-Dimethoxy-1-propanol	106	Ethyl acetate
107	2-Methoxy-1,3-propanediol	108	Tributyl citrate
109	2-Hydroxypropanoic acid	110	3-Ethoxy-1,2-propanediol
111	1,2,3-Propanetriyl triacetate	112	2-Ethoxy-2-methylpropane
113	Alpha-Terpineol	114	2-(2-Butoxyethoxy)ethanol
115	2,3-Diethoxy-1-propanol	116	3-Butoxy-1,2-propanediol
117	2-Methoxy-2-methylbutane	118	Acetone
119	(2,2-Dimethyl-1,3-dioxolan-4-yl)methanol	120	2-Hydroxy-N,N-dimethylpropanamide
121	2-Ethylhexyl lactate	122	3-Hydroxypropanoic acid
123	Geraniol	124	2-Ethoxy-1,3-propanediol
125	O-Acetylcholine	126	Glycerol
127	1-Decanol	128	1,4-Bis(aminoxy)-1,4-butanedione
129	1,2-Pentanediol	130	N,N-Bis(2-hydroxyethyl)octanamide
131	Cyclademol	132	2-Butoxy-1,3-propanediol
133	Butyl stearate	134	Dimethyl carbonate
135	12-Hydroxy-9-octadecenoic acid	136	Methoxy(trimethyl)silane
137	9-Octadecen-1-ol	138	Isopropanol
139	Ethanol	140	Butyl 3-hydroxybutanoate
141	Methyl 9,12-octadecadienoate		

Appendix 9.5: The candidates provided by IBSS®CAMD with a *GloPerf* > 0.6 for P3HT:PC<sub>71</sub>BM.

Candidates	1,2-dichlorobenzene	Anisole	p-Xylene	Isoamyl Acetate	Benzyl Benzoate	p-Cymene	Terpinolene	Butyl Acetate	Tetrahydrofuran
CAS	95-50-1	100-66-	106-	123-92-2	120-51-4	99-87-6	586-62-9	123-86-4	109-99-9
<i>GloPerf</i>	1	0.997	0.853	0.674	0.667	0.628	0.626	0.621	0.609
Melting Point ( $T_m$ , K)	255	239	229	202	307	224	221	201	179
$ProPerf_p - T_m$	1	1	1	1	≈ 0	1	1	1	1
Boiling Point ( $T_b$ , K)	449	428	419	420	573	450	448	407	323
$ProPerf_p - T_b$	1	1	1	1	≈ 0	1	1	1	≈ 0
Flash Point ( $T_f$ , K)	332	314	301	312	420	323	308	305	243
$ProPerf_p - T_f$	1	1	1	1	1	1	1	1	≈ 0
$\Delta H_{vap}$ (kJ/mol)	50.1	46.5	43.4	48.9	85.8	50.1	38.3	46.0	32.0
$ProPerf_p - \Delta H_{vap}$	1	1	1	1	≈ 0	1	0.34	1	≈ 0



Density (g/cm <sup>3</sup> )	1.280	0.974	0.873	0.868	1.123	0.864	0.855	0.873	0.872
<i>ProPerf<sub>p</sub></i> - Density	1	1	1	1	1	1	1	1	1
$\delta_D$ (MPa <sup>1/2</sup> )	19.5	18.1	18.6	15.8	19.8	17.4	16.9	15.8	16.9
<i>ProPerf<sub>p</sub></i> - $\delta_D$	1	1	1	≈ 0	1	0.21	0.005	≈ 0	0.005
$\delta_P$ (MPa <sup>1/2</sup> )	5.1	4.9	3.8	4	6.3	2.3	1.8	5.1	4.2
<i>ProPerf<sub>p</sub></i> - $\delta_P$	1	1	0.88	1	0.68	≈ 0	≈ 0	1	1
$\delta_H$ (MPa <sup>1/2</sup> )	3.1	6.1	1.6	6	4.7	2.4	4.8	6.5	4.1
<i>ProPerf<sub>p</sub></i> - $\delta_H$	1	0.96	≈ 0	1	1	≈ 0	1	0.34	1
$R_a$ (MPa <sup>1/2</sup> )	2.77	1.39	3.54	5.59	3.04	4.20	4.35	5.67	3.42
<i>ProPerf<sub>p</sub></i> - $R_a$	1	1	0.66	≈ 0	0.99	0.13	0.08	≈ 0	0.78
<i>RED</i>	0.59	0.30	0.75	1.19	0.65	0.89	0.93	1.21	0.73
<i>ProPerf<sub>p</sub></i> - <i>RED</i>	1	1	1	≈ 0	1	1	1	0.58	1
Viscosity (mPa s)	1.089	0.569	0.568	0.903	5.224	0.897	0.748	0.724	0.557
<i>ProPerf<sub>p</sub></i> - Viscosity	1	1	1	1	≈ 0	1	1	1	1

Appendix 9.6: The candidates provided by IBSS®CAMD with a *GloPerf* > 0.6 for P3HT:EH-IDTBR.

Candidates	Chlorobenzene	Anisole	p-Xylene	p-Cymene	Isoamyl acetate	Terpinolene	Tetrahydrofuran	Butyl acetate	Cyclopentyl methyl ether
CAS	108-90-7	100-66-	106-42-	99-87-6	123-92-2	586-62-9	109-99-9	123-86-4	5614-37-9
<i>GloPerf</i>	1	0.997	0.861	0.680	0.674	0.640	0.624	0.621	0.612
Melting Point ( $T_m$ , K)	226	239	229	224	202	221	179	201	185
<i>ProPerf<sub>p</sub></i> - $T_m$	1	1	1	1	1	1	1	1	1
Boiling Point ( $T_b$ , K)	409	428	419	450	420	448	323	407	385
<i>ProPerf<sub>p</sub></i> - $T_b$	1	1	1	1	1	1	≈ 0	1	1
Flash Point ( $T_f$ , K)	300	314	301	323	312	308	243	305	281
<i>ProPerf<sub>p</sub></i> - $T_f$	1	1	1	1	1	1	≈ 0	1	≈ 0
$\Delta H_{\text{vap}}$ (kJ/mol)	41.3	46.5	43.4	50.1	48.9	38.3	32.0	46.0	37.3
<i>ProPerf<sub>p</sub></i> - $\Delta H_{\text{vap}}$	1	1	1	1	1	0.34	≈ 0	1	0.07
Density (g/cm <sup>3</sup> )	1.099	0.974	0.873	0.864	0.868	0.855	0.872	0.873	0.857
<i>ProPerf<sub>p</sub></i> -Density	1	1	1	1	1	1	1	1	1

$\delta_D$ (MPa <sup>1/2</sup> )	19.3	18.1	18.6	17.4	15.8	16.9	16.9	15.8	16.6
<i>ProPerf<sub>p</sub></i> - $\delta_D$	1	1	1	0.96	≈ 0	0.21	0.21	≈ 0	0.03
$\delta_P$ (MPa <sup>1/2</sup> )	4.8	4.9	3.8	2.3	4	1.8	4.2	5.1	3.7
<i>ProPerf<sub>p</sub></i> - $\delta_P$	1	1	1	0.01	1	≈ 0	1	1	1
$\delta_H$ (MPa <sup>1/2</sup> )	2.7	6.1	1.6	2.4	6	4.8	4.1	6.5	3.7
<i>ProPerf<sub>p</sub></i> - $\delta_H$	1	0.96	≈ 0	≈ 0	1	1	1	0.34	1
$R_a$ (MPa <sup>1/2</sup> )	1.58	1.39	3.54	4.20	5.59	4.35	3.42	5.67	4.20
<i>ProPerf<sub>p</sub></i> - $R_a$	1	1	0.66	0.130	≈ 0	0.08	0.78	≈ 0	0.13
<i>RED</i>	0.41	0.3	0.75	0.89	1.12	0.93	0.73	1.21	0.89
<i>ProPerf<sub>p</sub></i> - <i>RED</i>	1	1	1	1	0.64	1	1	0.58	1
Viscosity (mPa s)	0.682	0.569	0.568	0.897	0.903	0.748	0.557	0.724	0.494
<i>ProPerf<sub>p</sub></i> -Viscosity	1	1	1	1	1	1	1	1	0.87

**Appendix 9.7: List of the best solvent candidates selected from the results of molecular design provided by IBSS<sup>®</sup>CAMD  
for P3HT:PC<sub>71</sub>BM. (Y: yes, N: no, /: missing data)**

Candidates	4-Ethynyltoluene	3-Ethylcyclopentane-1-Carbaldehyde	4-Methylphenyl Vinyl Ether	Anisole	Allyl Phenyl Ether	Phenyl Vinyl Ether	4-Acetylcyclohexene
CAS	766-97-2	/	1005-62-5	100-66-	1746-13-0	766-94-9	7353-76-6
<i>GloPerf</i>	1	1	0.998	0.997	0.989	0.978	0.977
Melting Point ( $T_m$ , K)	238	242	262	239	247	255	252
<i>ProPerf<sub>p</sub></i> - $T_m$	1	1	1	1	1	1	1
Boiling Point ( $T_b$ , K)	446	450	474	428	451	453	469
<i>ProPerf<sub>p</sub></i> - $T_b$	1	1	0.99	1	1	1	1
Flash Point ( $T_f$ , K)	323	328	338	314	330	330	342
<i>ProPerf<sub>p</sub></i> - $T_f$	1	1	1	1	1	1	1

$\Delta H_{\text{vap}}$ (kJ/mol)	47.9	51.8	55.3	46.5	51.4	51.4	55.2
$ProPerf_p - \Delta H_{\text{vap}}$	1	1	0.98	1	1	1	0.99
Density (g/cm <sup>3</sup> )	0.946	0.912	0.971	0.974	0.957	0.963	0.969
$ProPerf_p -$ Density	1	1	1	1	1	1	1
$\delta_D$ (MPa <sup>1/2</sup> )	18.2	18.1	18.5	18.1	17.8	18.8	17.7
$ProPerf_p - \delta_D$	1	1	1	1	0.84	1	0.68
$\delta_P$ (MPa <sup>1/2</sup> )	4.4	6	5	4.9	4.4	5.7	4.4
$ProPerf_p - \delta_P$	1	1	1	1	1	1	1
$\delta_H$ (MPa <sup>1/2</sup> )	4.5	4.4	5.7	6.1	4.5	6.3	5.2
$ProPerf_p - \delta_H$	1	1	1	0.96	1	0.68	1
$R_a$ (MPa <sup>1/2</sup> )	0.89	1.70	0.75	1.39	1.58	1.72	1.69
$ProPerf_p - R_a$	1	1	1	1	1	1	1
<i>RED</i>	0.19	0.36	0.16	0.30	0.34	0.37	0.36
$ProPerf_p - RED$	1	1	1	1	1	1	1
Viscosity (mPa s)	0.721	1.090	0.759	0.569	0.721	0.668	0.820

<i>ProPerf<sub>p</sub></i> - Viscosity	1	1	1	1	1	1	1
Stability	N	N	/	Y	Y	N	/
Commerciality	Y	N	N	Y	Y	Y	Y
Cost (€/g)	9.3	/	/	0.4	1.9	4230	1961.6

## Appendix 9.7 (continued)

Candidates	2-Methyl Anisole	2-Vinyl Anisole	Methyl Benzoate	4-Methoxystyrene	(1R,2R)-2-Vinyl Cyclohexanecarbaldehyde	3-Cyclohexen-1-yl Methyl Ether	Cyclopentyl Formate
CAS	578-58-5	612-15-7	93-58-3	637-69-4	/	15766-93-5	62781-99-1
<i>GloPerf</i>	0.946	0.931	0.923	0.923	0.920	0.916	0.901
Melting Point ( $T_m$ , K)	234	240	246	260	258	210	209
<i>ProPerf<sub>p</sub></i> - $T_m$	1	1	1	1	1	1	1
Boiling Point ( $T_b$ , K)	449	472	466	476	480	416	405
<i>ProPerf<sub>p</sub></i> - $T_b$	1	1	1	0.94	0.67	1	1
Flash Point ( $T_f$ , K)	329	350	343	353	350	301	302
<i>ProPerf<sub>p</sub></i> - $T_f$	1	1	1	1	1	1	1
$\Delta H_{\text{vap}}$ (kJ/mol)	52.3	/	55.6	/	53.7	41.7	46.9
<i>ProPerf<sub>p</sub></i> - $\Delta H_{\text{vap}}$	1	0	0.89	0	1	1	1
Density (g/cm <sup>3</sup> )	0.964	0.972	1.068	0.971	0.925	0.892	1.001

<i>ProPerf<sub>p</sub></i> -Density	1	1	1	1	1	1	1
$\delta_D$ (MPa <sup>1/2</sup> )	18.6	18.4	18.7	18.5	17.6	17.1	17
<i>ProPerf<sub>p</sub></i> - $\delta_D$	1	1	1	1	0.5	0.03	0.01
$\delta_P$ (MPa <sup>1/2</sup> )	4.4	4.5	7.5	5	5.9	3.7	5.4
<i>ProPerf<sub>p</sub></i> - $\delta_P$	1	1	≈ 0	1	1	0.75	1
$\delta_H$ (MPa <sup>1/2</sup> )	6.6	5.9	5.3	5.7	4.3	5.2	6.1
<i>ProPerf<sub>p</sub></i> - $\delta_H$	0.21	1	1	1	1	1	0.96
$R_a$ (MPa <sup>1/2</sup> )	1.60	0.92	2.86	0.75	2.35	3.02	3.32
<i>ProPerf<sub>p</sub></i> - $R_a$	1	1	1	1	1	0.99	0.86
<i>RED</i>	0.34	0.20	0.61	0.16	0.50	0.64	0.71
<i>ProPerf<sub>p</sub></i> - <i>RED</i>	1	1	1	1	1	1	1
Viscosity (mPa s)	0.668	0.759	1.340	0.759	1.382	0.611	0.944
<i>ProPerf<sub>p</sub></i> -Viscosity	1	1	1	1	1	1	1
Stability	Y	N	Y	Y	N	/	N
Commerciality	Y	Y	Y	Y	N	Y	N
Cost (€/g)	0.7	39.8	0.9	20.0	/	3712	/



**Appendix 9.8: The list of solvents used in HSPs measurements of PF2  
and KNSF2. (/:Not used for HSP measurements)**

Solvents	$\delta_D$	$\delta_P$	$\delta_H$	Score-PF2	Score-KNSF2
Methyl Ethyl Ketone (MEK)	16	9	5.1	6	0
1,4-Dioxane	17.5	1.8	9	5	0
n-Butyl Acetate	15.8	3.7	6.3	5	0
Hexane	14.9	0	0	3	0
Tetrahydrofuran (THF)	16.8	5.7	8	2	2
Chloroform	17.8	3.1	5.7	2	3
Tetrahydronaphthalene	19.6	2	2.9	1	0
o-Dichlorobenzene	19.2	6.3	3.3	1	1
Chlorobenzene	19	4.3	2	1	3
o-Xylene	17.8	1	3.1	1	1
Iodobenzene	19.9	5.6	6.1	1	5
Tetrachloroethylene	18.3	5.7	0	1	/
Toluene	18	1.4	2	1	1
Ethanol	15.8	8.8	19.4	0	0
Diethylene Glycol	16.6	12	19	0	/
N-Methyl-2-Pyrrolidone (NMP)	18	12.3	7.2	0	/
Acetonitrile	15.3	18	6.1	0	0
Diacetone Alcohol	15.8	8.2	10.8	0	0
2-Phenoxy Ethanol	17.8	5.7	14.3	0	/
Dipropylene Glycol	16.5	10.6	17.7	0	0
Cyclohexanol	17.4	4.1	13.5	0	/
Acetone	15.5	10.4	7	0	0

## 9. APPENDIX

Propylene Glycol Monomethyl Ether	15.6	6.3	11.6	0	0
Dimethyl Sulfoxide (DMSO)	18.4	16.4	10.2	0	0
Propylene Carbonate	20	18	4.1	0	/
Dimethyl Formamide (DMF)	17.4	13.7	11.3	0	0
Propylene Glycol Monomethyl Ether Acetate	15.6	5.6	9.8	0	0
1-Butanol	16	5.7	15.8	0	0
$\gamma$ -Butyrolactone (GBL)	18	16.6	7.4	0	0
Dibasic Esters (DBE)	16.2	6.5	8.4	0	/
Ethyl Acetate	15.8	5.3	7.2	0	0
Methyl Isobutyl Ketone (MIBK)	15.3	6.1	4.1	0	0
Cyclohexane	16.8	0	0.2	0	4
Methanol	14.7	12.3	22.3	0	/
Anisole	17.8	4.4	6.9	0	5
Phenetole (Ethyl Phenyl Ether)	18.4	4.5	4	/	6
1,2,3-Trichloropropane	17.8	12.3	3.4	/	0
Butyl Benzoate	18.3	5.6	5.5	/	0
1,3-Dioxolane	18.1	6.6	9.3	/	0
Ethanolamine	17	15.5	21	/	0

**Appendix 9.9: The candidates provided by IBSS<sup>®</sup>CAMD with a *GloPerf* > 0.5 for PF2:PC<sub>71</sub>BM.**

Candidates	1,2-dichlorobenzene	p-xylene	Anisole	p-Cymene	Benzyl Benzoate	Glycerol -1,2,3-triethyl ether	Isoamyl acetate	Butyl acetate	Ethylene carbonate
CAS	95-50-1	106-42-3	100-66-3	99-87-6	120-51-4	162614-45-1	123-92-2	123-86-4	96-49-1
<i>GloPerf</i>	1	0.931	0.724	0.693	0.566	0.517	0.517	0.517	0.514
Melting Point ( $T_m$ , K)	255	229	239	224	306	210	202	201	283
$ProPerf_p - T_m$	1	1	1	1	≈ 0	1	1	1	1
Boiling Point ( $T_b$ , K)	449	419	428	450	573	467	420	407	413
$ProPerf_p - T_b$	1	1	1	1	≈ 0	1	1	1	1
Flash Point ( $T_f$ , K)	332	301	314	323	419	343	312	305	324
$ProPerf_p - T_f$	1	1	1	1	1	1	1	1	1
$\Delta H_{vap}$ (kJ/mol)	50.1	43.4	46.5	50.1	85.75	60.2	48.9	46.0	49.3
$ProPerf_p - \Delta H_{vap}$	1	1	1	1	≈ 0	≈ 0	≈ 0	≈ 0	≈ 0

Density (g/cm <sup>3</sup> )	1.280	0.873	0.974	0.864	1.123	0.893	0.868	0.873	1.30
<i>ProPerf<sub>p</sub></i> - Density	1	1	1	1	1	1	1	1	1
$\delta_D$ (MPa <sup>1/2</sup> )	19.5	18.6	18.1	17.4	19.8	15.5	15.8	15.8	18.4
<i>ProPerf<sub>p</sub></i> - $\delta_D$	1	1	0.50	0.01	1.00	≈ 0	≈ 0	≈ 0	0.96
$\delta_P$ (MPa <sup>1/2</sup> )	5.1	3.8	4.9	2.3	6.3	4.8	4	5.1	21.2
<i>ProPerf<sub>p</sub></i> - $\delta_P$	1	1	1	0.02	0.03	1	1	1	≈ 0
$\delta_H$ (MPa <sup>1/2</sup> )	3.1	1.6	6.1	2.4	4.7	3.6	6	6.5	6.3
<i>ProPerf<sub>p</sub></i> - $\delta_H$	1	≈ 0	≈ 0	1	0.68	1	≈ 0	≈ 0	≈ 0
$R_a$ (MPa <sup>1/2</sup> )	1.51	1.70	4.12	4.10	3.36	7.51	7.52	7.85	17.82
<i>ProPerf<sub>p</sub></i> - $R_a$	1	1	0.17	0.18	0.83	≈ 0	≈ 0	≈ 0	≈ 0
<i>RED</i>	0.38	0.42	1.03	1.03	0.84	1.88	1.88	1.96	4.46
<i>ProPerf<sub>p</sub></i> - <i>RED</i>	1	1	0.99	0.99	1	≈ 0	≈ 0	≈ 0	≈ 0
Viscosity (mPa s)	1.089	0.568	0.569	0.897	5.224	0.962	0.903	0.724	0.824
<i>ProPerf<sub>p</sub></i> - Viscosity	1	1	1	1	≈ 0	1	1	1	1

**Appendix 9.10: The candidates provided by IBSS<sup>®</sup>CAMD with a *GloPerf* > 0.5 for PF2:EH-IDTBR.**

Candidates	1,2-dichlorobenzene	p-Xylene	Anisole	p-Cymene	Benzyl Benzoate	Glycerol -1,2,3-triethyl ether
CAS	95-50-1	106-42-3	100-66-3	99-87-6	120-51-4	162614-45-1
<i>GloPerf</i>	1	0.931	0.758	0.714	0.564	0.517
Melting Point ( $T_m$ , K)	255	229	239	224	307	210
$ProPerf_p - T_m$	1	1	1	1	5.52E-14	1
Boiling Point ( $T_b$ , K)	449	419	428	450	573	467
$ProPerf_p - T_b$	1	1	1	1	1.73E-39	1
Flash Point ( $T_f$ , K)	332	301	314	323	420	343
$ProPerf_p - T_f$	1	1	1	1	1	1
$\Delta H_{vap}$ (kJ/mol)	50.1	43.4	46.5	50.1	85.8	60.2
$ProPerf_p - \Delta H_{vap}$	1	1	1	1	$\approx 0$	$\approx 0$
Density (g/cm <sup>3</sup> )	1.280	0.873	0.974	0.864	1.123	0.893
$ProPerf_p - \text{Density}$	1	1	1	1	1	1

$\delta_D$ (MPa <sup>1/2</sup> )	19.5	18.6	18.1	17.4	19.8	15.5
<i>ProPerf<sub>p</sub></i> - $\delta_D$	1	1	1	0.21	1	0.00
$\delta_P$ (MPa <sup>1/2</sup> )	5.1	3.8	4.9	2.3	6.3	4.8
<i>ProPerf<sub>p</sub></i> - $\delta_P$	1	1	1	0.13	≈ 0	1
$\delta_H$ (MPa <sup>1/2</sup> )	3.1	1.6	6.1	2.4	4.7	3.6
<i>ProPerf<sub>p</sub></i> - $\delta_H$	1	0.00	0.00	1	0.68	1
$R_a$ (MPa <sup>1/2</sup> )	1.51	1.70	4.12	4.10	3.36	7.51
<i>ProPerf<sub>p</sub></i> - $R_a$	1	1	0.17	0.18	0.83	≈ 0
<i>RED</i>	0.38	0.42	1.03	1.03	0.84	1.88
<i>ProPerf<sub>p</sub></i> - <i>RED</i>	1	1.00	0.99	0.99	1	≈ 0
Viscosity (mPa s)	1.089	0.568	0.569	0.897	5.224	0.962
<i>ProPerf<sub>p</sub></i> -Viscosity	1	1	1	1	0	1

## Appendix 9.10 (continued)

Candidates	Isoamyl acetate	Butyl acetate	Ethylene carbonate	2-Furaldehyde	Dibutyl ether	Propylene carbonate
CAS	123-92-2	123-86-4	96-49-1	98-01-1	142-96-1	108-32-7
<i>GloPerf</i>	0.517	0.517	0.517	0.517	0.516	0.511
Melting Point ( $T_m$ , K)	202	201	283	249	187	287
<i>ProPerf<sub>p</sub></i> - $T_m$	1	1	1	1	1	0.50
Boiling Point ( $T_b$ , K)	420	407	413	417	426	433
<i>ProPerf<sub>p</sub></i> - $T_b$	1	1	1	1	1	1
Flash Point ( $T_f$ , K)	312	305	324	310	311	334
<i>ProPerf<sub>p</sub></i> - $T_f$	1	1	1	1	1	1
$\Delta H_{\text{vap}}$ (kJ/mol)	48.9	46.0	49.3	45.9	46.7	52.7
<i>ProPerf<sub>p</sub></i> - $\Delta H_{\text{vap}}$	1	1	1	1	1	1
Density (g/cm <sup>3</sup> )	0.868	0.873	1.303	1.113	0.770	1.195

<i>ProPerf<sub>p</sub></i> -Density	1	1	1	1	0.10	1
$\delta_D$ (MPa <sup>1/2</sup> )	15.8	15.8	18.4	18	15.4	17.9
<i>ProPerf<sub>p</sub></i> - $\delta_D$	0.00	0.00	1	1	0.00	0.96
$\delta_P$ (MPa <sup>1/2</sup> )	4	5.1	21.2	12.5	2.9	18.3
<i>ProPerf<sub>p</sub></i> - $\delta_P$	1	1	≈ 0	≈ 0	0.88	≈ 0
$\delta_H$ (MPa <sup>1/2</sup> )	6	6.5	6.3	8.8	2.7	5
<i>ProPerf<sub>p</sub></i> - $\delta_H$	0.00	0.00	0.00	0.00	1	0.21
$R_a$ (MPa <sup>1/2</sup> )	7.52	7.85	17.82	10.84	7.65	14.89
<i>ProPerf<sub>p</sub></i> - $R_a$	≈ 0	≈ 0	≈ 0	≈ 0	≈ 0	≈ 0
<i>RED</i>	1.88	1.96	4.46	2.71	1.91	3.72
<i>ProPerf<sub>p</sub></i> - <i>RED</i>	≈ 0	≈ 0	≈ 0	≈ 0	≈ 0	≈ 0
Viscosity (mPa s)	0.903	0.724	0.824	1.142	0.612	0.797
<i>ProPerf<sub>p</sub></i> -Viscosity	1	1	1	1	1	1



**Appendix 9.11: List of the best solvent candidates selected from the results of molecular design provided by IBSS®CAMD for PF2:PC<sub>71</sub>BM. (Y: yes, N: no, NA: no data available)**

Candidates	benzyl methyl ether	Methyl phenethyl ether	p-xylene	N,N-Dimethylaniline	1-(3-Buten-2-yl)-4-methylbenzene	4-Methylstyrene	1-Phenyl-2-butene	1-Methyl-2-(2-propyn-1-yl)benzene
CAS	538-86-3	3558-60-9	106-	121-69-7	97664-18-1	622-97-9	935-00-2	NA
<i>GloPerf</i>	0.975	0.966	0.931	0.931	0.931	0.912	0.909	0.901
Melting Point ( $T_m$ , K)	238	227	229	262	224	235	220	232
<i>ProPerf<sub>p</sub></i> - $T_m$	1	1	1	1	1	1	1	1
Boiling Point ( $T_b$ , K)	446	465	419	461	466	446	459	463
<i>ProPerf<sub>p</sub></i> - $T_b$	1	1	1	1	1	1	1	1
Flash Point ( $T_f$ , K)	323	337	301	338	332	327	329	332
<i>ProPerf<sub>p</sub></i> - $T_f$	1	1	1	1	1	1	1	1
$\Delta H_{\text{vap}}$ (kJ/mol)	47.9	52.8	43.4	52.8	52.8	NA	51.8	54.0

$ProPerf_p - \Delta H_{vap}$	1	1	1	1	1	0	1	1
Density (g/cm <sup>3</sup> )	0.946	0.935	0.873	0.937	0.883	0.889	0.888	0.918
$ProPerf_p -$ Density	1	1	1	1	1	1	1	1
$\delta_D$ (MPa <sup>1/2</sup> )	18.2	18.1	18.6	18.6	17.8	18.3	18.2	18.4
$ProPerf_p - \delta_D$	0.68	0.50	1	1	0.12	0.84	0.68	0.96
$\delta_P$ (MPa <sup>1/2</sup> )	4.4	3.9	3.8	3.9	3.2	3.2	1.9	3
$ProPerf_p - \delta_P$	1	1	1	1	0.88	0.88	≈ 0	0.60
$\delta_H$ (MPa <sup>1/2</sup> )	4.5	4.3	1.6	4.1	2.9	2.4	3.2	3.1
$ProPerf_p - \delta_H$	0.96	1	≈ 0	1	1	1	1	1
$R_a$ (MPa <sup>1/2</sup> )	2.69	2.66	1.70	1.77	2.87	1.94	2.79	1.81
$ProPerf_p - R_a$	1	1	1	1	1	1	1	1
<i>RED</i>	0.67	0.67	0.42	0.44	0.72	0.48	0.70	0.45
$ProPerf_p - RED$	1	1	1.00	1	1	1	1	1
Viscosity (mPa s)	0.721	0.902	0.568	NA	1.012	0.655	0.815	NA
$ProPerf_p -$ Viscosity	1	1	1	0	1	1	1	0

Commerciality	Y	Y	Y	Y	N	Y	N	N
Cost (€/g)	2.66	1.32	0.18	0.21	NA	0.52	NA	NA
Stable (at room temperature)	Y	Y	Y	Y	N	N	N	N

**Appendix 9.12: List of the best solvent candidates selected from the results of molecular design provided by IBSS®CAMD for PF2:EH-IDTBR. (Y: yes, N: no, NA: no data available)**

Target properties with performance values	Methyl phenethyl ether	benzyl methyl ether	1-(3-Buten-2-yl)-4-methylbenzene	Allylbenzene	1-Phenyl-2-butene	p-xylene	4-Methylstyrene
CAS	3558-60-9	538-86-3	97664-18-1	300-57-2	935-00-2	106-42-3	622-97-9
<i>GloPerf</i>	1	0.997	0.989	0.932	0.932	0.931	0.931
Melting Point ( $T_m$ , K)	227	238	224	197	220	229	235
<i>ProPerf<sub>n</sub></i> - $T_m$	1	1	1	1	1	1	1
Boiling Point ( $T_b$ , K)	465	446	466	435	459	419	446
<i>ProPerf<sub>n</sub></i> - $T_b$	1	1	1	1	1	1	1
Flash Point ( $T_f$ , K)	337	323	332	311	329	301	327
<i>ProPerf<sub>n</sub></i> - $T_f$	1	1	1	1	1	1	1
$\Delta H_{vap}$ (kJ/mol)	52.8	47.9	52.8	46.1	51.8	43.4	NA
<i>ProPerf<sub>n</sub></i> - $\Delta H_{vap}$	1	1	1	1	1	1	0
Density (g/cm <sup>3</sup> )	0.935	0.946	0.883	0.888	0.888	0.873	0.889

<i>ProPerf<sub>n</sub></i> -Density	1	1	1	1	1	1	1
$\delta_D$ (MPa <sup>1/2</sup> )	18.1	18.2	17.8	18.1	18.2	18.6	18.3
<i>ProPerf<sub>n</sub></i> - $\delta_D$	1	1	0.84	1.00	1.00	1	1.00
$\delta_P$ (MPa <sup>1/2</sup> )	3.9	4.4	3.2	2	1.9	3.8	3.2
<i>ProPerf<sub>n</sub></i> - $\delta_P$	1	1	1	0.02	0.01	1	1
$\delta_H$ (MPa <sup>1/2</sup> )	4.3	4.5	2.9	3.1	3.2	1.6	2.4
<i>ProPerf<sub>n</sub></i> - $\delta_H$	1.00	0.96	1.00	1.00	1.00	≈ 0	1.00
$R_a$ (MPa <sup>1/2</sup> )	2.66	2.69	2.87	2.86	2.79	1.70	1.94
<i>ProPerf<sub>n</sub></i> - $R_a$	1	1	1	1	1	1	1
RED	0.67	0.67	0.72	0.71	0.70	0.42	0.48
<i>ProPerf<sub>n</sub></i> -RED	1	1	1	1	1	1	1
Viscosity (mPa s)	0.902	0.721	1.012	0.707	0.815	0.568	0.655
<i>ProPerf<sub>n</sub></i> -Viscosity	1	1	1	1	1	1	1
Commerciality	Y	Y	N	Y	N	Y	Y
Cost (€/g)	1.32	2.66	NA	2.84	NA	0.18	0.52
Stable (at room temperature)	Y	Y	N	N	N	Y	N

### Appendix 9.12 (continued):

Target properties with performance values	N,N-Dimethylaniline	3-Butenylbenzene	1-Methyl-2-(2-propyn-1-yl)benzene	4-Ethynyltoluene	2-Methylstyrene	phenylallene
CAS	121-69-7	768-56-9	NA	622-96-8	611-15-4	2327-99-3
<i>GloPerf</i>	0.931	0.930	0.929	0.923	0.914	0.903
Melting Point ( $T_m$ , K)	262	207	232	212	211	253
$ProPerf_p - T_m$	1	1	1	1	1	1
Boiling Point ( $T_b$ , K)	461	458	463	441	442	465
$ProPerf_p - T_b$	1	1	1	1	1	1
Flash Point ( $T_f$ , K)	338	328	332	316	324	333
$ProPerf_p - T_f$	1	1	1	1	1	1
$\Delta H_{vap}$ (kJ/mol)	52.8	51.0	54.0	47.3	NA	48.3
$ProPerf_p - \Delta H_{vap}$	1	1	1	1	0	1
Density (g/cm <sup>3</sup> )	0.937	0.883	0.918	0.869	0.891	0.903

<i>ProPerf<sub>p</sub></i> -Density	1	1	1	1	1	1
$\delta_D$ (MPa <sup>1/2</sup> )	18.6	18	18.4	18.2	18.1	18.3
<i>ProPerf<sub>p</sub></i> - $\delta_D$	1	1	1	1	1	1
$\delta_P$ (MPa <sup>1/2</sup> )	3.9	1.9	3	2.9	2.8	2.7
<i>ProPerf<sub>p</sub></i> - $\delta_P$	1	0.01	0.97	0.88	0.75	0.60
$\delta_H$ (MPa <sup>1/2</sup> )	4.1	3	3.1	1.8	2.7	4.1
<i>ProPerf<sub>p</sub></i> - $\delta_H$	1.00	1.00	1.00	0.00	1	1
$R_a$ (MPa <sup>1/2</sup> )	1.77	3.07	1.81	2.41	2.42	2.48
<i>ProPerf<sub>p</sub></i> - $R_a$	1	0.99	1	1	1	1
<i>RED</i>	0.44	0.77	0.45	0.60	0.60	0.62
<i>ProPerf<sub>p</sub></i> - <i>RED</i>	1	1	1	1	1	1
Viscosity (mPa s)	NA	0.888	NA	0.722	0.655	NA
<i>ProPerf<sub>p</sub></i> -Viscosity	0	1	0	1	1	0
Commerciality	Y	Y	N	Y	Y	N
Cost (€/g)	0.21	9.73	NA	7.04	19.01	NA
Stable	Y	N	N	N	N	N

**Appendix 9.13: The candidates provided by IBSS® CAMD with a *GloPerf* > 0.6 for KNSF2:PC<sub>71</sub>BM.**

Candidates	<i>o</i> -DCB	<i>p</i> -Xylene	<i>p</i> -Cymene	1,4-Cineol	Anisole	Cyclopentyl methyl ether	$\alpha$ -Pinene
CAS	95-50-1	106-42-3	99-87-6	470-67-7	100-66-3	5614-37-9	80-56-8
<i>GloPerf</i>	0.977	0.874	0.812	0.751	0.742	0.725	0.699
Melting Point ( $T_m$ , K)	255	229	224	271	239	185	227
<i>ProPerf<sub>p</sub></i> - $T_m$	1	1	1	1	1	1	1
Boiling Point ( $T_b$ , K)	449	419	450	444	428	385	430
<i>ProPerf<sub>p</sub></i> - $T_b$	1	1	1	1	1	1	1
Flash Point ( $T_f$ , K)	332	301	323	319	314	281	301
<i>ProPerf<sub>p</sub></i> - $T_f$	1	1	1	1	1	$\approx 0$	1
$\Delta H_{\text{vap}}$ (kJ/mol)	50.1	43.35	50.06	54.22	46.52	37.30	47.70
<i>ProPerf<sub>p</sub></i> - $\Delta H_{\text{vap}}$	1	1	1	1	1	1	1
Density (g/cm <sup>3</sup> )	1.280	0.873	0.864	0.927	0.974	0.857	0.872
<i>ProPerf<sub>p</sub></i> -Density	1	1	1	1	1	1	1



$\delta_D$ (MPa <sup>1/2</sup> )	19.5	18.6	18.5	17	18.1	16.6	17
<i>ProPerf<sub>p</sub></i> - $\delta_D$	1	1	1	0.339	1	0.030	0.339
$\delta_P$ (MPa <sup>1/2</sup> )	5.1	3.8	2.6	3.4	4.9	3.7	1.3
<i>ProPerf<sub>p</sub></i> - $\delta_P$	1	1	0.075	0.969	1	1	≈0
$\delta_H$ (MPa <sup>1/2</sup> )	3.1	1.6	1.9	3.7	6.1	3.7	2
<i>ProPerf<sub>p</sub></i> - $\delta_H$	1	1	1	0.841	≈0	0.841	1
$R_a$ (MPa <sup>1/2</sup> )-KNSF2	4.37	2.31	2.66	2.47	4.74	2.80	3.13
<i>ProPerf<sub>p</sub></i> - $R_a$ -KNSF2	0.824	1	1	1	0.465	1	1
RED-KNSF2	0.88	0.47	0.54	0.50	0.97	0.57	0.64
<i>ProPerf<sub>p</sub></i> -RED-KNSF2	1	1	1	1	1	1	1
$R_a$ (MPa <sup>1/2</sup> )-PC <sub>71</sub> BM	2	4.61	5.11	6.75	4.52	7.44	8.00
<i>ProPerf<sub>p</sub></i> - $R_a$ -PC <sub>71</sub> BM	1	0.026	0.002	≈0	0.038	≈0	≈0
RED-PC <sub>71</sub> BM	0.24	0.55	0.61	0.80	0.54	0.89	0.95
<i>ProPerf<sub>p</sub></i> -RED-PC <sub>71</sub> BM	1	1	1	1	1	1	1
Viscosity (mPa s)	1.089	0.568	0.897	/	0.569	0.494	/
<i>ProPerf<sub>p</sub></i> -Viscosity	1	1	1	≈0	1	0.870	≈0

### Appendix 9.13 (continued)

Candidates	Glycerol -1,2,3-triethyl ether	Pinane	Dibutyl ether	$\beta$ -Pinene	Terpinolene	d-Limonene	Isoamyl acetate
CAS	162614-45-1	473-55-2	142-96-1	127-91-3	586-62-9	138-86-3	123-92-2
<i>GloPerf</i>	0.694	0.689	0.640	0.626	0.619	0.610	0.600
Melting Point ( $T_m$ , K)	210	225	187	228	221	189	202
<i>ProPerf<sub>p</sub></i> - $T_m$	1	1	1	1	1	1	1
Boiling Point ( $T_b$ , K)	467	433	426	436	448	452	420
<i>ProPerf<sub>p</sub></i> - $T_b$	1	1	1	1	1	1	1
Flash Point ( $T_f$ , K)	343	306	311	305	308	311	312
<i>ProPerf<sub>p</sub></i> - $T_f$	1	1	1	1	1	1	1
$\Delta H_{vap}$ (kJ/mol)	60.16	50.38	46.71	/	38.26	44.44	48.89
<i>ProPerf<sub>p</sub></i> - $\Delta H_{vap}$	$\approx 0$	1	1	$\approx 0$	1	1	1
Density (g/cm <sup>3</sup> )	0.893	0.845	0.770	0.868	0.855	0.843	0.868
<i>ProPerf<sub>p</sub></i> -Density	1	1	0.102	1	1	1	1

$\delta_D$ (MPa <sup>1/2</sup> )	15.5	17	15.4	16.9	16.9	16.7	15.8
$ProPerf_p$ - $\delta_D$	≈0	0.339	≈0	0.210	0.210	0.062	≈0
$\delta_P$ (MPa <sup>1/2</sup> )	4.8	1.6	2.9	1.6	1.8	2.2	4
$ProPerf_p$ - $\delta_P$	1	≈0	0.317	≈0	≈0	0.005	1
$\delta_H$ (MPa <sup>1/2</sup> )	3.6	1.4	2.7	1.8	4.8	4.9	6
$ProPerf_p$ - $\delta_H$	0.958	0.841	1	1	0.001	≈0	≈0
$R_a$ (MPa <sup>1/2</sup> )-KNSF2	4.46	2.83	4.50	2.90	4.21	4.20	5.55
$ProPerf_p$ - $R_a$ -KNSF2	0.741	1	0.703	1	0.940	0.945	0.034
RED-KNSF2	0.91	0.58	0.92	0.59	0.86	0.86	1.13
$ProPerf_p$ -RED -KNSF2	1	1	1	1	1	1.000	0.801
$R_a$ (MPa <sup>1/2</sup> )-PC <sub>71</sub> BM	9.46	8.06	10.08	8.08	7.52	7.71	9.04
$ProPerf_p$ - $R_a$ -PC <sub>71</sub> BM	≈0	≈0	≈0	≈0	≈0	≈0	≈0
RED-PC <sub>71</sub> BM	1.13	0.96	1.20	0.96	0.90	0.92	1.08
$ProPerf_p$ -RED -PC <sub>71</sub> BM	0.815	1	0.599	1	1	1	0.929
Viscosity (mPa s)	0.962	/	0.612	/	/	/	0.903
$ProPerf_p$ -Viscosity	1	≈0	1	≈0	≈0	≈0	1

## Resumé

### **Recherche par ingénierie inversée de solvants alternatifs, non-toxiques et bio-sourcés, pour la fabrication de cellules solaires organiques**

#### *1. Introduction*

Les cellules photovoltaïques organiques (PVO) à base d'hétérojonction donneur-accepteur distribuée en volume constituent une alternative intéressante aux technologies photovoltaïques conventionnelles. Elles ouvrent en effet la perspective de produire des modules photovoltaïques flexibles, légers, et facilement intégrables, par des techniques d'impression à bas coût. En outre, la fabrication de modules PVO bénéficie d'un temps de retour sur investissement énergétique beaucoup plus court (de l'ordre de quelques jours) et un impact environnemental bien plus faible que les autres technologies. L'augmentation récente du rendement de conversion d'énergie (RCE) des dispositifs PVO (un rendement de 18% a été atteint en 2020)<sup>1</sup> augmente également le potentiel de cette technologie à contribuer efficacement à la production d'énergie renouvelable à grande échelle. Toutefois, en ce qui concerne le développement industriel de modules PVO, la possibilité d'utiliser des moyens de fabrication écologiques et économiquement viables reste incertaine et dépendra entre autres de la disponibilité de solvants non toxiques et compatibles avec les techniques d'impression. En effet, à l'échelle du laboratoire, l'élaboration de cellules solaires organiques de petites dimensions se fait généralement en utilisant des solvants halogénés tels que le chloroforme (CF)<sup>2-5</sup>, le 1,2-dichlorobenzène (*o*-DCB)<sup>2,6-9</sup> ou le chlorobenzène (CB)<sup>8,10-12</sup>, car ceux-ci offrent une bonne solubilité pour de nombreux polymères semi-conducteurs et permettent d'atteindre des performances élevées. Cependant, les solvants halogénés sont toxiques et incompatibles avec une production de dispositifs de grande taille. Il est donc urgent d'identifier des solvants alternatifs qui

permettent de fabriquer des dispositifs PVO de grande surface avec un impact négligeable sur l'environnement et la santé humaine, sans réduire l'efficacité de conversion du dispositif.

Parmi les nombreux nouveaux matériaux organiques qui ont été développés pour augmenter l'efficacité des dispositifs de PVO, seuls quelques exemples ont été mis en œuvre avec des solvants alternatifs non ou moins toxiques. La solubilité étant fonction de la structure moléculaire du soluté, les solvants de remplacement ne peuvent cependant pas être appliqués universellement à tous les semi-conducteurs organiques. De fait, jusqu'à présent, la sélection des solvants de remplacement était principalement le résultat d'une approche empirique et fastidieuse, de type essais-erreurs, laquelle risque de manquer des solvants candidats plus appropriés. La recherche de nouveaux solvants est en effet un problème complexe nécessitant la prise en compte simultanée de nombreuses propriétés interdépendantes, l'augmentation en performance d'une propriété pouvant entraîner la réduction de la performance d'une autre. Ainsi, la recherche d'un solvant de remplacement est souvent le compromis d'un problème à objectifs multiples. Des propriétés telles que la solubilité, la viscosité, la sécurité, la durabilité, la toxicité..., sont toutes importantes pour l'application finale et ont toutes un impact sur les performances du dispositif. Comme de nouveaux matériaux donneurs ou accepteurs sont continuellement conçus et synthétisés dans les laboratoires de recherche afin d'améliorer encore les performances des dispositifs PVO, le développement d'une méthode plus efficace et rapide pour identifier des solvants alternatifs serait particulièrement utile. Il convient de noter que la recherche de solvants alternatifs est également nécessaire pour les dispositifs autres que les PVO, tels que les diodes électroluminescentes organiques, les transistors organiques à effet de champ ou encore les cellules solaires pérovskites. Enfin, dans le cadre du développement durable, les solvants synthétisés à partir de produits issus de l'agriculture (i.e. les « biosolvants ») suscitent un intérêt croissant. Toutefois, étant moins « polyvalents » que la plupart des solvants chlorés ou

hydrocarbonés, la recherche de solvants bio-sourcés efficaces est encore plus difficile.

Dans ce contexte, l'objectif principal de cette thèse a été d'appliquer une méthode d'« ingénierie inversée », reposant sur la conception assistée par ordinateur de molécules organiques, à la recherche de solvants de remplacement pour les matériaux photovoltaïques. Cette méthode a été développée initialement, et utilisée avec succès, pour la recherche de solvants alternatifs en cosmétique. Dans ce travail, il s'agissait d'appliquer une approche similaire à la problématique du PVO et de rendre la recherche de solvants alternatifs, voire bio-sourcés, moins empirique. La méthode a été appliquée avec succès aux mélanges de poly (3-hexylthiophène) (P3HT) et de PC<sub>71</sub>BM (un dérivé soluble du fullerène) ainsi qu'au P3HT mélangé avec du EH-IDTBR, un accepteur non-fullerène. Deux polymères à haut rendement (PF2 et KNSF2), synthétisés par les équipes de N. Leclerc d'ICPEES et de S. Méry à l'IPCMS, ont également été étudiés.

## *2. Effets de la morphologie sur l'efficacité de conversion photovoltaïque*

Une cellule photovoltaïque organique à base d'une hétérojonction donneur-accepteur distribuée en volume (HJV) est un composant à couches minces, dont la couche principale est constituée d'un mélange de deux matériaux semi-conducteurs organiques : un matériau donneur d'électrons (D) et un matériau accepteur d'électrons (A). Les molécules D et A sont déposées par une technique d'impression (ex : spin-coating) à partir d'une solution organique et forment l'HJV. Pendant le dépôt, les deux matériaux se séparent en phase et forment des domaines plus ou moins purs et de taille moyenne pouvant aller de quelques nanomètres à quelques dizaines de nanomètres. La conversion de la lumière en électricité se fait en quatre étapes consécutives : (1) absorption de la lumière et génération d'excitons par l'HJV, (2) diffusion des excitons jusqu'à l'interface D/A (3) séparation des excitons en porteurs de charge libres, et (4) transport de charges vers les électrodes.

Dans une HJV, la dissociation des excitons en charges libres a lieu uniquement à l'interface D/A. Elle est engendrée par la différence entre respectivement les affinités électroniques et les potentiels d'ionisation des matériaux D et A. Par conséquent, il est nécessaire que les excitons soient photo-générés à une distance de l'interface D/A inférieure à leur longueur de diffusion (typiquement de l'ordre de qqs nanomètres). Après génération, les porteurs de charge dérivent vers les électrodes respectives sous l'influence d'un champ électrique interne. Cette dérive nécessite l'existence d'un chemin continue (percolation) pour chaque type de domaine (D ou A). La morphologie de la couche active à l'échelle nanométrique est par conséquent un facteur clé pour l'efficacité de génération et de collecte des charges libres, et bien sûr pour l'efficacité de conversion énergétique d'une cellule PVO.

Les propriétés du solvant utilisé pour le dépôt de l'HJV influencent considérablement la morphologie du film et doivent être prises en compte lors de la recherche de solvants organiques. La séparation de phases entre D et A se produit pendant l'évaporation du solvant et détermine la taille des domaines D et A. Le phénomène est complexe car il dépend non seulement des propriétés intrinsèques des composants D et A telles que le degré de cristallinité, leur miscibilité et les propriétés de cristallisation auto-limitante, mais aussi des conditions expérimentales de mise en œuvre (tel que la nature du solvant ou des additifs éventuels, les traitements thermiques ou recuits en phase vapeur du solvant post-dépôt,...). Deux aspects sont à prendre en compte pour obtenir la morphologie HJV adéquate : la séparation de phases entre domaines donneur et accepteur et l'organisation moléculaire au sein des domaines. Idéalement, la séparation de phase entre les matériaux donneur et accepteur dans la HJV doit conduire à des tailles de domaine de l'ordre de la longueur de diffusion des excitons, minimisant ainsi la recombinaison des excitons et permettant la dissociation des excitons en charges libres.

### *3. Solvants et performances photovoltaïques*

Dans le cas des dispositifs élaborés à partir d'encres, la morphologie de la couche active dépend fortement de propriétés thermodynamiques et cinétiques liées au solvant. Les propriétés thermodynamiques sont associées à diverses propriétés physico-chimiques des matériaux donneurs et accepteurs et des solvants, telles que leurs interactions intermoléculaires, leur miscibilité ou encore leurs diagrammes de phases. La cinétique du séchage du film influence fortement la morphologie et dépend de propriétés telles que le point d'ébullition ou la pression de vapeur du solvant. Actuellement, le choix d'un solvant pour les dispositifs PVO est principalement basé sur sa capacité à solubiliser les semi-conducteurs organiques qui forment l'HJV et son point d'ébullition.

De nombreuses études ont porté sur l'influence de la solubilité des D et A dans le solvant sur la formation d'agrégats de dérivés du fullerène (A). L'étude de Brabec et al.<sup>13</sup> d'un mélange MDMO-PPV : PC<sub>61</sub>BM a ainsi été l'une des premières à apporter des éclaircissements sur la relation entre solubilité et morphologie à l'échelle nanométrique. La morphologie des films minces a en particulier pu être corrélée à la limite de solubilité du PC<sub>61</sub>BM dans divers solvants. De plus, la morphologie du film mince est fonction de la cinétique de séchage. Ainsi, en utilisant des solvants très volatils, la cinétique d'évaporation est plus rapide que la cinétique de cristallisation. Dans ce cas, la morphologie résultante est loin de celle observée dans des conditions d'équilibre. Les effets de la cinétique de séchage sur le degré d'agrégation des chaînes de polymères ont été largement étudiés en utilisant diverses techniques de dépôt et de solvants ayant des points d'ébullition différents. Dans le cas du P3HT:PC<sub>61</sub>BM, un solvant à point d'ébullition élevé permet d'obtenir une meilleure efficacité de conversion sans avoir recours à un traitement thermique. En outre, il a également été démontré que le choix du solvant avait un impact sur d'autres aspects de la morphologie de la HJV, tels que la séparation de phase verticale et l'orientation des chaînes de polymères. Pour les mélanges P3HT:PC<sub>61</sub>BM, les solvants à point d'ébullition élevé sont également préférables afin de laisser le temps aux chaînes de



polymères de s'auto-organiser.

Un solvant unique aux propriétés appropriées pourrait en principe suffire pour atteindre une morphologie adéquate. Cependant, comme le nombre de solvants pouvant solubiliser simultanément les deux composants, D et A, est souvent limité, d'autres méthodes sont nécessaires. Ainsi, l'ajout d'additifs dans la solution principale s'est avéré être un moyen complémentaire très efficace pour contrôler la morphologie du film mince. Par additif on désigne un solvant qui est introduit en petite proportion (généralement quelques % en volume) dans le solvant hôte utilisé pour solubiliser les matières actives. Pour les mélanges polymères:petites molécules, les additifs modifient souvent la séparation de phases et la cristallisation du polymère en dissolvant sélectivement les petites molécules (ex : dérivés de fullerène). Néanmoins, l'impact de l'additif sur la morphologie dépend du mélange D:A en question. Dans certains cas, les additifs ont augmenté le degré de séparation de phase, alors que dans d'autres c'est l'inverse. Tout dépend des propriétés physicochimiques de l'additif et de ces interactions avec les molécules photo-actives.

#### *4. Sélection de solvants alternatifs*

Comme mentionné ci-dessus, la morphologie de l'HJV peut être optimisée par un choix approprié de solvants, de mélanges de solvants et/ou d'additifs. Compte tenu de tous ces paramètres et de la grande variété de solvants et d'additifs existants, le choix de la formulation optimale en utilisant une approche de type essais - erreurs nécessite la formulation de nombreux mélanges de matériaux et la fabrication de nombreux dispositifs PVO. Par conséquent, l'optimisation de la morphologie peut être extrêmement coûteuse et prendre beaucoup de temps. Il est donc nécessaire de trouver des méthodes plus efficaces pour choisir les formulations adaptées. Une méthode récente repose sur la théorie de la solubilité de Hansen. Cette théorie utilise trois paramètres de solubilité (les « paramètres de Hansen » ou HSP) pour décrire les

interactions entre soluté et solvant. Les HSP ont été largement utilisés pour les solvants dans l'industrie des revêtements, mais ils n'ont émergé que récemment dans le domaine de l'électronique organique. La solubilité d'un matériau donné peut être évaluée expérimentalement pour un nombre déterminé de solvants et permet de classer ces derniers comme « bon » ou « mauvais » solvant. Ces résultats permettent ensuite de définir la sphère de solubilité du matériau séparant les bons solvants (situés à l'intérieur de la sphère) des mauvais en fonction de leurs paramètres HSP. Cependant, trouver un solvant adéquat pour le PVO est un problème complexe, qui nécessite de prendre en compte de multiples autres propriétés, au-delà de la solubilité. Pour la plupart d'entre elles l'impact sur les propriétés du dispositif est difficilement prévisible et mais doit être prise en compte lors du processus de sélection. Il y a donc un intérêt considérable à développer des méthodologies plus systématiques pour assister la sélection des solvants alternatifs. L'« ingénierie inverse » est l'une des voies possibles et fait l'objet principal de cette thèse.

L'ingénierie inverse suit les préceptes de la conception moléculaire assistée par ordinateur (CAMD) en définissant d'abord un ensemble de valeurs cibles pour un groupe de propriétés physico-chimiques sélectionnées et en dirigeant la construction *in silico* des structures moléculaires qui les satisfont le mieux. L'outil IBSS®CAMD<sup>14</sup> est un outil numérique innovant dédié à la conception de bio-solvants. Le principal avantage d'IBSS®CAMD réside dans la construction de structures moléculaires en imposant des bio-blocs comme fragments de départ pour assurer le développement de bio-solvants. IBSS®CAMD peut être utilisé selon deux modes différents pour la sélection de solvants : (a) pour évaluer les performances d'une liste de solvants existants présélectionnés, ou (b) pour concevoir de nouvelles molécules et évaluer leurs performances. Les deux modes sont utilisés dans cette thèse, avec un focus sur les solvants bio-sourcés, car ceux-ci devraient présenter de plus faibles impacts sur la santé et l'environnement.

## 5. Etudes de cas

Dans le cadre de cette thèse, des solvants durables ont été sélectionnés à l'aide de l'outil IBSS®CAMD pour cinq systèmes D:A. Les structures chimiques des trois polymères (P3HT, PF2 et KNSF2) et des deux petites molécules (PC<sub>71</sub>BM et EH-EDTBR) étudiés sont illustrées à la figure 1. Le P3HT est un polymère donneur d'électrons bien connu et largement étudié pour les applications PVO. Il constitue une bonne référence pour tester notre méthodologie. En outre, malgré les nombreuses données de la littérature sur les cellules solaires à base de P3HT, seuls quelques exemples ont traité la question des solvants verts. L'EH-IDTBR est un accepteur non-fullerène prometteur qui a récemment suscité beaucoup d'intérêt pour le remplacement des dérivés du fullerène et l'amélioration du PCE des dispositifs basés sur le P3HT. Nous avons donc choisi le P3HT:EH-IDTBR comme deuxième exemple pour illustrer comment l'IBSS®CAMD s'applique à différents matériaux et ouvre la voie à une approche plus polyvalente et plus efficace pour identifier les solvants de substitution.

Le PF2 et le KNSF2 sont deux copolymères di-fluorés dont les propriétés sont particulièrement appropriées pour le photovoltaïque. La fluoration de polymères conjugués a été utilisée initialement pour ajuster les niveaux d'énergie des orbitales frontières. De manière inattendue, d'autres effets positifs des polymères fluorés ont été découverts. Par exemple, des orientations mixtes "face on" et "edge on" du squelette des polymères fluorés par rapport au substrat du dispositif ont été fréquemment observées et engendrent une mobilité des trous hors plan très élevée. En outre, il a été constaté que la pureté des domaines dans les mélanges polymère:fullerène est améliorée lorsque des atomes de fluor sont introduits dans le squelette du polymère. En conséquence, les polymères fluorés ont conduit à une augmentation significative du RCE des cellules solaires HJV.

En 2018, O. A. Ibraikulov et al.<sup>15</sup> ont publié une étude portant sur une série de copolymères fluorés de même structure conjuguée mais avec différents nombres

d'atomes de fluor, dont le PF2. Des rendements supérieurs à 10 % ont pu être atteints avec le PF2 comme donneur d'électrons et le PC<sub>71</sub>BM comme accepteur en élaborant des dispositifs à partir de solution d'o-CDB chauffée à 90°C. Le PF2 présente en effet des caractéristiques exceptionnelles, telles que des niveaux d'énergie des orbitales frontières optimaux, d'excellentes capacités de collecte de la lumière, des propriétés de transport de charge élevées et une morphologie en film mince adéquate, qui se traduisent par un RCE élevé.

L'influence des "chaînes latérales" des polymères conjugués sur leurs propriétés opto-électroniques et photovoltaïques a également suscité un intérêt considérable. En effet, les chaînes latérales ne sont pas seulement nécessaires aux polymères conjugués pour les rendre solubles et manipulables sous forme d'encre, elles ont également un impact sur l'auto-assemblage moléculaire, la morphologie des mélanges D:A et donc sur les performances photovoltaïques. Ainsi, une étude récente a montré l'impact de chaînes siloxanes sur l'organisation moléculaire des polymères conjugués à base d'isoindigo. Le KNSF2 est un polymère de même cœur conjugué que le PF2, mais avec des chaînes siloxanes linéaires (Figure 1). L'objectif de notre travail a été d'évaluer dans quelle mesure les chaînes siloxanes influencent les propriétés de solubilité du polymère et peuvent modifier le choix de solvants alternatifs.

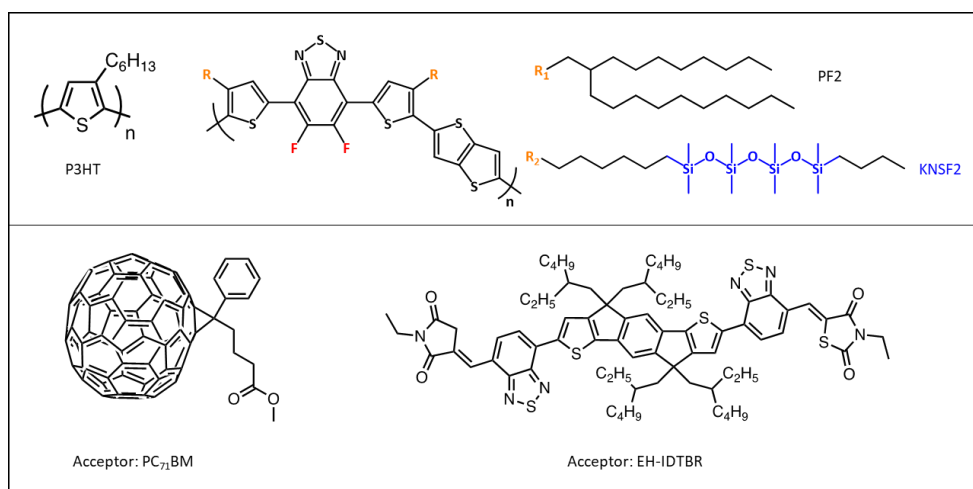


Figure 1. The chemical structures of donors and acceptors.

L'utilisation de l'IBSS®CAMD pour les matériaux semiconducteurs organiques a nécessité un travail préalable pour identifier les paramètres physico-chimiques du solvant qui ont un fort impact sur les performances photovoltaïques. En prenant en compte les propriétés des matériaux organiques étudiés et celles des solvants à remplacer, 11 propriétés et les valeurs cibles correspondantes ont pu être définies. Les solvants alternatifs ont ensuite été sélectionnés sur la base d'une fonction de performance globale englobant toutes les propriétés souhaitées. Les performances des solvants sélectionnés ont ensuite été vérifiées expérimentalement en élaborant des dispositifs avec les solvants alternatifs et en comparant leurs rendements de conversion à ceux obtenus à partir de solutions halogénées. Pour chaque mélange étudié, les performances des dispositifs obtenus avec les solvants alternatifs sont similaires à celles des dispositifs standard, confirmant la pertinence de l'ingénierie inversée pour la sélection des solvants alternatifs dans le domaine du photovoltaïque organique.

- *Le mélange P3HT:PC<sub>71</sub>BM*

Ce mélange a été utilisé comme système de référence, même si ses performances photovoltaïques sont aujourd'hui largement dépassées. En effet, ce matériau a fait l'objet de nombreuses études dans le monde entier et représente aujourd'hui le système donneur/accepteur dont les propriétés sont les mieux comprises. 5 solvants alternatifs ont pu être identifiés grâce aux deux modes de l'IBSS®CAMD (anisole, 2-méthyl anisole, p-xylène, p-cymène et terpinolène) et ont permis d'atteindre des performances similaires à celles du solvant toxique d'origine (*o*-DCB).

- *Le mélange P3HT:EH-IDTBR*

L'EH-IDTBR est une molécule acceptrice d'électrons récemment mise au point pour remplacer les dérivés du fullerène (comme le PC<sub>71</sub>BM) et améliorer les performances des dispositifs de PVO. Quatre solvants non toxiques ont pu être identifiés par le premier mode de l'outil IBSS®CAMD : anisole, p-xylène, p-cymène et

terpinolène. Un RCE moyen de 4,55 %, proche des résultats de la littérature, a été obtenu en utilisant l'anisole comme solvant de traitement.

- *Le mélange PF2:PC<sub>71</sub>BM*

La même approche a été utilisée pour le mélange PF2:PC<sub>71</sub>BM et nous a permis d'identifier le p-xylène, un solvant bio-sourcé, comme alternative à l'o-DCB. Un PCE de 9%, légèrement inférieur à celui obtenu à partir de solvants chlorés, a été obtenu. Il est probable qu'une optimisation supplémentaire des paramètres de fabrication permettra d'égaliser les performances de référence. A noter également que le p-xylène a permis de réduire la température pour solubiliser le polymère de 20°, ce qui facilite la fabrication des dispositifs de grande surface.

- *Le mélange PF2:EH-IDTBR*

Comme pour le cas précédent, le p-xylène a été le seul solvant alternatif identifié par l'IBSS®CAMD. Le faible rayon de solubilité du PF2 est à l'origine de cette limitation. Néanmoins, un RCE de 8,03% a pu être atteint, dépassant cette fois-ci celui obtenu avec l'o-DCB.

- *Le mélange KNSF2:PC<sub>71</sub>BM*

Les mesures des paramètres HSP ont démontré que le KNSF2 est plus soluble que le PF2. Les résultats de l'IBSS®CAMD valident également cette conclusion en fournissant davantage de solvants candidats. Cependant, la faible solubilité du PC<sub>71</sub>BM dans les solvants candidats pour le KNSF2 (due à un écart sensible entre les sphères de solubilités des deux composés) limite cette fois-ci la mise en œuvre des PVO. La prochaine étape, qui consistera à utiliser d'autres accepteurs que le PC<sub>71</sub>BM, n'a cependant pas encore pu être réalisée par manque de temps. L'IBSS®CAMD, sera appliqué en mode conception moléculaire à divers mélanges KNSF2 : NFA (molécules accepteurs non-fullerène).

## 6. Conclusion

Une nouvelle méthode basée sur l'ingénierie inversée et reposant sur l'outil numérique IBSS®CAMD a été utilisée avec succès pour concevoir et sélectionner des solvants alternatifs non-toxiques et durables pour les dispositifs photovoltaïques organiques, en remplacement des solvants toxiques actuels (CB, *o*-DCB, CF...). Cette approche a nécessité l'identification des paramètres des solvants ayant un impact fort sur les performances des dispositifs photovoltaïques, leur traduction en propriétés physico-chimiques et la définition de valeurs cibles que doivent atteindre les solvants alternatifs. En résolvant un problème d'optimisation multi-objectifs avec un outil de conception moléculaire assistée par ordinateur (IBSS®CAMD), les solvants alternatifs ont été classés selon une valeur de performance globale, qui évalue la correspondance du comportement des solvants alternatifs avec un ensemble de propriétés physico-chimiques cibles multiples. En explorant la diversité des structures moléculaires, l'approche de l'ingénierie inverse élargit considérablement la liste des solvants candidats par rapport aux méthodes plus empiriques de type essais-erreurs et peut donner lieu à des solvants présentant de meilleures performances.

Les cinq cas étudiés dans cette thèse ont clairement fait ressortir que l'approche de l'ingénierie inverse est un moyen efficace pour sélectionner des solvants de remplacement pour les semi-conducteurs organiques. Il convient en outre de noter que si la méthode n'a été appliquée dans ce travail qu'aux matériaux conçus pour des applications photovoltaïques, elle devrait également présenter un intérêt pour tout dispositif optoélectronique élaboré à partir de solutions organique.

#### *References :*

- (1) Liu, Q.; Jiang, Y.; Jin, K.; Qin, J.; Xu, J.; Li, W.; Xiong, J.; Liu, J.; Xiao, Z.; Sun, K.; Yang, S.; Zhang, X.; Ding, L. 18% Efficiency Organic Solar Cells. *Sci. Bull.* **2020**, *65* (4), 272–275.
- (2) Manley, E. F.; Strzalka, J.; Fauvell, T. J.; Marks, T. J.; Chen, L. X. In Situ Analysis of Solvent and Additive Effects on Film Morphology Evolution in Spin-Cast

- Small-Molecule and Polymer Photovoltaic Materials. *Adv. Energy Mater.* **2018**, *8* (23), 1–20.
- (3) Bilal Ahmed Siddique, M.; Hussain, R.; Ali Siddique, S.; Yasir Mehboob, M.; Irshad, Z.; Iqbal, J.; Adnan, M. Designing Triphenylamine-Configured Donor Materials with Promising Photovoltaic Properties for Highly Efficient Organic Solar Cells. *ChemistrySelect* **2020**, *5* (25), 7358–7369.
- (4) Li, S.; Zhan, L.; Zhao, W.; Zhang, S.; Ali, B.; Fu, Z.; Lau, T. K.; Lu, X.; Shi, M.; Li, C. Z.; Hou, J.; Chen, H. Revealing the Effects of Molecular Packing on the Performances of Polymer Solar Cells Based on A-D-C-D-A Type Non-Fullerene Acceptors. *J. Mater. Chem. A* **2018**, *6* (25), 12132–12141.
- (5) Jalan, I.; Lundin, L.; van Stam, J. Using Solubility Parameters to Model More Environmentally Friendly Solvent Blends for Organic Solar Cell Active Layers. *Materials (Basel)*. **2019**, *12* (23).
- (6) Meng, B.; Fu, Y.; Xie, Z.; Liu, J.; Wang, L. Phosphonated Conjugated Polymers for Polymer Solar Cells with a Non-Halogenated Solvent Process. *Polym. Chem.* **2015**, *6* (5), 805–812.
- (7) Zhao, W.; Ye, L.; Zhang, S.; Sun, M.; Hou, J. A Universal Halogen-Free Solvent System for Highly Efficient Polymer Solar Cells. *J. Mater. Chem. A* **2015**, *3* (24), 12723–12729.
- (8) Bouzid, H.; Prosa, M.; Bolognesi, M.; Chehata, N.; Gedefaw, D.; Albonetti, C.; Andersson, M. R.; Muccini, M.; Bouazizi, A.; Seri, M. Impact of Environmentally Friendly Processing Solvents on the Properties of Blade-Coated Polymer Solar Cells. *J. Polym. Sci. Part A Polym. Chem.* **2019**, *57* (4), 487–494.
- (9) Liu, D.; Wang, Z.; Zhang, S.; Zheng, Z.; Yang, B.; Ma, W.; Hou, J. Rational Selection of Solvents and Fine Tuning of Morphologies toward Highly Efficient Polymer Solar Cells Fabricated Using Green Solvents. *RSC Adv.* **2015**, *5* (85), 69567–69572.



- (10) Wang, H.; Fan, Q.; Chen, L.; Xiao, Y. Amino-Acid Ester Derived Perylene Diimides Electron Acceptor Materials: An Efficient Strategy for Green-Solvent-Processed Organic Solar Cells. *Dye. Pigment.* **2019**, *164* (December 2018), 384–389.
- (11) Abdulahi, B. A.; Li, X.; Mone, M.; Kiros, B.; Genene, Z.; Qiao, S.; Yang, R.; Wang, E.; Mammo, W. Structural Engineering of Pyrrolo[3,4-: F] Benzotriazole-5,7(2 H,6 H)-Dione-Based Polymers for Non-Fullerene Organic Solar Cells with an Efficiency over 12%. *J. Mater. Chem. A* **2019**, *7* (33), 19522–19530.
- (12) Morvillo, P.; Grimaldi, I. A.; Diana, R.; Loffredo, F.; Villani, F. Study of the Microstructure of Inkjet-Printed P3HT:PCBM Blend for Photovoltaic Applications. *J. Mater. Sci.* **2013**, *48* (7), 2920–2927.
- (13) Shaheen, S. E.; Brabec, C. J.; Sariciftci, N. S.; Padinger, F.; Fromherz, T.; Hummelen, J. C. 2.5% Efficient Organic Plastic Solar Cells. *Appl. Phys. Lett.* **2001**, *78* (6), 841–843.
- (14) Rodriguez-Donis, I.; Thiebaud-Roux, S.; Lavoine, S.; Gerbaud, V. Computer-Aided Product Design of Alternative Solvents Based on Phase Equilibrium Synergism in Mixtures. *Comptes Rendus Chim.* **2018**, *21* (6), 606–621.
- (15) Ibraikulov, O. A.; Ngov, C.; Chávez, P.; Bulut, I.; Heinrich, B.; Boyron, O.; Gerasimov, K. L.; Ivanov, D. A.; Swaraj, S.; Méry, S.; Leclerc, N.; Lévêque, P.; Heiser, T. Face-on Orientation of Fluorinated Polymers Conveyed by Long Alkyl Chains: A Prerequisite for High Photovoltaic Performances. *J. Mater. Chem. A* **2018**, *6* (25), 12038–12045.

## Searching sustainable solvents for high-performance organic solar cells by reverse engineering

### Résumé

Pour la production de modules photovoltaïques organiques (OPV), le remplacement des solvants halogénés par des solvants "verts" est indispensable. En raison des liens complexes entre propriétés des solvants et performances OPV, la sélection de solvants s'est basée jusqu'à présent sur une approche de type essai – erreur. Ici, nous explorons une méthode moins empirique, de type conception moléculaire assistée par ordinateur, en utilisant l'outil IBSS®CAMD, initialement développé pour la recherche de bio-solvants en cosmétique. IBSS®CAMD modélise les propriétés physico-chimiques de molécules et applique un algorithme génétique pour concevoir des molécules aux propriétés souhaitées. A partir de valeurs cibles de multiples propriétés, IBSS®CAMD établit une classification de solvants en terme de performances globales. Les performances réelles des solvants sélectionnés sont évaluées en élaborant des dispositifs OPV et en comparant les rendements de conversion avec des références. Pour chacun des matériaux étudiés, les résultats obtenus avec les solvants alternatifs sont équivalents aux références, confirmant l'efficacité de la méthode.

Mots-clés: Photovoltaïque organique, solvants durables, conception de produits assistée par ordinateur

### Résumé en anglais

For a sustainable scale-up of organic photovoltaic (OPV) modules, the replacement of halogenated solvents by "green" solvents is a critical pre-requisite. Due to the complex relationship between solvent properties and device performance, the selection of alternative solvents has so far relied primarily on a trial-and-error approach. In this thesis, we introduce a less empirical solvent selection tool, IBSS®CAMD, and apply it to the fabrication of OPVs. IBSS®CAMD models the physicochemical properties of molecules and applies a genetic algorithm to design molecules with the desired properties. This allows us to establish lists of alternative solvents ranked by a global performance function encompassing a given number of desired properties. The actual performances of the selected solvents are evaluated by elaborating photovoltaic devices and comparing the performance with those obtained with devices processed from halogenated solvents. For each of studied blends, the performances of the devices obtained with the alternative solvents were similar to those of standard devices processed from halogenated solvents, corroborating the relevance of the proposed method.

Keywords: Organic photovoltaics, sustainable solvents, computer-aided product design